

University of Windsor

Scholarship at UWindor

Electronic Theses and Dissertations

Theses, Dissertations, and Major Papers

2005

Self-assembled platinum(II) complexes for anion recognition.

Chantelle R. Bondy
University of Windsor

Follow this and additional works at: <https://scholar.uwindsor.ca/etd>

Recommended Citation

Bondy, Chantelle R., "Self-assembled platinum(II) complexes for anion recognition." (2005). *Electronic Theses and Dissertations*. 3412.
<https://scholar.uwindsor.ca/etd/3412>

This online database contains the full-text of PhD dissertations and Masters' theses of University of Windsor students from 1954 forward. These documents are made available for personal study and research purposes only, in accordance with the Canadian Copyright Act and the Creative Commons license—CC BY-NC-ND (Attribution, Non-Commercial, No Derivative Works). Under this license, works must always be attributed to the copyright holder (original author), cannot be used for any commercial purposes, and may not be altered. Any other use would require the permission of the copyright holder. Students may inquire about withdrawing their dissertation and/or thesis from this database. For additional inquiries, please contact the repository administrator via email (scholarship@uwindsor.ca) or by telephone at 519-253-3000ext. 3208.

INFORMATION TO USERS

This manuscript has been reproduced from the microfilm master. UMI films the text directly from the original or copy submitted. Thus, some thesis and dissertation copies are in typewriter face, while others may be from any type of computer printer.

The quality of this reproduction is dependent upon the quality of the copy submitted. Broken or indistinct print, colored or poor quality illustrations and photographs, print bleedthrough, substandard margins, and improper alignment can adversely affect reproduction.

In the unlikely event that the author did not send UMI a complete manuscript and there are missing pages, these will be noted. Also, if unauthorized copyright material had to be removed, a note will indicate the deletion.

Oversize materials (e.g., maps, drawings, charts) are reproduced by sectioning the original, beginning at the upper left-hand corner and continuing from left to right in equal sections with small overlaps.

ProQuest Information and Learning
300 North Zeeb Road, Ann Arbor, MI 48106-1346 USA
800-521-0600

UMI[®]

Self-Assembled Platinum(II) Complexes For Anion Recognition

By

Chantelle R. Bondy

A Dissertation

Submitted to the Faculty of Graduate Studies and Research
through the Department of Chemistry and Biochemistry
in Partial Fulfillment of the Requirements for
the Degree of Doctor of Philosophy at the
University of Windsor.

Windsor, Ontario, Canada

October 21, 2005



Library and
Archives Canada

Bibliothèque et
Archives Canada

0-494-09719-1

Published Heritage
Branch

Direction du
Patrimoine de l'édition

395 Wellington Street
Ottawa ON K1A 0N4
Canada

395, rue Wellington
Ottawa ON K1A 0N4
Canada

Your file *Votre référence*

ISBN:

Our file *Notre référence*

ISBN:

NOTICE:

The author has granted a non-exclusive license allowing Library and Archives Canada to reproduce, publish, archive, preserve, conserve, communicate to the public by telecommunication or on the Internet, loan, distribute and sell theses worldwide, for commercial or non-commercial purposes, in microform, paper, electronic and/or any other formats.

The author retains copyright ownership and moral rights in this thesis. Neither the thesis nor substantial extracts from it may be printed or otherwise reproduced without the author's permission.

AVIS:

L'auteur a accordé une licence non exclusive permettant à la Bibliothèque et Archives Canada de reproduire, publier, archiver, sauvegarder, conserver, transmettre au public par télécommunication ou par l'Internet, prêter, distribuer et vendre des thèses partout dans le monde, à des fins commerciales ou autres, sur support microforme, papier, électronique et/ou autres formats.

L'auteur conserve la propriété du droit d'auteur et des droits moraux qui protègent cette thèse. Ni la thèse ni des extraits substantiels de celle-ci ne doivent être imprimés ou autrement reproduits sans son autorisation.

In compliance with the Canadian Privacy Act some supporting forms may have been removed from this thesis.

Conformément à la loi canadienne sur la protection de la vie privée, quelques formulaires secondaires ont été enlevés de cette thèse.

While these forms may be included in the document page count, their removal does not represent any loss of content from the thesis.

Bien que ces formulaires aient inclus dans la pagination, il n'y aura aucun contenu manquant.


Canada

© Chantelle R. Bondy 2005

All Rights Reserved

Abstract

The focus of this thesis is the development of novel anion receptors possessing conformational flexibility through the use of a simple inorganic framework. The complex cation, $[\text{PtL}_4]^{2+}$, can adopt four conformations inspired by calix[4]arene-based receptors: 'cone', 'partial cone', '1,2-alternate' or '1,3-alternate'. The first part of the thesis involves the synthesis, characterization and examination of the binding properties of three generations of anion receptors using ^1H NMR spectroscopy and X-ray crystallography.

The first generation receptor is $[\text{PtL}_4]^{2+}$ where $\text{L} = 3\text{-}n\text{butylnicotinamide}$. Solution studies show moderate binding constants in polar solvents with preference for 1:2 binding of planar bidentate anions such as CH_3CO_2^- and NO_3^- .

Conformational flexibility is removed in the second generation receptor. The receptor is preorganized for 1:2 binding of planar bidentate anions with two *bis*-3,5-*n*butylnicotinamide ligands coordinated to $[\text{Pt}(2,2'\text{-bipy})]^{2+}$. The results show diminished receptor:anion interactions in both solution and solid state.

The third generation receptor consists of $[\text{PtL}_4]^{2+}$ where $\text{L} = 8\text{-}n\text{butylurea}i\text{soquinoline}$. The association constants are high in very polar solvent with the 1,2-alternate conformation preferred for the binding of spherical halide anions. The cone conformation is seen when binding tetrahedral shaped oxo-anions. This trend is also confirmed by X-ray crystal structure data.

The second part of the thesis investigates the conformational stability and interconversion barriers of several rotameric model complexes using ^1H NMR spectroscopy and molecular mechanics. The number of possible conformations in most

of the compounds is simplified to two, *syn* and *anti*. The *anti* conformation is the most stable and interconversion barriers range from 69 – 76 kJ/mol.

Finally, the last section of the thesis explores the use of mass spectrometry and fluorescence spectroscopy as tools for qualitative analysis of the binding interactions between our third generation receptor and several different anions. Trends in anion selectivity are monitored.

This work is dedicated to my father, mother and brother.

Acknowledgments

I would like to thank my boss Steve Loeb for all his guidance and patience throughout the years.

I would also like to thank all the members of the Loeb group, past and present, especially: Greg Davidson, Sarah Vella, Roopa Patel, Dave Tramontozzi, Derek Beauchamp, Iavor Mihalkov, Dennis Hoffart, Ana De La Torre, Jason Jolicoeur, Amy Root, Norma Georges, Natalie Suhan and Clare Sullivan. Thanks for making the last six years so enjoyable!

Thanks to Phil Gale for all the discussions about my project. A special thanks to Jorge Tiburcio for helping and teaching me so much. Thanks to James Gauld for proofreading my thesis and for putting up with me.

Thanks to Mike Fuerth for the help running NMR experiments and Shuanquan Zhang for the help acquiring the mass spectrometry data.

I would like to thank my parents for believing in me and encouraging me throughout all my endeavors. Finally, I would like to thank my brother for setting the bar very high and for being the best role model a little sister could have ever asked for.

Table of Contents

Abstract	iv
Dedication	vi
Acknowledgements	vii
List of Figures	xiv
List of Tables	xxv
List of Abbreviations	xxvi
Chapter 1 - Introduction	1
1.1 Supramolecular Chemistry of Anions	1
1.1.1 Anion Recognition	1
<i>Anion Characteristics</i>	<i>1</i>
<i>Types of Interactions</i>	<i>3</i>
<i>Functional Groups</i>	<i>5</i>
<i>Frameworks</i>	<i>6</i>
<i>Organic Frameworks</i>	<i>6</i>
<i>Inorganic Frameworks</i>	<i>13</i>
<i>Metal Functionality</i>	<i>16</i>
1.2 Scope of the Project	18
Chapter 2 - Amide Receptor	22
2.1 Introduction	22
2.2 Results and Discussion	25
2.2.1 Synthesis and Characterization of [Pt(3- <i>n</i> butylnicotinamide) ₄][PF ₆] ₂ (1)	25

	<i>Synthesis</i>	25
	<i>¹H NMR Spectroscopy</i>	27
	<i>Mass Spectrometry</i>	29
	<i>X-ray Structure of [Pt(3-<i>n</i>butylnicotinamide)₄][PF₆]₂·2CH₂Cl₂ (1)</i>	31
2.2.2	Binding Studies	33
	<i>¹H NMR Titrations</i>	33
	<i>X-Ray Structure of [Pt(3-<i>n</i>butylnicotinamide)₄][CF₃SO₃]₂</i>	39
	<i>X-Ray Structure of [Pt(3-<i>n</i>butylnicotinamide)₄][ReO₄]₂</i>	41
2.3	Conclusions	44
2.4	Experimental	46
	2.4.1 General Methods	46
	2.4.2 General Methods for X-Ray Crystallography	46
	2.4.3 3- <i>n</i> Butylnicotinamide	47
	2.4.4 [Pt(3- <i>n</i> butylnicotinamide) ₄][PF ₆] ₂ (1)	49
	2.4.5 [Pt(3- <i>n</i> butylnicotinamide) ₄][CF ₃ SO ₃] ₂	51
	2.4.6 [Pt(3- <i>n</i> butylnicotinamide) ₄][ReO ₄] ₂	52
	2.4.7 Titration Methods	53
	2.4.8 Method of Continuous Variation (Job Method)	56
	Chapter 3 - Bis-Amide Receptor	58
3.1	Introduction	58
3.2	Results and Discussion	60

3.2.1 Synthesis and Characterization of [Pt(3,5- <i>di-n</i> butylamidepyridine) ₂ (<i>t</i> butylbipy)][PF ₆] ₂ (2)	60
<i>Synthesis</i>	60
¹ H NMR Spectroscopy	62
<i>Mass Spectrometry</i>	64
3.2.2 Binding Studies	65
¹ H NMR Titrations	65
<i>X-Ray Structure of</i> [Pt(3,5- <i>di-n</i> butylamidepyridine) ₂ (<i>t</i> butylbipy)][NO ₃] ₂	68
<i>X-Ray Structure of</i> [Pt(3,5- <i>di-n</i> butylamidepyridine) ₂ (<i>bipy</i>)] [ReO ₄] ₂	71
<i>X-Ray Structure of</i> [Pt(C ₆ H ₅ CO ₂) ₂ (<i>t</i> butylbipy)]	72
3.3 Conclusions	73
3.4 Experimental	75
3.4.1 General Methods	75
3.4.2 3,5- <i>Di-n</i> butylamidepyridine	75
3.4.3 [Pt(3,5- <i>di-n</i> butylamidepyridine) ₂ (<i>t</i> butylbipy)][PF ₆] ₂ (2)	77
3.4.4 [Pt(3,5- <i>di-n</i> butylamidepyridine) ₂ (<i>t</i> butylbipy)][NO ₃] ₂	79
3.4.5 [Pt(3,5- <i>di-n</i> butylamidepyridine) ₂ (<i>bipy</i>)] [ReO ₄] ₂	80
3.4.6 [Pt(C ₆ H ₅ CO ₂) ₂ (<i>t</i> butylbipy)]	81
3.4.7 Titration Methods	82
Chapter 4 - Urea Receptor	83
4.1 Introduction	83
4.2 Results and Discussion	86
4.2.1 Synthesis of [Pt(8- <i>n</i> butylurea <i>iso</i> quinoline) ₄][BF ₄] ₂ (3)	86

	<i>Synthesis</i>	86
	¹ H NMR Spectroscopy	88
	Mass Spectrometry	90
	<i>X-ray Structure of</i> <i>[Pt(8-nbutylureaisoquinoline)₄][BF₄]₂ (3)</i>	91
4.2.2	Binding Studies	92
	¹ H NMR Titrations	92
	<i>X-Ray Structure of</i> <i>[Pt(8-nbutylureaisoquinoline)₄][Cl]₂</i>	98
	<i>X-Ray Structure of</i> <i>[Pt(8-nbutylureaisoquinoline)₄][SO₄]</i>	100
4.3	Conclusions	104
4.4	Experimental	105
	4.4.1 General Methods	105
	4.4.2 8- <i>n</i> Butylureaisoquinoline	106
	4.4.3 [Pt(8- <i>n</i> butylureaisoquinoline) ₄][BF ₄] ₂ (3)	108
	4.4.4 [Pt(8- <i>n</i> butylureaisoquinoline) ₄][Cl] ₂	110
	4.4.5 [Pt(8- <i>n</i> butylureaisoquinoline) ₄][SO ₄]	111
	4.4.6 Titration Methods	112
	Chapter 5 - Model Compounds	114
5.1	Introduction	114
5.2	Results and Discussion	119
	5.2.1 <i>cis</i> -[PtCl ₂ (3- <i>n</i> butylamidequinoline) ₂] (7)	119
	<i>Synthesis</i>	120

^1H NMR Spectroscopy	121
Conformational Analysis	126
Conclusions	127
5.2.2 [Pt(3- <i>n</i> butylnicotinamide) ₂ (<i>t</i> butylbipy)][PF ₆] ₂ (5)	127
Synthesis	128
^1H NMR Spectroscopy	129
Mass Spectrometry	131
Conformational Analysis	132
Conclusions	134
5.2.3 [Pt(8- <i>n</i> butylureaisoquinoline) ₂ (<i>t</i> butylbipy)][BF ₄] ₂ (6)	134
Synthesis	135
^1H NMR Spectroscopy	136
X-Ray Crystallography	139
Mass Spectrometry	140
Conformational Analysis	141
Conclusions	143
5.2.4 [Pt(3- <i>n</i> butylamidequinoline) ₄][PF ₆] ₂ (4)	143
Synthesis	144
^1H NMR Spectroscopy	145
Conformational Analysis	147
Conclusions	148
5.3 Conclusions	149
5.4 Experimental	150

5.4.1 General Methods	150
5.4.2 3- <i>n</i> Butylamidequinoline	151
5.4.3 [Pt(3- <i>n</i> butylamidequinoline) ₄][PF ₆] ₂ (4)	153
5.4.4 [Pt(3- <i>n</i> butylnicotinamide) ₂ (<i>t</i> butylbipy)][PF ₆] ₂ (5)	155
5.4.5 [Pt(8- <i>n</i> butylureaisoquinoline) ₂ (<i>t</i> butylbipy)][BF ₄] ₂ (6)	157
5.4.6 <i>cis</i> -[PtCl ₂ (3- <i>n</i> butylamidequinoline) ₂] (7)	159
Chapter 6 - Anion Sensing	161
6.1 Introduction	161
6.2 Results and Discussion	163
6.2.1 ESI-TOF Mass Spectrometric Investigation	163
<i>The experiment</i>	164
6.2.2 Fluorescence-Emission Spectroscopic Investigation	167
6.3 Conclusions	171
6.4 Experimental	173
6.4.1 General Methods	173
6.4.2 Mass Spectrometry Solution Preparation	173
6.4.3 Fluorescence-Emission Titration Methods	175
Chapter 7 - Summary and Future Work	177
7.1 Summary	177
7.2 Future Work	183
References	186
Vita Auctoris	192

List of Figures

Figure 1.1	The complementary shape and size of the host and guest as they interact, non-covalently.	1
Figure 1.2	First synthetic anion receptor, reported in 1967 by Park and Simmons.	2
Figure 1.3	Geometries of various anions.	3
Figure 1.4	Types of interactions available for receptor:anion binding.	4
Figure 1.5	Functional groups providing hydrogen bonding interactions.	5
Figure 1.6	Functional groups providing both hydrogen bonding and electrostatic interactions.	6
Figure 1.7	Simple aromatic ring framework, by Crabtree.	7
Figure 1.8	A bicyclic (1.6) and tripodal (1.7) 1,3,5- <i>trisubstituted</i> benzene framework, by Anslyn, with an example of a strongly binding enolate (1.8).	7
Figure 1.9	Cyclic and acyclic receptors based on a cholic acid framework, by Davis.	8
Figure 1.10	Pyrrole based clefts containing single and dipyrrole frameworks, by Gale.	9
Figure 1.11	Cyclophane framework containing polyammonium functional groups, by Bowman-James.	10
Figure 1.12	Macrocyclic peptides form the framework for the anion receptors by Kubik.	10
Figure 1.13	Calixarene frameworks are utilized by Ungaro.	11
Figure 1.14	Various calixpyrroles used the frameworks to study anion binding, by Sessler.	12
Figure 1.15	Cyclodextrins provide a hydrophobic environment for binding anions which is used by Kano. 1.42 and 1.43 are examples of the anions bound by these receptors.	13

Figure 1.16	Atwood developed metallated calixarenes which also provide a hydrophobic and electron deficient environment for binding anions.	14
Figure 1.17	Beer utilizes Ru(II)(bipy) ₃ complexes as a framework to append functionalized ligands.	15
Figure 1.18	A cage structure (1.52) by Fabbrizzi contains coordinating metal ion to bind anions.	15
Figure 1.19	Metallated porphyrins used by Beer provide a large framework to append functional groups.	16
Figure 1.20	i) Mercuracarborane receptor 1.56 contains six coordinating metal ions. ^{50,51} ii) Calix[4]pyrrole, 1.57 , with an appended ferrocene group used as a reporter group for anion binding. ⁵² iii) Ruthenium(II) used as a scaffold for three <i>bis</i> -amide substituted bipyridine ligands, 1.48-1.51 . ⁴²⁻⁴⁵ iv) Cr(CO) ₃ coordinated to the receptor, 1.58 , as electron withdrawing substituents to increase the acidity of the amide proton. ⁵³	17
Figure 1.21	Neutral small molecule receptor, by Gokel and Atwood, where the iron(II) metal centres allow for structural functionality and conformational change upon binding the guest.	18
Figure 1.22	The basic structure of our inorganic scaffold.	19
Figure 1.23	The basic structure for our anion receptors.	20
Figure 1.24	Structural similarity between calix[4]arene and our receptor framework when functional groups placed in the 3 position.	21
Figure 2.1	Enzyme <i>Threonine synthase</i> binding serine phosphate through amide functional groups.	22
Figure 2.2	1,3-amide substituted calix[4]arene in pinched cone conformation binding benzoate.	23
Figure 2.3	Comparison of possible placement of the amide groups for convergence toward the anion a) 2-position b) 3-position and c) 4-position.	24
Figure 2.4	First generation receptor [Pt(3- <i>n</i> butylnicotinamide) ₄][PF ₆] ₂ , 1 , arbitrarily shown in the 1,2-alternate conformation.	25

Figure 2.5	Synthesis of nicotinic ethyl ester. i) Reflux for 24 hours in EtOH and H ₂ SO ₄ (conc).	26
Figure 2.6	Synthesis of 3- <i>n</i> -butylnicotinamide.	26
Figure 2.7	Synthesis of 1 .	26
Figure 2.8	¹ H NMR spectrum of 3- <i>n</i> -butylnicotinamide in MeCN- <i>d</i> ₃ with inset of aromatic region.	27
Figure 2.9	¹ H NMR spectrum of 1 in MeCN- <i>d</i> ₃ with inset of aromatic region.	28
Figure 2.10	The ESI-TOF mass spectra showing the calculated (top) and raw (bottom) data obtained from [L-H] ⁺ .	30
Figure 2.11	The ESI-TOF mass spectra showing the calculated (top) and raw (bottom) data for [1-PF ₆] ⁺ .	30
Figure 2.12	X-ray crystal structure of [Pt(3- <i>n</i> -butylnicotinamide) ₄][PF ₆] ₂ ·2CH ₂ Cl ₂ , side view demonstrating electrostatic interaction between Pt(II) and PF ₆ ⁻ . Pt...F distances (Å) and angles (°): Pt(1)...F(1) 3.42, Pt(1)...F(1)-P(1) 147; Pt(1)...F(8) 3.28, Pt(1)...F(1)-P(2) 155.	31
Figure 2.13	X-ray crystal structure of [Pt(3- <i>n</i> -butylnicotinamide) ₄][PF ₆] ₂ ·2CH ₂ Cl ₂ , front view demonstrating H-bonding between C=O of receptor with C-H of solvent, CH ₂ Cl ₂ . C-H...O distances (Å) and angles (°): C(50)...O(4) 3.01, C(50)-H(50A)...O(4) 155; C(50)...O(1) 3.26, C(50)-H(50B)...O(1) 153; C(60)...O(2) 3.26, C(60)-H(60A)...O(2) 155; C(60)...O(3) 3.37, C(60)-H(60B)...O(3) 140.	32
Figure 2.14	The ¹ H NMR titration of 1 with NO ₃ ⁻ , in MeCN- <i>d</i> ₃ , at several different quantities of anion. The receptor:anion interactions are fast on the NMR timescale therefore, a gradual downfield change in chemical shift is observed for the N-H resonance.	34
Figure 2.15	Plot of continuous variation experiment with CF ₃ SO ₃ ⁻ , showing the 1:1 interaction of receptor and anion.	36
Figure 2.16	Conformations available for receptor 1 to interact with the first guest. A change in conformation for interaction with the second anion may require an unfavorable amount of energy.	37

Figure 2.17	Plot of continuous variation experiment with CH_3CO_2^- showing the 1:2 interactions of receptor and anions.	38
Figure 2.18	Scheme representing the positive allosteric effect observed upon binding CH_3CO_2^- .	39
Figure 2.19	X-ray crystal structure of $[\text{Pt}(3\text{-}n\text{butylnicotinamide})_4][\text{CF}_3\text{SO}_3]_2$, front view. N-H...O and C-H...O distances (Å) and angles (°): N(2)...O(5) 2.94, N(2)-H(2A)...O(5) 158; N(4)...O(4) 3.05, N(4)-H(4A)...O(4) 154; C(15)...O(3) 3.13, C(15)-H(15A)...O(3) 157.	40
Figure 2.20	X-ray crystal structure of $[\text{Pt}(3\text{-}n\text{butylnicotinamide})_4][\text{CF}_3\text{SO}_3]_2$, side view. Pt...O distances (Å) and angles (°): Pt(1)...O(3) 3.60, Pt(1)...O(3)-S(1) 111; Pt(1)...O(4) 4.70, Pt(1)...O(4)-S(1) 67; Pt(1)...O(5) 4.36, Pt(1)...O(5)-S(1) 80. Pt(1)...S(1) 4.34.	41
Figure 2.21	X-ray crystal structure of $[\text{Pt}(3\text{-}n\text{butylnicotinamide})_4][\text{ReO}_4]_2$, side view showing 1,2-alternate conformation. Pt...O distances (Å) and angles (°): Pt(1)...O(10) 4.16, Pt(1)...O(10)-Re(2) 86; Pt(1)...O(11) 4.11, Pt(1)...O(11)-Re(2) 89; Pt(1)...O(12) 4.12, Pt(1)...O(12)-Re(2) 87. Pt(1)...Re(2) 4.42.	42
Figure 2.22	X-ray crystal structure of $[\text{Pt}(3\text{-}n\text{butylnicotinamide})_4][\text{ReO}_4]_2$ where orange ligand is twisted 23° to allow the acidic C-H proton (H21A) to interaction with the oxygen of the anion.	43
Figure 2.23	X-ray crystal structure of $[\text{Pt}(3\text{-}n\text{butylnicotinamide})_4][\text{ReO}_4]_2$, front view showing hydrogen bonding interactions. N-H...O and C-H...O distances (Å) and angles (°): N(2)...O(12) 3.49, N(2)-H(2A)...O(12) 137; N(8)...O(10) 3.01, N(8)-H(8A)...O(10) 168; C(11)...O(11) 3.31, C(11)-H(11A)...O(7) 142; C(21)...O(7) 3.32, C(21)-H(21A)...O(11) 171.	44
Figure 3.1	Schematic representation of the possible mode of 1:2 binding for receptors 1 and 2 .	58
Figure 3.2	Scheme representing the convergence of possible interactions towards the guest with amide substitution in the 3 position and the 3,5 position.	59

Figure 3.3	Second generation receptor [Pt(3,5- <i>di-n</i> butylamidepyridine) ₂ (<i>t</i> butylbipy)][PF ₆] ₂ , 2 .	60
Figure 3.4	Synthesis of 3,5-pyridine ethyl ester. i) Reflux in EtOH and H ₂ SO ₄ (conc).	60
Figure 3.5	Synthesis of 3,5- <i>di-n</i> butylamidepyridine.	61
Figure 3.6	Synthesis of 2 .	61
Figure 3.7	¹ H NMR spectrum of 3,5- <i>di-n</i> butylamidepyridine in MeCN- <i>d</i> ₃ .	62
Figure 3.8	Partial ¹ H NMR spectrum of 2 in MeCN- <i>d</i> ₃ .	63
Figure 3.9	The isotopic profile of the calculated (top) and raw (bottom) spectra of [2-PF ₆] ⁺ .	65
Figure 3.10	Scheme representing the ability of receptor 1 and 2 to bind anions in a 1:2 ratio. A positive allosteric effect is observed with receptor 1 while a negative allosteric effect is observed with receptor 2 .	67
Figure 3.11	X-ray crystal structure of [Pt(3,5- <i>di-n</i> butylamidepyridine) ₂ (<i>t</i> butylbipy)][NO ₃] ₂ , front view showing the tilt of the ligands and the hydrogen bonding interactions with NO ₃ ⁻ , <i>t</i> butyl groups have been omitted for clarity. N-H...O distances (Å) and angles (°): N(106)...O(10) 2.96, N(106)-H(10D)...O(10) 161; N(103)...O(10) 2.93, N(103)-H(10B)...O(10) 149; N(102)...O(9) 2.88, N(15)-H(10A)...O(9) 141.	69
Figure 3.12	X-ray crystal structure of [Pt(3,5- <i>di-n</i> butylamidepyridine) ₂ (<i>t</i> butylbipy)][NO ₃] ₂ , side view showing the placement of the anions with respect to the platinum(II), <i>t</i> butyl groups have been omitted for clarity. Pt...O distances (Å) and angles (°): Pt(1)...O(12) 4.19, Pt(1)...O(12)-N(4) 83; Pt(1)...O(8) 3.39, Pt(1)...O(8)-N(3) 172. Pt(1)...N(3) 4.63; Pt(1)...N(4) 4.22.	70
Figure 3.13	X-ray crystal structure of [Pt(3,5- <i>di-n</i> butylamidepyridine) ₂ (bipy)][ReO ₄] ₂ , front view showing the hydrogen bonding between the receptor and two ReO ₄ ⁻ anions. N-H...O and C-H...O distances (Å) and angles (°): N(202)...O(8) 3.05, N(202)-H(202A)...O(8) 163; C(220)...O(3) 3.05, C(220)-H(22A)...O(3) 164.	71

Figure 3.14	A side view of X-ray crystal structure of [Pt(3,5- <i>di-n</i> butylamidepyridine) ₂ (bipy)][ReO ₄] ₂ showing the electrostatic interactions. Pt...O distances (Å) and angles (°): Pt(2)...O(6) 4.14, Pt(2)...O(6)-Re(2) 84; Pt(2)...O(1) 3.59, Pt(2)...O(1)-Re(1) 104. Pt(2)...Re(2) 4.31; Pt(2)...Re(1) 4.00.	72
Figure 3.15	X-ray crystal structure of [Pt(C ₆ H ₅ CO ₂) ₂ (<i>t</i> butylbipy)].	73
Figure 4.1	Systematic replacement of amide by urea functional groups in a biphenyl receptor, by Albrecht, demonstrating the effect of increasing the number of hydrogen bond donors.	83
Figure 4.2	The placement of the functional group on the pyridine ligand is important for convergence towards the coordinating anion.	85
Figure 4.3	Comparison of the N-H hydrogen bond donor position in the first generation amide based receptor 1 and the third generation urea based receptor 3 .	85
Figure 4.4	Third generation receptor [Pt(8- <i>n</i> butylurea <i>iso</i> quinoline) ₄][BF ₄] ₂ , 3 , arbitrarily in the 1,2-alternate conformation.	86
Figure 4.5	Synthesis of 8-amino <i>iso</i> quinoline from 5-amino <i>iso</i> quinoline. i) NaNO ₂ (aq) at 0 °C; CuCl in HCl(conc) at 75 °C, ii) KNO ₃ in H ₂ SO ₄ (conc), iii) H ₂ N=NH ₂ and Pd on carbon in EtOH at reflux.	87
Figure 4.6	Synthesis of 8- <i>n</i> butylurea <i>iso</i> quinoline. i) Stir in CH ₂ Cl ₂ with excess <i>n</i> butylisocyanate.	87
Figure 4.7	Synthesis of 3 .	88
Figure 4.8	¹ H NMR spectrum of the aromatic region for 8- <i>n</i> butylurea <i>iso</i> quinoline in DMSO- <i>d</i> ₆ .	89
Figure 4.9	Partial ¹ H NMR spectrum of 3 , in DMSO- <i>d</i> ₆ .	89
Figure 4.10	The calculated (top) and observed (bottom) mass spectra of 3 as the [3-BF ₄] ⁺ species.	91

- Figure 4.11 X-ray crystal structure of **3** in the 1,2-alternate conformation. N-H...F distances (Å) and angles (°): N(2)...F(2) 2.95, N(2)-H(2A)...F(2) 162; N(3)...F(2) 2.99, N(3)-H(3A)...F(2) 162; N(5)...F(6) 2.97, N(5)-H(5A)...F(6) 155; N(6)...F(6) 2.96, N(6)-H(6B)...F(6) 146; N(8)...F(8) 2.98, N(8)-H(8A)...F(8) 153; N(9)...F(8) 3.27, N(9)-H(9A)...F(8) 148; N(11)...F(4) 3.07, N(11)-H(11A)...F(4) 160; N(12)...F(4) 3.32, N(12)-H(12A)...F(4) 147. Pt...B distances (Å) : Pt(1)...B(1) 4.37; Pt(1)...B(2) 4.36. 92
- Figure 4.12 ¹H NMR spectra from the titration of **3** with Cl⁻ at 0 and 2 equivalents. Arrows depict the change in chemical shift observed for each respective proton found in the binding site. 95
- Figure 4.13 Spectra from the titration of **3** with H₂PO₄⁻ at several different points. Uncomplexed peaks become broad while new broad complexed peaks grow in. At 1:1 ratio the uncomplexed peaks disappear and the complexed peaks sharpen. Red letters represent uncomplexed receptor while blue represents complexed. 96
- Figure 4.14 Spectra from the titration of **3** with SO₄²⁻ at several different points. Sharp complexed peaks grow in as anion is added. At 1:1 ratio the uncomplexed peaks disappear with only the complexed peaks remaining. Red letters represent uncomplexed receptor while blue represents complexed. 97
- Figure 4.15 Side view of [Pt(8-*n*butylurea*iso*quinoline)₄][Cl]₂ in the 1,2-alternate conformation showing Cl⁻ pulled into the hydrogen bonding pockets, off-set from direct alignment with the platinum(II). 98
- Figure 4.16 X-ray crystal structure of [Pt(8-*n*butylurea*iso*quinoline)₄][Cl]₂ in the 1,2-alternate conformation with a total of 12 hydrogen bonds with the Cl⁻ anions. 99
- Figure 4.17 X-ray crystal structure of [Pt(8-*n*butylurea*iso*quinoline)₄][SO₄] in the cone conformation. 101
- Figure 4.18 Front view of [Pt(8-*n*butylurea*iso*quinoline)₄][SO₄] where the green ligand is tilted 29° out of the plane in order hydrogen bond to the same oxygen of the SO₄²⁻ as the red ligand. 102

Figure 4.19	Top view of [Pt(8- <i>n</i> butylurea <i>iso</i> quinoline) ₄][SO ₄] where one oxygen, O(8), from the SO ₄ ²⁻ is directly over top of the platinum(II) metal centre.	104
Figure 5.1	Schematic of the four <i>pseudo</i> -calix[4]arene conformations.	114
Figure 5.2	Model compound 4 based on receptor 1 .	115
Figure 5.3	Schematic diagram of <i>syn</i> and <i>anti</i> conformations.	116
Figure 5.4	Model compound 5 , shown in the <i>syn</i> conformation, based on receptor 1 .	117
Figure 5.5	Model compound 6 , shown in the <i>syn</i> conformation, based on receptor 3 .	117
Figure 5.6	Model compound 7 , shown in the <i>syn</i> conformation, based on receptor 1 .	118
Figure 5.7	<i>cis</i> -[PtCl ₂ (quinoline) ₂] in the <i>syn</i> and <i>anti</i> conformations.	119
Figure 5.8	Model compound <i>cis</i> -[PtCl ₂ (3- <i>n</i> butylamidequinoline) ₂], 7 , where only two conformations are possible, <i>syn</i> and <i>anti</i> .	120
Figure 5.9	Synthesis of 3- <i>n</i> butylamidequinoline by refluxing 3-quinolinic ethyl ester in <i>n</i> butylamine.	120
Figure 5.10	Synthesis of 7 .	121
Figure 5.11	Aromatic region of the ¹ H NMR spectrum of 3- <i>n</i> butylamidequinoline in DMF- <i>d</i> ₇ .	122
Figure 5.12	Partial spectrum of 7 at 0 °C, in DMF- <i>d</i> ₇ , where two sets of peaks representing the <i>syn</i> and <i>anti</i> isomers are seen.	122
Figure 5.13	¹ H NMR spectra of 7 at several temperatures with the proton H _a highlighted.	125
Figure 5.14	Potential energy curve of 7 showing the <i>anti</i> conformation as the most stable and the interconversion barrier of 73 kJ/mol.	126
Figure 5.15	Model compound [Pt(3- <i>n</i> butylnicotinamide) ₂ (<i>t</i> butylbipy)][PF ₆] ₂ , 5 , where only two conformations are possible, <i>syn</i> and <i>anti</i> .	128
Figure 5.16	Synthesis of 5 .	129

Figure 5.17	Aromatic region of the ^1H NMR spectrum of 5 at 0 °C in MeCN- d_3 . Two sets of peaks representing the <i>syn</i> and <i>anti</i> conformations are seen.	130
Figure 5.18	^1H NMR spectra of 5 at several temperatures with the proton H_a highlighted.	131
Figure 5.19	The ESI-TOF mass spectra showing the calculated (top) and raw (bottom) isotopic profile of the $[\mathbf{5}\text{-PF}_6]^+$ species.	132
Figure 5.20	The ESI-TOF mass spectrum showing the raw isotopic profile of the $[\mathbf{5}]^{2+}$ species.	132
Figure 5.21	Potential energy curve of 5 showing the <i>anti</i> conformation as the most stable and the interconversion barrier as 6 kJ/mol.	133
Figure 5.22	Model compound $[\text{Pt}(8\text{-}n\text{butylureaisoquinoline})_2(\textit{t}\text{butylbipy})][\text{BF}_4]_2$, 6 , where only two conformations are possible, <i>syn</i> and <i>anti</i> .	135
Figure 5.23	Synthesis of the complex 6 .	135
Figure 5.24	Aromatic region of the ^1H NMR spectrum of 6 at -5 °C in MeCN- d_3 . Two sets of peaks representing the <i>syn</i> and <i>anti</i> conformations are seen for several protons.	136
Figure 5.25	^1H NMR spectra of 6 at several temperatures with the proton H_a highlighted.	138
Figure 5.26	X-ray crystal structure of 6 showing the front view with the <i>t</i> butyl groups omitted for clarity. N-H...F distances (Å) and angles (°): N(2)...F(6) 2.92, N(2)-H(2B)...F(6) 160; N(3)...F(6) 3.17, N(3)-H(3B)...F(6) 147; N(3)...F(7) 3.01, N(3)-H(3B)...F(7) 157; N(5)...F(3) 3.13, N(5)-H(5B)...F(3) 162; N(6)...F(3) 3.29, N(6)-H(6B)...F(3) 153; N(6)...F(1) 3.29, N(6)-H(6B)...F(1) 152. Pt...F distances (Å) and angles (°): Pt(1)...F(6) 3.85, Pt(1)...F(6)-B(2) 85; Pt(1)...F(3) 4.02, Pt(1)...F(3)-B(1) 109.	140
Figure 5.27	The ESI-TOF mass spectra showing the calculated (top) and raw (bottom) isotopic profile of the $[\mathbf{6}\text{-BF}_4]^+$ species.	141
Figure 5.28	The ESI-TOF mass spectrum showing the raw data isotopic profile of the $[\mathbf{6}]^{2+}$ species.	141

Figure 5.29	Potential energy curve of 6 showing the <i>anti</i> conformation as the most stable and the interconversion barrier as 2 kJ/mol.	142
Figure 5.30	Model compound [Pt(3- <i>n</i> butylamidequinoline) ₄][PF ₆] ₂ , 4 , in the 1,2-alternate conformation.	144
Figure 5.31	Synthesis of 4 .	144
Figure 5.32	Partial ¹ H NMR spectrum of 4 at -40 °C in DMF- <i>d</i> ₇ . Several sets of peaks representing the different <i>pseudo-calix[4]arene</i> conformations are seen.	145
Figure 5.33	<i>Pseudo-calix[4]arene</i> conformations assumed by 4 with the number of sets of peaks possible in the ¹ H NMR spectrum.	146
Figure 5.34	Relative stabilities of the isomers compared to the 1,3-alternate conformation.	148
Figure 6.1	Host-guest interaction where the host acts as a sensor and undergoes an optical change when interacting with the guest.	162
Figure 6.2	Tris(2,2'-bipyridine)ruthenium(II) based anion sensor where a change in fluorescence-emission occurs upon binding anions.	163
Figure 6.3	Mass spectrum obtained from a mixture of 3 and CF ₃ SO ₃ ⁻ , I ⁻ , H ₂ PO ₄ ⁻ , Br ⁻ , NO ₃ ⁻ and Cl ⁻ .	166
Figure 6.4	The relative binding ratio of the anions with 3 after correction for the ESI response factor.	167
Figure 6.5	Fluorescence-emission spectrum of 3 in MeCN when excited at 270 nm. The peak maxima are 410 nm and 452 nm.	168
Figure 6.6	Fluorescence-emission spectra of 3 with several anions at 10 equivalents.	169
Figure 6.7	Change in intensity observed after the addition of 10 equivalents of anion.	170
Figure 6.8	Spectra showing the bathochromic shift observed upon addition of 10 equivalents of SO ₄ ²⁻ .	171
Figure 7.1	Structural similarity between calix[4]arene and our receptor framework.	177

Figure 7.2	First generation receptor [Pt(3- <i>n</i> butylnicotinamide) ₄][PF ₆] ₂ , 1 , arbitrarily shown in the 1,2-alternate conformation.	178
Figure 7.3	Second generation receptor [Pt(3,5- <i>di-n</i> butylamidepyridine) ₂ (<i>t</i> butylbipy)][PF ₆] ₂ , 2 .	179
Figure 7.4	Third generation receptor [Pt(8- <i>n</i> butylurea <i>iso</i> quinoline) ₄][BF ₄] ₂ , 3 , arbitrarily in the 1,2-alternate conformation.	180
Figure 7.5	Model complexes [Pt(3- <i>n</i> butylamidoquinoline) ₄][PF ₆] ₂ , 4 , arbitrarily in the 1,2-alternate conformation and <i>cis</i> -[PtCl ₂ (3- <i>n</i> butylamidoquinoline) ₂], 7 , in the <i>syn</i> conformation.	181
Figure 7.6	Model complexes [Pt(3- <i>n</i> butylnicotinamide) ₂ (<i>t</i> butylbipy)][PF ₆] ₂ , 5 , and [Pt(8- <i>n</i> butylurea <i>iso</i> quinoline) ₂ (<i>t</i> butylbipy)][BF ₄] ₂ , 6 , arbitrarily in the <i>syn</i> conformation.	182

List of Tables

Table 2.1	Comparison of ^1H chemical shifts of the ligand before and after coordination to Pt(II).	29
Table 2.2	Association constants, K_a (M^{-1}), obtained for 1 with various oxo-anions, at 30 °C (error < 10 %).	35
Table 2.3	Amount of anion added for a typical ^1H NMR titration.	53
Table 2.4	Volume of receptor and anion required for each NMR sample when performing a Job Plot.	56
Table 3.1	Comparison of ^1H chemical shifts of the ligand before and after coordination to Pt(II).	64
Table 3.2	Association constants, K_a (M^{-1}), obtained for 2 with various oxo-anions, at 30 °C (error < 10 %).	66
Table 4.1	Comparison of ^1H chemical shifts of the ligand before and after coordination to Pt(II).	90
Table 4.2	Association constants, K_a (M^{-1}), obtained for 3 with various anions, at 30 °C (error < 10 %).	94
Table 4.3	Observed Hydrogen bond distances (Å) and angles (°) for $[\text{Pt}(8\text{-}n\text{butylurea}i\text{soquinoline})_4][\text{Cl}]_2$.	100
Table 4.4	Observed Hydrogen bond distances (Å) and angles (°) for $[\text{Pt}(8\text{-}n\text{butylurea}i\text{soquinoline})_4][\text{SO}_4]$.	103
Table 5.1	Comparison of ^1H chemical shifts of the ligand before and after coordination to Pt(II).	123
Table 6.1	An example of the aliquots of anion added during a titration.	175

List of Abbreviations

a, b, c	unit cell dimensions (in Å)
α, β, γ	unit angles (in °)
Å	Angstrom
bipy	2,2'-bipyridine
b	broad
<i>t</i> butylbipy	4,4'- <i>t</i> butyl-2,2'-bipyridine
°	degrees
°C	degrees Celsius
δ	chemical shift
CH ₂ Cl ₂	methylene chloride
CHCl ₃	chloroform
d	doublet
dd	doublet of doublets
DMF	<i>N-N'</i> -dimethylformamide
DMSO	dimethyl sulfoxide
E	energy
ESI-TOF	electrospray ionization time of flight
Et ₂ O	diethyl ether
EtOH	ethanol
g	grams
h	hour(s)
Hz	hertz

$i\text{Pr}_2\text{O}$	<i>di</i> -isopropyl ether
ITC	isothermal titration calorimetry
J	joules
K	degrees kelvin
kJ	kilo Joules
μ	absorption coefficient
M	molarity
M	multiplet
MLCT	metal-to-ligand charge-transfer
MeCN	acetonitrile
MeOH	methanol
MHz	megahertz
min	minutes
mL	milliliters
mm^{-1}	reciprocal millimeters
mmol	millimole
mol	mole
nm	nanometer
MW	molecular weight
MeNO ₂	nitromethane
NMR	nuclear magnetic resonance
ppm	parts per million
PDB	protein data bank
ρ	density

R	agreement factor
wR	weighted agreement factor
s	singlet
<i>t</i>	tertiary
tba	tetrabutylammonium
t	triplet
T	temperature
UV-VIS	Ultraviolet/visible spectroscopy
X-ray	X-ray diffraction
V	Volume
Z	number of formula units per unit cell

Chapter 1

Introduction

1.1 Supramolecular Chemistry of Anions

In supramolecular chemistry, non-covalent intermolecular interactions between two or more molecules in a unique structural arrangement is known as host-guest chemistry. Typically, the host is a larger molecule with a pocket or cavity possessing convergent binding sites for selectivity of a specific guest. The guest molecule possesses divergent binding sites and can vary in size from a single atom to a complex biological assembly (Figure 1.1).¹

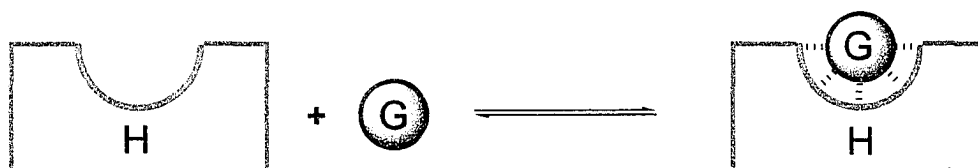


Figure 1.1 The complementary shape and size of the host and guest as they interact, non-covalently.

1.1.1 Anion Recognition

Anions have a ubiquitous role in the world; they have biological, chemical, industrial and environmental implications. Some examples include: i) over 70% of enzyme substrates in the human body contain anions, e.g., adenosine triphosphate (ATP) and deoxyribonucleic acid (DNA), ii) chloride anions make up a large fraction of extracellular ions and the transport of chloride ions across the cell membrane is an extremely important process that is thought to lead to cystic fibrosis when the channel is

not functioning correctly, iii) from an industrial standpoint by-products such as TcO_4^- are derived from the manufacturing of nuclear fuel reprocessing and iv) our lakes and ponds are at risk due to the runoff of fertilizers from our crops where the nitrates and phosphates cause eutrophication.²

The first synthetic anion receptor was reported in 1968 by Park and Simmons³, Figure 1.2. Earlier the same year Pedersen⁴ reported the first synthetic cation receptor and it was not long after that the literature was filled with novel cation receptors. However, host-guest chemistry involving anion binding did not come into prominence until the late 1980s. The delay in the development of synthetic anion receptors was likely due to the innate properties of anions. As shall be seen, designing receptors for these negatively charged guests can be a challenging task.

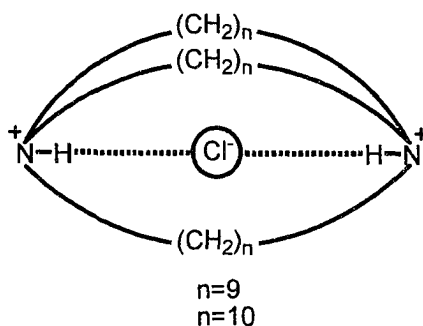


Figure 1.2 First synthetic anion receptor, reported in 1968 by Park and Simmons.

Anion Characteristics

The sizes of anions are large compared to their isoelectronic cation counterparts. Therefore, the charge density of anions is more diffuse which lessens their ability to interact electrostatically. The ‘in solution’ existence of an anion in its charged form is often pH dependent, e.g. H_2PO_4^- can be H_3PO_4 ($\text{pK}_b = 11.8$), and consequently the

receptor must function at the appropriate pH. The design of the receptor must also be suitable for a specific geometry since anions can vary in shape from spherical to octahedral, as shown in Figure 1.3. Therefore, the synthetic receptor should provide a binding site that complements the size and shape of the larger ion in order to overcome the higher solvation energies.²

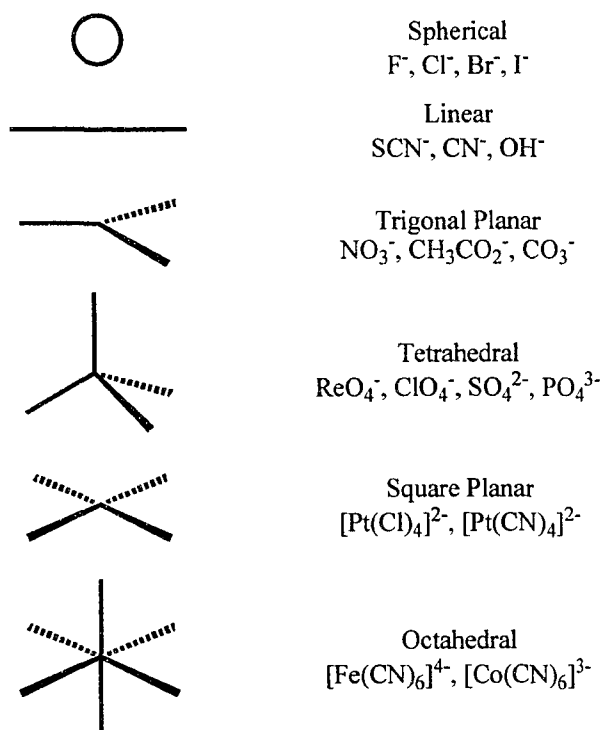


Figure 1.3 Geometries of various anions.

Types of Interactions

Several types of interactions are available for the coordination of anions into receptor binding sites. These interactions can be incorporated through either the functional groups or the framework of the receptor. The broad categories of interactions include hydrogen bonding, electrostatics, metal ion coordination and hydrophobicity, as shown in Figure 1.4. The hydrogen bond interactions occur between a relatively acidic

hydrogen atom, due to its coordination to an electronegative atom (oxygen or nitrogen), and an electron rich atom, ion or molecule. This interaction involves directionality with an X-H...A⁻ angle of 150 ° - 160 ° being typical.

Electrostatic interactions are a non-directional mutual attraction between oppositely charge species (ion-ion, ion-dipole and dipole-dipole). For example, metal ion coordination involves an electron deficient metal centre coordinating to an anion through orbital overlap and the hydrophobic effect is association of non-polar molecules in aqueous solution.¹

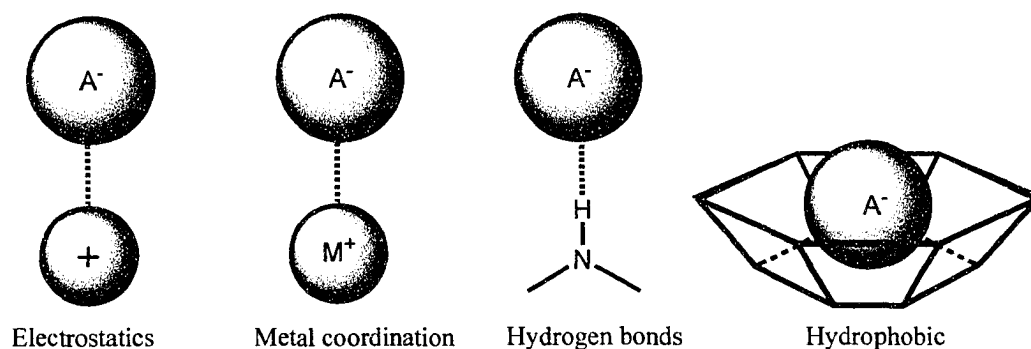
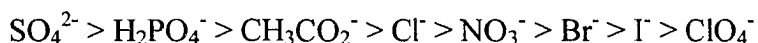


Figure 1.4 Types of interactions available for receptor:anion binding.

These interactions can be incorporated into receptors through functional groups or the framework of the system. Functional groups provide, for the most part, the hydrogen bonding interactions, while the framework usually provides the metal coordination and hydrophobic effects. Electrostatic interactions can be observed through either the functional groups or the framework.

One measure of anion coordination ability is the Hofmeister series which closely parallels pK_b . Formally, the Hofmeister series is derived from the ability of an ion to cause a mixture of hen egg proteins to precipitate from an aqueous solution. This is due to the stabilization of the protein.⁵ The series for anions is as follows:



Therefore, for a receptor to show selectivity it should deviate from this series.

Functional Groups

Anions are electron-rich and act as a hydrogen bond acceptors attracting molecules (hosts) with electron-deficient hydrogen atoms. Functional groups such as amides, sulphonamides, ureas, thioureas and pyrroles possess electron-deficient hydrogen atoms and are therefore capable of acting as hydrogen bond donors.⁶ These groups are neutral with varying acidities and number of hydrogen bond donor sites (Figure 1.5). The acidity of sulphonamide is slightly higher than amide and both contain a single hydrogen bond donor site. The urea and thiourea functional groups contain two protons available for hydrogen bonding. The N-H proton found on pyrroles can also interact with anions.

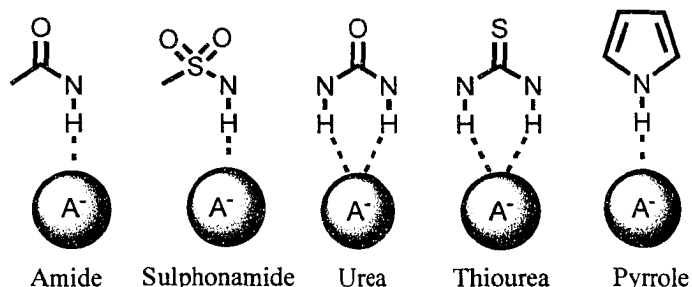


Figure 1.5 Functional groups providing hydrogen bonding interactions.

Functional groups that offer both hydrogen bond donors and electrostatic interactions include ammonium, guanidinium, amidinium and thiouronium (Figure 1.6).⁶ The groups all have positively charged quaternary nitrogens. While guanidinium, amidinium and thiouronium possess two hydrogen bond donor groups, ammonium only has a single site.

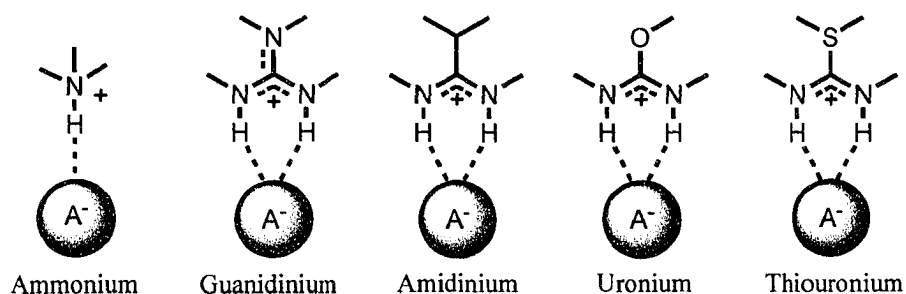


Figure 1.6 Functional groups providing both hydrogen bonding and electrostatic interactions.

Frameworks

The framework is a scaffold used to build a receptor with a binding site that is preorganized and complements the shape and size of the guest. The preorganization of the host should maintain the binding sites in an appropriate spatial arrangement for the interactions to converge on the incoming guest. These frameworks can either be organic or inorganic however, most of the literature examples are based on purely organic backbones. The following are several examples of different frameworks, both organic and inorganic. All methods for the determination of association constants discussed are by ^1H Nuclear Magnetic Resonance (NMR) titrations unless otherwise stated.

Organic Frameworks

Organic frameworks can be as simple as a single, rigid aromatic ring used to append functional groups. Crabtree^{7,8} has used a very simple example where a *bis*-amide or sulphonamide substituted phenyl or pyridine ring (Figure 1.7) can bind anions in a 1:1 stoichiometry. Both amide N-H groups rotate to point into the cavity forming a cleft for the anion to bind. Receptor **1.2** binds Cl^- with the highest association constant of $6.1 \times 10^4 \text{ M}^{-1}$ in a $\text{CH}_2\text{Cl}_2-d_2$ solution.

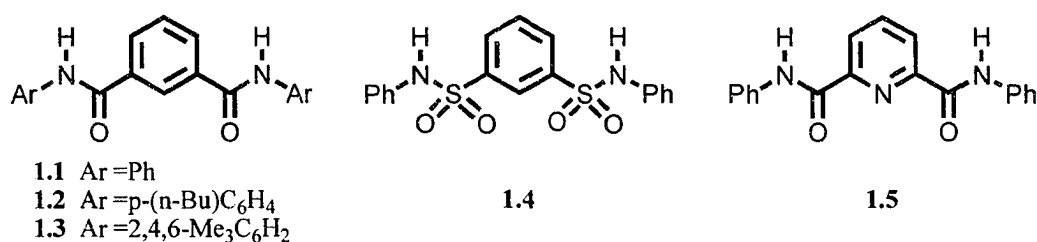


Figure 1.7 Simple aromatic ring framework, by Crabtree.

A slight modification of the *di*-substituted aromatic ring is a 1,3,5-*trisubstituted* benzene ring used by Anslyn⁹⁻¹⁴, as shown in Figure 1.8. The bicyclic receptor, **1.6**, possesses 3-fold symmetry where the placement of the six hydrogen bonding amides provides the correct placement for the interaction with the anion's π system. Initial studies showed good binding with CH₃CO₂⁻ (770 M⁻¹) and the enolate, **1.8**, (3060 M⁻¹) which have the ideal planar geometry for interaction of the receptor with their π -electron system. The guanidinium receptor, **1.7**, was designed to complement the geometry of citrate which bound very strongly (7×10^3 M⁻¹) in pure water.

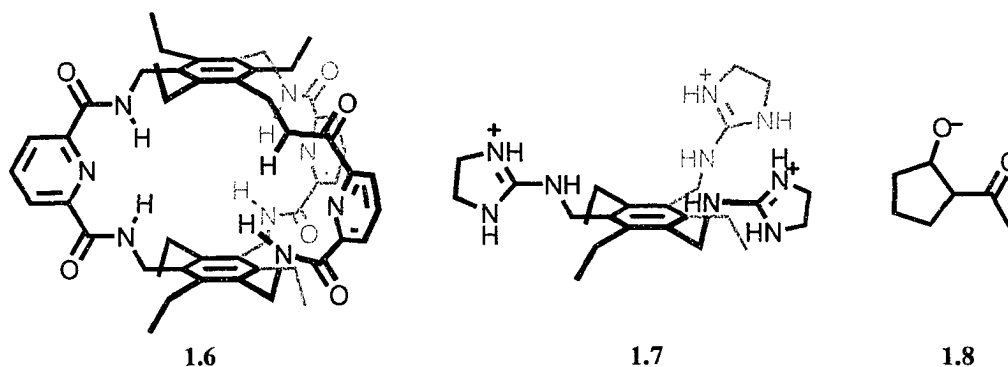


Figure 1.8 A bicyclic (**1.6**) and tripodal (**1.7**) 1,3,5-*trisubstituted* benzene framework, by Anslyn, with an example of a strongly binding enolate (**1.8**).

The use of a steroid-based backbone, cholic acid, allows several functional groups to be appended (Figure 1.9). Davis^{15,16} and co-workers used this motif where initially

only two amides were incorporated into both cyclic, **1.9**, and acyclic, **1.10-1.13**, versions. The macrocyclic version forms a small, rigid cavity with four hydroxyl groups and two amide N-H groups directed towards the cavity. When compared with the acyclic version the preorganized macrocycle proved to be a much better host for halide anions. Acyclic receptors have been synthesized containing carbamates, amides, sulphonamides, ureas and thioureas. The amide receptors show moderate binding to halides whereas the urea receptors show extremely strong binding to Br⁻ and Cl⁻.

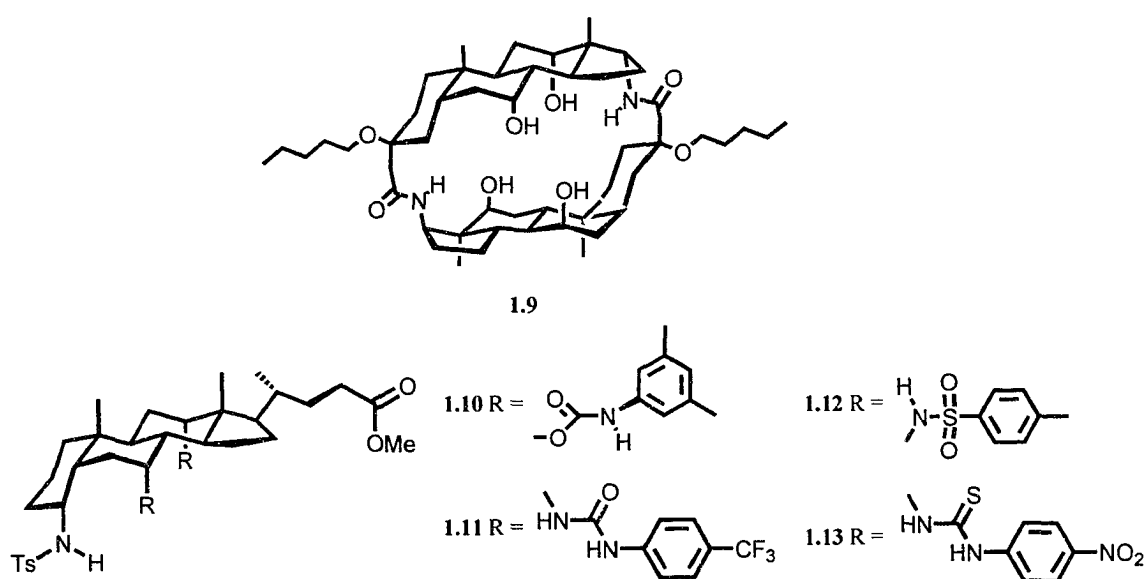


Figure 1.9 Cyclic and acyclic receptors based on a cholic acid framework, by Davis.

Gale¹⁷⁻²¹ and co-workers have used pyrroles as the framework with amide functional groups, see Figure 1.10, in their study of anion recognition. The single pyrrole receptors, **1.14-1.17**, show a semi-cleft arrangement in the solid state in which both amide protons are pointing away from the binding site. Upon addition of anions, the amide groups rotate so the amide N-H groups are now pointing into the binding site forming a cleft. Adding electron-withdrawing groups increased binding of anions ten-fold compared to the electron donating versions. Receptor **1.17** is a colourimetric

receptor in the presence of F^- . That is, the receptor solution changes from colourless to blue in the presence of F^- . The dipyrrole receptors, **1.18-1.22**, form clefts that bind anions in very polar solvent. The receptors have shown to bind $H_2PO_4^-$ in DMSO- d_6 / 25% H_2O with an affinity of $234 M^{-1}$.

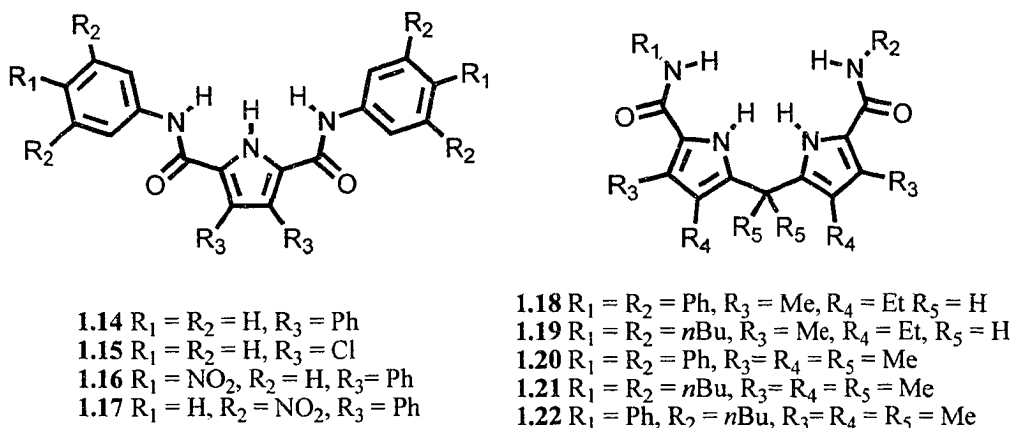


Figure 1.10 Pyrrole based clefts containing single and dipyrrole frameworks, by Gale.

Cyclophanes containing ammoniums, as shown in Figure 1.11, are the frameworks employed by Bowman-James.²²⁻²⁴ The ability of these receptors to bind halides was studied over a wide range of pH values. The tetraprotonated receptor **1.23** is a flexible receptor that has been shown to form a pocket upon binding NO_3^- . The small cavity of receptor **1.24** shows selectivity for F^- or Cl^- , depending on the pH. When the pH value is below 2.5 the receptor preferentially binds Cl^- however, above this pH F^- is bound. Finally, receptor **1.25** possesses an ability to encapsulate F^- over a broad range of pH values.

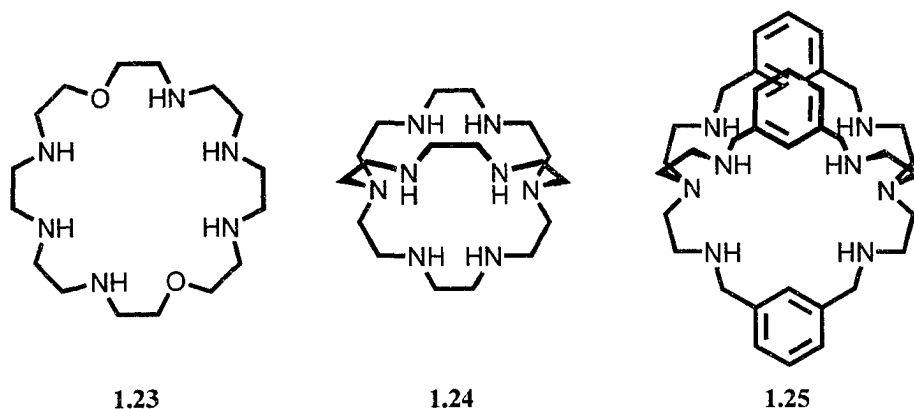


Figure 1.11 Cyclophane framework containing polyammonium functional groups, by Bowman-James.

Peptides are another feasible framework for an anion receptor (Figure 1.12). Peptides consist of many amide functional groups and work by Kubik²⁵⁻³⁰ shows the anion binding ability of this backbone. The single macrocycle, **1.26**, is a hexapeptide which has the ability to complex a variety of anions in a very polar 80% D₂O / MeOH-*d*₄ solution. The solid state structure with I⁻ shows two receptors sandwiching the anion and interacting through six N-H hydrogen bonds. When two of these macrocycles, **1.27-1.30**, are tethered together they act as a molecular oyster upon binding anions.

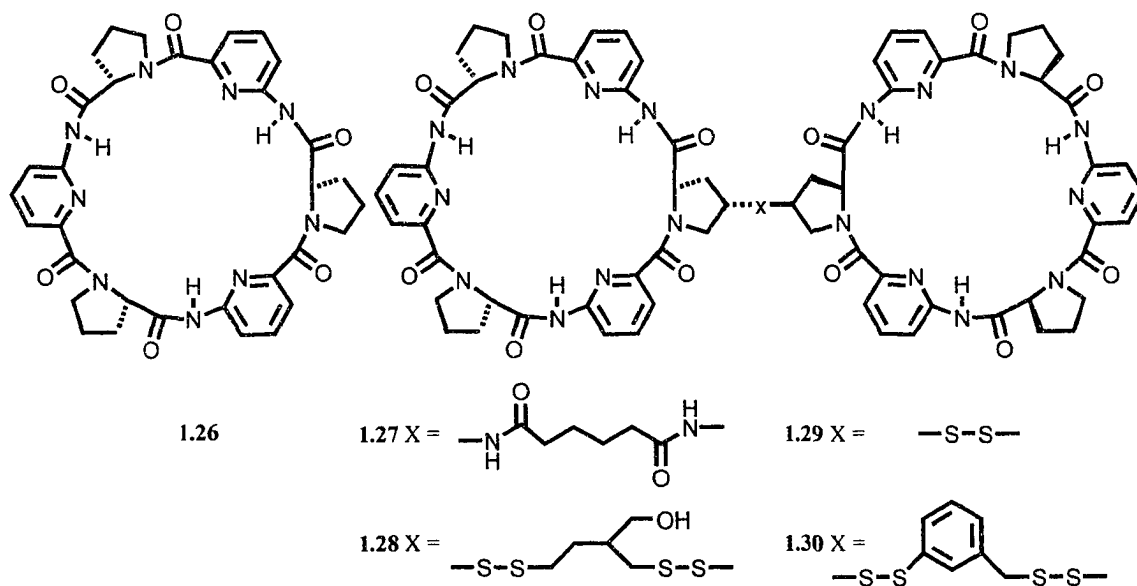


Figure 1.12 Macrocyclic peptides form the framework for the anion receptors by Kubik.

Calixarenes have been used as the framework for many different anion receptors. The flexibility of this framework allows four different conformations to be attained. Ungaro³¹⁻³³ used this motif in several receptors including a calix[4]arene with the upper rim substituted by C-linked peptides, **1.31**. This receptor binds CH_3CO_2^- with an association constant of 33 M^{-1} in $\text{DMSO-}d_6$. The strapped C-linked peptidocalix[4]arenes, **1.32** and **1.33**, locks the receptor in a cone conformation. The binding site formed provides four hydrogen bonds through the N-H units and π - π stacking through the phenyl or pyridine ring. Receptor **1.33** shows less flexibility and higher association constants than **1.32** with binding constants for $\text{C}_6\text{H}_5\text{CO}_2^-$ of $4.0 \times 10^4 \text{ M}^{-1}$ in $\text{acetone-}d_6$.

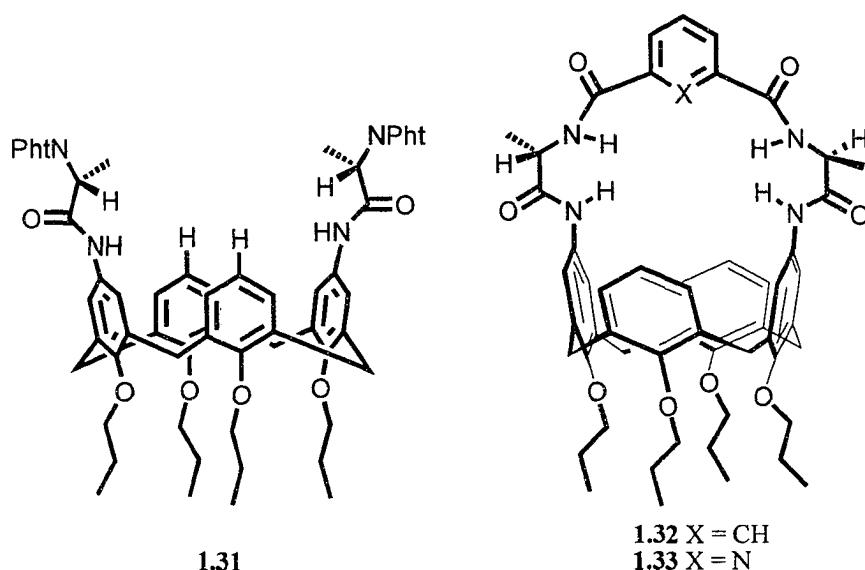


Figure 1.13 Calixarene frameworks are utilized by Ungaro.

A wide variety of calixpyrroles have been used as receptor frameworks by Sessler³⁴⁻³⁶, as shown in Figure 1.14. By using the pyrrole functional group as part of the macrocycle these receptors are able to bind halides. The number of pyrroles incorporated into the macrocycle can vary between four and eight, **1.34** and **1.37**, and the substituents

can vary between electron-donating and electron-withdrawing groups. Electron-withdrawing groups increase the acidity of the pyrroles and therefore increase the overall affinity of the receptor for the anions. Receptor **1.34** binds F^- preferentially with an association of $1.7 \times 10^4 M^{-1}$ in $CH_2Cl_2-d_2$. The calix[5]pyrrole, **1.35**, binds Cl^- preferentially over the calix[8]pyrrole, **1.37**, with a binding of $4.1 \times 10^4 M^{-1}$ in $MeCN-d_3$ 0.5% D_2O . Calixbipyrroles **1.38** and **1.39** have also been studied and the calix[4]bipyrrole, **1.39**, binds Cl^- very strongly with an association constant of $2.9 \times 10^6 M^{-1}$, obtained by isothermal titration calorimetry (ITC).

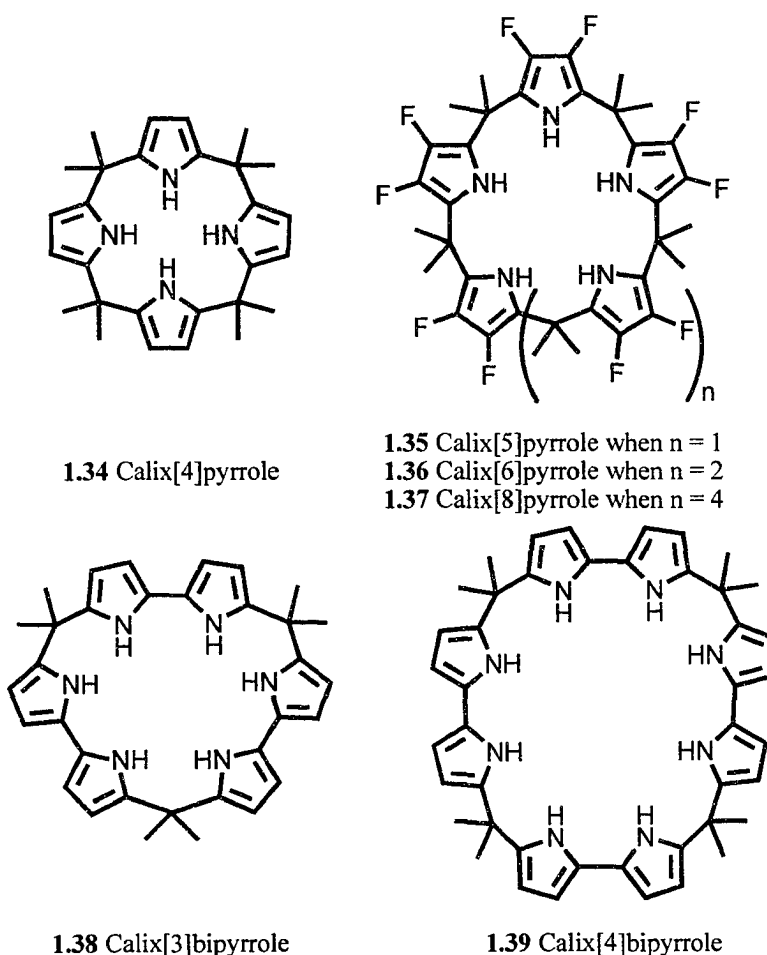


Figure 1.14 Various calixpyrroles used as frameworks to study anion binding, by Sessler.

The final organic frameworks discussed are cyclodextrins³⁷ (CD), as shown in Figure 1.15. These frameworks provide a large hydrophobic core for the interaction with anions. The anions tested were carboxylates possessing a large aromatic surface, **1.42** and **1.43**. These receptors are placed in aqueous solution and the anion interacts with the receptor by inserting the aromatic rings into the hydrophobic core of the receptor while the carboxylates are left exposed to interact with the aqueous solution.

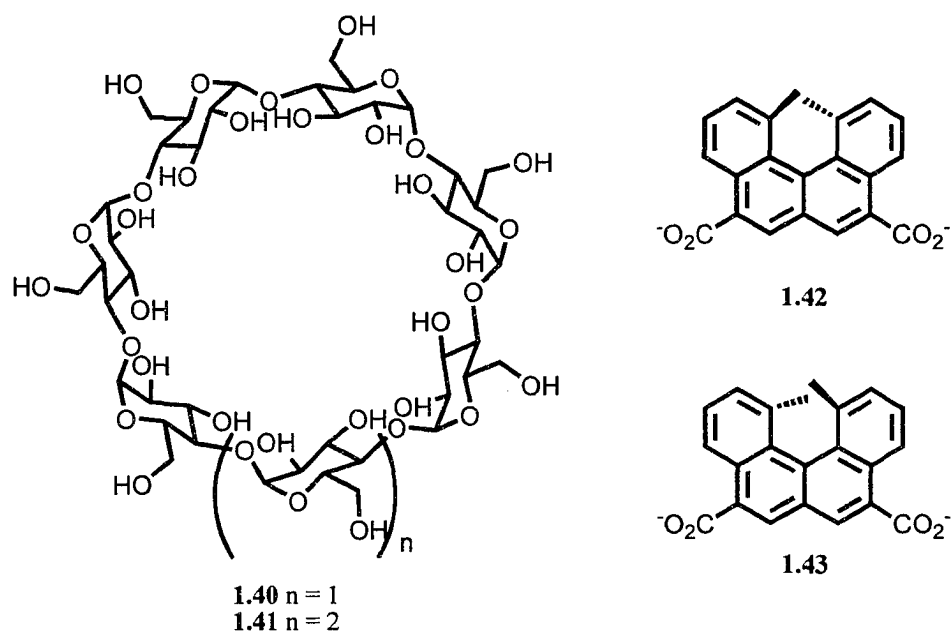


Figure 1.15 Cyclodextrins provide a hydrophobic environment for binding anions which is used by Kano. **1.42** and **1.43** are examples of the anions bound by these receptors.

Inorganic Frameworks

The first of the inorganic frameworks discussed also operates by the hydrophobic effect. The metallated calixarenes were initially studied by Atwood (Figure 1.16).³⁸⁻⁴¹ The electron deficient metal centre reduces the electron density of the calixarene. This in turn produces an excellent hydrophobic, electron deficient, pocket for the electron rich

anions to interact with. These receptors have measured association constants as high as 550 M^{-1} for Cl^- in aqueous solution.

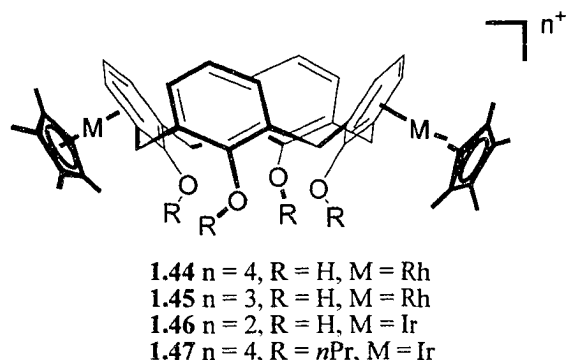


Figure 1.16 Atwood developed metallated calixarenes which also provide a hydrophobic and electron deficient environment for binding anions.

The framework of tris(2,2'-bipyridine)ruthenium(II) has been explored extensively by Beer⁴²⁻⁴⁵ where the ruthenium(II) acts as a scaffold to organize the functional groups (Figure 1.17). These receptors are attractive due to their ability to recognize and sense anions in a variety of manners. These complexes can be tested and characterized by optical and NMR spectroscopies and electrochemistry. Receptors **1.48-1.51** all possessing a 2,2'-bipyridyl ligand, substituted with amido groups at the 5 and 5'-positions, were titrated with both Cl^- and Br^- in $\text{DMSO-}d_6$. The association constants obtained revealed that none of the receptors showed a large affinity for Cl^- (all values $\sim 45 \text{ M}^{-1}$) and receptor **1.48** was the only receptor to complex Br^- (40 M^{-1}). Therefore, differentiating the substituents on the amide group did not aid in the selectivity towards a specific anion in these systems. Cyclic and square wave voltammetry along with fluorescence emission have both demonstrated chloride recognition through considerable cathodic perturbation and quenching of the metal-to-ligand charge-transfer (MLCT) emission band.

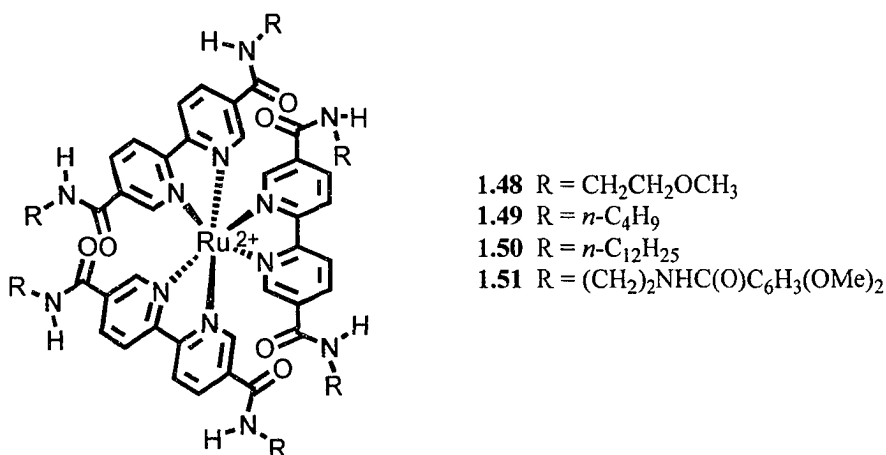


Figure 1.17 Beer utilizes Ru(II)(bipy)₃ complexes as a framework to append functionalized ligands.

Anions can also be recognized in receptors containing metal ions with vacant coordination sites. A *bis*-tren cage framework was used by Fabbrizzi⁴⁶ where the receptor contains two metal ions. The example in Figure 1.18 shows receptor **1.52** containing two Zn²⁺ metal ions which fluoresces when no anions are present but is quenched upon addition of N₃⁻. The anion is situated in the centre of the cage in between the two metal ions. The electron transfer from the electron rich anion to the anthracene is thought to be the cause of the quenching.

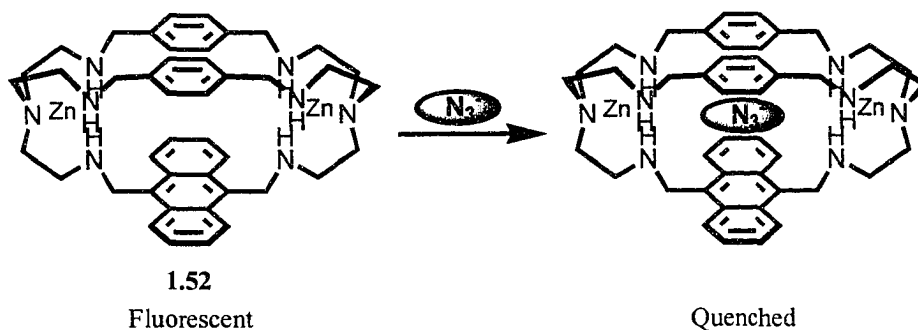


Figure 1.18 A cage structure (**1.52**) by Fabbrizzi contains coordinating metal ion to bind anions.

The final inorganic frameworks discussed are porphyrins which can be substituted with many different functional groups as shown in Figure 1.19. Beer^{47,48} also synthesized

amide functionalized zinc(II) porphyrin receptors that show affinity for Cl^- , Br^- , NO_3^- and HSO_4^- while their metal-free analogues did not show any significant interactions. Metal-free cobaltocenium analogues did show association to Cl^- , Br^- and NO_3^- in MeCN-d_3 . Therefore a combination of both electrostatic interactions with the metallocene or metallated porphyrin and the amide hydrogen bonds contributed to the binding of the anions. The atropisomer receptors **1.53-1.55** also demonstrate some selectivity. Receptor **1.53** showed selectivity for NO_3^- over Cl^- and HSO_4^- while the halides were preferred by the other isomers.

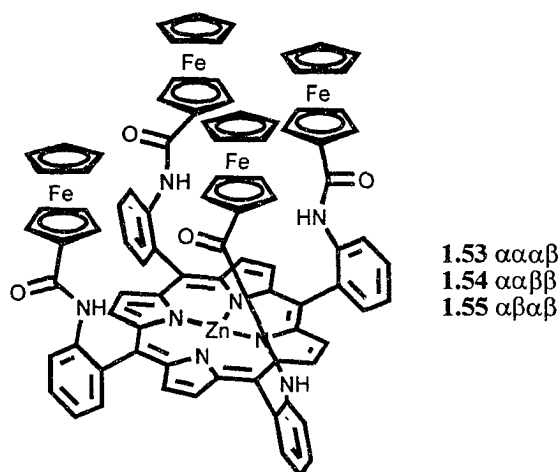


Figure 1.19 Metallated porphyrins used by Beer provide a large framework to append functional groups.

Metal Functionality

The functionality of a metal ion in the framework of anion receptors can be divided into four different types, as shown in Figure 1.20. Based on the frameworks discussed above the metal ions can act as i) coordination sites / electrostatic interactions ii) reporter groups iii) a scaffold to arrange functional groups and iv) electron-withdrawing groups.⁴⁹

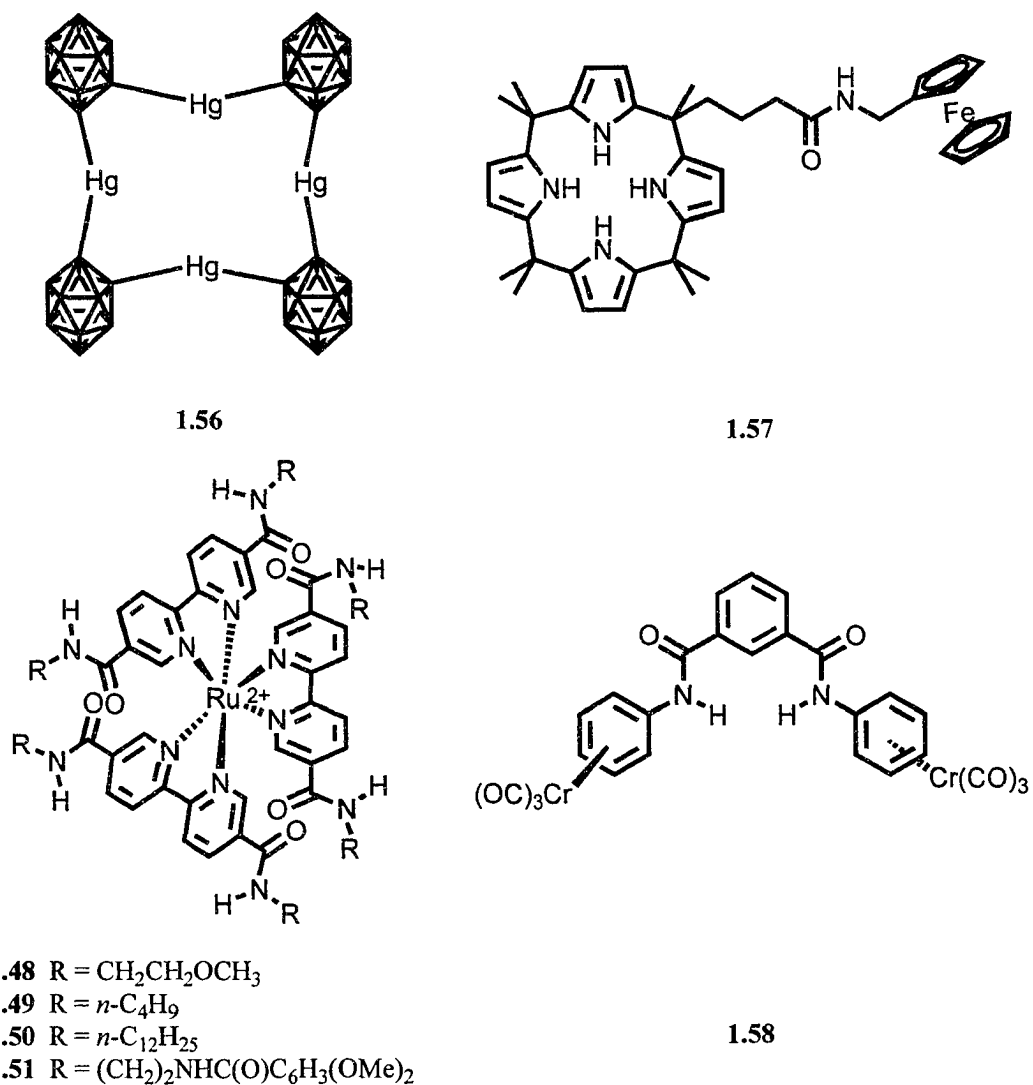


Figure 1.20 i) Mercuracarborane receptor **1.56** contains four coordinating metal ions.^{50,51} ii) Calix[4]pyrrole, **1.57**, with an appended ferrocene group used as a reporter group for anion binding.⁵² iii) Ruthenium(II) used as a scaffold for three *bis*-amide substituted bipyridine ligands, **1.48-1.51**.⁴²⁻⁴⁵ iv) Cr(CO)₃ coordinated to the receptor **1.58**, as electron withdrawing substituents to increase the acidity of the amide proton.⁵³

To date there are no examples of the metal ion acting as an electron-deficient site for electrostatic interactions as well as possessing structure functionality beyond a stationary scaffold. There is, however, an example of this type of receptor, reported Gokel^{54,55} and Atwood, designed for small neutral molecules based on the rotational ability of the

cyclopentadienyl (C_p) groups in ferrocene. Two ferrocene units are linked together through an aromatic bridge between one C_p ring on each ferrocene unit. The lower two C_p rings are mono substituted with carboxylates. The solid state structure shows the two carboxylates are pointing in opposite directions, however, in solution they are able to come together and bind small molecules. This is due to the ease of rotation the rings have about the iron(II) centre (Figure 1.21).

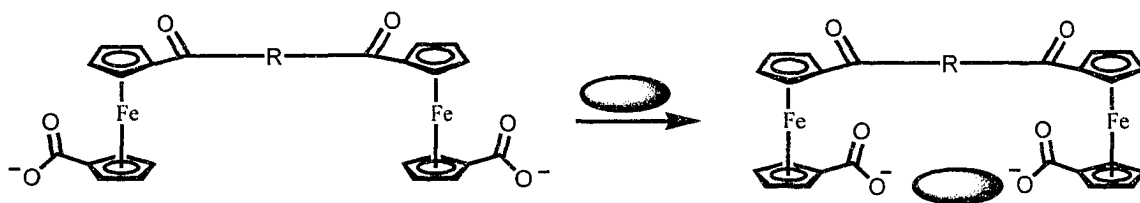


Figure 1.21 Neutral small molecule receptor, by Gokel and Atwood, where the iron(II) metal centres allow for structural functionality and conformational change upon binding the guest.

1.1.2 Scope of the Project

As outlined, a high proportion of the anion receptors reported thus far are ‘built’ on complicated organic scaffolds such as the cyclodextrins, cholic acid or calixarenes. The preparation of these types of receptors can often be synthetically challenging, a fact that prompted us to look for alternative means of arranging hydrogen bond donating groups in space. It occurred to us that some easy to prepare metal-ligand complexes could be exploited as simple pieces of *inorganic* molecular scaffolding. We chose to study square planar platinum(II) complexes due to their relative inertness towards ligand substitution and pyridine or *isoquinoline* ligands due to their ease of synthesis. Brammer⁵⁶ and co-workers have studied the application of related PtL_4^{2+} ($L =$ nicotinamide) complexes in the construction of crystal-engineered networks while Steed⁵⁷

and co-workers have investigated the role anions can play in stabilizing discrete complexes using similar organic ligands and kinetically labile templating metal centres.

One of the major goals in our receptor design was conformational flexibility. That is, the receptor should be able to adopt different conformations depending on the type of anion it is binding. The second criterion for the receptor was simplicity of synthesis. The main component facilitating these two requirements will be the platinum(II) metal centre. This single atom is the inorganic scaffold of the receptor and will support the convergent hydrogen bond donor sites as well as provide the electrostatic interactions of the system. The metal centre will have square planar geometry and therefore will coordinate to four nitrogen ligands. The conformational flexibility arises from the coordination of monodentate ligands which can exhibit free rotation of the metal ligand bond. Pyridine and related ligands will be used to due to their ease of synthesis, variety of functionalization and ability to form inert coordinate bonds with platinum(II) (Figure 1.22).

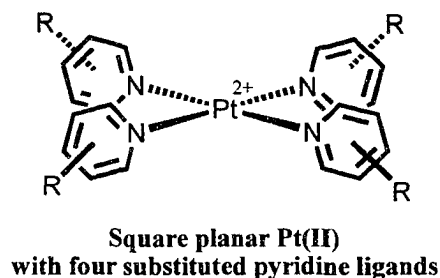


Figure 1.22 The basic structure of our inorganic scaffold.

The platinum(II) metal centre provides the electrostatic interactions and the scaffolding for the receptor. The monodentate pyridine base ligands allow for free rotation around the Pt-N and an inert coordination complex. The final requirement is the hydrogen bonding interactions. These will be provided by amide (Chapter 2 and 3) or

urea (Chapter 4) functional groups. Many anion receptors, including those found in nature, possess amide functional groups. To increase the number of hydrogen bond donors urea groups will also be investigated (Figure 1.23).

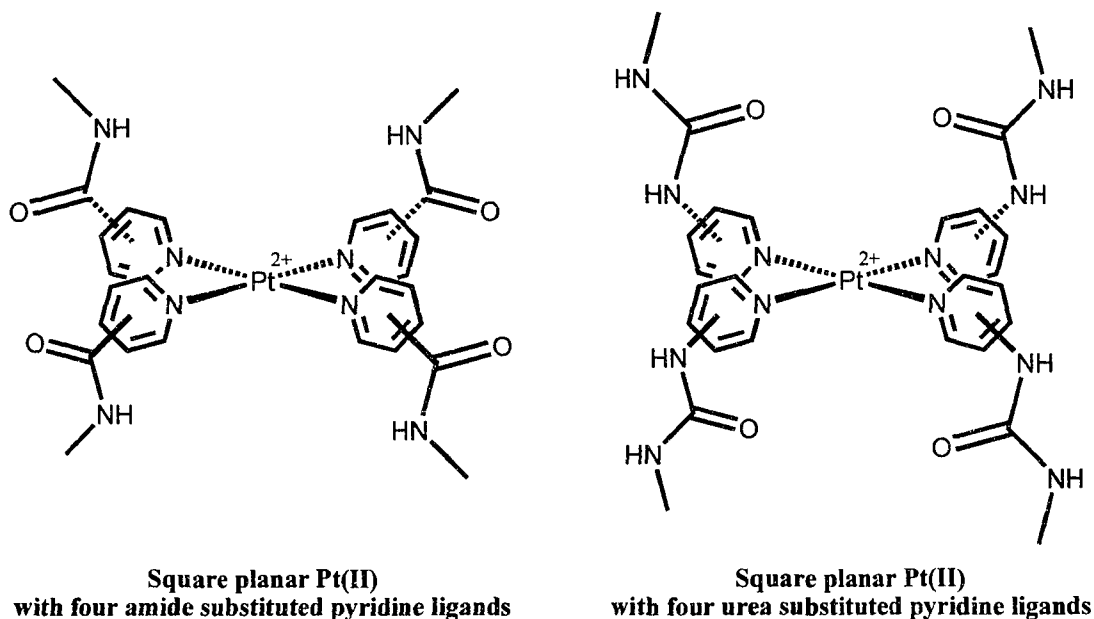


Figure 1.23 The basic structure for our anion receptor.

As a convenient way of viewing the possible conformations of these complexes, we will use calix[4]arenes as an analogy. Calix[4]arenes are known to adopt four different conformations, (i) the cone, (ii) the 1,2-alternate, (iii) the 1,3-alternate and (iv) the partial cone. The *pseudo-calix[4]arene* conformations that our inorganic receptor may adopt occur when (i) all four ligand are oriented in the same direction (cone), (ii) ligands *cis* to one another point in the same direction (1,2-alternate), (iii) ligands *trans* to one another are positioned in the same direction (1,3-alternate) and (iv) when all but one ligand are pointing in the same direction (partial cone) (Figure 1.24). The flexibility of this system should allow the receptor to change conformation depending on the size and shape of the anion with which it is interacting.

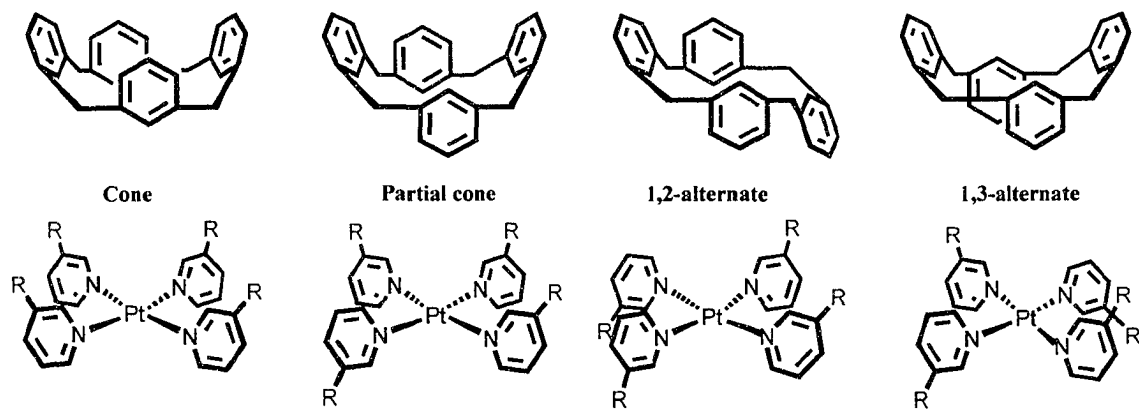


Figure 1.24 Structural similarity between calix[4]arene and our receptor framework when functional groups placed in the 3 position.

Finally, the platinum(II) metal centre provides an electrostatic component for the receptor and since the four pyridine ligands are neutral the complex will have an overall 2+ charge. In order to counterbalance this positive charge, the system must have some anions already present. Hexafluorophosphate (PF_6^-) is a common non-competitive anion and is utilized as the counterion for these receptor systems in order to eliminate, or at least minimize, competition with targeted guest anions.

Chapter 2

Amide Receptor

2.1 Introduction

The selection of amides as the hydrogen bond donors for our first generation anion receptor is related to their biological importance. In biological systems, enzymes can recognize and bind anionic substrates through amide hydrogen bond donors. For example, the enzyme *Threonine synthase* catalyzes the conversion of serine phosphate to threonine and inorganic phosphate. Thus, it must specifically bind the anionic substrate serine phosphate, which is achieved via amide hydrogen bonds from the protein's peptide. A schematic representation of the binding site is shown in Figure 2.1 (taken from PDB: 1UIM).⁵⁸

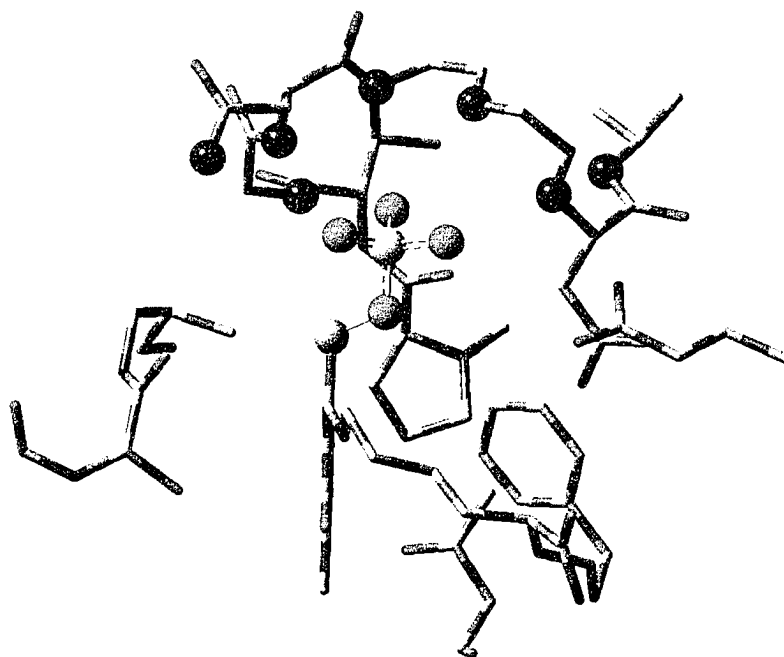


Figure 2.1 Enzyme *Threonine synthase* binding serine phosphate through amide functional groups.

Amide functional groups have also been employed in synthetic anion receptors. Previously, our research group has studied anion binding using calix[4]arenes substituted on the upper rim with amide groups, as shown in Figure 2.2. These receptors are able to adopt a pinched cone conformation which allows the amide groups in the 1,3 positions to be parallel to one another. This type of alignment is optimal for the association of “Y-shaped” carboxylate anions. Therefore, these receptors show preference for the binding of carboxylates and, in particular, benzoate which has an association constant of 5100 M^{-1} when $X = \text{CHCl}_2$ in CH_2Cl_2 .⁵⁹

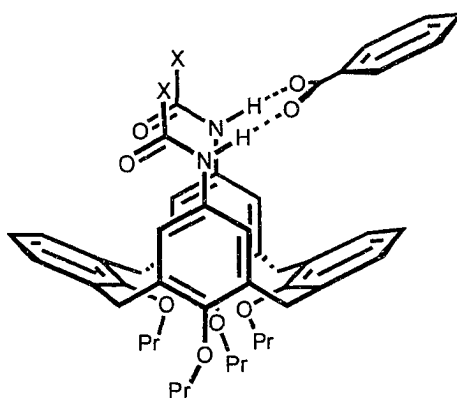


Figure 2.2 1,3-amide substituted calix[4]arene in pinched cone conformation binding benzoate.

Our first generation receptor is comprised of four pyridine-based ligands coordinated to a central platinum(II) metal centre. Each ligand contains an amide functional group. Hence, the binding cavity consists of an electrostatic component as well as four N-H hydrogen bond donors.

It is important to place the hydrogen bond donor sites in the correct position within the cavity in order to optimize their interaction with the guest anion. In particular, the positioning must allow the hydrogen bond donors to converge towards the hydrogen bond acceptor sites on the anion (Figure 2.3).¹ Placement of the amide group in the 3

position on the pyridine ring fulfils this need for convergence by allowing all four N-H groups to point toward one another, into the cavity, parallel to the Pt-N bonds. This should also optimize the electrostatic interaction with the platinum(II) metal centre by placing the binding site directly above the metal centre.

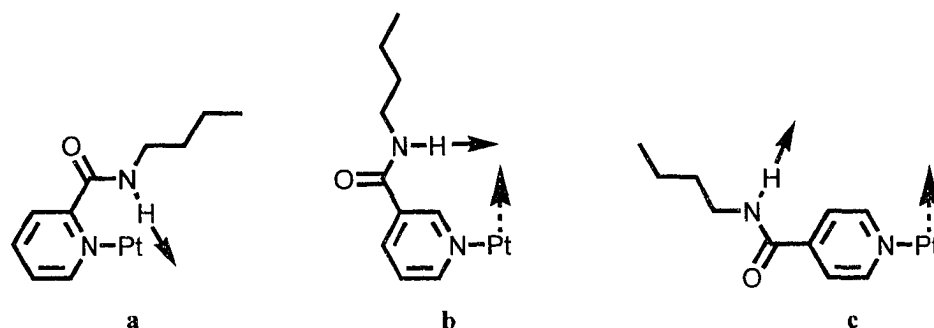


Figure 2.3 Comparison of possible placement of the amide groups for convergence toward the anion a) 2-position b) 3-position and c) 4-position.

The R group chosen for the ligand may seem unimportant but it will have a great influence on the solubility of the receptor, ability for crystal growth and the size of the cavity available for the guest. In order to balance all three of these phenomena the R group was selected to be an *n*butyl chain. The short alkane chain is not bulky and should not interfere with the binding cavity; the four carbon chain should aid with maintaining the solubility in organic solvents and it will not likely interfere in the packing ability of the receptor in the solid state.

The ever present counterion may also potentially interact with the receptor. To minimize competition, PF_6^- was chosen as the counterion. In polar solvents such as MeCN the N-H...F PF_5^- should be minimized and ion pairing with PF_6^- should be insignificant relative to receptor:anion interactions.⁶⁰

Therefore, our first generation anion receptor is $[\text{Pt}(3\text{-}n\text{butylnicotinamide})_4][\text{PF}_6]_2$, **1**, shown in Figure 2.4; the receptor possesses four hydrogen bond donors, an electropositive metal centre for electrostatic interactions and conformational flexibility for interactions with guest anions.

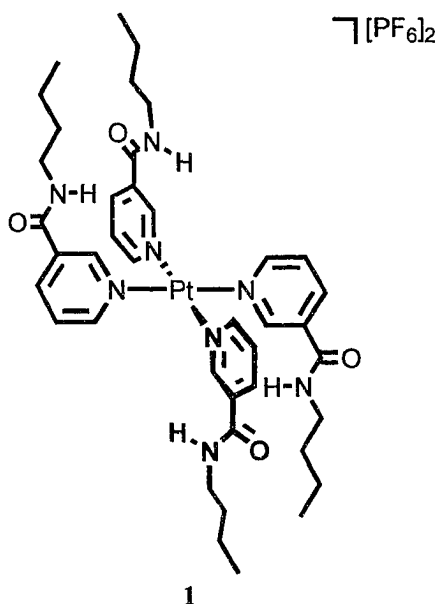


Figure 2.4 First generation receptor $[\text{Pt}(3\text{-}n\text{butylnicotinamide})_4][\text{PF}_6]_2$, **1**, arbitrarily shown in the 1,2-alternate conformation.

2.2 Results and Discussion

2.2.1 Synthesis and Characterization of $[\text{Pt}(3\text{-}n\text{butylnicotinamide})_4][\text{PF}_6]_2$ (**1**)

Synthesis

The ligand for the first generation receptor, $[\text{Pt}(3\text{-}n\text{butylnicotinamide})_4][\text{PF}_6]_2$, was synthesized from nicotinic acid. First, the acid was refluxed in EtOH using $\text{H}_2\text{SO}_{4(\text{conc})}$ as the catalyst to produce the nicotinic ethyl ester *via* an esterification reaction (Figure 2.5).⁶¹

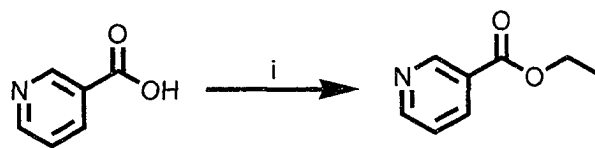


Figure 2.5 Synthesis of nicotinic ethyl ester. i) Reflux for 24 hours in EtOH and $\text{H}_2\text{SO}_{4(\text{conc})}$.

This was followed by the formation of the amide by refluxing the nicotinic ethyl ester in 15 mL of *n*butylamine. The excess *n*butylamine was removed to obtain the desired 3-*n*butylnicotinamide in nearly quantitative yield. (Figure 2.6)

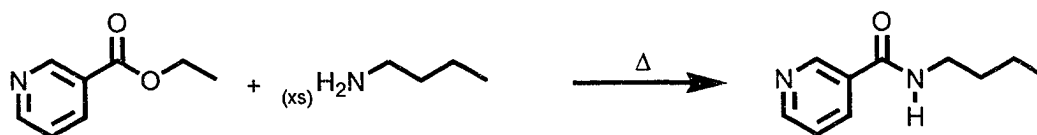


Figure 2.6 Synthesis of 3-*n*butylnicotinamide.

The $[\text{Pt}(3\text{-}n\text{butylnicotinamide})_4][\text{PF}_6]_2$, **1**, was synthesized by reacting $[\text{PtCl}_2(\text{C}_2\text{H}_5\text{CN})_2]$,⁶² 2.2 equivalents of AgPF_6 and 4 equivalents of 3-*n*butylnicotinamide ligand in refluxing MeCN (Figure 2.7). The receptor was obtained in 87 % yield.

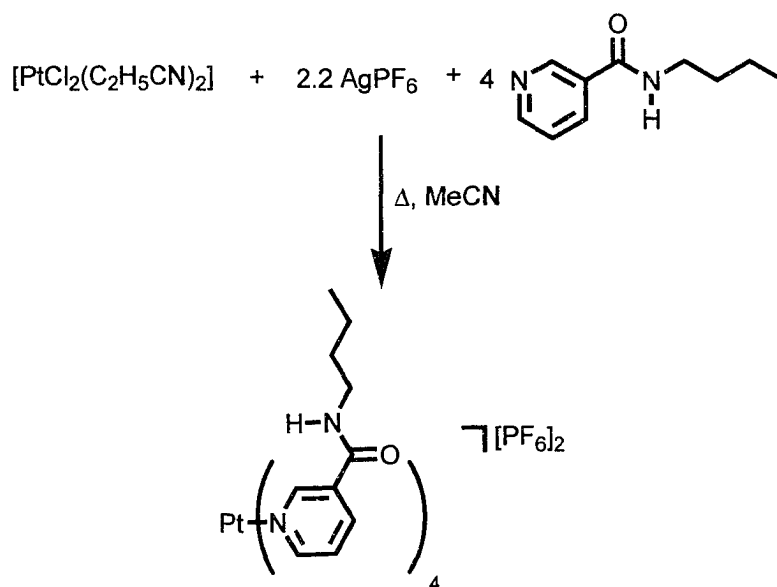


Figure 2.7 Synthesis of **1**.

¹H NMR Spectroscopy

The ¹H NMR spectrum of 3-*n*butylnicotinamide in MeCN-*d*₃ reveals characteristic chemical shifts for all the protons (Figure 2.8). The chemical shifts representing the *n*butyl group protons are found in the region of 0 - 4 ppm. The resonance for H_i appears as a triplet at 0.95 ppm while H_h and H_g have chemical shifts of 1.40 and 1.57 ppm and appear as a sextet and quintet. Due to its proximity to the amide group, the *n*butyl proton with the highest frequency is H_f, with a chemical shift of 3.36 ppm. The aromatic proton H_a is a singlet with a chemical shift of 8.94 ppm due to the proximity of both the aromatic nitrogen of the pyridine and the carbonyl group of the amide. Protons H_b and H_d are both doublets with chemical shifts of 8.67 and 8.08 ppm, respectively. The doublet of doublets at 7.41 ppm is from the resonance of H_c. The amide proton H_e at 7.08 ppm is a broad singlet due to its proximity to the quadrupolar nitrogen.

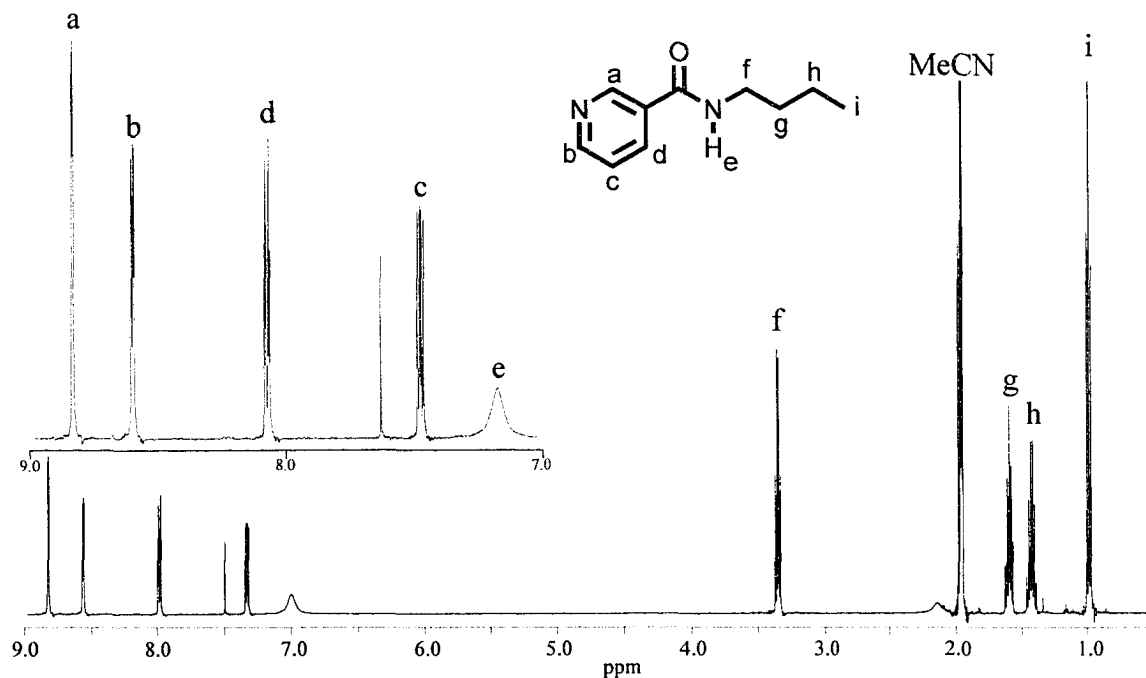


Figure 2.8 ¹H NMR spectrum of 3-*n*butylnicotinamide in MeCN-*d*₃ with inset of aromatic region.

Upon coordination of four of these ligands to the platinum(II) centre, the protons on the pyridine ring undergo changes to their chemical shifts while the *n*butyl portion exhibits negligible changes (Table 2.1). The changes in resonances are due to the coordination of an electropositive metal centre causing the closest protons to become deshielded and shift to a higher frequency. The ^1H NMR spectrum of **1** in $\text{MeCN-}d_3$ (Figure 2.9) shows that protons H_a (9.36 ppm) and H_b (8.94 ppm) experience the largest changes in chemical shift of 0.42 and 0.27 ppm along with H_e (7.36 ppm) which changes by 0.29 ppm. The smallest change in chemical shift is observed for the proton furthest from the electropositive metal center, H_d (8.23 ppm), with 0.15 ppm.

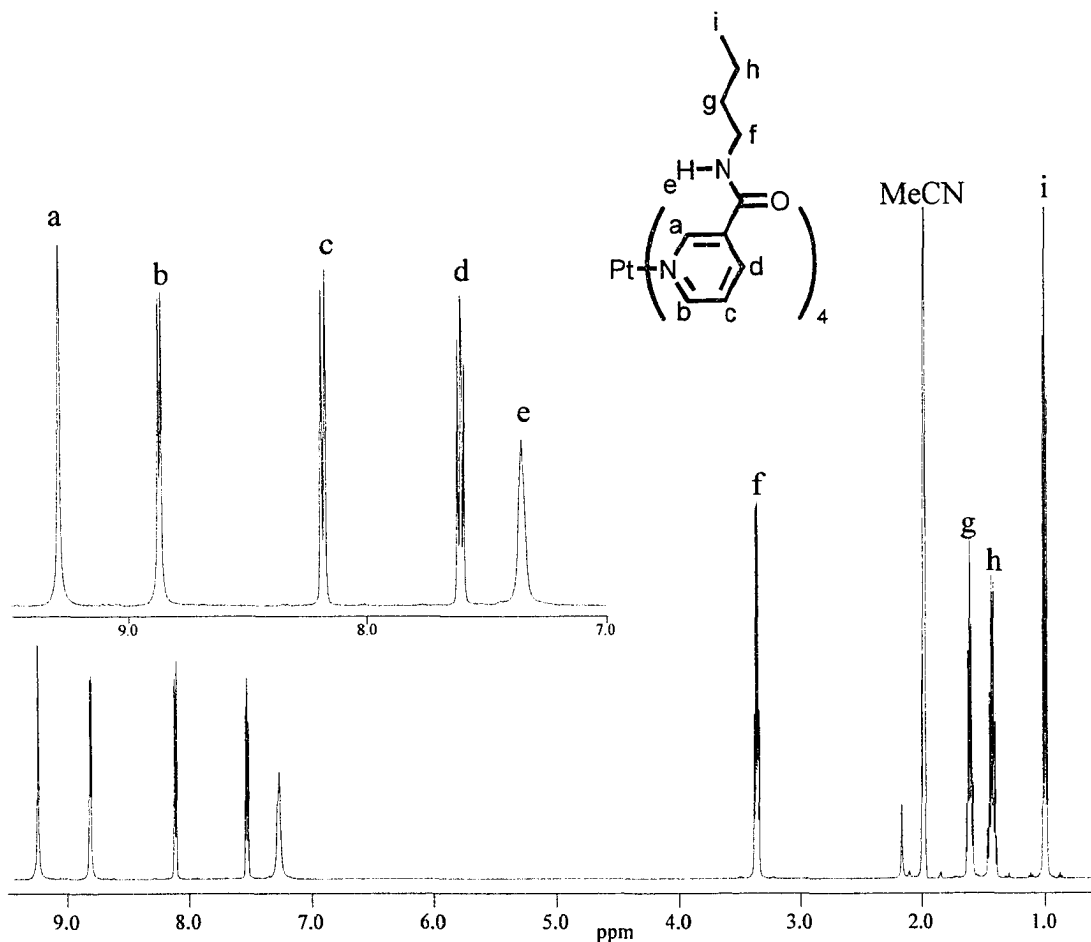


Figure 2.9 ^1H NMR spectrum of **1** in $\text{MeCN-}d_3$ with inset of aromatic region.

Table 2.1 Comparison of ^1H chemical shifts of the ligand before and after coordination to Pt(II).

Proton	Receptor δ (ppm)	Ligand δ (ppm)	$\Delta \delta$
a	9.36	8.94	0.42
b	8.94	8.67	0.27
c	7.62	7.41	0.21
d	8.23	8.08	0.15
e	7.36	7.07	0.29
f	3.36	3.36	0.00
g	1.58	1.57	0.01
h	1.39	1.40	0.01
i	0.94	0.95	0.01

The ^1H NMR spectrum for this complex shows a single set of ligand peaks representing all four conformational isomers. This indicates that the rate of rotation about the Pt-N bond is fast on the NMR timescale, i.e., the rotational energy barrier is low enough to see an average set of peaks representing all the conformations.

Mass Spectrometry

Further characterization of both the ligand and receptor **1** was obtained from electrospray ionization time of flight (ESI-TOF) mass spectrometry. The mass spectrum for the protonated 3-*n*butylnicotinamide ligand, $[\text{L-H}]^+$, shows a mass of 179.1182. This mass is within 1.3 ppm of the calculated mass, 179.1184. The theoretical and raw spectra obtained for the compound are shown in Figure 2.10.

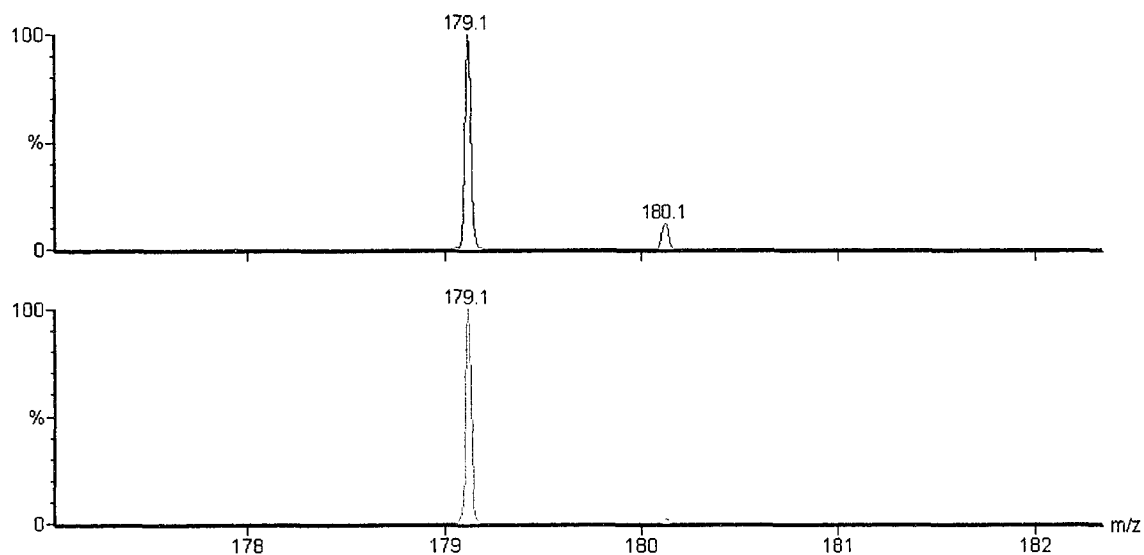


Figure 2.10 The ESI-TOF mass spectra showing the calculated (top) and raw (bottom) data obtained from $[L-H]^+$.

The exact mass obtained for the receptor $[1-PF_6]^+$ complex is 1052.3696 which is within 1.7 ppm of the calculated mass, 1052.3714. The isotopic profile is similar to that predicted for this platinum(II) complex (Figure 2.11).

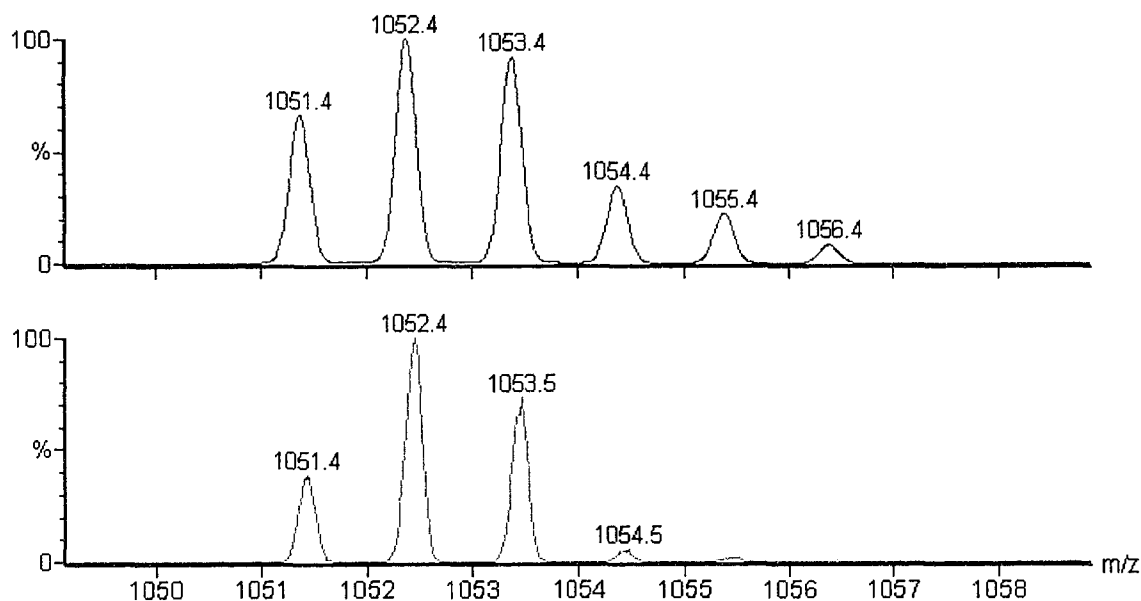


Figure 2.11 The ESI-TOF mass spectra showing the calculated (top) and raw (bottom) data for $[1-PF_6]^+$.

X-ray Structure of [Pt(3-nbutylnicotinamide)₄][PF₆]₂·2CH₂Cl₂

Single crystals of [Pt(3-nbutylnicotinamide)₄][PF₆]₂ as the CH₂Cl₂ solvate suitable for X-ray diffraction were obtained through slow diffusion of *i*Pr₂O into a solution of CH₂Cl₂. The clear colourless blocks appeared after several days. The structural information obtained shows the receptor adopts the 1,2-alternate conformation, as seen in Figure 2.12. This conformation orients two nicotinamide ligands *cis* to one another in the same direction. Therefore, the receptor contains two binding sites each comprised of a minimum of two hydrogen bond donor groups and electrostatic interactions. The two binding sites allow for 1:2 ratio of receptor to anion.

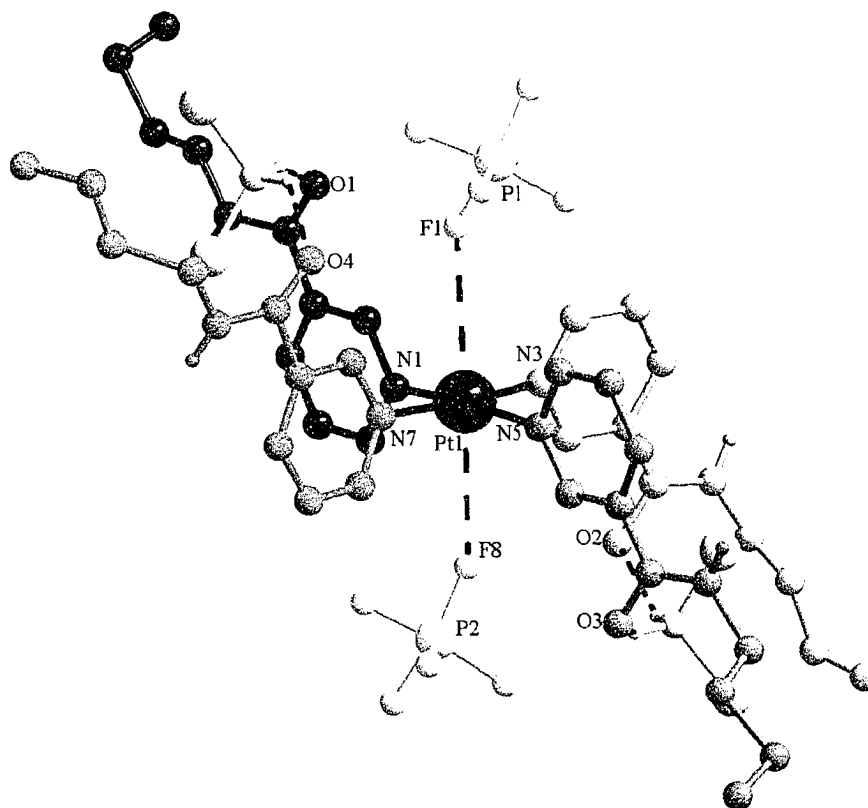


Figure 2.12 X-ray crystal structure of [Pt(3-nbutylnicotinamide)₄][PF₆]₂·2CH₂Cl₂, side view demonstrating electrostatic interaction between Pt(II) and PF₆⁻. Pt...F distances (Å) and angles (°): Pt(1)...F(1) 3.42, Pt(1)...F(1)-P(1) 147; Pt(1)...F(8) 3.28, Pt(1)...F(1)-P(2) 155.

Interestingly, there are no hydrogen bonding interactions between the receptor and the PF_6^- anions. The hydrogen bonding interactions observed in this structure are between the C=O of the amide group, that are pointing into the cavity, and the hydrogen atoms of the CH_2Cl_2 solvent molecules (Figure 2.13). In this thesis, all hydrogen bond distances are quoted as heavy atom...heavy atom distances. The interactions between the receptor and the solvent molecules demonstrate the deficiency PF_6^- has in its ability to hydrogen bond with the receptor.

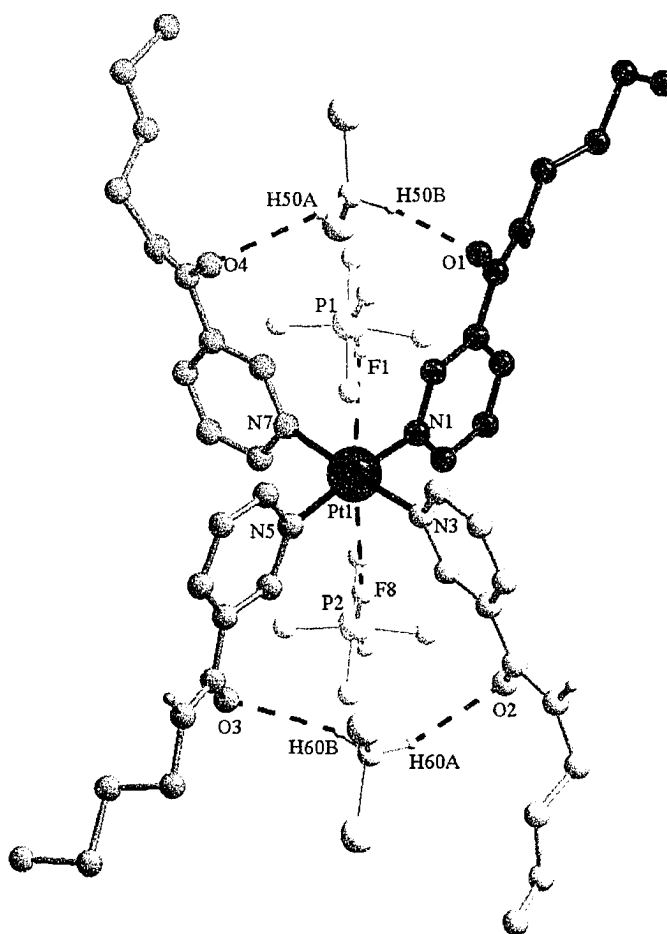


Figure 2.13 X-ray crystal structure of $[\text{Pt}(3\text{-}n\text{butylnicotinamide})_4][\text{PF}_6]_2 \cdot 2\text{CH}_2\text{Cl}_2$, front view demonstrating H-bonding between C=O of receptor with C-H of solvent, CH_2Cl_2 . C-H...O distances (Å) and angles ($^\circ$): C(50)...O(4) 3.01, C(50)-H(50A)...O(4) 155; C(50)...O(1) 3.26, C(50)-H(50B)...O(1) 153; C(60)...O(2) 3.26, C(60)-H(60A)...O(2) 155; C(60)...O(3) 3.37, C(60)-H(60B)...O(3) 140.

The PF_6^- anions are however interacting electrostatically with the platinum(II) metal centre in each binding site; one above the plane and the other below the plane of the metal centre. The structure shows the receptor:anion electrostatic interactions occur at a Pt...F(1) distance of 3.42 Å and a Pt...F(8) distance of 3.28 Å, as shown in Figure 2.12. Therefore, the requirement that the receptor counterions exhibit minimal interactions with the binding site is satisfied. The close approach of the cation and anions is likely a solid state phenomenon. It is likely that in polar solutions there will be negligible ion-pairing and therefore no real competition with target anions.

2.2.2 Binding Studies

¹H NMR Titrations

The determination of binding constants for this receptor in solution was obtained using ¹H NMR spectroscopy. The NMR titrations are carried out in several different solvents depending on the solubility of the receptor alone as well as the solubility of the receptor:anion adduct.

The host-guest interactions for all these titrations are fast on the NMR timescale. Hence, a single average peak for each resonance is observed representing both the complex and uncomplexed receptor. Thus, in order to obtain valid association constants, this type of dynamic receptor:anion interaction requires the stepwise addition of anion until the receptor is saturated (Figure 2.14).

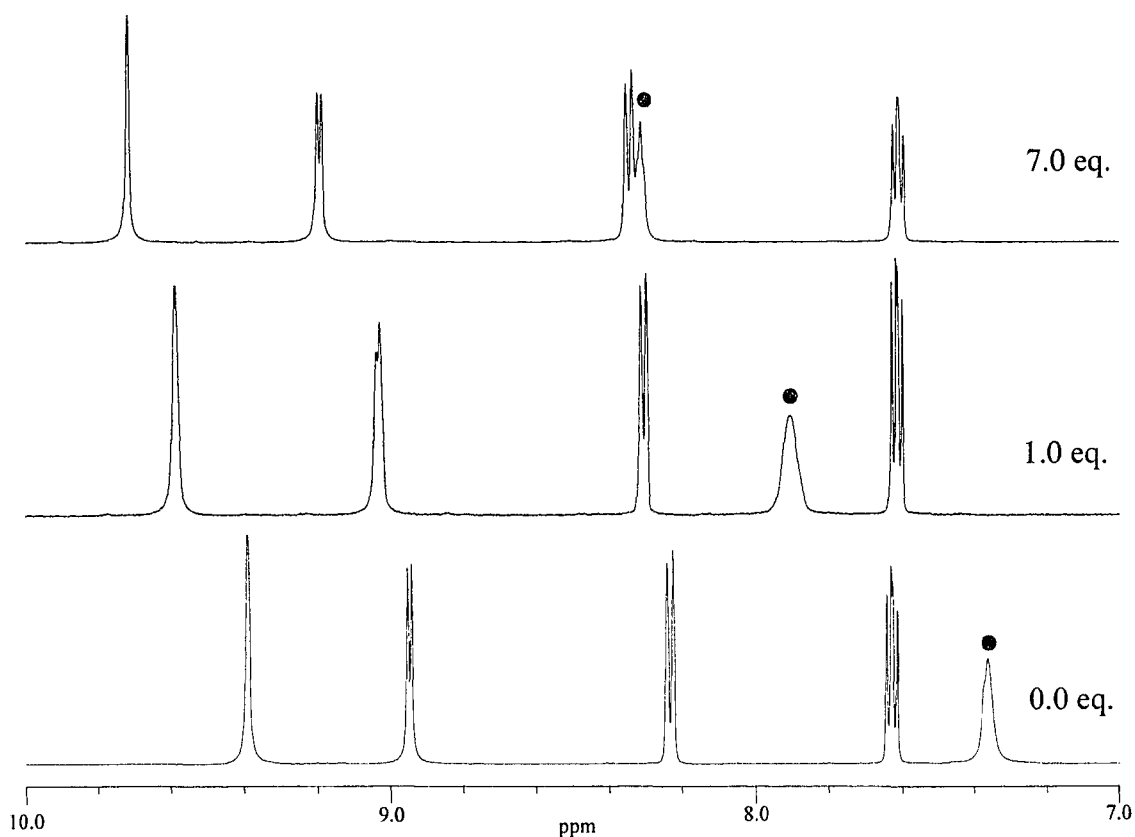


Figure 2.14 The ^1H NMR titration of **1** with NO_3^- , in $\text{MeCN-}d_3$, at several different quantities of anion. The receptor:anion interactions are fast on the NMR timescale therefore a gradual downfield change in chemical shift is observed for the N-H resonance.

Ideally, all the association constants could be measured in a single solvent to allow direct comparisons of the receptor:anion binding strength and selectivity. Unfortunately, this was not possible as a number of the combinations studied precipitated in less polar solvent or showed no interaction in strongly competitive solvents. However, measurements in a small number of solvents allowed basic trends to be evaluated.

The association constants obtained from the addition of CF_3SO_3^- and ReO_4^- in $\text{MeCN-}d_3$ are 129 and 150 M^{-1} . The result from HSO_4^- in $25\% \text{ DMSO-}d_6$ $75\% \text{ MeCN-}d_3$ is an association constant of 149 M^{-1} and from H_2PO_4^- in $\text{DMSO-}d_6$ is 264 M^{-1} . The

binding constant for H_2PO_4^- is the highest of the tetrahedral shaped anions even though it was measured in the most polar solvent system (Table 2.2).

Table 2.2 Association constants, K_a (M^{-1}), obtained for **1** with various oxo-anions, at 30 °C (error <10%).

Anion	K_a (M^{-1})	Solvent
CF_3SO_3^-	129	MeCN- d_3
ReO_4^-	150	MeCN- d_3
NO_3^-	K_1 562 K_2 132	MeCN- d_3
HSO_4^-	149	MeCN- d_3 / DMSO- d_6 3:1 v/v
CH_3CO_2^-	precipitate	MeCN- d_3 / DMSO- d_6 3:1 v/v
H_2PO_4^-	precipitate	MeCN- d_3 / DMSO- d_6 1:9 v/v
CH_3CO_2^-	K_1 230 K_2 491	MeCN- d_3 / DMSO- d_6 1:9 v/v
H_2PO_4^-	264	DMSO- d_6

The stoichiometries in solution for the binding of CF_3SO_3^- , ReO_4^- , HSO_4^- and H_2PO_4^- are all 1:1. This was determined by the continuous variation method^{63,64} and by comparing the titration curves to both 1:1 and 1:2 models using non-linear least squares curve fitting analysis. An example of the graph (Job plot) obtained from the continuous variation method with CF_3SO_3^- shows the peak of the curve at 0.5 mole fraction of host (Figure 2.15). Therefore, the binding of the anion to the receptor is occurring in a 1:1 ratio.

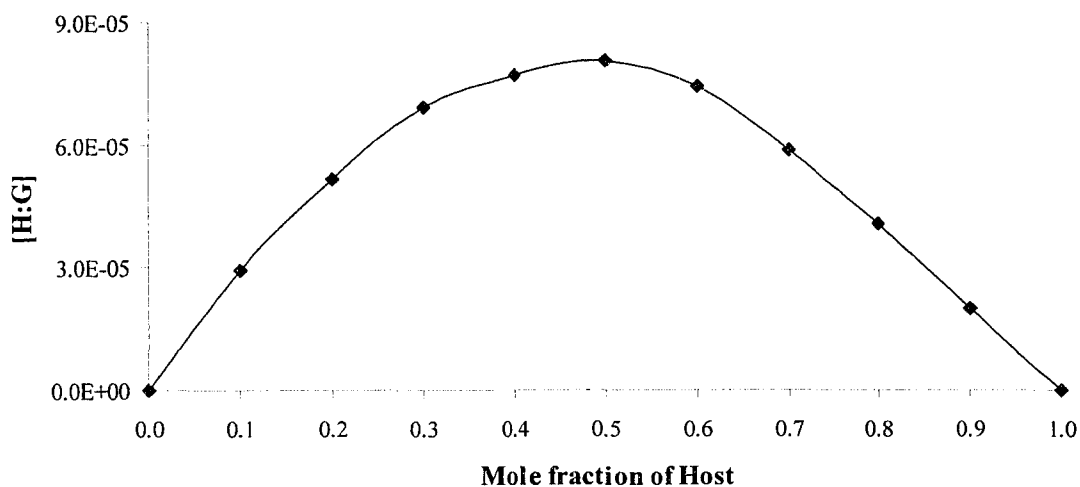


Figure 2.15 Plot of continuous variation experiment with CF_3SO_3^- , showing the 1:1 interaction of receptor and anion.

Intuitively, one might expect to observe a 1:2 ratio of receptor:anion in order to facilitate charge balance with the 2+ charge on the receptor. Some simple explanations for this discrepancy are i) the anions are coordinating in a 1:2 ratio but the second association constant is too small to be measured by this technique and ii) the receptor may have adjusted its conformation to optimize its interaction with a single anion and it is energetically unfavourable to undergo rearrangement to interaction with the second anion (Figure 2.16).

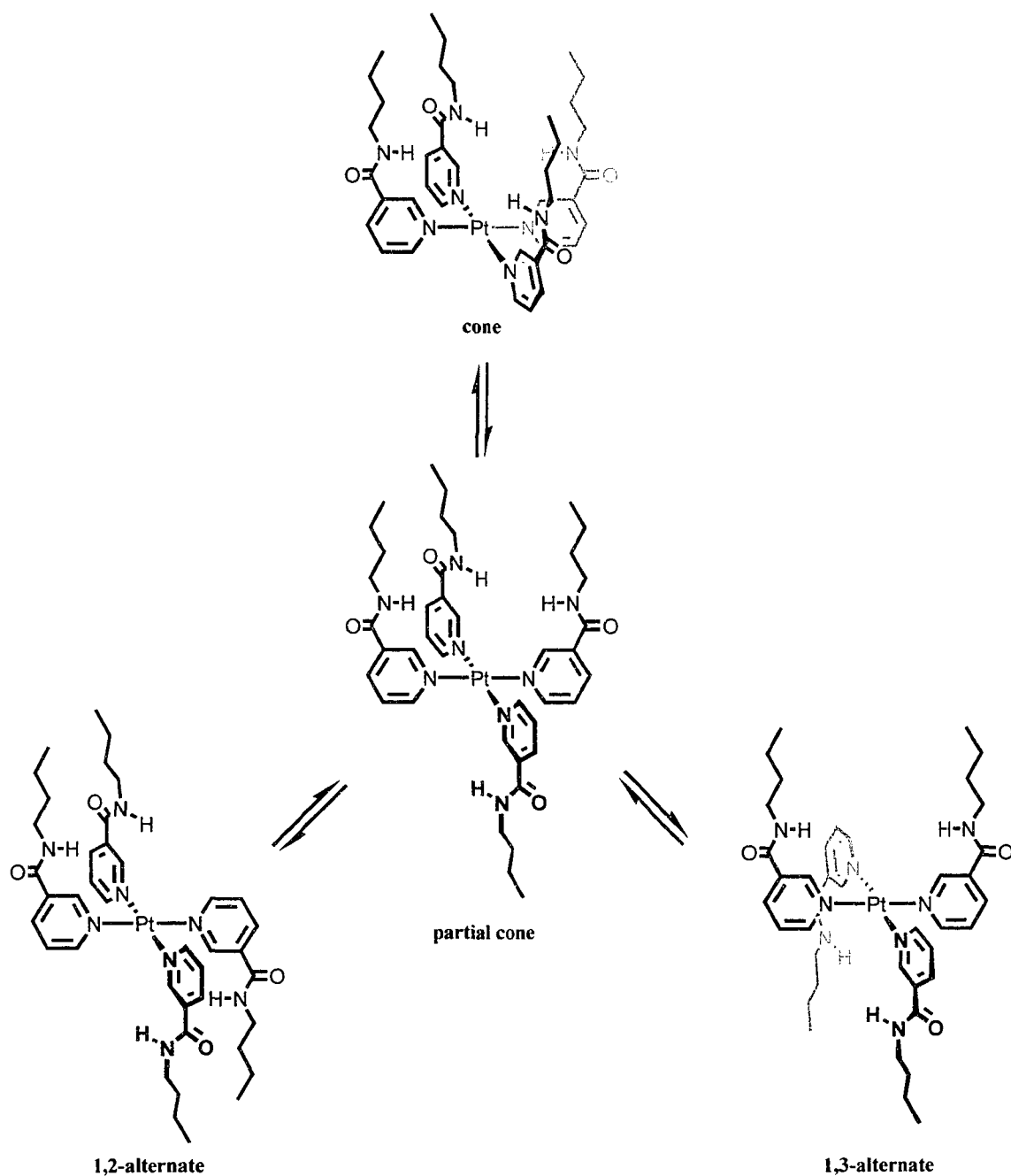


Figure 2.16 Conformations available for receptor **1** to interact with the first anionic guest. A change in conformation for interaction with the second anion may require an unfavourable amount of energy.

The final two anions NO_3^- and CH_3CO_2^- show a 1:2 binding ratio with the receptor. The graph from the continuous variation method with CH_3CO_2^- , shown in Figure 2.17, has a maximum at 0.3 mole fractions of host. That is, one part host and two

parts guest are interacting together during the binding. Therefore, the stoichiometry is a 1:2 binding ratio of receptor to anion.

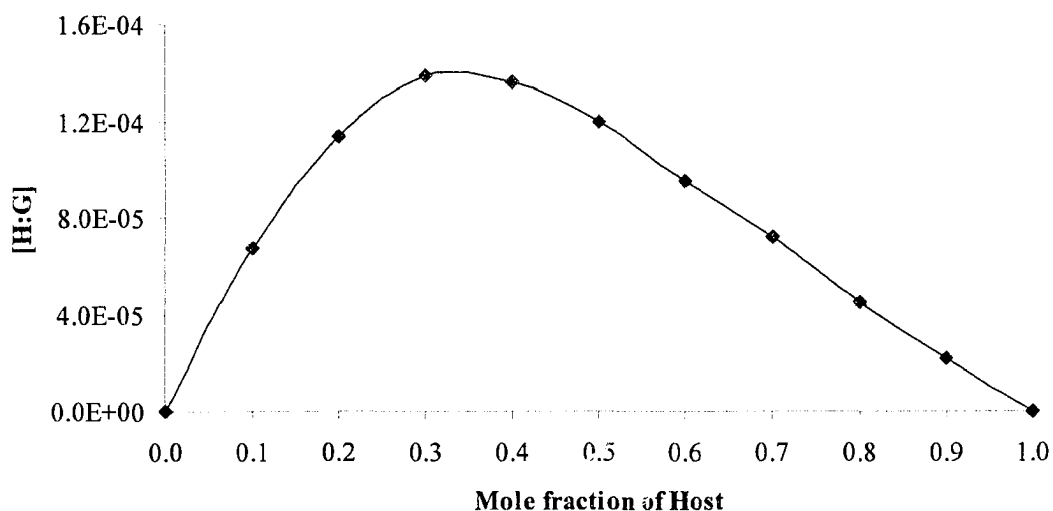


Figure 2.17 Plot of continuous variation experiment with CH_3CO_2^- showing the 1:2 interactions of receptor and anions.

The association constants for NO_3^- were measured in $\text{MeCN-}d_3$ as $K_1 = 562 \text{ M}^{-1}$ and $K_2 = 132 \text{ M}^{-1}$. The binding with CH_3CO_2^- was measured in a much more polar solvent mixture 10% MeCN 90 % $\text{DMSO-}d_6$, where $K_1 = 230 \text{ M}^{-1}$ and $K_2 = 491 \text{ M}^{-1}$. Importantly, the second association constant is higher than the first for CH_3CO_2^- . This can be attributed to a allosteric interaction between the receptor and the anions. That is, the binding of a guest at a one site in the receptor enhances the binding of a second guest at another site. A positive allosteric interaction occurs when the binding of the first guest to the receptor increases the affinity of the second anion towards the receptor.⁶⁵ Therefore, binding of the first anion preorganizes the receptor for the binding of the second anion. The receptor does not require any further adjustments to its conformation

allowing the binding constant for the second anion to be higher than the first (Figure 2.18).

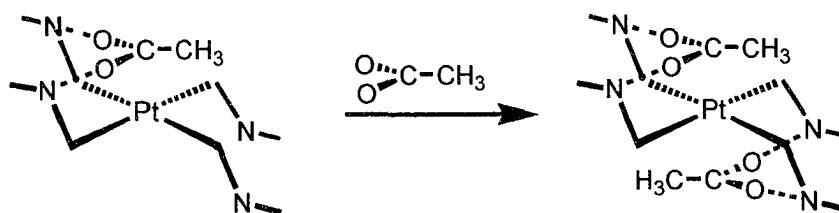


Figure 2.18 Scheme representing the positive allosteric effect observed upon binding CH_3CO_2^- .

*X-Ray Structure of [Pt(3-*n*butylnicotinamide)₄][CF₃SO₃]₂*

Single crystals of $[\text{Pt}(3\text{-}n\text{butylnicotinamide})_4][\text{CF}_3\text{SO}_3]_2$ suitable for X-ray diffraction were obtained by slow diffusion of *i*Pr₂O into a solution of MeCN. The structure shows the receptor in a 1,2-alternate conformation. The CF_3SO_3^- anions interact electrostatically with the platinum(II) metal centre as well as through hydrogen bonds with the amide groups.

Three hydrogen bonding interactions between the receptor and each guest anion are observed; two via N-H groups of two receptor amides and one via a relatively acidic C-H group on an adjacent ligand. The NH...O hydrogen bond lengths are 3.05 and 2.94 Å with angles of 158 ° and 154 °. The CH...O(3) interaction length is 3.13 Å at an angle of 157 °. This type of orientation between the anion and the receptor (two NH and one CH hydrogen bond) optimizes the interactions of the 3-fold symmetric anion with the 4-fold symmetric receptor, as shown in Figure 2.19.

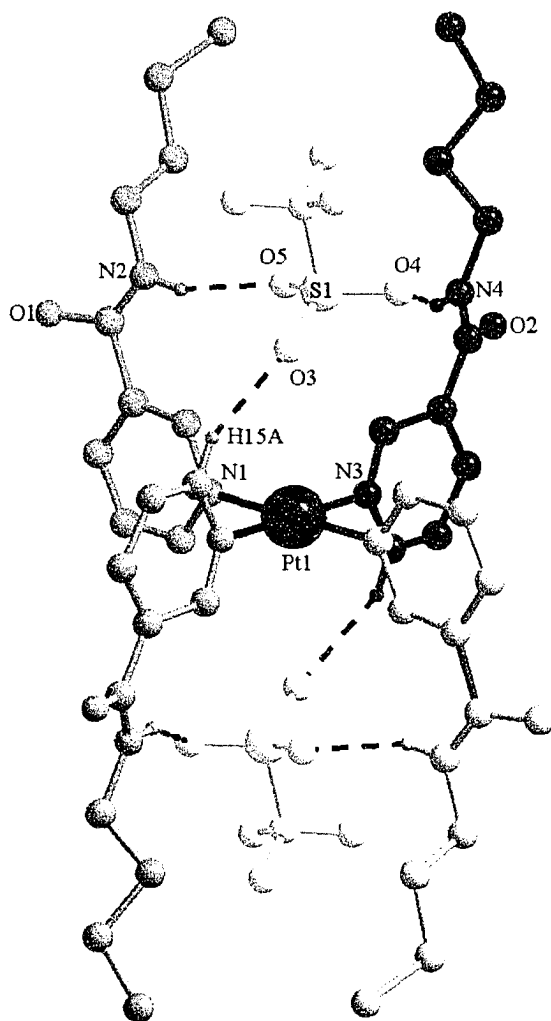


Figure 2.19 X-ray crystal structure of $[\text{Pt}(3\text{-}n\text{butylnicotinamide})_4][\text{CF}_3\text{SO}_3]_2$, front view. N-H...O and C-H...O distances (Å) and angles ($^\circ$): N(2)...O(5) 2.94, N(2)-H(2A)...O(5) 158; N(4)...O(4) 3.05, N(4)-H(4A)...O(4) 154; C(15)...O(3) 3.13, C(15)-H(15A)...O(3) 157.

The anions above and below the plane of the platinum(II) metal centre are interacting at a Pt...O(3) distance of 3.60 Å and a Pt...S(1) distance of 4.34 Å. A rotation of the amide group compared to the PF_6^- structure orients the hydrogen bond donors into the receptor cavity (Figure 2.20).

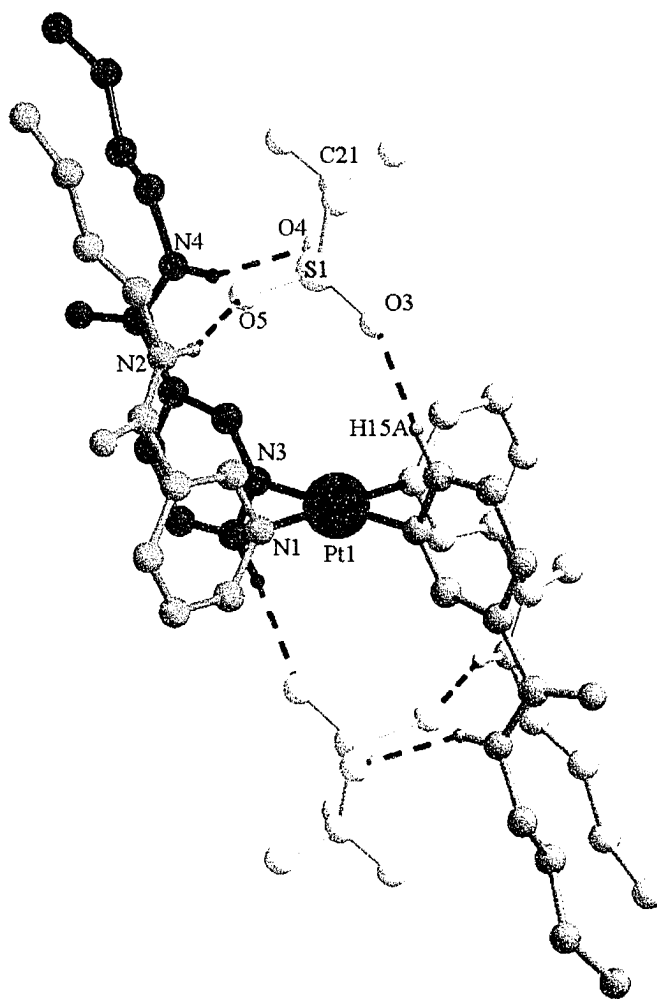


Figure 2.20 X-ray crystal structure of $[\text{Pt}(3\text{-}n\text{butylnicotinamide})_4][\text{CF}_3\text{SO}_3]_2$, side view. Pt...O distances (Å) and angles ($^\circ$): Pt(1)...O(3) 3.60, Pt(1)...O(3)-S(1) 111; Pt(1)...O(4) 4.70, Pt(1)...O(4)-S(1) 67; Pt(1)...O(5) 4.36, Pt(1)...O(5)-S(1) 80. Pt(1)...S(1) 4.34.

X-Ray Structure of $[\text{Pt}(3\text{-}n\text{butylnicotinamide})_4][\text{ReO}_4]_2$

X-ray quality single crystals of $[\text{Pt}(3\text{-}n\text{butylnicotinamide})_4][\text{ReO}_4]_2$ were obtained through slow diffusion of $i\text{Pr}_2\text{O}$ into a solution of MeCN. After several days clear colourless blocks were obtained. This complex is also in the 1,2-alternate conformation but the receptor to anion binding ratio is 1:1, as shown in Figure 2.21. This ratio is due to the acidic C-H(21A) protons from the adjacent *cis* ligand (orange ligand) twisting out of

the vertical plane by 23 ° in order to interact with the anion in the binding site below. The twisting of the ligand optimizes the interaction between a 3-fold symmetric anion and a 4-fold symmetric receptor. The flexibility of the receptor allows this type of slight singular adjustments to be made in order to maximize the number of hydrogen bonds to a single anion (Figure 2.22).

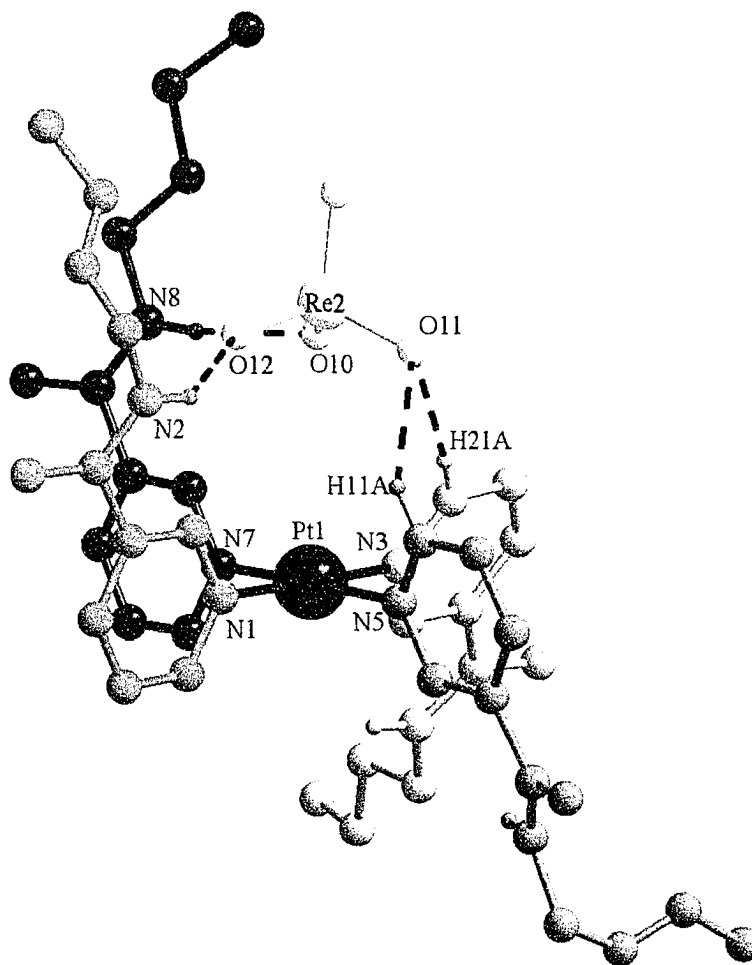


Figure 2.21 X-ray crystal structure of [Pt(3-*n*butylnicotinamide)₄][ReO₄]₂, side view showing 1,2-alternate conformation. Pt...O distances (Å) and angles (°): Pt(1)...O(10) 4.16, Pt(1)...O(10)-Re(2) 86; Pt(1)...O(11) 4.11, Pt(1)...O(11)-Re(2) 89; Pt(1)...O(12) 4.12, Pt(1)...O(12)-Re(2) 87. Pt(1)...Re(2) 4.42.

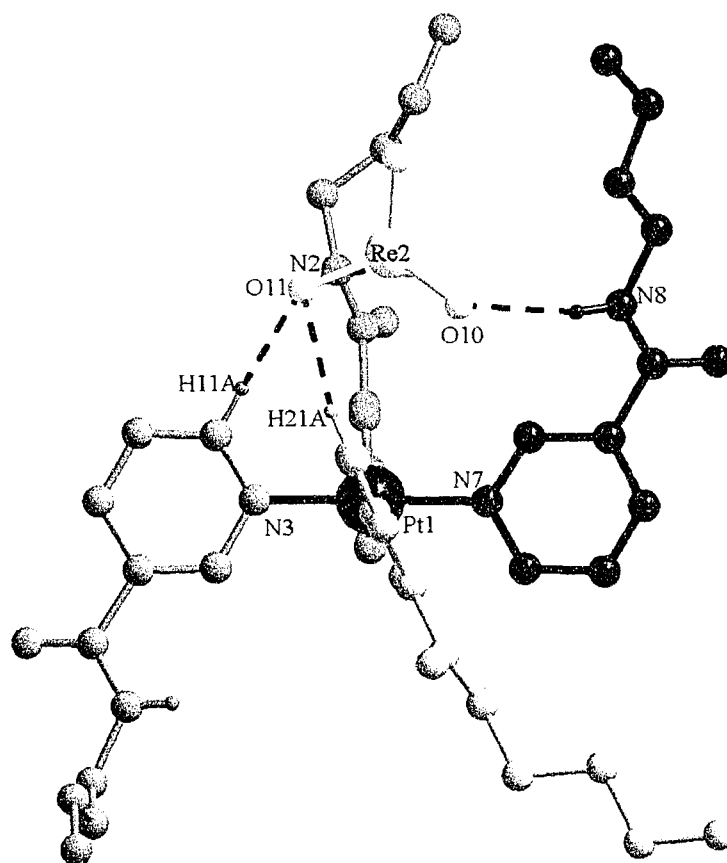


Figure 2.22 X-ray crystal structure of $[\text{Pt}(\text{3-nbutylnicotinamide})_4][\text{ReO}_4]_2$ where orange ligand is twisted 23° to allow the acidic C-H proton (H21A) to interaction with the oxygen of the anion.

The single binding site in this structure is made up of two N-H and two C-H hydrogen bond donors (Figure 2.23). The N-H...O hydrogen bonds are at a distance of 2.88 and 3.10 Å with angles of 137° and 168° . The CH...O hydrogen bonding lengths are 3.32 and 3.31 Å with angles of 171° and 143° , respectively. The electrostatic interactions between the ReO_4 and the receptor occur at a Pt...Re(2) distance of 4.42 Å. The structural information obtained aids in understanding the solution data obtained for the tetrahedral shaped anions binding in a 1:1 stoichiometry.

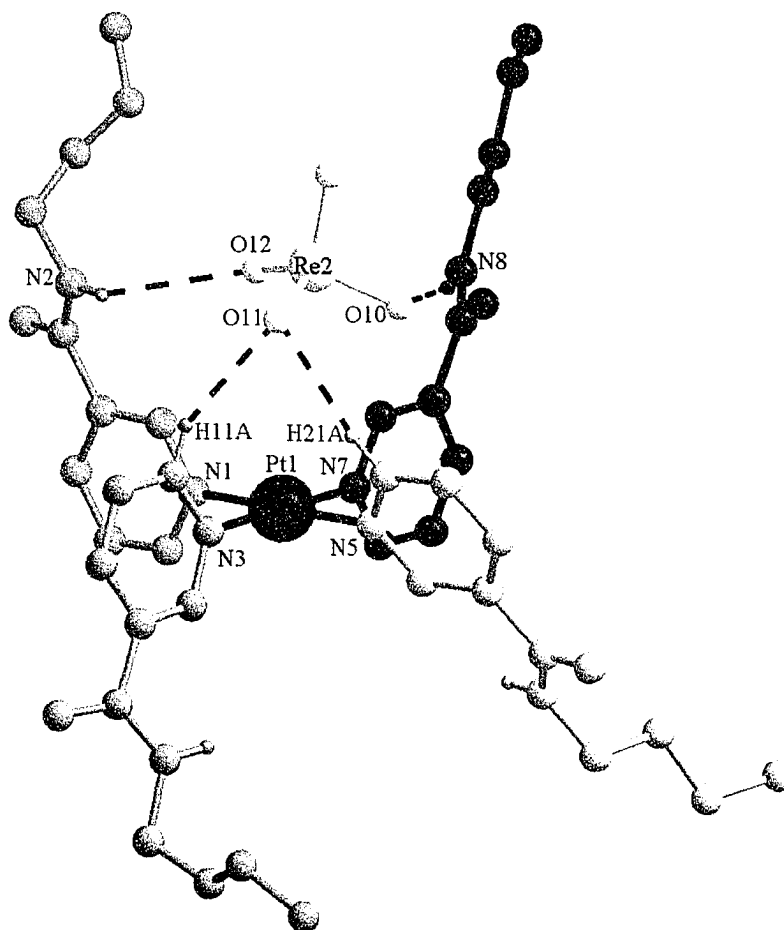


Figure 2.23 X-ray crystal structure of $[\text{Pt}(\text{3-}n\text{butylnicotinamide})_4][\text{ReO}_4]_2$, front view showing hydrogen bonding interactions. N-H...O and C-H...O distances (Å) and angles ($^\circ$): N(2)...O(12) 3.49, N(2)-H(2A)...O(12) 137; N(8)...O(10) 3.01, N(8)-H(8A)...O(10) 168; C(11)...O(11) 3.31, C(11)-H(11A)...O(7) 142; C(21)...O(7) 3.32, C(21)-H(21A)...O(11) 171.

2.3 Conclusions

The use of platinum(II) as an electropositive scaffold to append four amide hydrogen bond donor groups to bind anions was successful. The placement of the amide groups in the 3 position is effective for aligning the hydrogen bond donor sites into the cavity above the metal centre. The use of *n*butyl chains allowed the receptor to be quite soluble even in non-polar solvents such as CH_2Cl_2 . The increase in solvent polarity to

MeCN and DMSO was only required when precipitation occurred upon addition of strongly interacting anions.

The use of PF_6^- as the non-coordinating counterion was also shown to be an effective choice. The solid state results showed only electrostatic interactions between the receptor and the PF_6^- anion while the hydrogen bonding occurred with the solvent. The receptor exhibits free rotation around the Pt-N bond and the ^1H NMR spectrum shows a single set of peaks representing an average of all four *pseudo-calix[4]arene* conformations.

Overall, the solution data shows selectivity for the planar bidentate oxo-anions such as CH_3CO_2^- and NO_3^- . These anions bind in a 1:2 ratio with CH_3CO_2^- having the highest association constant. The CH_3CO_2^- ion also interacts with the receptor through a positive allosteric interaction where the association of the second anion is higher than the first. The tetrahedral shaped anions interact with the receptor in a 1:1 ratio with H_2PO_4^- binding the strongest.

The X-ray structures of the receptor with various anions show the preference for the 1,2-alternate conformation. The number of anions bound to the receptor varies; either 1:1 or 1:2 stoichiometry. Therefore, the receptor is able to maximize its hydrogen bonding interactions with one or two anions while maintaining a 1,2-alternate conformation. No solid state information has been obtained showing different conformations, but this does not preclude their existence in solution.

The selectivity of the receptor is demonstrated by a variation from the Hofmeister series. The series places CH_3CO_2^- midrange in the order, however, when interacting with this receptor it shows the highest association constant.

2.4 Experimental

2.4.1 General Methods

All chemical were purchased from Aldrich Chemicals and used without further purification. The mass spectra were obtained using a Micromass LCT electrospray ionization, time of flight spectrometer. The samples were run in a 1:1 MeCN/H₂O solvent mixture from EM Science OmniSolv[®] High Purity Solvents.

¹H NMR spectra were recorded on a Brüker Avance 500 MHz spectrometer. All peak positions are listed in ppm and are relative to the residual solvent resonance. All deuterated solvents were purchased from Cambridge Isotope Laboratories and used without further drying or distillation. Stability constants were obtained using non-linear least squares curve fitting program, WinEQNMR version 1.10.⁶⁶

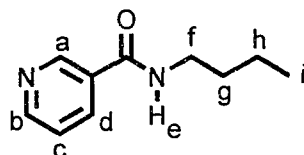
2.4.2 General Methods for X-Ray Crystallography

X-ray crystal structures were determined by first mounting the crystal on a glass fiber or placing it in paratone oil inside a cryoloop if the crystals lost solvent. A full hemisphere of data was collect on a Brüker APEX diffractometer with 10 or 30 s frames. This diffractometer is fitted with a CCD based detector using MoK_α radiation ($\lambda = 0.71073 \text{ \AA}$). Diffraction data and unit-cell parameters were consistent with assigned space groups. The structures were solved by Patterson or direct methods, completed by subsequent Fourier syntheses and refined with full-matrix least-squares methods against $|F^2|$ data. All hydrogen atoms were calculated and treated as idealized contributions. Scattering factors and anomalous dispersion coefficients are contained in the SHELXTL

5.03 program library (Sheldrick, G.M., Madison, WI).⁶⁷ All ball-and-stick diagrams were prepared using DIAMOND, version 3.0.⁶⁸

All X-ray structure solutions were determined by S. J. Loeb, J. Tiburcio-Baez or G. J. E. Davidson.

2.4.3 3-*n*Butylnicotinamide



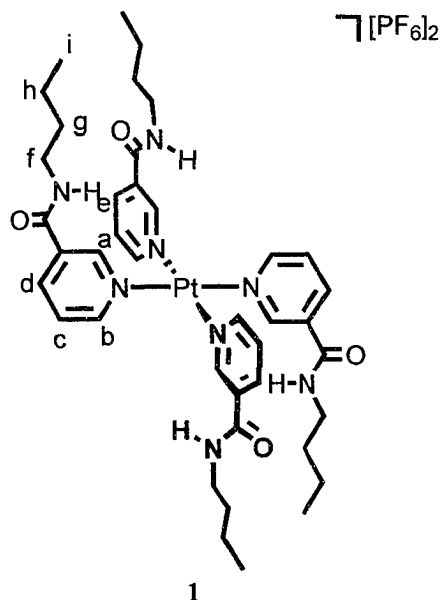
The ligand, 3-*n*butylnicotinamide, was synthesized from 3-nicotinic ethyl ester. The ethyl ester was first synthesized from an esterification reaction of the nicotinic acid. This involved the dropwise addition of H₂SO₄ (enough to ensure the nicotinic acid remained in solution, ~ 10 mL) to the nicotinic acid (5.00 sg, 40.60 mmol) that was stirring in 50 mL of EtOH. The solution was refluxed for 24 hours and then poured over 50 mL of ice. The solution was basified with NH₄OH and the white precipitate was collected by vacuum filtration. The ethyl ester was obtained in quantitative yield.

3-Nicotinic ethyl ester (1.00 g, 5.61 mmol) was dissolved in 15 mL of *n*butylamine and refluxed for 5 days. The excess *n*butylamine was removed and the desired 3-*n*butylnicotinamide was obtained in 94 % yield as a brown oil. HRMS (ESI): Calcd. for: C₁₀H₁₅N₂O [L-H]⁺; Found: 179.1182.

¹H NMR data in MeCN-*d*₃:

Proton	δ (ppm)	Multiplicity	Coupling Constant (Hz)	# of Protons
a	8.94	d	${}^4J_{ad} = 1.9$	1
b	8.67	dd	${}^3J_{bc} = 7.9$ ${}^4J_{ba} = 1.9$	1
c	7.41	dd	${}^3J_{cb} = 7.9$ ${}^3J_{cd} = 5.1$	1
d	8.08	d	${}^3J_{cd} = 5.1$ ${}^4J_{da} = 1.9$	1
e	7.07	bs	---	1
f	3.36	q	${}^3J_{fe} = 6.0$ ${}^3J_{fg} = 7.2$	2
g	1.57	tt	${}^3J_{gf} = 7.2$ ${}^3J_{gh} = 7.5$	2
h	1.40	tq	${}^3J_{hg} \approx {}^3J_{hi} = 7.5$	2
i	0.95	t	${}^3J_{ih} = 7.5$	3

2.4.4 [Pt(3-*n*butylnicotinamide)₄][PF₆]₂ (1)



The synthesis of [Pt(3-*n*butylnicotinamide)₄][PF₆]₂ involved refluxing [PtCl₂(C₂H₅CN)₂]⁶² (0.100 g, 0.27 mmol) with 4 equivalents of 3-*n*butylnicotinamide (0.192 g, 1.08 mmol) and 2.2 equivalents of AgPF₆ (0.150 g, 0.59 mmol) in MeCN for 24 h. The resulting mixture was allowed to cool to room temperature and was filtered through a Büchner funnel with a very fine fritted disc, to remove the AgCl. The filtrate was concentrated to approximately 10 mL and the product was precipitated by slow addition of Et₂O. The white powder was filtered and the clean product was obtained in 87 % yield. X-ray quality crystals of [Pt(3-*n*butylnicotinamide)₄][PF₆]₂·2CH₂Cl₂ were obtained through slow diffusion of *i*Pr₂O into a CH₂Cl₂ solution of this Pt(II) complex. HRMS (ESI): Calcd. for C₄₀H₅₆PF₆N₈O₄Pt [1-PF₆]⁺: 1052.3714; Found: 1052.3696. Crystal data: for [1.2(CH₂Cl₂)]: C₄₂H₆₀Cl₄F₁₂N₈O₄P₂Pt, M = 1367.81, monoclinic, space group Cc, a = 16.2726(4), b = 8.9587(2), c = 39.2903(5) Å, β = 96.253(1)°, V = 5693.7(2) Å³, T = 293(2) K, Z = 4, μ = 2.793 mm⁻¹, 5449 independent reflections (R_{int} =

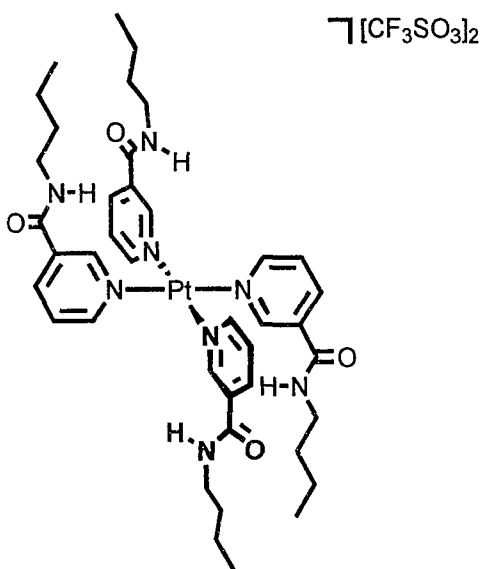
0.0159). R1 = 0.0310, wR1 = 0.0802, (I > 2σI), R2 = 0.0369, wR2 = 0.0844, (all data),

Goodness-of-fit = (F²) = 1.033.

¹H NMR data (500 MHz, MeCN-d₃):

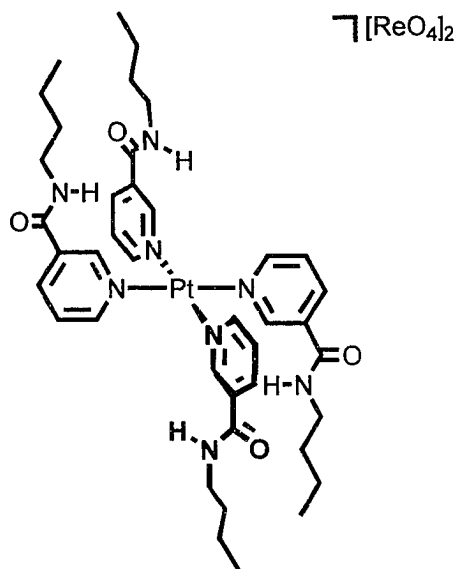
Proton	δ(ppm)	Multiplicity	Coupling Constant (Hz)	# of Protons
a	9.36	s	---	4
b	8.94	d	³ J _{ab} = 5.7	4
c	7.62	dd	³ J _{ba} = 5.7 ³ J _{bc} = 8.1	4
d	8.23	d	³ J _{cb} = 8.1	4
e	7.36	bs	---	4
f	3.36	q	³ J _{fe} = 6.2 ³ J _{fg} = 7.5	8
g	1.58	tt	³ J _{gf} = 7.5 ³ J _{gh} = 7.5	8
h	1.39	tq	³ J _{hg} ≈ ³ J _{hi} = 7.5	8
i	0.94	t	³ J _{ih} = 7.5	12

2.4.5 [Pt(3-*n*butylnicotinamide)₄][CF₃SO₃]₂



The synthesis of [Pt(3-*n*butylnicotinamide)₄][CF₃SO₃]₂ was only undertaken in an attempt to grow crystals and obtain solid state information. The synthesis involved refluxing [PtCl₂(C₂H₅CN)₂] (0.050 g, 0.14 mmol) with 4 equivalents of 3-*n*butylnicotinamide (0.096 g, 0.54 mmol) and 2.2 equivalents of AgCF₃SO₃ (0.075 g, 0.30 mmol) in MeCN for 24 hrs. The resulting mixture was allowed to cool to room temperature and was filtered through a Büchner funnel with a very fine fritted disc, to remove the AgCl. The filtrate was concentrated to approximately 5 mL. The crystals were grown by the slow diffusion of *i*Pr₂O into the MeCN solution. Crystal data: C₄₂H₄₈F₆N₈O₁₀PtS₂, M = 1198.09, monoclinic, space group P-1, a = 10.0946(4), b = 10.7405(3), c = 12.4085(5) Å, α = 83.8350(10), β = 82.243(2), γ = 81.1200(10), V = 1311.90(8) Å³, T = 293(2) K, Z = 1, μ = 2.833 mm⁻¹, 5608 independent reflections (R_{int} = 0.0509). R1 = 0.1146, wR1 = 0.0863, (3402 data, I > 2σI), R2 = 0.3083, wR2 = 0.2312, Goodness-of-fit = (F²) = 1.204.

2.4.6 [Pt(3-*n*butylnicotinamide)₄][ReO₄]₂



The synthesis of [Pt(3-*n*butylnicotinamide)₄][ReO₄]₂ was, once again, an attempt to grow crystal and obtain solid state information. The synthesis involved refluxing [PtCl₂(C₂H₅CN)₂] (0.050 g, 0.14 mmol) with 4 equivalents of 3-*n*butylnicotinamide (0.096 g, 0.54 mmol) and 2.2 equivalents of AgReO₄ (0.075 g, 0.30 mmol) in MeCN for 24 hrs. The resulting mixture was allowed to cool to room temperature and was filtered through a Büchner funnel with a very fine fritted disc, to remove the AgCl. The filtrate was concentrated to approximately 5 mL. The crystals were grown by the slow diffusion of *i*Pr₂O into the MeCN solution. Crystal data: C₅₆H₄₂N₈O₁₂PtRe₂, M = 1586.47, triclinic, space group P-1, a = 10.182(1), b = 14.618(1), c = 17.408(2) Å, α = 72.888(3), β = 88.487(3), γ = 71.773(2)°, V = 2346.0(6) Å³, T = 293(2) K, Z = 2, μ = 8.203 mm⁻¹, 6103 independent reflections (R_{int} = 0.0719). R1 = 0.0698, wR1 = 0.1518, (I > 2σI), R2 = 0.1062, wR2 = 0.1714, (all data), Goodness-of-fit = (F²) = 1.028

2.4.7 Titration Method

Two solutions were prepared. The first was a 1.00 mL, 1.0×10^{-2} M solution of $[\text{Pt}(3\text{-}n\text{butylnicotinamide})_4][\text{PF}_6]_2$ (0.006 g, 0.003 mmol) dissolved in the desired solvent system. The second was a 5.0×10^{-2} M solution prepared by dissolving the selected anion as the tetrabutylammonium (tba) salt (0.003 mmol) in 1.0 mL of the same solvent system.

The ^1H NMR titrations were performed by the systematic addition of small amounts of anion to the receptor solution. After each addition of anion the ^1H NMR spectrum was recorded and the chemical shift from the N-H proton was monitored.

The addition were comprised of 10 μL aliquots of the tba salt solution corresponding to 0.1 equivalents of anion to the solution containing **1** until minimal change in chemical shift occurred (approximately 3 equivalents). At this point 50 μL (0.5 equivalents) aliquots of anion were added to the receptor solution until no further change in chemical shift was observed. An example of this is shown in Table 2.3.

Table 2.3 Amount of anion added for a typical ^1H NMR titration.

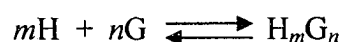
Volume per addition (μL)	Concentration of Receptor (M)	Concentration of Anion (M)	Equivalents of Anion present
0	1.00×10^{-2}	0	0
10	9.80×10^{-3}	9.80×10^{-4}	0.1
10	9.62×10^{-3}	1.92×10^{-3}	0.2
10	9.43×10^{-3}	2.83×10^{-3}	0.3
10	9.26×10^{-3}	3.70×10^{-3}	0.4
10	9.09×10^{-3}	4.55×10^{-3}	0.5
10	8.93×10^{-3}	5.36×10^{-3}	0.6

10	8.77×10^{-3}	6.14×10^{-3}	0.7
10	8.62×10^{-3}	6.90×10^{-3}	0.8
10	8.47×10^{-3}	7.63×10^{-3}	0.9
10	8.33×10^{-3}	8.33×10^{-3}	1.0
10	8.20×10^{-3}	9.02×10^{-3}	1.1
10	8.06×10^{-3}	9.68×10^{-3}	1.2
10	7.94×10^{-3}	1.03×10^{-2}	1.3
10	7.81×10^{-3}	1.09×10^{-2}	1.4
10	7.69×10^{-3}	1.15×10^{-2}	1.5
10	7.58×10^{-3}	1.21×10^{-2}	1.6
10	7.46×10^{-3}	1.27×10^{-2}	1.7
10	7.35×10^{-3}	1.32×10^{-2}	1.8
10	7.25×10^{-3}	1.38×10^{-2}	1.9
10	7.14×10^{-3}	1.43×10^{-2}	2.0
10	7.04×10^{-3}	1.48×10^{-2}	2.1
10	6.94×10^{-3}	1.53×10^{-2}	2.2
10	6.85×10^{-3}	1.58×10^{-2}	2.3
10	6.76×10^{-3}	1.62×10^{-2}	2.4
10	6.67×10^{-3}	1.67×10^{-2}	2.5
10	6.58×10^{-3}	1.71×10^{-2}	2.6
10	6.49×10^{-3}	1.75×10^{-2}	2.7
10	6.41×10^{-3}	1.79×10^{-2}	2.8
10	6.33×10^{-3}	1.84×10^{-2}	2.9
10	6.25×10^{-3}	1.88×10^{-2}	3.0
50	5.88×10^{-3}	2.06×10^{-2}	3.5
50	5.56×10^{-3}	2.22×10^{-2}	4.0
50	5.26×10^{-3}	2.37×10^{-2}	4.5
50	5.00×10^{-3}	2.50×10^{-2}	5.0

100	4.55×10^{-3}	2.73×10^{-2}	6.0
100	4.17×10^{-3}	2.92×10^{-2}	7.0

The association constants were determined using WinEQNMR.⁶⁶ This program is a non-linear least squares curve fitting program that requires several factors in order to determine the binding constants. These factors include the concentration of host and guest throughout the titration, the chemical shift of the peak of interest, the overall binding ratio, the chemical shift at complete saturation as well as an initial guess at the association constant.

From the reaction equation



where H is the host receptor and G is the guest anion. The calculation involves the determination of the calculated chemical shift for the weighted average of the chemical shift of the various Host-Guest complexes. The equation used to refine this non-linear least square calculation is

$$\delta_{calc} = \sum_{m=1}^{m=i} \sum_{n=0}^{n=j} \frac{\delta_{mn} \beta_{mn} m [H]^m [G]^n}{[H]_{total}}$$

where i and j represent the maximum values for m and n . The output from this calculation is the chemical shift, the association constant and the error. The errors are determined by the deviation in the chemical shift between the calculated and experimental data. The equation employed is the “merit function”

$$R = 100 \left(\frac{\sum W_i (\delta_{obs} - \delta_{calc})^2}{\sum W_i (\delta_{obs})^2} \right)^{1/2}$$

where W is the weight attributed to observation i .

2.4.8 Method of Continuous Variation (Job Method)

A solution of $[\text{Pt}(3\text{-}n\text{butylnicotinamide})_4][\text{PF}_6]_2$ (0.0180 g, 0.015 mmol) was made with a concentration of 5×10^{-3} M and a total volume of 3.00 mL. An equimolar solution of the desired tba salt was made with a total volume of 3.00 mL.

The ^1H NMR experiment required ten NMR samples containing varying amounts of host and guest where the total volume is constant. Table 2.4 shows the exact volumes of host and guest to be added.

Table 2.4 Volume of receptor and anion required for each NMR sample when performing a Job Plot.

NMR tube #	Receptor Volume (μL)	Anion Volume (μL)
1	50	450
2	100	400
3	150	350
4	200	300
5	250	250
6	300	200
7	350	150
8	400	100
9	450	50
10	500	0

The stoichiometry is obtained by plotting the [H:G] versus the mole fraction of host.⁶⁴ The peak of the curve represents the mole fraction of host interacting with the anion. [H:G] is calculated by

$$[H : G] = \frac{\delta_{\text{observed}} - \delta_{\text{initial}}}{\delta_{\text{max}}} [\text{Host}]$$

where $\delta_{observed}$ is the chemical shift observed for each sample, $\delta_{initial}$ is the chemical shift when no anion is added and δ_{max} is the chemical shift when the receptor is saturated with anion.

Chapter 3

Bis-Amide Receptor

3.1 Introduction

In the previous chapter, it was shown that the amide based receptor **1** is well suited for the binding of planar bidentate anions such as NO_3^- and CH_3CO_2^- . The binding occurred with the receptor in the 1,2-alternate conformation favouring the 1:2 binding of receptor to anion.

The goal for the second generation receptor is to increase the binding affinity and specificity towards planar bidentate anions. The design involves preorganizing the receptor in to a *pseudo* 1,2-alternate conformation. Although the receptor will lose some of its conformational flexibility, it has the potential to demonstrate a higher degree of specificity due to the preorganization. (Figure 3.1)

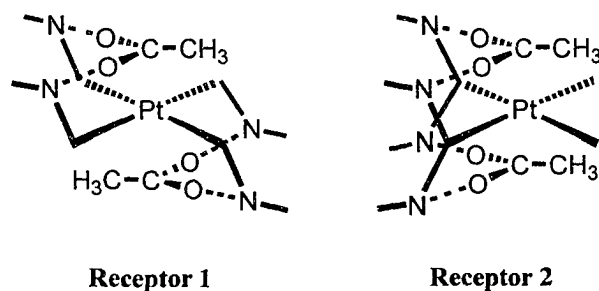


Figure 3.1 Schematic representation of the possible mode of 1:2 binding for receptors 1 and 2.

More specifically, receptor **2** is an amide based receptor possessing four hydrogen bond donor sites, an electrostatic component and a π -stacking unit. The four hydrogen bond donor sites are found on two pyridine ligands with amide substituents in the 3 and 5 positions. This is the same number of hydrogen bond donors as receptor **1**, however,

unlike the previous receptor there is only the possibility of two binding sites. By placing the amides in the 3 and 5 positions, the receptor maintains convergence of all the hydrogen bond donors into the cavity towards the incoming anion; Figure 3.2.

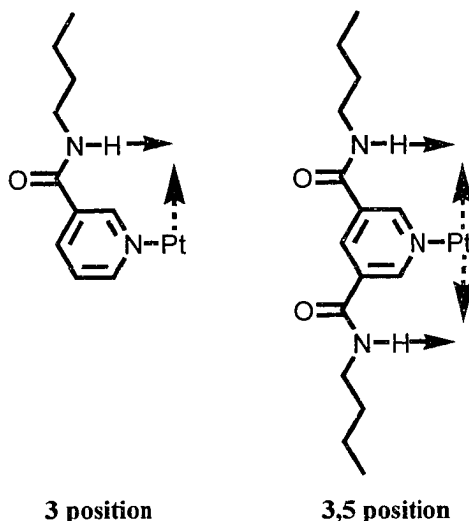


Figure 3.2 Scheme representing the convergence of possible interactions towards the guest with amide substitution in the 3 position and the 3,5 position.

The platinum(II) metal centre provides the opportunity for electrostatic interactions drawing the anion into the binding sites. The incorporation of a 2,2'-bipyridine (bipy) ligand offers the possibility for π -stacking interactions.

This second generation receptor will also maintain the use of the *n*butyl chain on the amide group. The length of this chain provides increased solubility of the receptors as seen in the first generation receptor. The incorporation of *t*butyl groups on the periphery of the bipy unit was also used to ensure solubility in solvents such as MeCN. The counterion for this receptor is PF_6^- , once again, due to its relative inertness.⁶⁰ Therefore, the overall structure of our second generation receptor is $[\text{Pt}(3,5\text{-di-}n\text{butylamidepyridine})_2(\text{tbutylbipy})][\text{PF}_6]_2$, **2**, as shown in Figure 3.3.

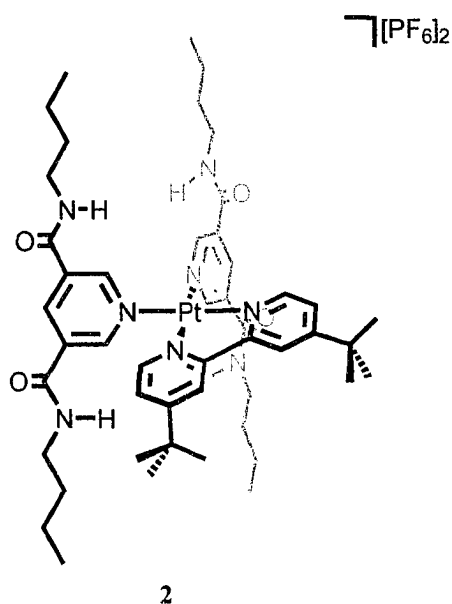


Figure 3.3 Second generation receptor $[\text{Pt}(3,5\text{-di-}n\text{butylamidepyridine})_2(\text{tbutylbipy})][\text{PF}_6]_2$, **2**.

3.2 Results and Discussion

3.2.1 Synthesis and Characterization of

$[\text{Pt}(3,5\text{-di-}n\text{butylamidepyridine})_2(\text{tbutylbipy})][\text{PF}_6]_2$ (**2**)

Synthesis

The 3,5-*di-n*butylamidepyridine ligand was synthesized from an ester precursor.⁶¹ The 3,5-pyridine-dicarboxylic acid was stirred in EtOH and H_2SO_4 was added dropwise until the starting material dissolved in solution. The solution was refluxed for 24 hours, basified and the diester was obtained in quantitative yield (Figure 3.4).

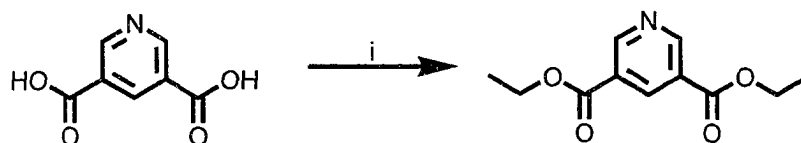


Figure 3.4 Synthesis of 3,5-pyridine ethyl ester. i) Reflux in EtOH and $\text{H}_2\text{SO}_{4(\text{conc})}$.

The 3,5-pyridine ethyl ester was refluxed in neat *n*butylamine for 5 days after which the desired 3,5-*di-n*butylamidepyridine product was obtained in quantitative yield (Figure 3.5).

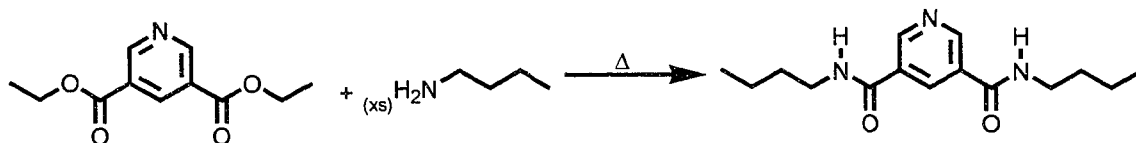


Figure 3.5 Synthesis of 3,5-*di-n*butylamidepyridine.

[PtCl₂(4,4'-*t*Bu-2,2'-bipyridine)] was synthesized by refluxing 4,4'-*t*Bu-2,2'-bipyridine (*t*butylbipy) with [PtCl₂(C₂H₅CN)₂] in acetone.⁶⁹ [Pt(3,5-*di-n*butylamidepyridine)₂(*t*butylbipy)][PF₆]₂, **2**, was synthesized by refluxing [PtCl₂(*t*butylbipy)] with 2.2 equivalents of AgPF₆ and 2 equivalents of 3,5-*di-n*butylamidepyridine in MeCN (Figure 3.6). Receptor **2** was obtained in 62 % yield.

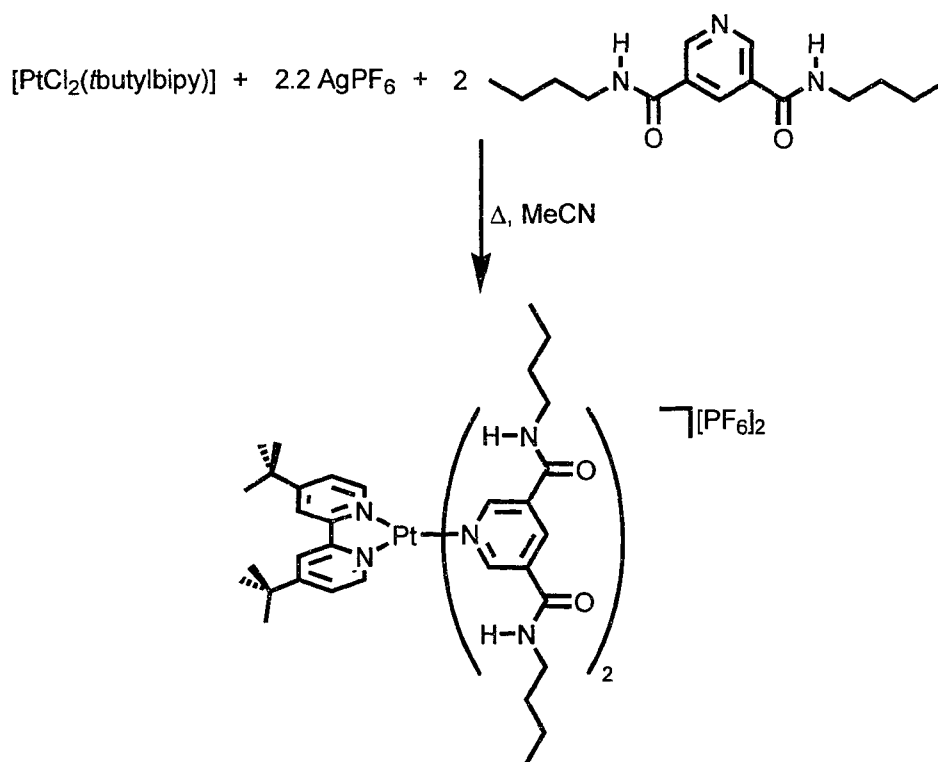


Figure 3.6 Synthesis of **2**.

¹H NMR Spectroscopy

The ¹H NMR spectrum of 3,5-*di*-*n*-butylamidepyridine in MeCN-*d*₃ has two peaks in the aromatic region. Protons H_a and H_b are singlets at 9.03 and 8.46 ppm, respectively. Amide proton H_c is a broad singlet at 7.25 ppm due to its proximity to a nitrogen atom. The peaks obtained in the aliphatic region are due to the butyl chain. These peaks range in chemical shift from 3.37 ppm for H_d, the proton closest to the amide group, to 0.95 ppm for H_g, the methyl proton at the end of the aliphatic chain, as shown in Figure 3.7.

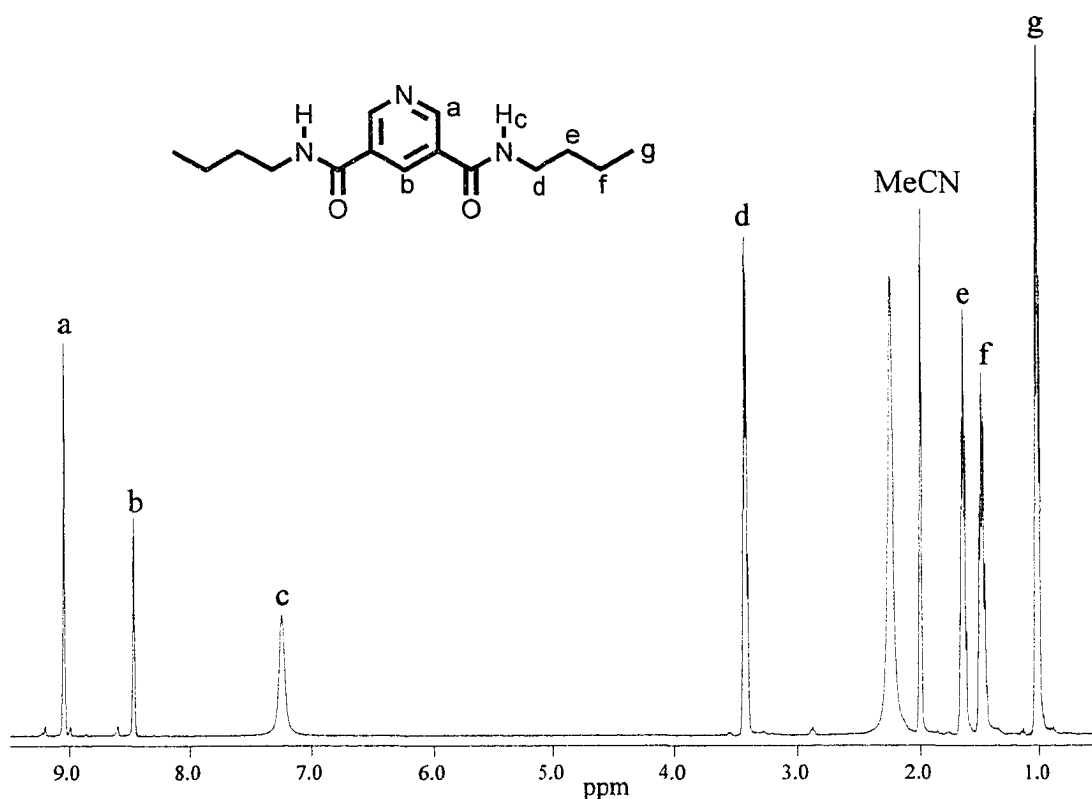


Figure 3.7 ¹H NMR spectrum of 3,5-*di*-*n*-butylamidepyridine in MeCN-*d*₃.

Upon complexation to the metal centre, characteristic changes in chemical shifts occurred for the protons in the aromatic region due to their proximity to the electropositive metal centre (Table 3.1). The ¹H NMR spectrum reveals proton H_a, the

proton closest to the metal, has a chemical shift of 9.53 ppm and the largest change in chemical shift of 0.50 ppm, while H_c (7.67 ppm) shifts by 0.32 ppm. Changes in chemical shifts in the aliphatic region are minimal. The chemical shifts observed for the protons on the *t*butylbipy ligand are 8.43 ppm for H_j, 7.47 ppm for H_h and 7.58 ppm for H_i (Figure 3.8). The singlet representing the *t*butyl peak, H_k, is found at 1.46 ppm.

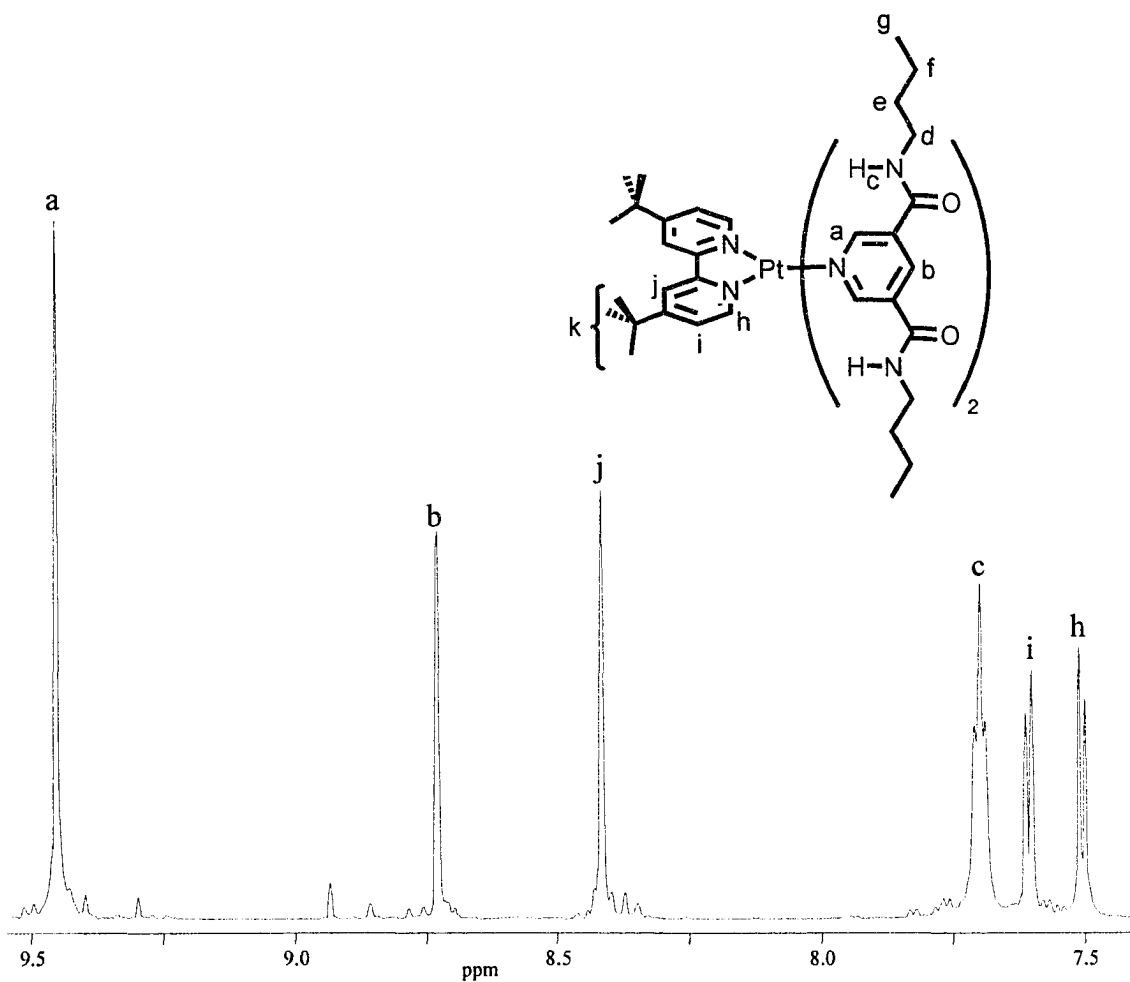


Figure 3.8 Partial ¹H NMR spectrum of **2** in MeCN-*d*₃.

Table 3.1 Comparison of ^1H chemical shifts of the ligand before and after coordination to Pt(II).

Proton	Receptor δ (ppm)	Ligand δ (ppm)	$\Delta \delta$
a	9.53	9.03	0.50
b	8.76	8.46	0.30
c	7.67	7.25	0.32
d	3.36	3.37	-0.01
e	1.58	1.58	-0.07
f	1.39	1.40	-0.01
g	0.95	0.95	0.00

Mass Spectrometry

Further characterization of the protonated ligand and receptor complex was obtained by ESI-TOF mass spectrometry. The exact mass of the singly protonated 3,5-*di-n*butylamidepyridine ligand of 278.1860 was obtained within 3.1 ppm of the calculated mass, 278.1869.

The $[\text{2-PF}_6]^+$ species has an exact mass of 1162.4822 where results show the exact mass to be within 0.7 ppm of the calculated mass. The isotopic profiles for the calculated and raw data are displayed in Figure 3.9.

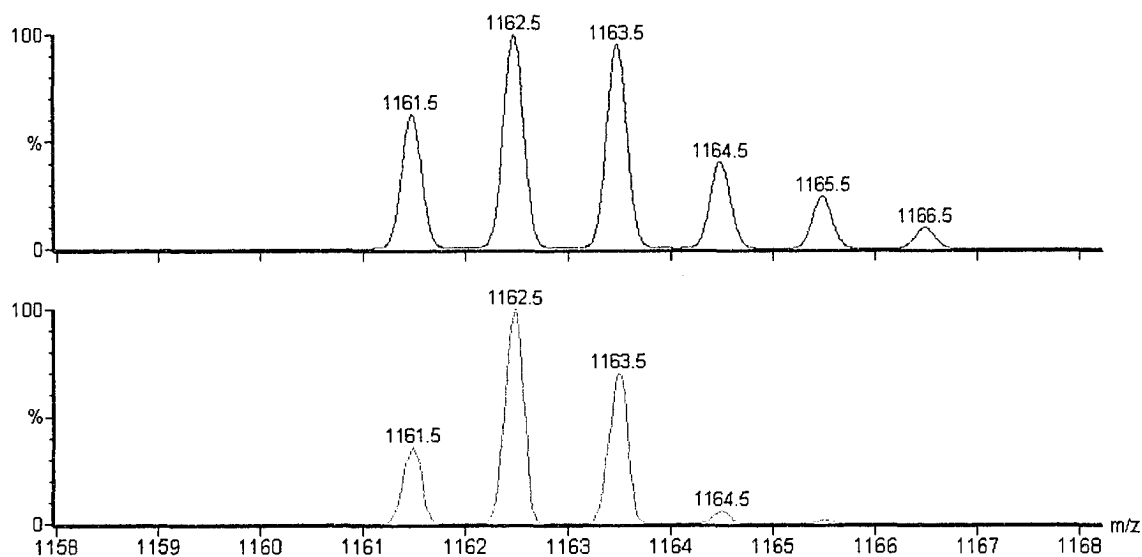


Figure 3.9 The isotopic profile of the calculated (top) and raw (bottom) spectra of $[2\text{-PF}_6]^+$.

3.2.2 Binding Studies

¹H NMR Titrations

In order to facilitate comparison with receptor **1**, the same anions (CF_3SO_3^- , ReO_4^- , NO_3^- , HSO_4^- , H_2PO_4^- and CH_3CO_2^-) were also tested with receptor **2**. In addition, benzoate ($\text{C}_6\text{H}_5\text{CO}_2^-$) was also considered to test the possible involvement of the third type of interaction; π -stacking.

The association constants for receptor **2** with various anions were determined using solution ^1H NMR spectroscopy. The titrations for this receptor were carried out in two different solvent systems. The binding constants for CF_3SO_3^- , ReO_4^- and NO_3^- were measured in $\text{MeCN-}d_3$ while HSO_4^- , H_2PO_4^- , CH_3CO_2^- and $\text{C}_6\text{H}_5\text{CO}_2^-$ were measured in 5% $\text{DMSO-}d_6$ 95 % $\text{MeCN-}d_3$ solution. The addition of 5% $\text{DMSO-}d_6$ in several of the titration solutions was necessary to overcome precipitation problems that occurred in the presence of strongly interacting anions.

The rate of complexation for all the anions tested is fast on the NMR timescale. Therefore, as the anion was titrated into the receptor solution an average signal representing the complexed and uncomplexed receptor was observed. The calculation of the binding constants in this situation requires monitoring the chemical shifts of the proton of interest, the amide proton in this case, upon stepwise addition of 0.1 equivalents of anion, until saturation.

The association constants obtained for ReO_4^- and CF_3SO_3^- are 101 and 148 M^{-1} , respectively (Table 3.2). These numbers are slightly lower compared to 129 and 150 M^{-1} obtained with receptor 1. The association constants obtained for the 1:2 binding of NO_3^- are $K_1 = 283 \text{ M}^{-1}$ and $K_2 = 2 \text{ M}^{-1}$ which is much lower than those of receptor 1 with values of $K_1 = 562 \text{ M}^{-1}$ and $K_2 = 132 \text{ M}^{-1}$.

Table 3.2 Association constants, K_a (M^{-1}), obtained for **2** with various oxo-anions, at 30 °C (error < 10%).

Anion	K_a (M^{-1})	Solvent
CF_3SO_3^-	101	$\text{MeCN-}d_3$
ReO_4^-	148	$\text{MeCN-}d_3$
NO_3^-	K_1 283 K_2 2	$\text{MeCN-}d_3$
HSO_4^-	decomposed	$\text{MeCN-}d_3/\text{DMSO-}d_6$ 95:5 v/v
H_2PO_4^-	decomposed	$\text{MeCN-}d_3/\text{DMSO-}d_6$ 95:5 v/v
CH_3CO_2^-	decomposed	$\text{MeCN-}d_3/\text{DMSO-}d_6$ 95:5 v/v
$\text{C}_6\text{H}_5\text{CO}_2^-$	decomposed	$\text{MeCN-}d_3/\text{DMSO-}d_6$ 95:5 v/v

The lower K_1 values obtained for all the anions is due to the presence of only the *pseudo* 1,2-alternate conformation which eliminates the possibility for more than two

hydrogen bond interactions occurring with the anion. Receptor **1** has the potential to form the cone or the partial cone conformation to increase the number of hydrogen bond interactions, with a single anion, but this has been eliminated with the preorganized design of **2**.

The decrease in the second association constant is due to the fact that the preorganized cavities are not an exact match to the planar NO_3^- anions. The slight pinching of the ligands required for the interaction with the first anion causes the expansion of the second binding site. The change to the second binding site is not favourable for interaction with the second anion causing a decrease in the observed association constant. While receptor **1** shows a positive allosteric effect, where binding of the first anion (CH_3CO_2^-) favourably preorganizes the receptor for the binding of the second anion, a negative allosteric interaction is observed in the binding of NO_3^- with the inflexible receptor, **2**, as shown in Figure 3.10.

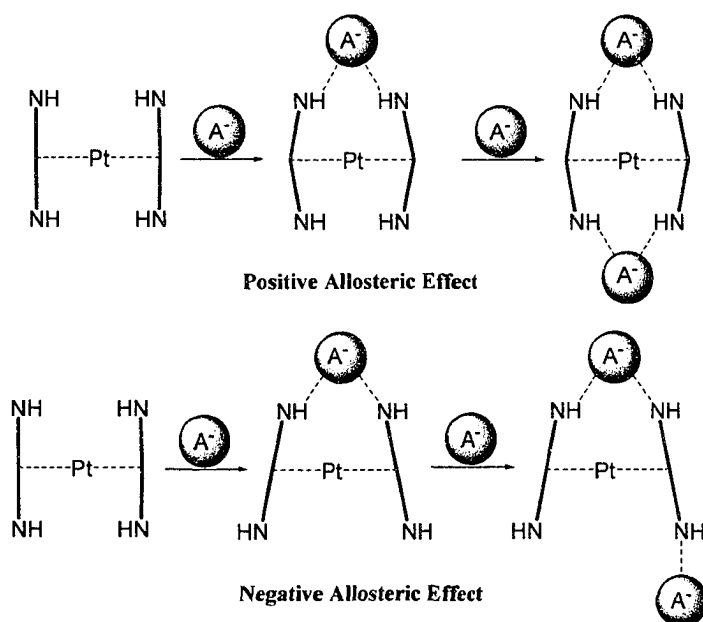


Figure 3.10 Scheme representing the ability of receptor **1** and **2** to bind anions in a 1:2 ratio. A positive allosteric effect is observed with receptor **1** while a negative allosteric effect is observed with receptor **2**.

During the titrations with the remaining anions the receptor decomposed. As the strongly hydrogen bonding anions were added to the receptor solution, the resonances representing free ligand appeared. The 3,5-*di-n*butylamidepyridine ligand contains two electron withdrawing amide groups on a single pyridine ring. The withdrawal of electrons from the ring diminishes the ability of the pyridine nitrogen to donate electrons to the metal centre. Therefore, the inertness of the Pt-N coordinate bond is diminished and substitution is more likely. This produces a competitive environment between the poorly coordinating ligands, the anions and the polar coordinating solvent. Solid state evidence also concurs with this solution data, *vide infra*.

X-Ray Structure of [Pt(3,5-*di-n*butylamidepyridine)₂(*t*butylbipy)][NO₃]₂

X-ray quality colorless block crystals of [Pt(3,5-*di-n*butylamidepyridine)₂(*t*butylbipy)][NO₃]₂ were obtained by slow diffusion of *i*PrO₂ into a MeCN solution over several days. The structure shows the 3,5-*di-n*butylamidepyridine ligands are oriented perpendicular to the square plane of the receptor at slight angles of 17.4 ° and 19.7 °. The N-H portions of the amides point into the cavity and the *t*butylbipy ligand is in the square plane of the receptor. The inclination of the pyridine rings causes N(103) and N(106) to have a distance of 5.42 Å between them while the distance between N(102) and N(105) is 6.37 Å. Figure 3.11 shows the tilt of the ligands as well as the hydrogen bonding interactions.

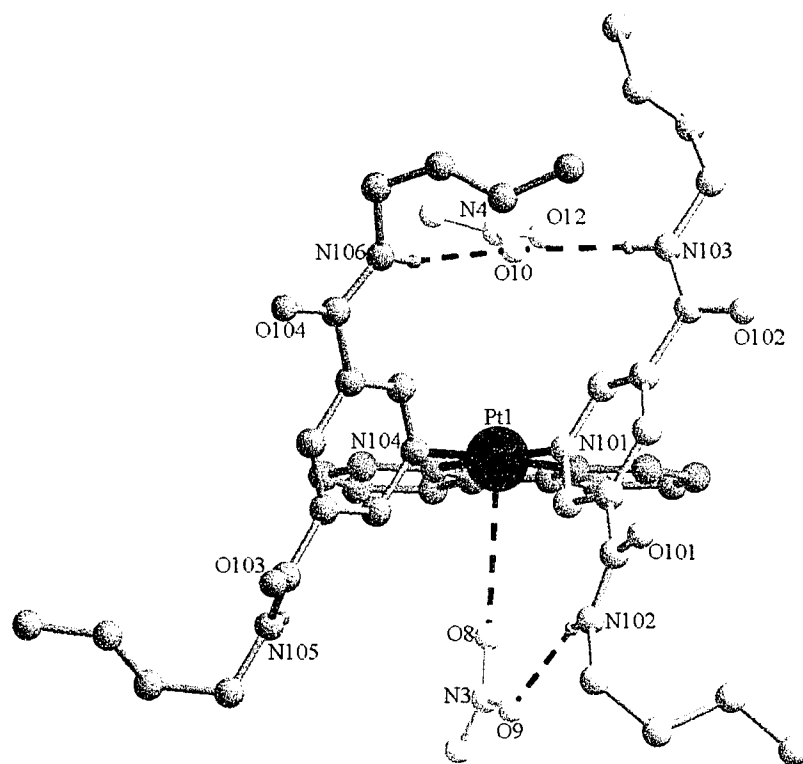


Figure 3.11 X-ray crystal structure of $[\text{Pt}(3,5\text{-di-}n\text{butylamidepyridine})_2(\text{tbutylbipy})][\text{NO}_3]_2$, front view showing the tilt of the ligands and the hydrogen bonding interactions with NO_3^- ; *t*butyl groups have been omitted for clarity. N-H...O distances (Å) and angles ($^\circ$): N(106)...O(10) 2.96, N(106)-H(10D)...O(10) 161; N(103)...O(10) 2.93, N(103)-H(10B)...O(10) 149; N(102)...O(9) 2.88, N(15)-H(10A)...O(9) 141.

The two hydrogen bonds above the plane occur between the N-H groups and a single oxygen, O(10), from the NO_3^- at N-H...O distances of 2.93 and 2.96 Å. Below the plane, only a single N-H unit is hydrogen bonded with the NO_3^- . The N-H...O(9) distance is 2.88 Å while the second non-hydrogen bonding N-H...O(8) distance is 4.24 Å. The electrostatic interactions occur at a distance of 4.22 Å above the plane and 4.63 Å below the plane (Figure 3.12).

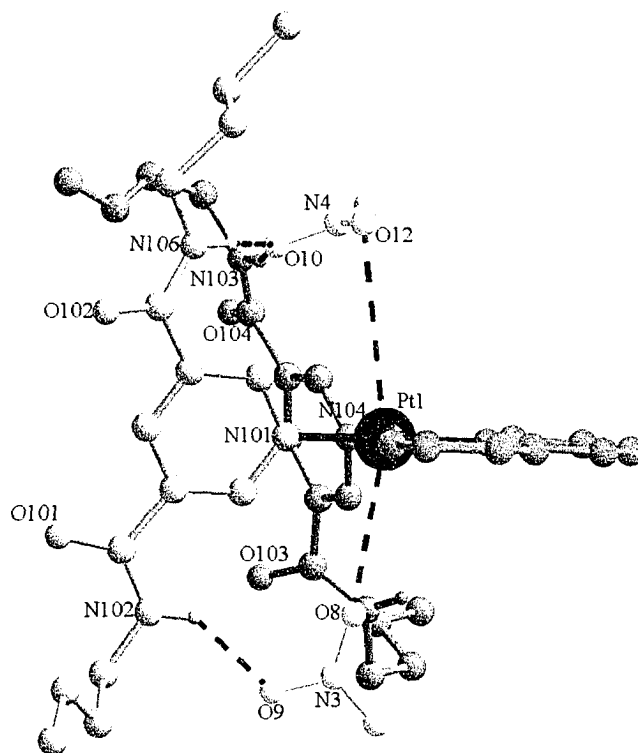


Figure 3.12 X-ray crystal structure of $[\text{Pt}(3,5\text{-di-}n\text{butylamidepyridine})_2(\text{tbutylbipy})][\text{NO}_3]_2$, side view showing the placement of the anions with respect to the platinum(II), *t*butyl groups have been omitted for clarity. Pt...O distances (Å) and angles (°): Pt(1)...O(12) 4.19, Pt(1)...O(12)-N(4) 83; Pt(1)...O(8) 3.39, Pt(1)...O(8)-N(3) 172. Pt(1)...N(3) 4.63; Pt(1)...N(4) 4.22.

The preorganization of the nicotinamide ligands in the *pseudo* 1,2-alternate conformation causes the binding sites to lose their independence. Since the binding sites are not a perfect match for NO_3^- , the receptor must compensate slightly to bind the first anion. In doing so, a negative allosteric effect is observed. The slight pinching required for two hydrogen bonding interactions to occur with the NO_3^- above the plane forces the two amide groups below the plane to move away from each other. This in turn inhibits the maximum amount of hydrogen bonding to occur below the plane.

X-Ray Structure of $[\text{Pt}(3,5\text{-di-}n\text{butylamidepyridine})_2(\text{bipy})][\text{ReO}_4]_2$

Single crystals of $[\text{Pt}(3,5\text{-di-}n\text{butylamidepyridine})_2(\text{bipy})][\text{ReO}_4]_2$ suitable for X-ray diffraction were obtained by slow diffusion of $i\text{PrO}_2$ into a MeCN solution. After several days, small colorless blocks were obtained. This structure shows the 3,5-*n*butylamidepyridine ligands perpendicular to the plane with only a single N-H group on each ligand pointing into the cavity. The bipy ligand is in the square plane of the receptor. There are only two interactions within acceptable hydrogen bonding distance in this structure. The single N-H...O(8) hydrogen bond distance occurs at 3.04 Å while the C-H...O(3) hydrogen bond interaction occurs at a distance of 3.03 Å, as shown in Figure 3.13. Proton H(20B) and H(20C) are hydrogen bonded neighbouring receptors while H(20D) is interacting with a water molecule.

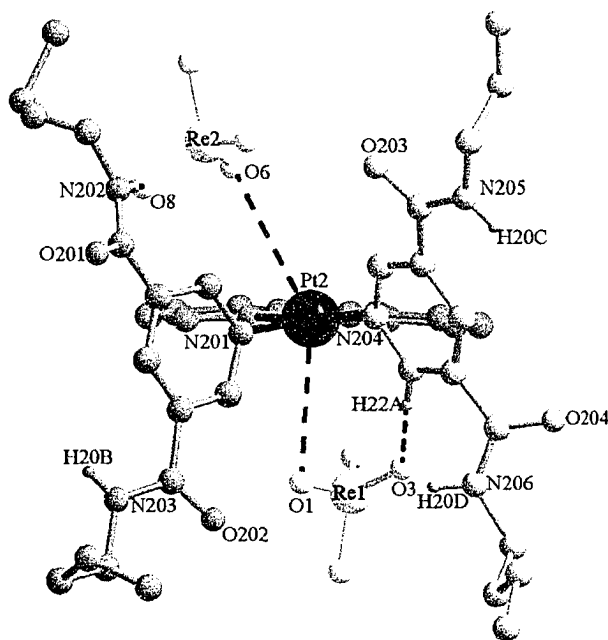


Figure 3.13 X-ray crystal structure of $[\text{Pt}(3,5\text{-di-}n\text{butylamidepyridine})_2(\text{bipy})][\text{ReO}_4]_2$, front view showing the hydrogen bonding between the receptor and two ReO_4^- anions. N-H...O and C-H...O distances (Å) and angles ($^\circ$): N(202)...O(8) 3.05, N(202)-H(202A)...O(8) 163; C(220)...O(3) 3.05, C(220)-H(22A)...O(3) 164.

The electrostatic interaction with the platinum(II) metal centre occurs below the plane with a Pt...O(1) distance of 3.59 Å while the interaction above the plane is much weaker with a Pt...O(6) distance of 4.14 Å (Figure 3.14). Therefore, the preorganization of the binding sites in the receptor causes an inhibition in the binding of ReO_4^- .

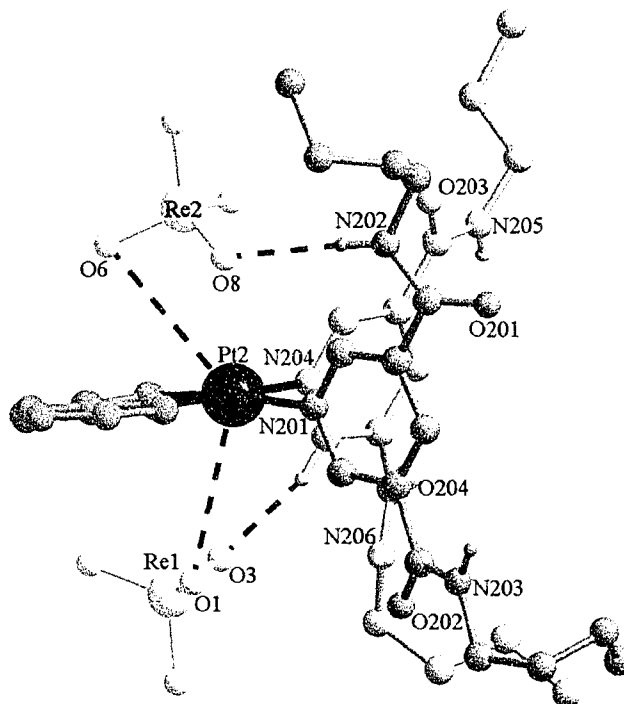


Figure 3.14 A side view of X-ray crystal structure of $[\text{Pt}(3,5\text{-di-}n\text{butylamidepyridine})_2(\text{bipy})][\text{ReO}_4]_2$ showing the electrostatic interactions. Pt...O distances (Å) and angles ($^\circ$): Pt(2)...O(6) 4.14, Pt(2)...O(6)-Re(2) 84; Pt(2)...O(1) 3.59, Pt(2)...O(1)-Re(1) 104. Pt(2)...Re(2) 4.31; Pt(2)...Re(1) 4.00.

X-Ray Structure of $[\text{Pt}(\text{C}_6\text{H}_5\text{CO}_2)_2(\text{tbutylbipy})]$

Small yellow single crystals suitable of X-ray diffraction of $[\text{Pt}(\text{C}_6\text{H}_5\text{CO}_2)_2(\text{tbutylbipy})]$ were obtained by slow diffusion of $i\text{PrO}_2$ into a 95% MeCN 5% DMSO solution. The polar solvent system is required to maintain the solubility of the strongly interacting receptor and anion. The solution initially contained $[\text{Pt}(3,5\text{-di-}n\text{butylamidepyridine})_2(\text{tbutylbipy})][\text{PF}_6]_2$ and two equivalents of tetrabutylammonium

benzoate. The crystals that formed are of a neutral platinum(II) compound where the two 3,5-*di-n*butylamidepyridine ligands are replaced by two benzoate anions coordinating to the metal centre (Figure 3.15).

The presence of competitive coordinating polar solvent, DMSO, and $C_6H_5CO_2^-$ anions allows the more labile *bis*-amide substituted ligand to exchange with the electron rich benzoate anions. This is in agreement with the solution data obtained where the receptor slowly decomposed upon addition of anions in the more polar 95% MeCN 5% DMSO solvent system.

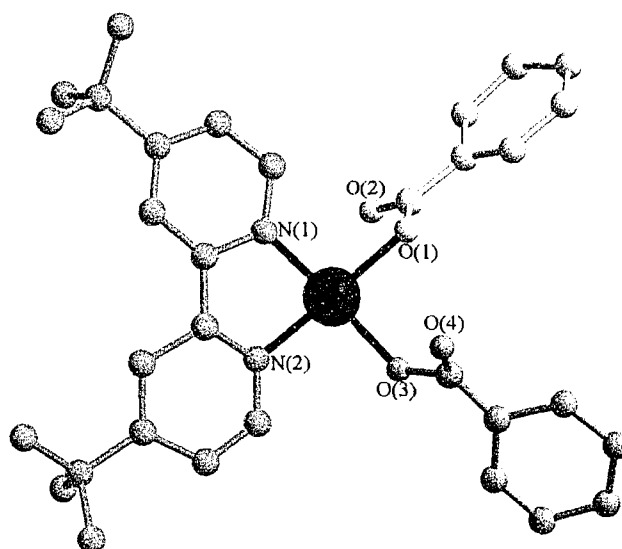


Figure 3.15 X-ray crystal structure of $[Pt(C_6H_5CO_2)_2(tbutylbipy)]$.

3.3 Conclusions

The modifications made for the design of the second generation receptor included the addition of a bipy ligand while maintaining four amide functional groups. This new arrangement preorganized **2** in the *pseudo* 1,2-alternate conformation which appeared to be the preferred conformation for receptor **1**.

The maintenance of the *n*butyl chains as an R group for the amide as well as the incorporation of the *t*butyl group on the bipy allowed the receptor to maintain its solubility in solvents such as MeCN. The PF_6^- counterion once again did not show measurable competition for the binding sites with the association constants being relatively unchanged compared to receptor 1.

The placement of amide groups in the 3 and 5 position on the pyridine ring maintained the proper convergence of the hydrogen bond donor into the binding cavities. However, one drawback of placing two electron withdrawing groups on a coordinating ligand is the decrease in inertness in the Pt-N bond. In order to maintain the solubility of the system in the presence of strongly coordinating anions the receptor was dissolved in a 5% DMSO 95 % MeCN solution. The labile *bis*-amide substituted ligand was displaced from the metal centre resulting in the decomposition of the receptor. Therefore, association constants for HSO_4^- , H_2PO_4^- , CH_3CO_2^- and $\text{C}_6\text{H}_5\text{CO}_2^-$ anions were not obtained.

The second drawback of having both hydrogen bond donor sites on the same ligand is the loss of flexibility of the receptor binding sites. This is seen in the decrease of association constants for both K_1 and K_2 . The first association constants are lower due to the elimination of the possibility of more than two hydrogen bond interactions with the anion in the first binding site. The second association constant is affected due to adjustments made for the binding of the first anion which changed the shape of the second binding site. This change in shape decreased the affinity of the second anion to the receptor which is also known as a negative allosteric effect. The X-ray structures

obtained also show the lack of complementarity between the binding site and the shape and size of the anions.

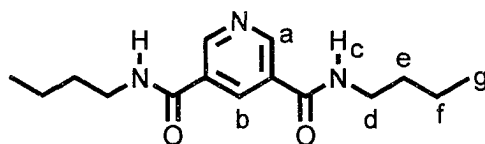
Overall, through both solution and solid state experiments it was determined that the *pseudo* 1,2-alternate conformation obtained in this receptor is not an exact match for the planar bidentate oxo-anions. The analysis shows this preorganization actually caused a decrease in binding strength and specificity in the receptor. The preferred spatial arrangement for the desired 1:2 complexation was not attained due to the lack of flexibility in the binding sites, resulting in a negative allosteric effect.

3.4 Experimental

3.4.1 General Methods

See description in section 2.4.1 and 2.4.2 for general procedure and instrumentation used in this chapter.

3.4.2 3,5-Di-*n*butylamidepyridine



The 3,5-pyridine ethyl ester was synthesized by an esterification reaction. The 3,5-pyridine-dicarboxylic acid (5.00g, 29.640 mmol) was added to 50 mL of EtOH. Concentrated H₂SO₄ was added dropwise to the mixture until the carboxylic acid dissolved in solution. The reaction was refluxed for 24 hours then cooled to room temperature. The mixture was poured over 50 mL of crushed ice and basified with

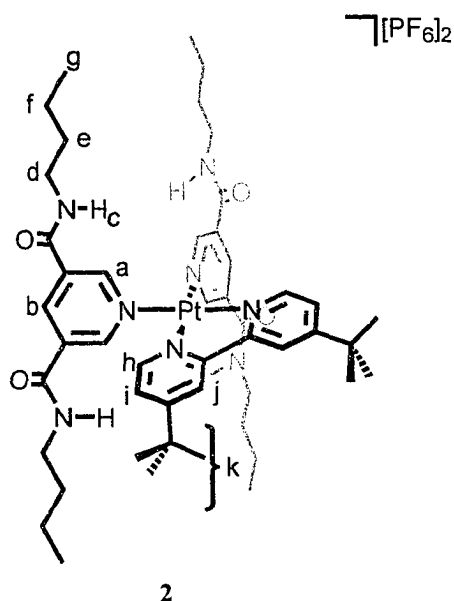
NH₄OH. The resulting white precipitate was filtered by vacuum filtration and washed with water.

The 3,5-pyridine ethyl ester (1.00 g, 4.48 mmol) was dissolved in 15 mL of *n*butylamine and refluxed for 4 days. The remaining *n*butylamine was removed by dynamic vacuum to give the product as a pale yellow powder, 1.15 g, 92 % yield. HRMS (ESI): Calcd. for: C₁₄H₂₄N₃O₂ [L-H]⁺: 278.1869; Found : 278.1860.

¹H NMR data (500 MHz, MeCN-*d*₃):

Proton	δ(ppm)	Multiplicity	Coupling Constant (Hz)	# of Protons
a	9.03	s	---	2
b	8.46	s	---	1
c	7.25	bs	---	2
d	3.37	t	³ J _{de} = 7.2	4
e	1.58	tt	³ J _{ed} ≈ ³ J _{ef} = 7.2	4
f	1.40	tq	³ J _{fe} ≈ ³ J _{fg} = 7.2	4
g	0.95	t	³ J _{gf} = 7.2	6

3.4.3 [Pt(3,5-*di-n*butylamidepyridine)₂(*t*butylbipy)] [PF₆]₂ (**2**)



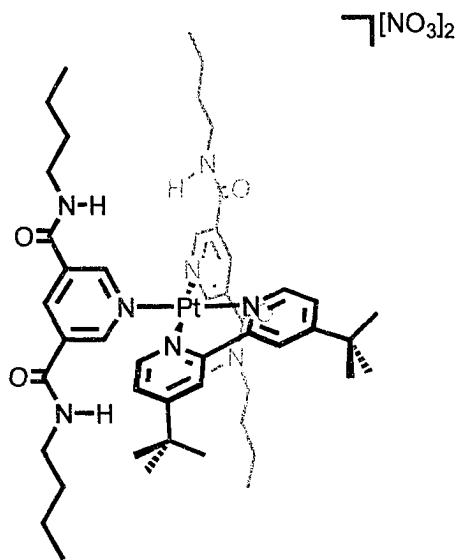
The [PtCl₂(*t*butylbipy)] starting material was synthesized by refluxing [PtCl₂(C₂H₅CN)₂]⁶² with *t*butylbipy in acetone for 40 hours.⁶⁹ The yellow precipitate was collected by filtering the solution while still hot.

The receptor, **2**, was synthesized by refluxing [PtCl₂(*t*butylbipy)] (0.133 g, 0.249 mmol) with 2 equivalents of both AgPF₆ (0.236 g, 0.498 mmol) and 3,5-*di-n*butylamidepyridine (0.126 g, 0.498 mmol) in 25 mL of MeCN for 48 hours. After cooling the reaction mixture to room temperature the AgCl was removed by filtering the mixture through a Büchner funnel fit with a fritted disc. The solvent from the filtrate was evaporated and the crude product was obtained as a white powder. The product was recrystallized from hot CHCl₃ in 62 % yield (0.202 g). HRMS (ESI): Calcd. for: C₄₈H₇₀N₈O₄PF₆Pt [**2**-PF₆]⁺: 1162.4822; Found : 1162.4822 and for C₄₈H₇₀N₈O₄Pt [**2**]²⁺: 508.7584; Found : 508.7587. Anal Calcd: C 44.07 %, H 5.39 %, N 8.57 %; Found: C 44.45 %, H 5.56 %, N 8.60 %.

¹H NMR data (500 MHz, MeCN-*d*₃):

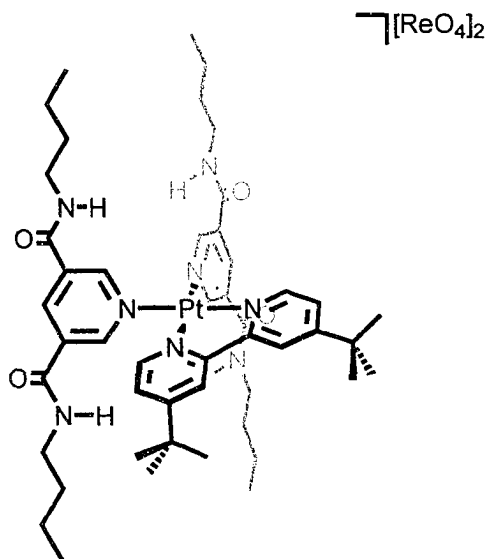
Proton	δ(ppm)	Multiplicity	Coupling Constant (Hz)	# of Protons
a	9.53	d	${}^4J_{ab} = 1.8$	4
b	8.76	d	${}^4J_{ba} = 1.8$	2
c	7.67	bs	---	4
d	3.36	t	${}^3J_{de} = 6.9$	8
e	1.58	tt	${}^3J_{ed} = 6.9$ ${}^3J_{ef} = 7.2$	8
f	1.39	tq	${}^3J_{fe} \approx {}^3J_{fg} = 7.2$	8
g	0.95	t	${}^3J_{gf} = 7.2$	12
h	7.47	d	${}^3J_{hi} = 6.2$	2
i	7.58	dd	${}^3J_{ih} = 6.2$ ${}^4J_{ij} = 2.1$	2
j	8.43	d	${}^4J_{ji} = 2.1$	2
k	1.46	s	---	18

3.4.4 [Pt(3,5-*di-n*butylamidepyridine)₂(*t*butylbipy)][NO₃]₂



The receptor was synthesized as the NO₃⁻ salt to obtain some solid state information about the receptor:anion interaction. This complex was synthesized by refluxing [PtCl₂(*t*butylbipy)] (0.050 g, 0.093 mmol) with 2 equivalents of both AgNO₃ (0.032 g, 0.187 mmol) and 3,5-*di-n*butylamidepyridine (0.052 g, 0.187 mmol) in 25 mL of MeCN for 48 hours. After cooling the reaction mixture to room temperature the AgCl was removed by filtering the mixture through a Büchner filter fit with a very fine fritted disc. The filtrate was concentrated to approximately 5 mL and crystals were grown by slow diffusion of *i*Pr₂O into this MeCN solution. Crystal data: C₄₉H₇₃N₁₁O₁₂Pt, $M = 1203.7$, triclinic, $P-1$, $a = 12.589(1)$, $b = 17.733(2)$, $c = 26.447(2)$ Å, $\alpha = 105.942(1)$, $\beta = 96.895(1)$, $\gamma = 99.343(1)^\circ$, $V = 5520.7(8)$ Å³, $Z = 4$, $T = 173(2)$ K, $\mu = 2.61$ cm⁻¹, 39776 data, $R(\text{int}) = 0.0314$, $R1 = 0.0423$, $wR1 = 0.0507$, (16068 data, $I > 2\sigma I$), $R2 = 0.1113$, $wR2 = 0.1164$ (all data), $\text{GoF}(F^2) = 1.074$.

3.4.5 [Pt(3,5-*di-n*butylamidepyridine)₂(bipy)][ReO₄]₂



The receptor was also synthesized as the ReO_4^- salt in order to obtain further solid state information about the receptor:anion interaction. This complex was synthesized by refluxing $[\text{PtCl}_2(\textit{t}\text{butylbipy})]$ (0.050 g, 0.093 mmol) with 2 equivalents of both AgReO_4 (0.067 g, 0.187 mmol) and 3,5-*di-n*butylamidepyridine (0.052 g, 0.187 mmol) in 25 mL of MeCN for 48 hours. After cooling the reaction mixture to room temperature, the AgCl was removed by filtering the mixture through a Büchner filter fit with a very fine fritted disc. The filtrate was concentrated to approximately 5 mL and crystals were grown by slow diffusion of *i*Pr₂O into this MeCN solution. Crystal data: $\text{C}_{41}\text{H}_{54}\text{N}_8\text{O}_{16}\text{PtRe}_2$, $M = 1509.43$, triclinic, $P2_1/c$, $a = 26.098(6)$, $b = 26.380(6)$, $c = 15.158(4)$ Å, $\alpha = 90.00$ $\beta = 90.344(4)$, $\gamma = 90.00$ °, $V = 90.00$ Å³, $Z = 8$, $T = 173(2)$ K, $\mu = 7.376$ cm⁻¹, 44803 data, $R(\text{int}) = 0.0544$, $R1 = 0.1103$, $wR1 = 0.0694$, (14987 data, $I > 2\sigma I$), $R2 = 0.1887$, $wR2 = 0.1548$ (all data), $\text{GoF}(F^2) = 1.106$.

3.4.6 [Pt(C₆H₅CO₂)₂(*t*butylbipy)]

The product of [Pt(C₆H₅CO₂)₂(*t*butylbipy)] was not the expected product. Initially 5 mL of 5% DMSO 95% MeCN solution was prepared containing [Pt(3,5-*di-n*butylamidepyridine)₂(*t*butylbipy)][PF₆]₂ (0.050g, 0.038 mmol) and two equivalents of tetrabutylammonium benzoate (0.028g, 0.076 mmol). The X-ray quality crystals were obtained by slow diffusion of *i*Pr₂O into the solution. Crystal data: C₃₂H₃₄N₂O₄Pt, *M* = 705.7, monoclinic, *P*2₁/*c*, *a* = 12.864(15), *b* = 24.05(3), *c* = 9.385(11) Å, β = 92.33(2)°, *V* = 5520.7(8) Å³, *Z* = 4, *T* = 293(2) K, μ = 4.87 cm⁻¹, 7864 data, R(int) = 0.1972, R1 = 0.0943, wR1 = 0.1228, (2286 data, I > 2σI), R2 = 0.2273, wR2 = 0.2392 (all data), GoF(*F*²) = 1.074. The poor quality and relatively small size of the crystals resulted in a structure solution which should be considered preliminary; only the Pt atom could be refined anisotropically. The determination did however allow for identification of basic atom connectivity.

3.4.7 Titration Methods

A 1.0×10^{-2} M solution of host was made by dissolving [Pt(3,5-*n*butylamidepyridine)₂(*t*butylbipy)][PF₆]₂ (0.0060 g, 0.005 mmol) in 0.5 mL of the desired solvent. The 5.0×10^{-2} M guest solution was made by dissolving the tetrabutylammonium salt of the desired anion in 1.0 mL of the desired solvent.

The ¹H NMR titrations were performed by the stepwise addition of 10 μL (0.1 equivalents) aliquots of the guest solution to the receptor solution until minimal change in chemical shift was observed (approximately 3 equivalents). This was followed by the addition of 50 μL (0.5 equivalents) until saturation occurred (approximately 7 equivalents). The amide proton was followed throughout the titration and the association constants were obtained using winEQNMR.⁶⁶

For further details about the titrations see section 2.4.7.

Chapter 4

Urea Receptor

4.1 Introduction

Albrecht et. al. have studied the complexation of a biphenyl based receptor with NO_3^- where the amide groups have been systematically replaced by urea groups, as shown in Figure 4.1. They have shown the stepwise addition of hydrogen bond donors increases the free enthalpy of complexation by approximately 3 kJ/mol. That is, increasing the number of hydrogen bond donor sites interacting with the guest molecule has an additive effect on the observed association constant.⁷⁰

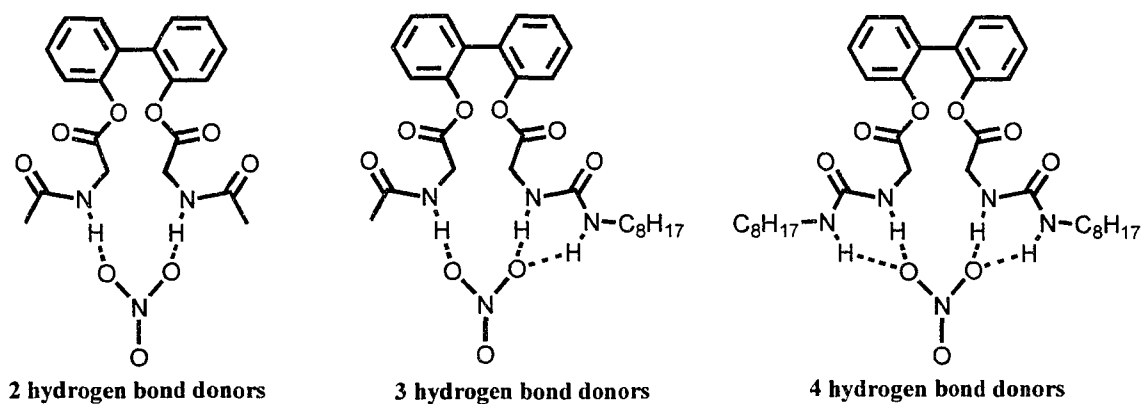


Figure 4.1 Systematic replacement of amide by urea functional groups in a biphenyl receptor, by Albrecht, demonstrating the effect of increasing the number of hydrogen bond donors.

In chapter 2, it was shown that the amide based receptor **1** was an effective host for oxo-anions. The receptor was flexible with a single hydrogen bond donor site on each ligand. This allowed for the interaction with the incoming anion to be optimized due to

independent placement of each hydrogen bond donor site. However, the magnitude of the association constants measured for the receptor:anion interaction was not substantial.

In chapter 3, it was shown that receptor **2** was preorganized for a 1:2 interaction with the incoming anions. This was accomplished by placing two hydrogen bond donor amide groups on each ligand. However, the rearrangement of the hydrogen bond donor sites caused a loss of flexibility in the receptor. The independent adjustments and fine tuning of the ligand placement, required for an increase in association with anions, was lost. The overall effect was a decrease in association constants.

In this chapter, a second attempt is made to increase the effectiveness of our platinum(II) based complex as an anion receptor. This time an increase in association with the anions will be attempted by maintaining the flexibility of receptor **1** while increasing the number of hydrogen bond donor sites. The use of urea functional groups provides the logical progression from the amide group. The urea group offers double the number of hydrogen bond donor sites. The electron donating ability of the urea is another beneficial feature for the inertness of the Pt-N bond.

In order to maintain consistency between receptor **1** and **3**, correct placement of the urea group within the receptor is important. The urea should be at an equivalent position from the platinum(II) centre and converge towards the inside of the binding site. Simply placing the hydrogen bond donors sites on to the pyridine ring would result in the bottom N-H being closer and pointing at a 60 ° angle above the plane of the platinum(II) (Figure 4.2).

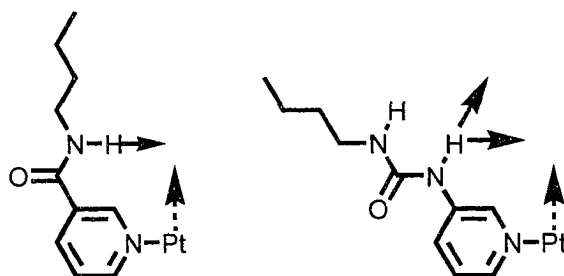


Figure 4.2 The placement of the functional group on the pyridine ligand is important for convergence towards the coordinating anion.

Therefore, in order to have the analogous distance between the bottom N-H of the urea and the N-H of the amide the pyridine ring is replaced with an *isoquinoline* fused ring system. Figure 4.3 demonstrates the overlap in hydrogen bond donor distances from the metal centre between pyridine and *isoquinoline*.

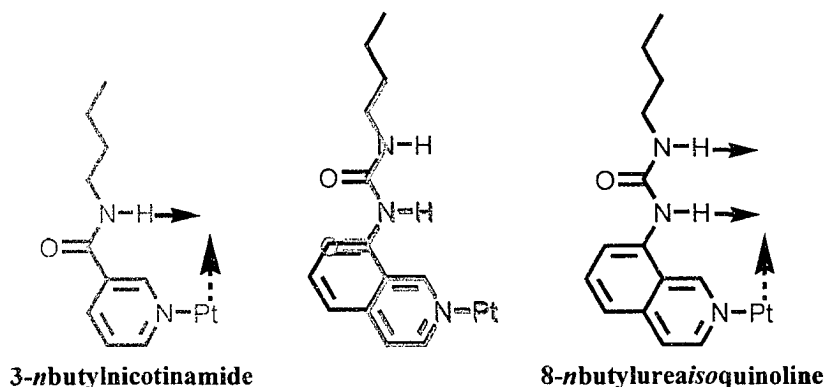


Figure 4.3 Comparison of the N-H hydrogen bond donor position in the first generation amide based receptor **1** and the third generation urea based receptor **3**.

Once again, *n*butyl chains will be employed as suitable R groups for the urea *isoquinoline* ligands. The length of the carbon chain should aid in the solubility of the receptor as well as not hinder the ability to produce X-ray quality crystals. Finally, the counterion for this receptor is BF_4^- . It has been shown that this anion behaves much the

same as the PF_6^- anion used in receptor 1 and 2.⁶⁰ Overall, our third generation receptor is $[\text{Pt}(8\text{-}n\text{butylureaisoquinoline})_4][\text{BF}_4]_2$, 3, with the structure shown in Figure 4.4.

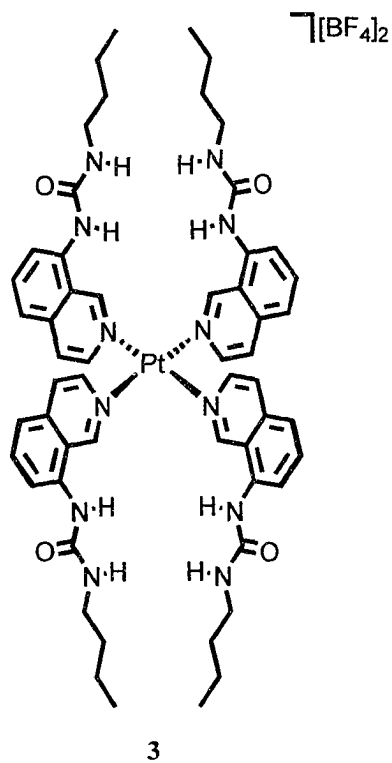


Figure 4.4 Third generation receptor $[\text{Pt}(8\text{-}n\text{butylureaisoquinoline})_4][\text{BF}_4]_2$, 3, arbitrarily in the 1,2-alternate conformation.

4.2 Results and Discussion

4.2.1 Synthesis and Characterization of $[\text{Pt}(8\text{-}n\text{butylureaisoquinoline})_4][\text{BF}_4]_2$ (3)

Synthesis

The 8-*n*butylureaisoquinoline ligand for the third generation receptor was synthesized from 8-aminoisoquinoline and *n*butylisocyanate. The 8-aminoisoquinoline was first prepared by literature methods starting from 5-aminoisoquinoline, as shown in Figure 4.5.^{71,72}

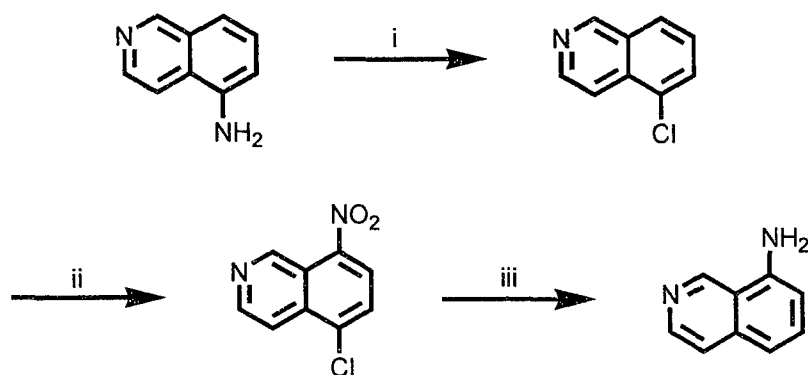


Figure 4.5 Synthesis of 8-aminoisoquinoline from 5-aminoisoquinoline. i) $\text{NaNO}_2(\text{aq})$ at $0\text{ }^\circ\text{C}$; CuCl in $\text{HCl}(\text{conc})$ at $75\text{ }^\circ\text{C}$, ii) KNO_3 in $\text{H}_2\text{SO}_4(\text{conc})$, iii) $\text{H}_2\text{N}=\text{NH}_2$ and Pd on carbon in EtOH at reflux.

The 8-aminoisoquinoline was dissolved in CH_2Cl_2 and excess *n*butylisocyanate was added. The solution was stirred for 5 days to obtain 8-*n*butylurea isoquinoline in quantitative yield (Figure 4.6).

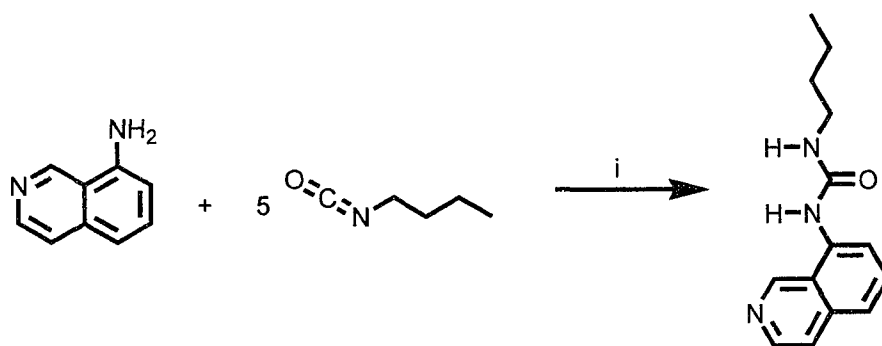


Figure 4.6 Synthesis of 8-*n*butylurea isoquinoline. i) Stir in CH_2Cl_2 with excess *n*butylisocyanate.

Receptor **3**, was synthesized by refluxing four equivalents of ligand, 2.2 equivalents of AgBF_4 with $[\text{PtCl}_2(\text{C}_2\text{H}_5\text{CN})_2]$ in MeCN . $[\text{Pt}(\text{8-}n\text{butylurea isoquinoline})_4][\text{BF}_4]_2$ was collected in 60 % yield (Figure 4.7).

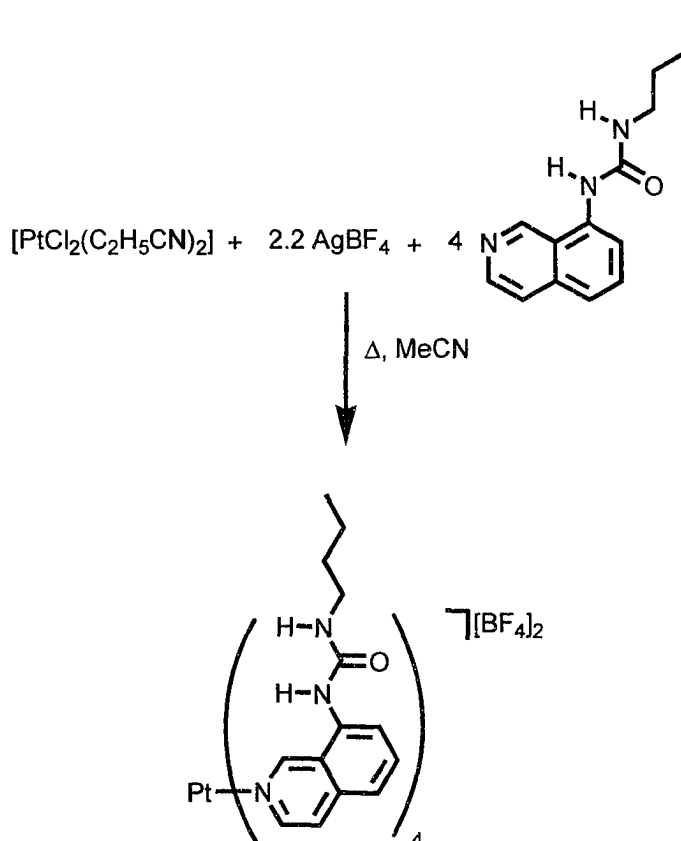


Figure 4.7 Synthesis of 3.

¹H NMR Spectroscopy

The ¹H NMR spectrum of 8-*n*butylureaisoquinoline in DMSO-*d*₆ shows chemical shifts varying from 9.49 to 0.91 ppm. The aromatic protons produce four doublets representing H_b, H_c, H_d and H_f with chemical shifts of 8.47, 7.76, 7.53 and 8.12 ppm, respectively. The triplet from H_e has a chemical shift of 7.65 ppm while the singlet from H_a appears at 9.49 ppm. The chemical shifts from the urea protons are found at 8.84 and 6.58 ppm for H_g and H_h respectively. The protons on the *n*butyl chain produce chemical shifts between 3.15 and 0.91 ppm, see Figure 4.8.

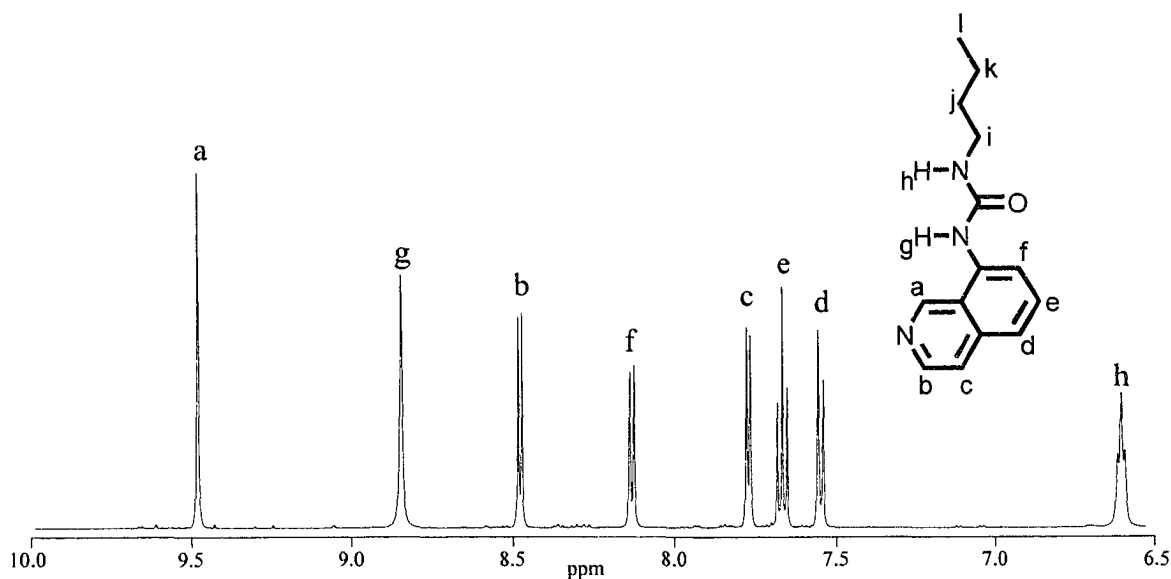


Figure 4.8 ^1H NMR spectrum of the aromatic region for 8-*n*-butylureaisoquinoline in $\text{DMSO-}d_6$.

The ^1H NMR spectrum of **3** in $\text{DMSO-}d_6$ shows protons H_a , H_g and H_h are singlets with chemical shifts of 9.51, 8.77 and 6.33 ppm. Doublets are seen for H_b , H_c , H_d and H_f with chemical shifts of 8.60, 7.93 and 7.70 ppm (overlapping H_d and H_f). Finally, H_e is a triplet with a chemical shift of 7.85 ppm, as shown in Figure 4.9.

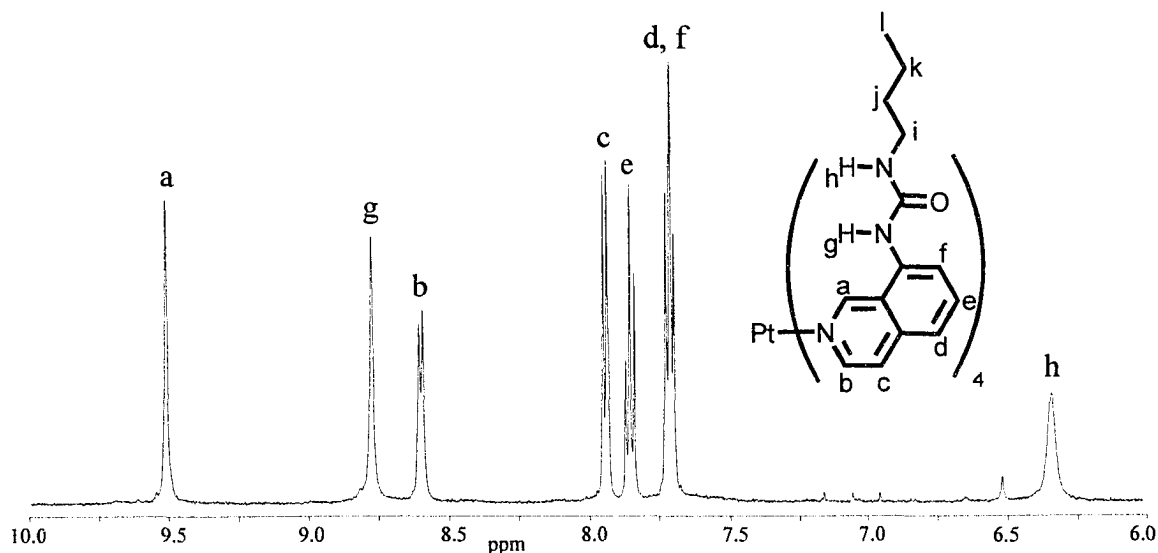


Figure 4.9 Partial ^1H NMR spectrum of **3**, in $\text{DMSO-}d_6$.

The coordination of four of these ligands to a platinum(II) metal centre causes some perturbations in the chemical shifts of the protons. The chemical shifts for proton H_a to H_e all shift to a higher frequency by varying amounts. The shift to a higher frequency upon coordination to platinum(II) is due the electropositive metal centre. The electron rich ligand donates its electron density to the metal causing the protons on the aromatic ring to become deshielded and shift to a higher frequency (Table 4.1).

Table 4.1 Comparison of ¹H chemical shifts of the ligand before and after coordination to Pt(II).

Proton	Receptor δ(ppm)	Ligand δ(ppm)	Δ δ
a	9.51	9.49	0.02
b	8.60	8.47	0.13
c	7.93	7.76	0.17
d	7.70	7.53	0.17
e	7.85	7.65	0.20
f	7.70	8.12	-0.42
g	8.77	8.84	-0.07
h	6.33	6.58	-0.25
i	2.75	3.15	-0.40
j	1.25	1.47	-0.22
k	1.20	1.35	-0.15
l	0.83	0.91	-0.08

Mass Spectrometry

The ESI-TOF mass spectrum of the protonated 8-*n*butylurea*iso*quinoline was obtained with the addition of formic acid as the source of protons from a 1:1 mixture of MeOH and H₂O. The exact mass is 244.1452 and the calculated mass is 244.1450 which is within 0.9 ppm of the exact mass.

The isotopic profile of receptor **3** as the $[3\text{-BF}_4]^+$ is shown in Figure 4.10. The exact mass for $[3\text{-BF}_4]^+$ is 1254.5168 and the calculated mass is within 0.4 ppm of this value.

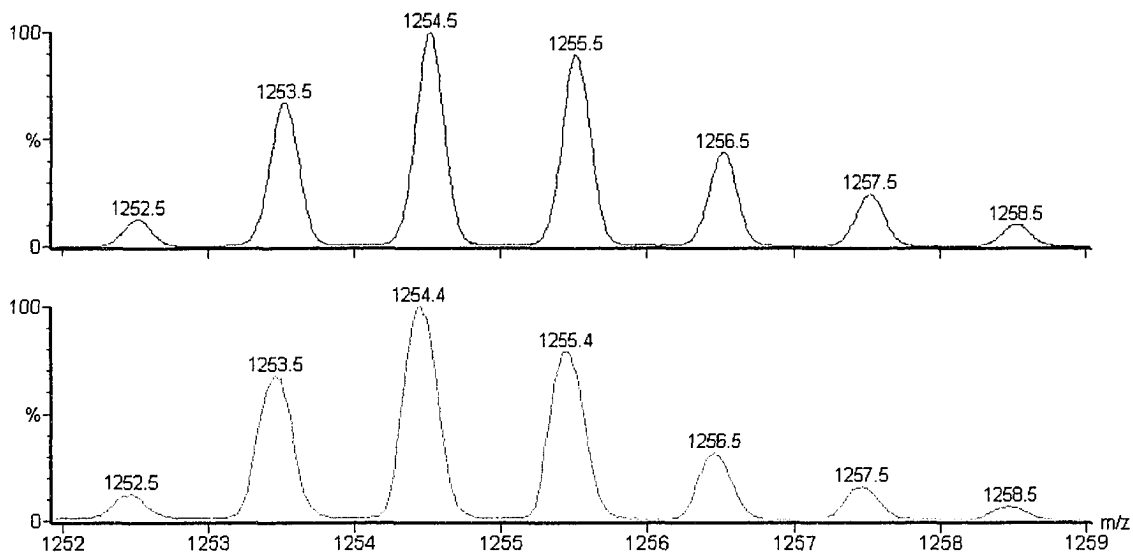


Figure 4.10 The calculated (top) and observed (bottom) mass spectra of **3** as the $[3\text{-BF}_4]^+$ species.

X-Ray Crystallography of $[\text{Pt}(8\text{-nbutylureaisoquinoline})_4][\text{BF}_4]_2$

X-ray quality colourless block crystals of **3** were obtained by slow diffusion of $i\text{PrO}_2$ into a DMF solution. The structure is in the 1,2-alternate conformation with BF_4^- interacting in each binding site through both hydrogen bonds and electrostatic interactions.

A total of eight hydrogen bonding interactions are present with varying N-H...F BF_3^- lengths ranging from 2.95 to 3.27 Å. The angles involved in these interactions vary between 145 ° and 161 °. The electrostatic interactions occur above and below the platinum(II) metal centre at Pt... BF_4^- distances of 4.36 and 4.37 Å (Figure 4.11).

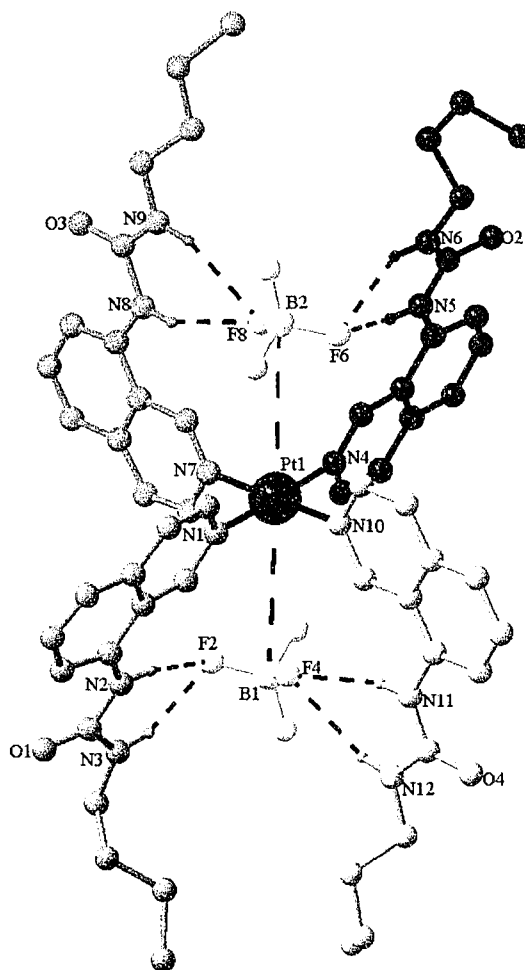


Figure 4.11 X-ray crystal structure of **3** in the 1,2-alternate conformation. N-H...F distances (Å) and angles (°): N(2)...F(2) 2.95, N(2)-H(2A)...F(2) 162; N(3)...F(2) 2.99, N(3)-H(3A)...F(2) 162; N(5)...F(6) 2.97, N(5)-H(5A)...F(6) 155; N(6)...F(6) 2.96, N(6)-H(6B)...F(6) 146; N(8)...F(8) 2.98, N(8)-H(8A)...F(8) 153; N(9)...F(8) 3.27, N(9)-H(9A)...F(8) 148; N(11)...F(4) 3.07, N(11)-H(11A)...F(4) 160; N(12)...F(4) 3.32, N(12)-H(12A)...F(4) 147. Pt...B distances (Å) : Pt(1)...B(1) 4.37; Pt(1)...B(2) 4.36.

4.2.2 Binding Studies

¹H NMR Titrations

The association constants for receptor **3** were obtained from ¹H NMR titrations. The titrations were carried out in two sets of solvent systems, the less polar being 35%

MeNO₂-*d*₃ 65% DMF-*d*₇ and the more polar being neat DMSO-*d*₆. The very high association constants obtained from some of the anions demanded a more polar solvent system to determine the association constants by this method.

Two different titration methods were used depending on the type of receptor:anion interaction during the NMR titrations. When the interaction was fast on the NMR timescale, an average set of peaks was obtained representing both the complexed and uncomplexed receptor. In this case, the titrations involved the stepwise addition of anion to the receptor until saturation occurred. The association constants were then obtained using non-linear least squares curve fitting analysis. The Cl⁻, Br⁻, I⁻, ReO₄⁻, CF₃SO₃⁻, NO₃⁻ and H₂PO₄⁻ anions fit into this category.

The second type of receptor:anion interaction obtained with this receptor was one that is slow on the NMR timescale. The ¹H NMR spectrum showed two separate sets of peaks, one representing the complexed receptor and the other the uncomplexed receptor. The association constants for this type of interaction were obtained by a single point analysis and simple integration of the complexed and uncomplexed peaks. The SO₄²⁻ anion falls into this category.

The solvent system of 35% MeNO₂-*d*₃ 65% DMF-*d*₇ was tested with Cl⁻, Br⁻, I⁻, ReO₄⁻, CF₃SO₃⁻, NO₃⁻ and H₂PO₄⁻. The titrations with ReO₄⁻, CF₃SO₃⁻ and NO₃⁻ produced minimal changes in the chemical shift therefore, association constants were not obtained for these anions. The titration with Cl⁻, Br⁻, I⁻ and H₂PO₄⁻ produced titration curves that were too sharp and non-linear least square analysis was not attainable. In order to decrease the association between the receptor and the anion to a measurable level a more polar solvent, DMSO-*d*₆, was used.

Overall the binding constants obtained with receptor **3** are much higher than the previous receptors tested. In table 4.2, the association constants for the halides show a 1:2 binding mode. The binding constant for Cl⁻ is the highest of the halides tested with $K_1 = 11693 \text{ M}^{-1}$ and $K_2 = 2223 \text{ M}^{-1}$. The Br⁻ and I⁻ have relatively similar binding constants for K_1 (~ 1400 M^{-1}) while K_2 for Br⁻ is a magnitude higher than I⁻ (450 vs. 52 M^{-1}). The difference in association between the halides suggests the Cl⁻ is the best fit for the binding site.

Table 4.2 Association constants, K_a (M^{-1}), obtained for **3** with various anions, at 30 °C (error < 10%).

Anion	K_a (M^{-1})		Solvent
CF ₃ SO ₃ ⁻	nil		MeNO ₂ - <i>d</i> ₃ / DMF- <i>d</i> ₇ 35:65 v/v
ReO ₄ ⁻	nil		MeNO ₂ - <i>d</i> ₃ / DMF- <i>d</i> ₇ 35:65 v/v
NO ₃ ⁻	nil		MeNO ₂ - <i>d</i> ₃ / DMF- <i>d</i> ₇ 35:65 v/v
Cl ⁻	K_1 11693	K_2 2223	DMSO- <i>d</i> ₆
Br ⁻	K_1 1364	K_2 450	DMSO- <i>d</i> ₆
I ⁻	K_1 1431	K_2 52	DMSO- <i>d</i> ₆
H ₂ PO ₄ ⁻	>10 ⁵		DMSO- <i>d</i> ₆
SO ₄ ²⁻	>10 ⁵		DMSO- <i>d</i> ₆

When the changes in chemical shift of all the protons are monitored throughout the titrations involving the halides, protons H_g, H_h and H_a show the largest changes in chemical shifts. The perturbation of these protons suggests the binding of the anion is taking place in the designed binding sites. This includes both the hydrogen bond donors

in the urea group as well as the relatively acidic C-H proton H_a . All other protons show negligible changes in chemical shifts (Figure 4.12).

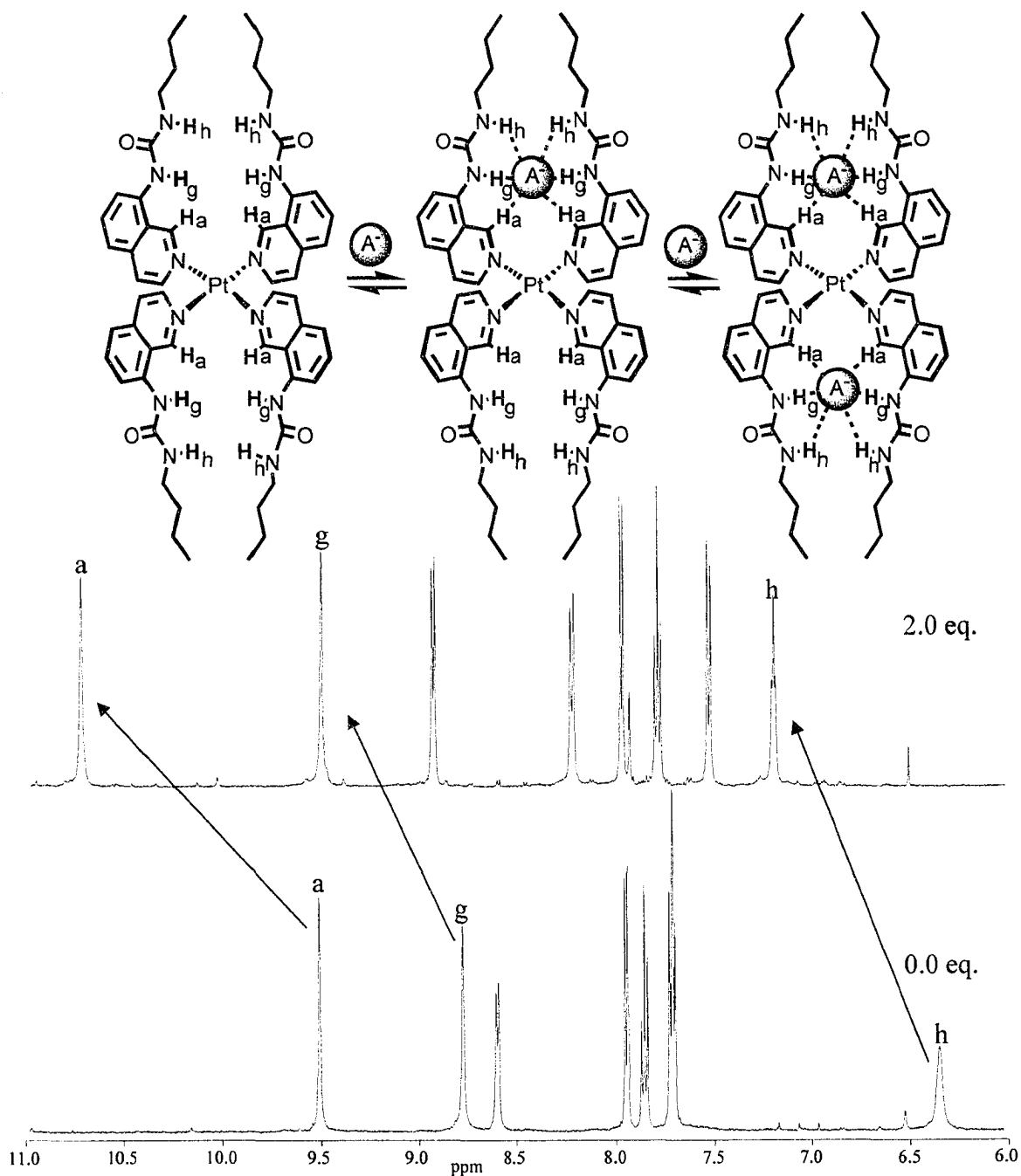


Figure 4.12 ^1H NMR spectra from the titration of **3** with Cl^- at 0 and 2 equivalents. Arrows depict the change in chemical shift observed for each respective proton found in the binding site.

Table 4.2 also shows very high binding constants for H_2PO_4^- and SO_4^{2-} . These anions are very tightly bound in a 1:1 binding mode. The rate of binding for H_2PO_4^- is close to the NMR timescale resulting in a broad spectrum at sub-stoichiometric amount of anion as well as peaks representing both the complexed and uncomplexed receptor. At equimolar amounts of receptor and anion the peaks become sharp, the uncomplexed peaks disappear and no further change in chemical shift is observed, as shown in Figure 4.13. Therefore, saturation occurs at a 1:1 ratio of receptor to anion likely indicative of a cone conformation.

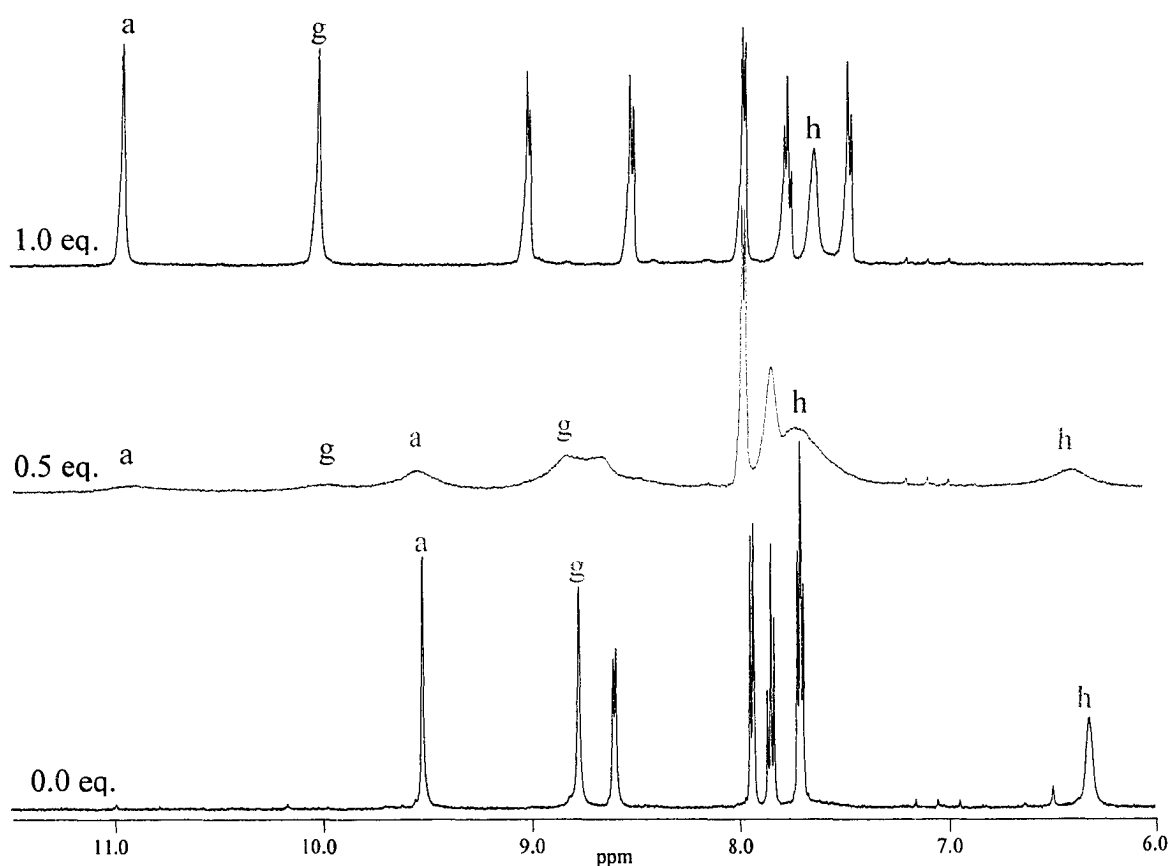


Figure 4.13 Spectra from the titration of **3** with H_2PO_4^- at several different points. Uncomplexed peaks become broad while new broad complexed peaks grow in. At 1:1 ratio the uncomplexed peaks disappear and the complexed peaks sharpen. Red lettering represents uncomplexed receptor while blue represents complexed.

Two peaks are observed upon titration with the SO_4^{2-} anion, indicative of a slow receptor:anion complexation rate. At 0.5 equivalents of anion, the complexed and uncomplexed peak ratio is 1:1. As anion is added to the receptor solution complete complexation is occurring with the receptor. The strong receptor:anion association shows saturation at one equivalent, once again, indicative of a cone conformation (Figure 4.14).

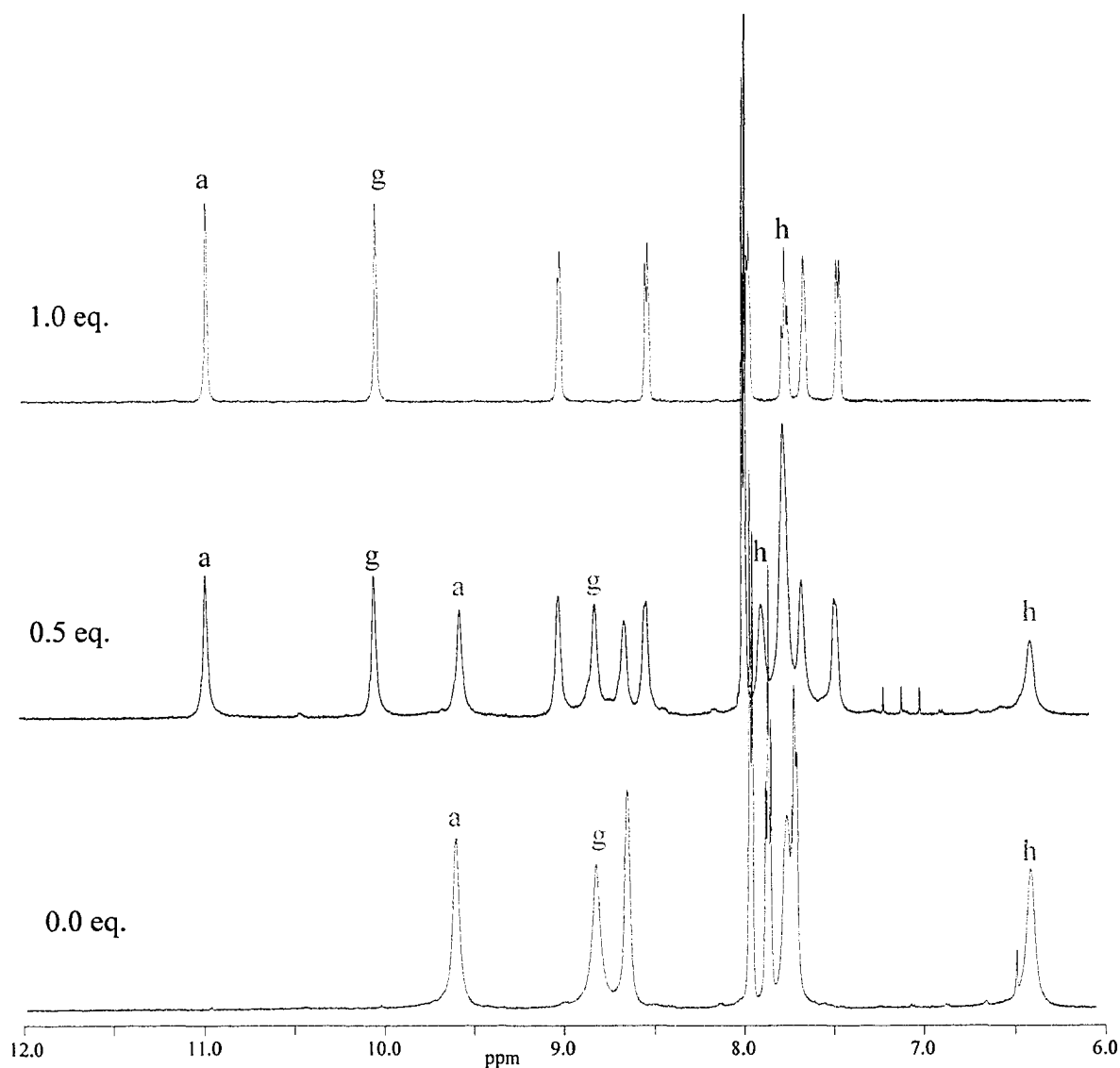


Figure 4.14 Spectra from the titration of **3** with SO_4^{2-} at several different points. Sharp complexed peaks grow as anion is added. At 1:1 ratio the uncomplexed peaks disappear with only the complexed peaks remaining. Red lettering represents uncomplexed receptor while blue represents complexed.

X-Ray Crystallography of [Pt(8-nbutylureaisoquinoline)₄][Cl]₂

Single crystals of [Pt(8-*n*butylureaisoquinoline)₄][Cl]₂ suitable for X-ray diffraction were grown over a few days by slow evaporation of a DMF solution. The results from this experiment show the receptor in a 1,2-alternate conformation interacting with two chloride anions (Figure 4.15). This 1:2 binding mode allows for an overall neutral complex.

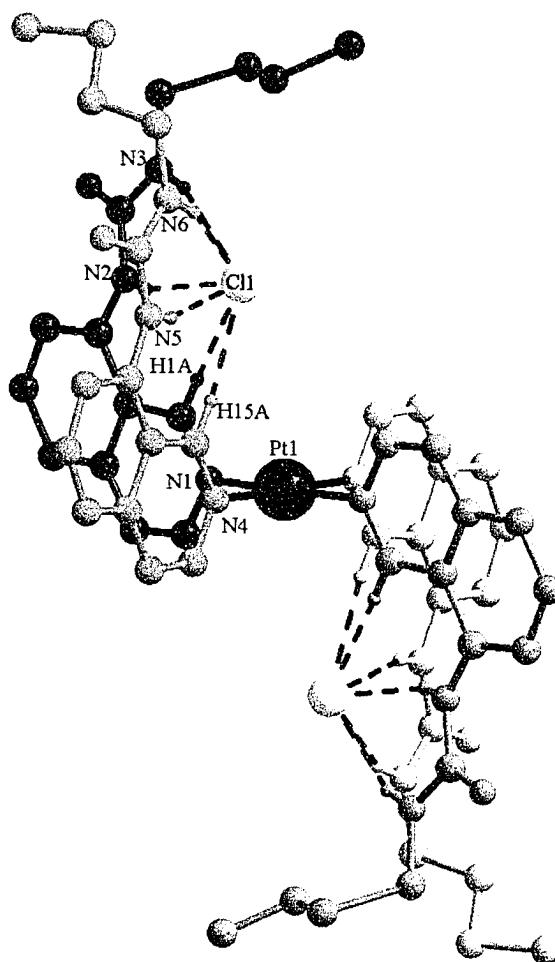


Figure 4.15 Side view of [Pt(8-*n*butylureaisoquinoline)₄][Cl]₂ in the 1,2-alternate conformation showing Cl⁻ pulled into the hydrogen bonding pockets, off-set from direct alignment with the platinum(II).

Each chloride anion is interacting through hydrogen bonds with two separate urea groups. The hydrogen bond distances between the anion and the N-H groups range from

3.33 to 3.40 Å and are at angles ranging from 153 ° to 160 °. There is also significant interaction between the anions and the relatively acidic C-H proton found on the *isoquinoline* between the nitrogen of the ring and the urea functional group. This interaction occurs at a distance of 3.50 and 3.53 Å and at angles of 169 ° and 175 ° (Figure 4.16). A complete list of hydrogen bond interactions is shown in Table 4.3.

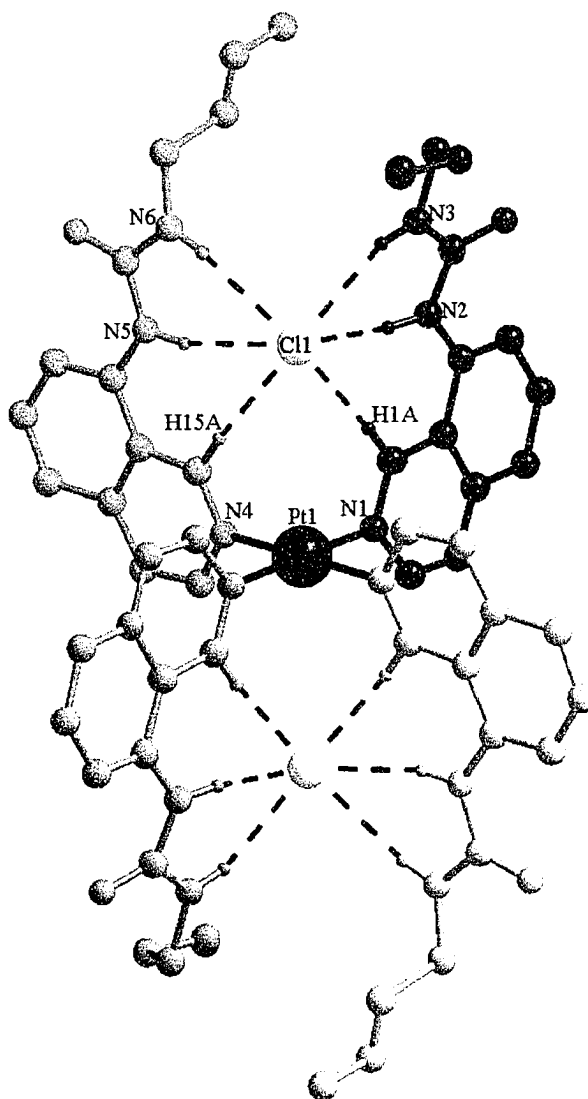


Figure 4.16 X-ray crystal structure of $[\text{Pt}(8\text{-}n\text{butylureaisoquinoline})_4][\text{Cl}]_2$ in the 1,2-alternate conformation with a total of 12 hydrogen bonds with the Cl⁻ anions.

Table 4.3 Observed Hydrogen bond distances (Å) and angles (°) for [Pt(8-*n*butylureaisoquinoline)₄][Cl]₂.

Hydrogen Bond	Cl...E Distance (Å)	Cl...H-E Angle (°)
red urea upper NH	3.34	158.2
red urea lower NH	3.33	155.4
red aromatic CH	3.50	175.7
blue urea upper NH	3.37	153.6
blue urea lower NH	3.40	160.4
blue aromatic CH	3.53	169.8

Therefore, a total of six hydrogen bonds are formed between each anion and the receptor. The anions are pulled towards the hydrogen bonding donors sitting in a pocket, slightly off-set from directly above the platinum(II) metal centre. The electrostatic interactions between the anion and the metal centre are at a distance of 4.06 and 4.21 Å (Figure 4.15).

X-Ray Crystallography of [Pt(8-*n*butylureaisoquinoline)₄][SO₄]

X-ray quality single crystals of [Pt(8-*n*butylureaisoquinoline)₄][SO₄] were obtained as colourless blocks by slow evaporation of a DMF solution. The structure shows a cone conformation where all four ligands are oriented in the same direction. One sulphate anion is nestled into the pocket formed by the receptor. There are a total of eight N-H...O and four C-H...O hydrogen bond interactions as shown in Figure 4.17.

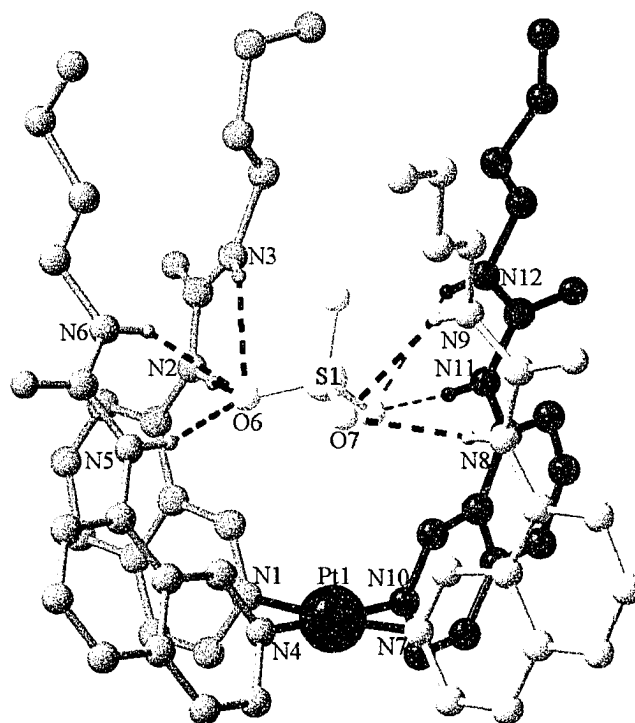


Figure 4.17 X-ray crystal structure of $[\text{Pt}(8\text{-}n\text{butylureaisoquinoline})_4][\text{SO}_4]$ in the cone conformation.

The receptor possesses 4-fold symmetry while the symmetry of the sulphate is 3-fold. The structure shows the green ligand is tilted out of the plane by 29° in order to compensate for the difference in symmetry. This allows all the ligands to maximize their hydrogen bonding with the anion. The urea groups from the green and red ligands form four hydrogen bonds to a single oxygen of the anion while blue and orange ligands form separate sets of hydrogen bonds to the other two oxygen atoms (Figure 4.18).

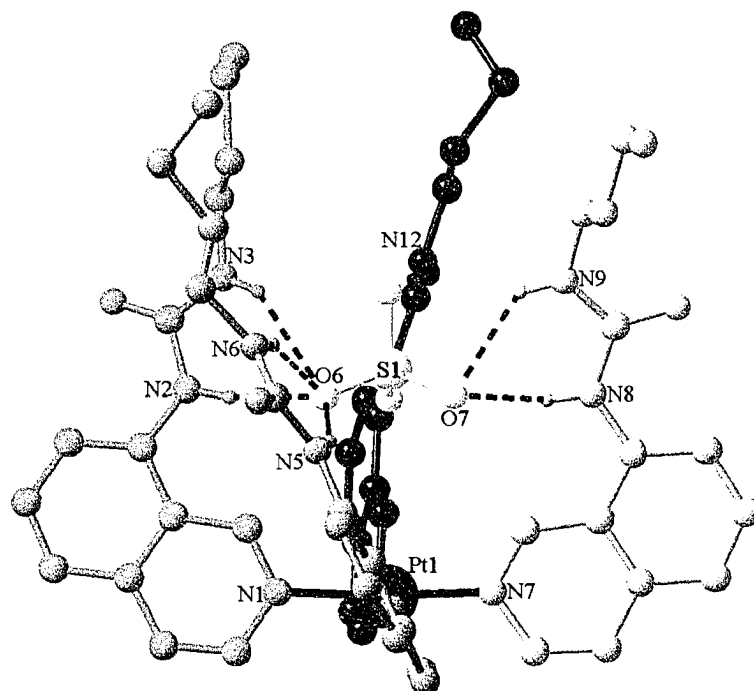


Figure 4.18 Front view of $[\text{Pt}(8\text{-}n\text{butylureaisoquinoline})_4][\text{SO}_4]$ where the green ligand is tilted 29° out of the plane in order hydrogen bond to the same oxygen of the SO_4^{2-} as the red ligand.

The N-H...O hydrogen bonding distances for the lower N-H of the urea group range from 2.89 to 2.94 Å with angles ranging from 137° to 168° . The N-H...O hydrogen bonding distances for the upper N-H of the urea group range from 2.98 to 3.23 Å with angles ranging from 132° to 150° . Hydrogen bonds also occur between the relatively acidic C-H *ortho* proton found between the nitrogen of the *isoquinoline* and the urea groups and the oxygen atoms of the sulphate. These interactions fall within acceptable ranges with distances of 3.03 to 3.36 Å and angles of 139° to 167° (Table 4.4).

Table 4.4 Observed Hydrogen bond distances (Å) and angles (°) for [Pt(8-*n*butylurea*isoquinoline*)₄][SO₄].

Hydrogen Bond	O...E Distance (Å)	O...H-E Angle (°)
red urea upper NH	3.23	144.4
red urea lower NH	2.92	163.7
red aromatic CH	3.30	139.4
green urea upper NH	2.98	150.8
green urea lower NH	2.93	157.9
green aromatic CH	3.33	167.4
orange urea upper NH	3.06	132.2
orange urea lower NH	2.94	137.9
orange aromatic CH	3.36	147.1
blue urea upper NH	3.23	140.1
blue urea lower NH	2.89	168.0
blue aromatic CH	3.03	164.8

The electrostatic interactions in this structure shows a Pt(II)...S(1) distance of 4.41 Å whilst the Pt(II)...O(8) distance with the oxygen atom found directly above the platinum(II) metal centre is found at a distance of 3.72 Å (Figure 4.19).

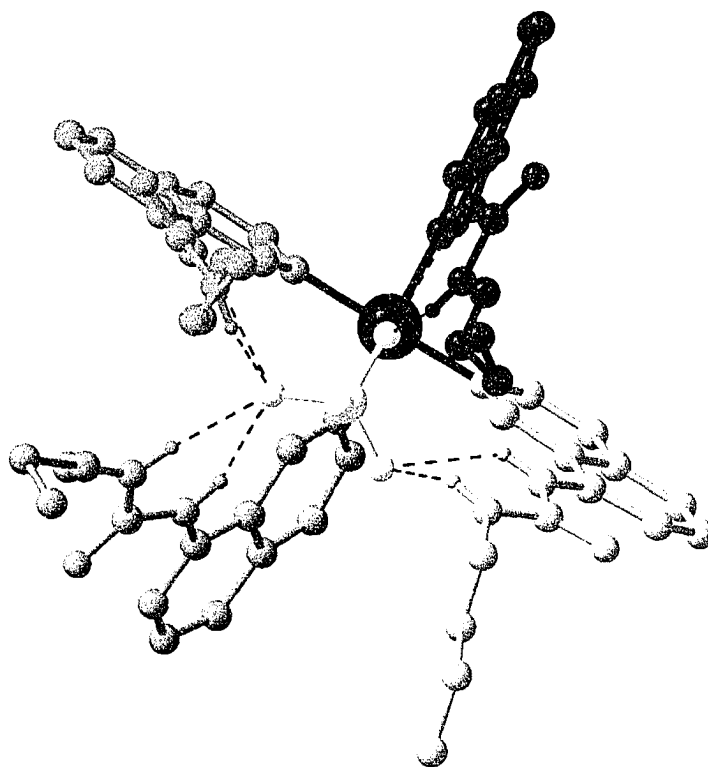


Figure 4.19 Top view of $[\text{Pt}(8\text{-}n\text{butylurea-isoquinoline})_4][\text{SO}_4]$ where one oxygen, O(8), from the SO_4^{2-} is directly over top of the platinum(II) metal centre.

4.3 Conclusions

This third generation receptor maintains the flexibility of the first generation receptor whilst incorporating twice as many hydrogen bond donor units. This was accomplished through the use of urea groups. The correct placement of the hydrogen bond donor groups is obtained by replacing the pyridine with *isoquinoline* units. The electron donating ability of the urea group also assisted in maintaining the inertness of the Pt-N coordinate bond even in very polar solvents such as DMSO.

The use of butyl groups did not maintain the solubility of the receptor in less polar organic solvents. The least polar solvent system able to solvate the receptor was 35% MeNO_2 65% DMF. This solvent system was too polar to measure the association

constants for ReO_4^- , CF_3SO_3^- and NO_3^- . However, the association constants for Cl^- , Br^- , I^- , H_2PO_4^- and SO_4^{2-} were too high to measure in this solvent system, and therefore they were obtained from DMSO.

The solution data obtained for this third generation receptor, **3**, showed there are two categories. First, the halides all show 1:2 binding with relatively high binding constants. The highest binding in this category is seen with Cl^- . The second category is the tetrahedral oxo-anions H_2PO_4^- and SO_4^{2-} which bind in a 1:1 ratio. These two anions are very strongly coordinating with saturation occurring at one equivalent and association constant $>10^5$. Therefore, the solution data shows two types of conformations were attained with a single receptor.

The conformational flexibility of the receptor is also shown in the solid state. The 1,2-alternate conformation is observed with the binding of Cl^- while the cone conformation is obtained upon coordination of SO_4^{2-} .

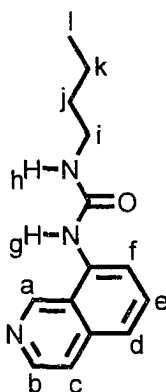
Overall, the association constants obtained for receptor **3** are much higher compared to the previous receptors **1** and **2**, however deviation from the Hofmeister series was not obtained.

4.4 Experimental

4.4.1 General Methods

See section 2.4.1 for general methods used. The exception to this is the sample solution for the mass spectrometry was a 1:1 solvent mixture of MeOH and H_2O .

4.4.2 8-*n*Butylureaisoquinoline



Under an inert N₂ atmosphere 8-aminoisoquinoline (0.500 g, 3.47 mmol) was dissolved in 20 mL of dry CH₂Cl₂. Five equivalents of *n*butylisocyanate (1.710 g, 17.34 mmol) was added and stirred for 5 days. The product was precipitated from solution upon the addition of hexanes as a yellow powder. The mixture was filtered by vacuum filtration and 0.767 g of clean ligand was obtained in 91% yield. HRMS (ESI): Calcd. for C₁₄H₁₈N₃O [L-H]⁺: 244.1452; Found: 244.1450. ¹H NMR data (500 MHz, MeCN-*d*₃ and DMSO-*d*₆):

¹H NMR data in MeCN-*d*₃

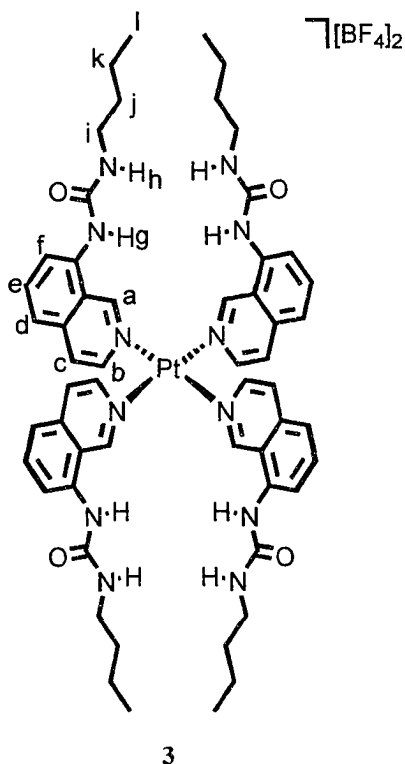
Proton	δ(ppm)	Multiplicity	Coupling Constant (Hz)	# of Protons
a	9.40	s	---	1
b	8.47	d	³ J _{bc} = 5.8	1
c	7.94	d	³ J _{cb} = 7.5	1
d	7.56	m	---	1
e	7.65	dd	³ J _{ed} ≈ ³ J _{ef} = 8.0	1
f	7.56	m	---	1
g	7.56	bs	---	1
h	5.58	bs	---	1
i	3.22	m	---	2

j	1.51	m	---	2
k	1.40	m	---	2
l	0.94	t	${}^3J_{lk} = 7.3$	3

${}^1\text{H}$ NMR data in DMSO- d_6

Proton	$\delta(\text{ppm})$	Multiplicity	Coupling Constant (Hz)	# of Protons
a	9.49	s	---	1
b	8.47	d	${}^3J_{bc} = 5.3$	1
c	7.76	d	${}^3J_{cb} = 5.3$	1
d	7.53	d	${}^3J_{de} = 7.7$	1
e	7.65	dd	${}^3J_{ed} \approx {}^3J_{ef} = 7.7$	1
f	8.12	d	${}^3J_{fe} = 7.7$	1
g	8.84	bs	---	1
h	6.58	bs	---	1
i	3.15	quartet	${}^3J_{ij} = 7.2$	2
j	1.47	tt	${}^3J_{ji} \approx {}^3J_{jk} = 7.2$	2
k	1.35	tq	${}^3J_{kj} \approx {}^3J_{kl} = 7.2$	2
l	0.91	t	${}^3J_{lk} = 7.2$	3

4.4.3 [Pt(8-*n*butylureaisoquinoline)₄][BF₄]₂

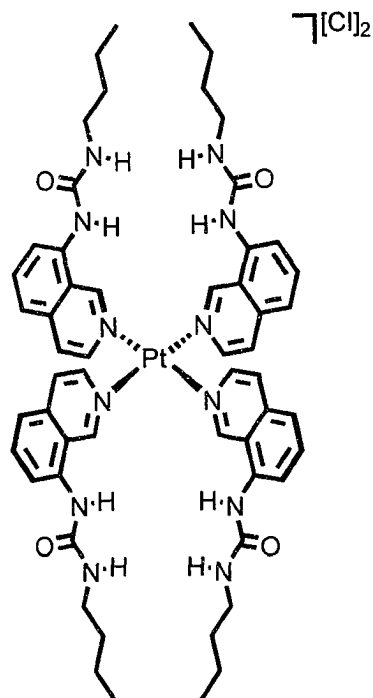


[PtCl₂(CH₃CH₂CN)₂] (0.081 g, 0.22 mmol) was refluxed with 4 equivalents of 8-*n*butylureaisoquinoline (0.210 g, 0.86 mmol) and 2.2 equivalents AgBF₄ (0.168 g, 0.47 mmol) in 15 mL of MeCN for 24 hours. The reaction mixture was cooled to room temperature and centrifuged. The solution was decanted and 1.5 mL of DMF was added to the gray-yellow pellet. The mixture was sonicated for 2 h and centrifuged once again. The yellow solution was collected and the solvent was removed by dynamic vacuum. The clean product was obtained as a yellow powder. Yield 0.174 g (60%). HRMS (ESI): Calcd. for C₅₆H₆₈BF₄N₁₂O₄Pt [3-BF₄]⁺: 1254.5168; Found: 1254.5164. Crystal data for [3]: colorless crystal, C₆₂H₈₂B₂F₈N₁₄O₆Pt, M= 1488.13, monoclinic, *Cc*, *a* = 10.7571(55), *b* = 18.7629(95), *c* = 34.3736(175) Å, β = 98.12(1)°, *V* = 6868 (6) Å³, *T* = 173(2) K, *Z* = 4, *R*₁ = 0.0656 (*I* > 2σ(*I*)), *wR*₂ = 0.0644 (all data).

¹H NMR data (500 MHz, DMSO-*d*₆):

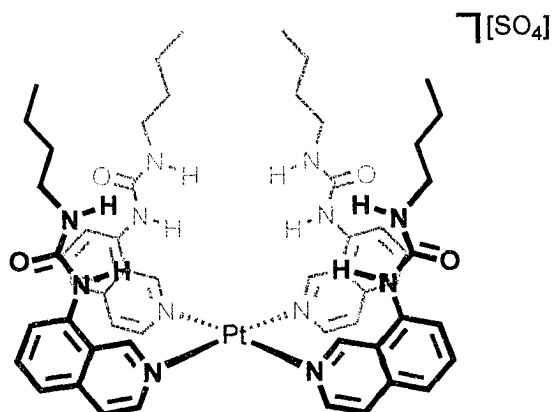
Proton	δ(ppm)	Multiplicity	Coupling Constant (Hz)	# of Protons
a	9.51	s	---	4
b	8.60	d	³ J _{bc} = 6.6	4
c	7.93	d	³ J _{cb} = 6.6	4
d	7.70	m	---	4
e	7.85	dd	³ J _{ed} ≈ ³ J _{ef} = 7.9	4
f	7.70	m	---	4
g	8.77	bs	---	4
h	6.33	bs	---	4
i	2.75	m	³ J _{gf} = 6.5	8
j	1.25	m	---	8
k	1.20	m	---	8
l	0.83	t	³ J _{lm} = 7.2	12

4.4.4 [Pt(8-*n*-butylureaisoquinoline)₄][Cl]₂



The synthesis of [Pt(8-*n*-butylureaisoquinoline)₄][Cl]₂ was an attempt to make the neutral [PtCl₂(8-*n*-butylureaisoquinoline)₂]. From the reaction mixture, X-ray quality crystals of [Pt(8-*n*-butylureaisoquinoline)₄][Cl]₂ were obtained. The synthesis involved refluxing [PtCl₂(CH₃CH₂CN)₂] (0.060g, 0.16 mmol) with 2 equivalents of 8-*n*-butylureaisoquinoline (0.077 g, 0.32 mmol) in 15 mL of DMF for 24 hours. The reaction mixture was concentrated to approximately 5 mL. X-ray quality crystals of [Pt(8-*n*-butylureaisoquinoline)₄][Cl]₂ were obtained by slow evaporation of the solution. Crystal data: colorless crystal, monoclinic, $P2_1/n$, $a = 20.029(5)$, $b = 21.508(5)$, $c = 21.244(5)$ Å, $\beta = 100.491(6)^\circ$, $V = 8999(4)$ Å³, $T = 173.5(1)$ K, $Z = 6$, $R1 = 0.0655$ ($I > 2\sigma(I)$), $wR2 = 0.1784$ (all data).

4.4.5 [Pt(8-*n*-butylureaisoquinoline)₄][SO₄]



The synthesis of [Pt(8-*n*-butylureaisoquinoline)₄][SO₄] was performed to attempt to grow X-ray quality crystals. The synthesis involved refluxing [PtCl₂(CH₃CH₂CN)₂] (0.060g, 0.16 mmol) with 4 equivalents of 8-*n*-butylureaisoquinoline (0.154 g, 0.63 mmol) and 1.2 equivalents AgSO₄ (0.060 g, 0.19 mmol) in 15 mL of CH₂Cl₂ for 24 hours. The reaction mixture was cooled to room temperature and centrifuged. The solution was decanted and 1.5 mL of DMF was added to the gray-yellow pellet. The mixture was sonicated for 2 h and centrifuged, once again. The yellow solution is collected and X-ray quality crystals were grown by slow evaporation of the solvent. Crystal data: colorless crystal, monoclinic, $P2_1/n$, $a = 20.700(3)$, $b = 11.4505(16)$, $c = 27.823(4)$ Å, $\beta = 96.944(3)^\circ$, $V = 6546.2(16)$ Å³, $T = 173.5(1)$ K, $Z = 4$, $R1 = 0.0750$ ($I > 2\sigma(I)$), $wR2 = 0.1646$ (all data).

4.4.6 Titration Methods

Two types of receptor:anion interactions were observed with this system, those that were fast on the NMR timescale (Cl^- , Br^- , I^- and H_2PO_4^-) and those that were slow (SO_4^{2-}). The titration required for the interactions that were fast on the timescale is the stepwise addition of anion. More specifically this involved the preparation of two solutions. The first contained **3** (0.0044 g, 3.25×10^{-6} mol) dissolved in 0.65 mL of $\text{DMSO-}d_6$. The second was a solution of desired anion as the desired salt. The solution contains 32.5×10^{-6} moles of the desired salt dissolved in 1.0 mL of $\text{DMSO-}d_6$. The ^1H NMR titration were carried out by the stepwise addition of 0.1 equivalents of anion to the receptor solution until minimal change in chemical shift was observed (approximately 3 equivalents). The titration was continued by the addition of 50 μL (0.5 equivalents) aliquots until complete saturation occurred (approximately 7 equivalents). The chemical shift of the bottom N-H proton, H_g , was monitored throughout the titration. For further information about the calculation of association constants by this type of titration see section 2.4.7.⁶⁶

The titration required for the kinetically slow interaction is a single point titration where one solution is required containing equimolar amounts of receptor and anion. The SO_4^{2-} anion was the only anion tested that required this type of titration. The titration involved preparing a single 5×10^{-3} M $\text{DMSO-}d_6$ solution (1.30 mL) containing both $[\text{Pt}(8\text{-}n\text{butylurea}i\text{soquinoline})_4][\text{BF}_4]_2$ (0.0087 g, 6.50×10^{-6} mol) and K_2SO_4 (0.0011 g, 6.50×10^{-6} mol). A single NMR experiment was recorded and the ratio of peaks from the bound and unbound receptor was obtained from the peak integration. This information was entered into the equation:

$$K_a = \frac{b[\textit{Receptor} : \textit{Anion}]}{u[\textit{Receptor}][\textit{Anion}]}$$

where u is the ratio of the unbound receptor and b is the ratio of the bound receptor and from this the association constant was determined directly.

Chapter 5

Model Compounds

5.1 Introduction

In previous chapters, it was shown that the homoleptic amide (1) and urea (3) based receptors exhibit free rotation around the Pt-N bond at room temperature. This was inferred from the ^1H NMR spectra of both 1 and 3, where an average set of proton peaks was observed for all of the possible *pseudo-calix[4]arene* conformations (Figure 5.1) even at low temperatures. In order to study the interconversion between the isomers and the relative stability of each conformation, the volume, or effective space an individual ligand assumes must be increased. In doing so, the internal rotational barrier may be increased to the point where ^1H NMR spectroscopy is a viable tool to study the conformational dynamics of these systems. This is tested with the aid of four model compounds.

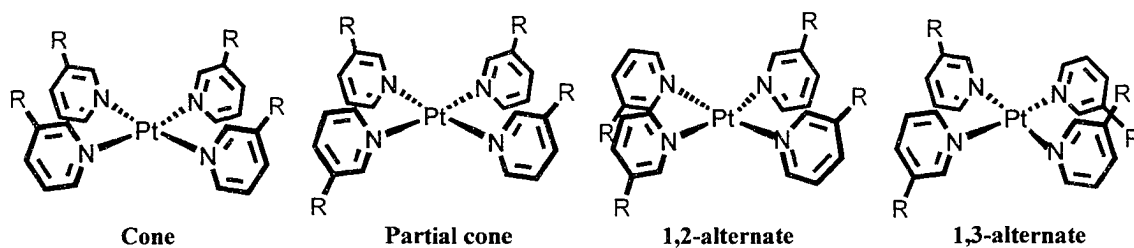


Figure 5.1 Schematic of the four *pseudo-calix[4]arene* conformations.

One method for increasing the effective volume of a ligand but still maintaining the functionality and basic structure of the receptor would be to extend the framework of the ligands themselves. This will initially be explored with model compound **4** as shown in Figure 5.2. It is based on extending the pyridine ring of receptor **1** into a quinoline ring. Presumably, the quinoline based complex would continue to possess free Pt-N rotation and attain all four *pseudo-calix[4]arene* conformations but the barrier for interconversion would be raised and thus the rate slowed enough to be observable on the NMR timescale at an accessible temperature. One potential drawback of the design of model compound **4** might be our ability to identify all four conformations (should they all be observable) simultaneously in a single ^1H NMR experiment.

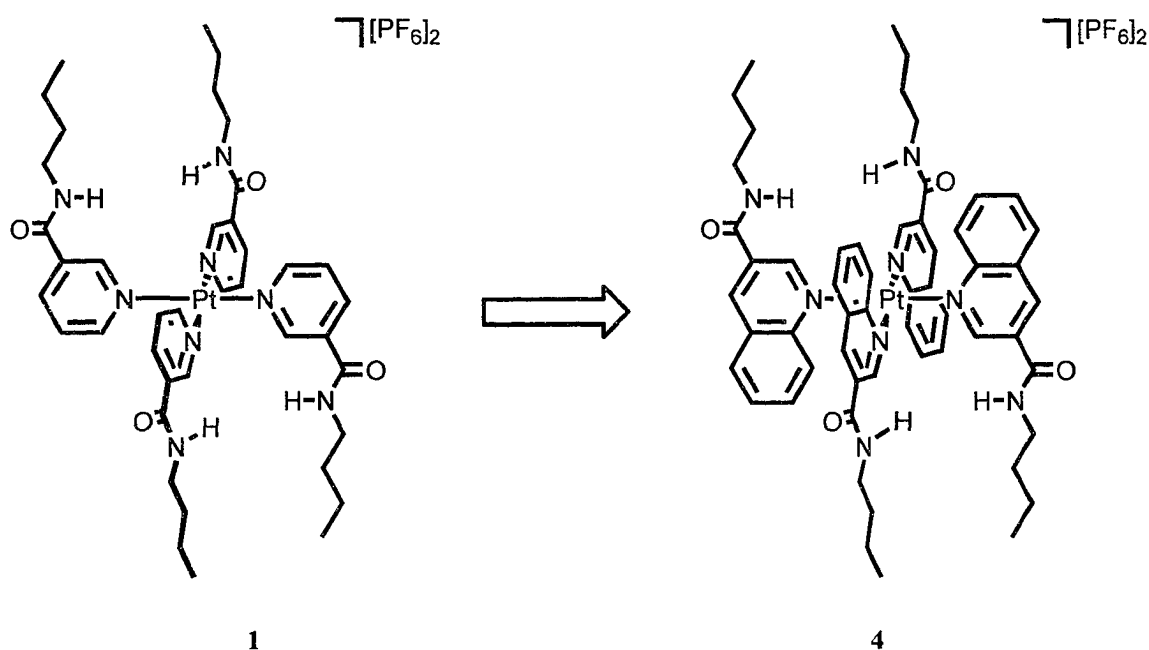


Figure 5.2 Model compound **4** based on receptor **1**.

A second resolution to the low interconversion barrier and a way of avoiding difficulties in interpreting the ^1H NMR spectra with the presence of four isomers is simply to minimize the number of possible isomers. The replacement of two of the

ligands with auxiliary bidentate ligands (L) will obviously decrease the number of possible conformations to two. The two possible conformations are now designated as *syn* and *anti*. The *syn* conformation occurs when both ligands are oriented in the same direction while the *anti* conformation occurs when the ligands are positioned in opposite directions, as shown in Figure 5.3.

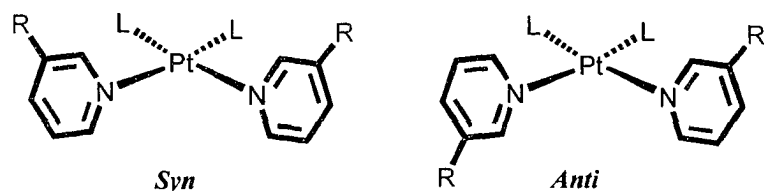


Figure 5.3 Schematic diagram of *syn* and *anti* conformations.

The simplification from four to two conformations is a respectable idea however, the bulk of the auxiliary ligands must also be increased in order to raise the barrier to interconversion. Based on this idea, model compounds **5** and **6** were designed (Figures 5.4 and 5.5). In these two model compounds, the use of 4,4'-*t*butyl-2,2'-bipyridine (*t*butylbipy) as the ancillary ligand may indirectly produce an effective increase in volume in order to slow the interconversion of the isomers. This is accomplished by locking this ligand in the square plane of the receptor. Thus, *t*butylbipy may restrict the ability of the monodentate ligands to rotate through the square plane of the complex thereby raising the interconversion barrier and slowing the rate of isomer exchange.

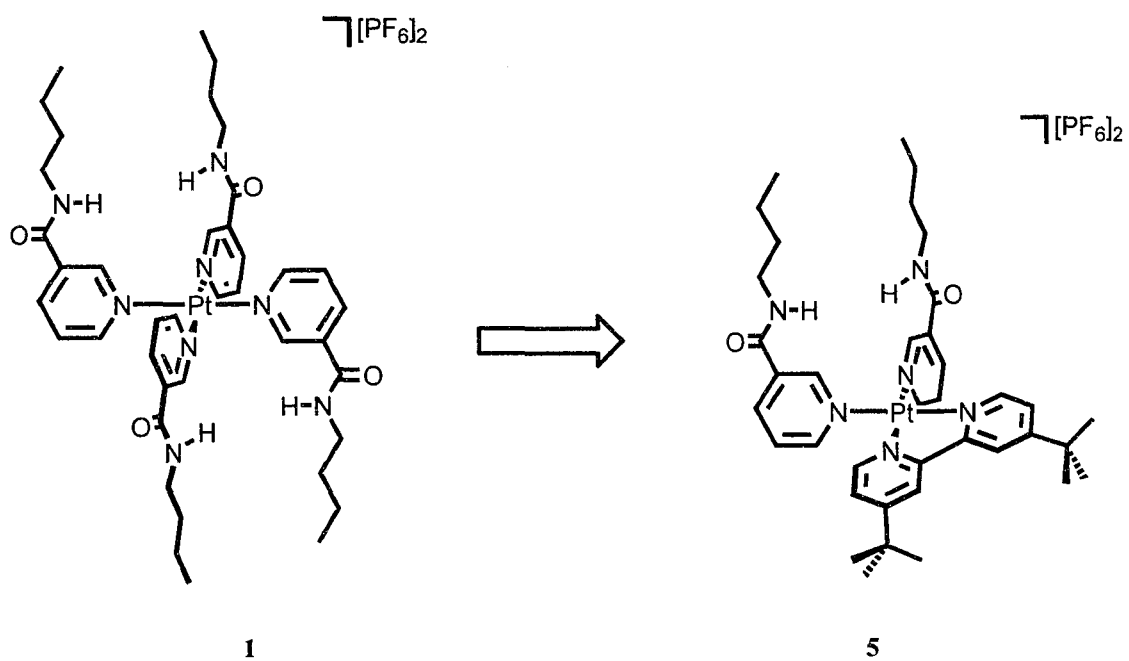


Figure 5.4 Model compound 5, shown in the *syn* conformation, based on receptor 1.

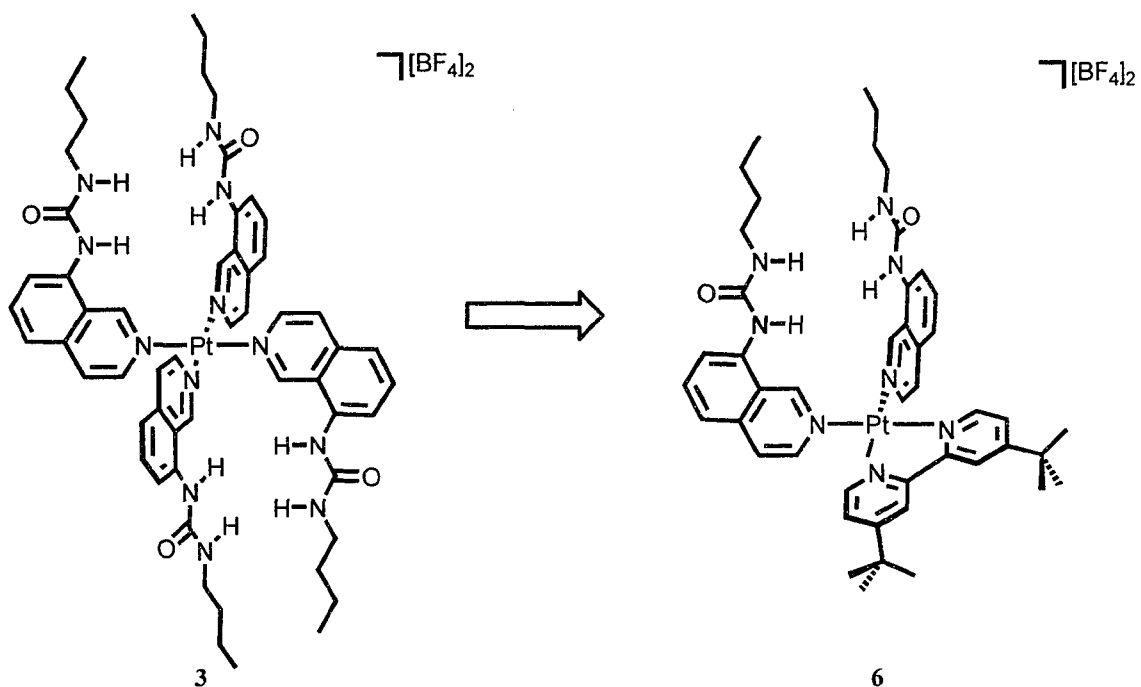


Figure 5.5 Model compound 6, shown in the *syn* conformation, based on receptor 3.

The fourth and final model compound (7) maintains the concept of simplifying the number of conformations to two, however, the bulk is added in a manner reminiscent of that used to create model 4. Model compound 7 consists of two ancillary chloride ligands in the *cis* conformation, with the bulk originating from the two quinoline ligands, as shown in Figure 5.6.

Another reason for simplifying the receptor model systems to this degree (i.e. compound 7) is that there are a number of studies in the literature reporting the stability and interconversion barriers for this class of compounds.⁷³⁻⁷⁵ Therefore, this is where we will begin.

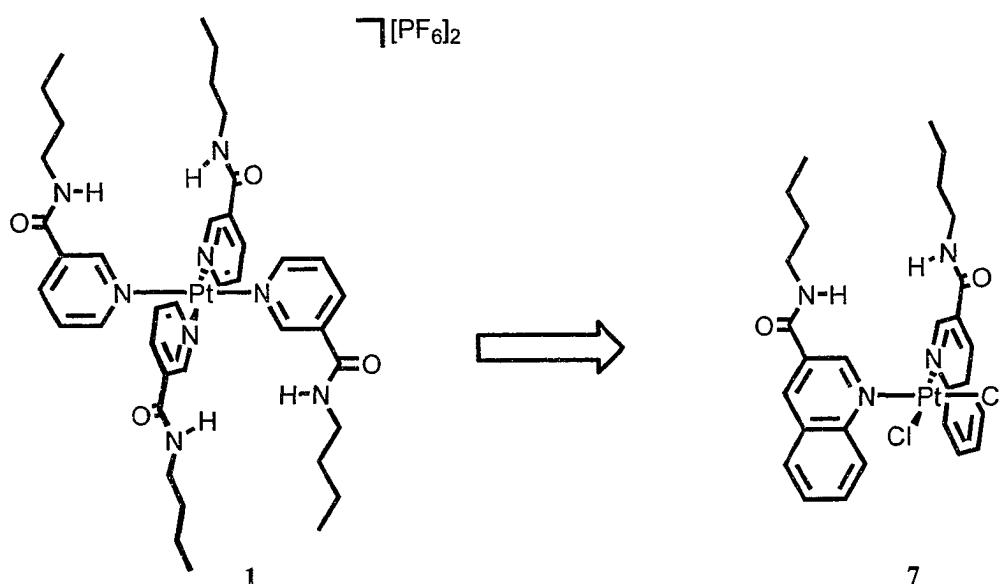


Figure 5.6 Model compound 7, shown in the *syn* conformation, based on receptor 1.

This chapter focuses on the four model compounds 4-7, investigating the relative stability and dynamics of the individual conformations. The rotational interconversion barriers are determined using variable temperature 1H NMR spectroscopy and molecular mechanics.

5.2 Results and Discussion

5.2.1 *cis*-[PtCl₂(3-*n*butylamidequinoline)₂] (7)

Hambley and co-workers determined the stability and interconversion barrier of the two rotamers of *cis*-[PtCl₂(quinoline)₂] using ¹H NMR spectroscopy and molecular mechanics.⁷⁶ The complex exhibits slow interconversion between the *syn* and *anti* rotamers at room temperature (Figure 5.7). The bulk of the quinoline ring is large enough to slow the Pt-N bond rotation on the NMR timescale. Using variable temperature ¹H NMR spectroscopy, the barrier was determined to be 82 kJ/mol while that calculated from molecular mechanics was 40 kJ/mol. The calculated energy of the optimized structures showed the *anti* conformation to be ~1 kJ/mol more stable than the *syn* conformation.

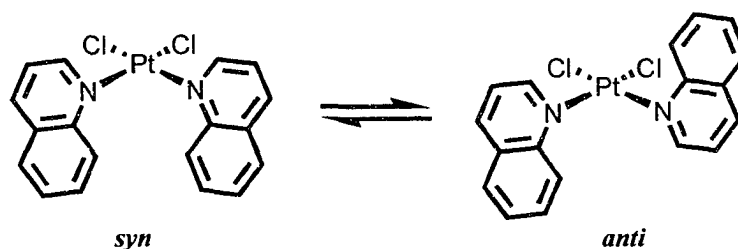


Figure 5.7 *cis*-[PtCl₂(quinoline)₂] in the *syn* and *anti* conformations.

This literature study lead us to investigate the simple model compound *cis*-[PtCl₂(3-*n*butylamidequinoline)₂], 7. This very basic model complex consists of two amide substituted quinoline ligands and two auxiliary chloride ligands. As previously noted, the use of only two 3-*n*butylamidequinoline ligands simplifies the number of possible conformations to two; *syn* and *anti*. The relative size increase from pyridine to quinoline is designed to increase the energy barrier for the rotation of the Pt-N bond, thus

allowing the study of the stability and interconversion barrier for the isomers (Figure 5.8).

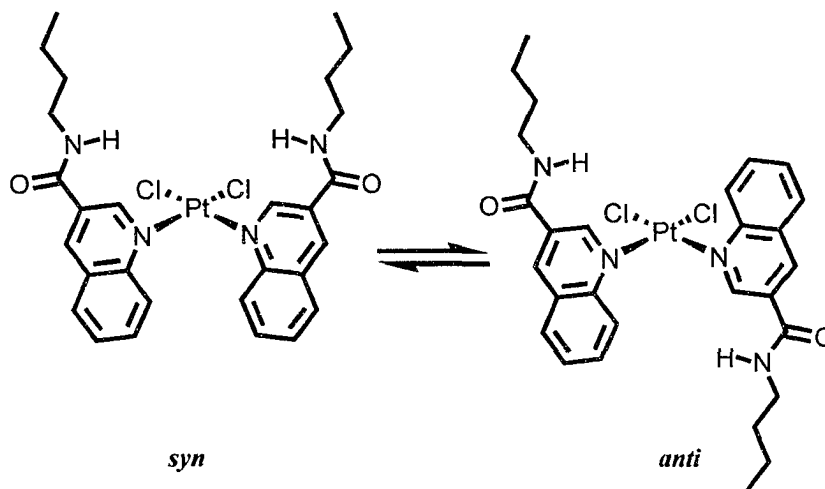


Figure 5.8 Model compound $cis-[PtCl_2(3-nbutylamidequinoline)_2]$, 7, where only two conformations are possible, *syn* and *anti*.

Synthesis

The synthesis of the ligand 3-*n*-butylamidequinoline involved the formation of the amide group by refluxing the 3-quinolinic ethyl ester in neat *n*-butylamine. After the removal of the remaining *n*-butylamine, the 3-*n*-butylamidequinoline was obtained in quantitative yield (Figure 5.9).

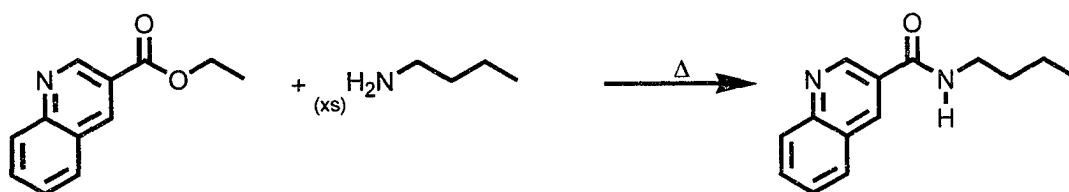


Figure 5.9 Synthesis of 3-*n*-butylamidequinoline by refluxing 3-quinolinic ethyl ester in *n*-butylamine.

The next step involved complexation of the ligand to the platinum(II) centre. The starting complex $[\text{PtCl}_2(\text{C}_2\text{H}_5\text{CN})_2]$ was refluxed with 2 equivalents of 3-*n*-butylamidequinoline in MeCN for 1 week to give 7 in 32 % yield (Figure 5.10).

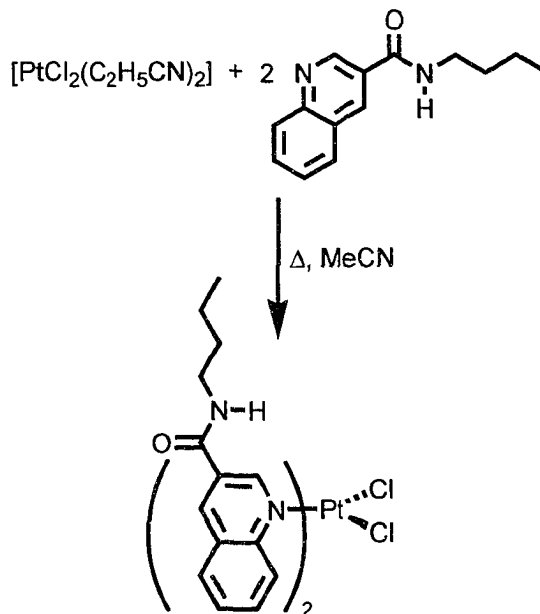


Figure 5.10 Synthesis of 7.

¹H NMR Spectroscopy

The ^1H NMR spectrum obtained for the ligand 3-*n*-butylamidequinoline in $\text{DMF-}d_7$, displayed in Figure 5.11, shows the chemical shifts of H_a and H_f at 9.55 and 9.04 ppm, respectively. Protons H_b and H_e overlap with a chemical shift of 8.23 ppm. The two triplets at 8.05 and 7.86 ppm are due to H_c and H_d , respectively. The proton from the amide group (H_g) has a resonance at 8.93 ppm as a broad singlet. The butyl chain produces peaks at 3.42, 1.61, 1.42 and 0.69 ppm. These resonances appear in order of increasing distance from the amide group with H_h producing the peak at the highest frequency and H_k producing the resonance at the lowest frequency.

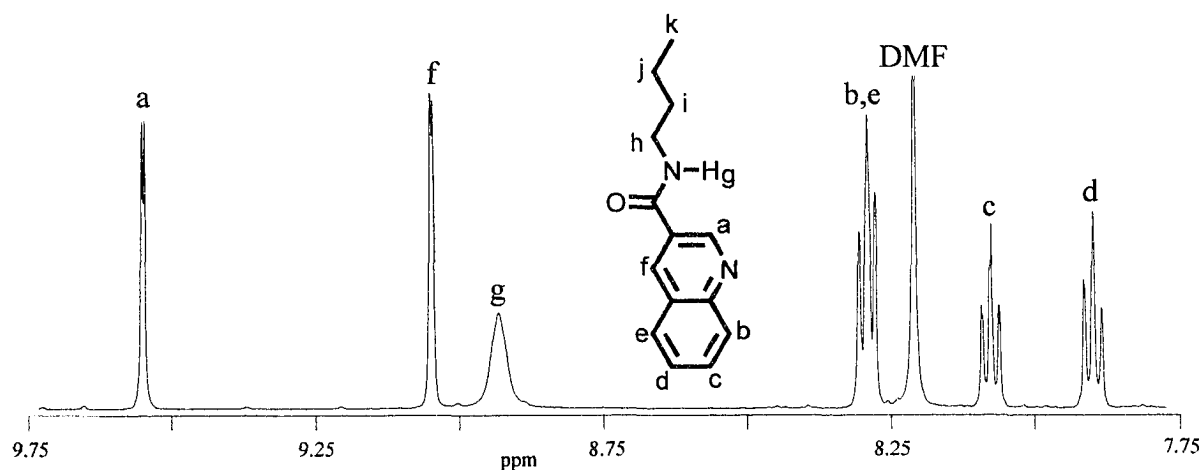


Figure 5.11 Aromatic region of the ^1H NMR spectrum of 3-*n*butylamidequinoline in $\text{DMF-}d_7$.

The ^1H NMR spectrum of the neutral complex **7**, at room temperature in the same solvent shows two sets of peaks originating from two different conformations. Therefore, the added bulk of the quinoline ligands was large enough to allow observation of both *syn* and *anti* isomers on the NMR timescale. The temperature dependent spectra show an average set of sharp resonances at 90 °C and two separate sets of sharp resonances below 0 °C, as shown in Figure 5.12.

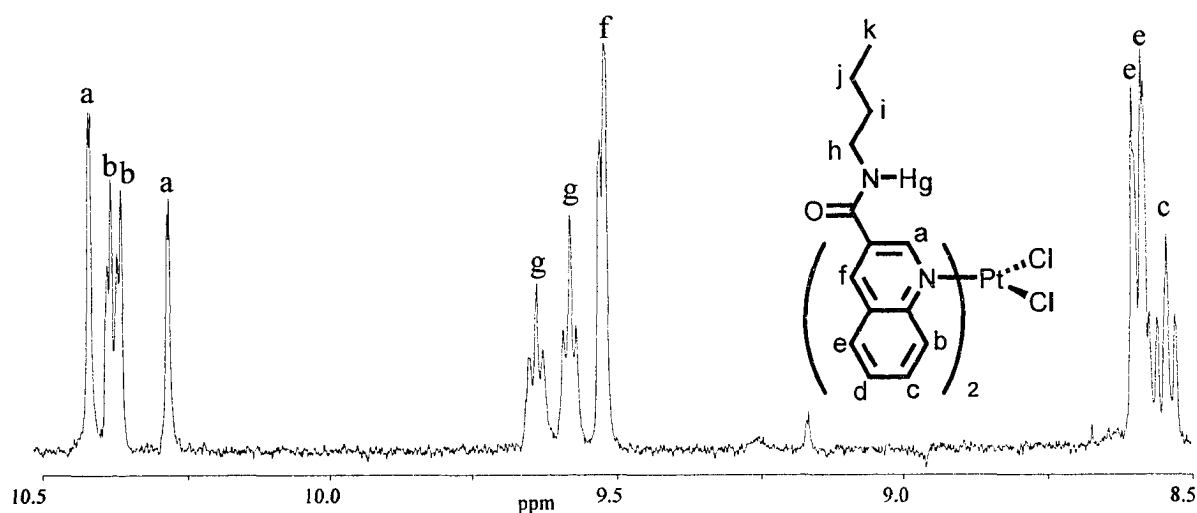


Figure 5.12 Partial spectrum of **7** at 0 °C, in $\text{DMF-}d_7$, where two sets of peaks representing the *syn* and *anti* isomers are seen.

A comparison of the chemical shifts for the ligand and the complex at 0°C shows all the aromatic peaks shifted to a higher frequency, with H_b and H_g surpassing H_f due to the proximity of the electropositive metal centre. Proton H_b in the complex has chemical shifts of 10.38 and 10.35 ppm and produces the largest changes in chemical shift, compared to the uncomplexed ligand, of $\Delta\delta = 2.14$ ppm. Proton H_a has chemical shifts from in the complex of 10.44 and 10.29 ppm with changes in chemical shifts of ~ 0.82 ppm. The chemical shifts for H_g when coordinated to the platinum(II) are 9.70 and 9.64 ppm with changes in chemical shifts of ~ 0.74 ppm. Proton H_c and H_d have chemical shifts of 8.51 and 8.19 ppm when in the complex with changes in chemical shifts of 0.46 and 0.33 ppm. The chemical shifts for H_f when in the complex are 9.53 and 9.52 ppm with changes in chemical shifts from the uncomplexed version of ~ 0.49 ppm. Finally, H_e has changes in chemical shift of 0.35 ppm and a chemical shift from in the metal complex of 8.58 ppm (Table 5.1).

Table 5.1 Comparison of ¹H chemical shifts of the ligand before and after coordination to Pt(II).

Proton	Receptor δ (ppm)	Ligand δ (ppm)	$\Delta \delta$
a	10.44	9.55	0.89
	10.29		0.74
b	10.38	8.23	2.15
	10.35		2.12
c	8.51	8.05	0.46
d	8.19	7.86	0.33
e	8.58	8.23	0.35
f	9.53	9.04	0.49
	9.52		0.48
g	9.70	8.93	0.77
	9.64		0.71

The low temperature spectrum shows the amide proton (H_g) as well as most of the aromatic protons split into two sets of peaks. The three most affected protons are H_a , H_b and H_g . H_a is the most perturbed with a difference in chemical shift between the two resonances of 0.15 ppm. Protons H_g shows a difference of 0.06 ppm and H_b experiences the smallest difference with 0.03 ppm.

Integration of the two sets of peaks shows the populations are not equal, indicating experimentally that one isomer is more stable than the other. The ratio is 0.6 to 0.4 and from applying the Boltzmann distribution equation at several different temperatures, the experimental difference in stability is calculated to be very small; ~ 1 kJ/mol.

The rotational energy barrier for the Pt-N bond in this complex was determined by variable temperature ^1H NMR spectroscopy and a full line shape analysis⁷⁷ of the experimental spectra. Proton H_a was followed at different temperatures, see Figure 5.13, and the interconversion rate constant were extracted. This data allows for the determination of activation parameters ΔG^\ddagger . The full line shape analysis yields an activation energy for the rotational barrier of 76 kJ/mol.

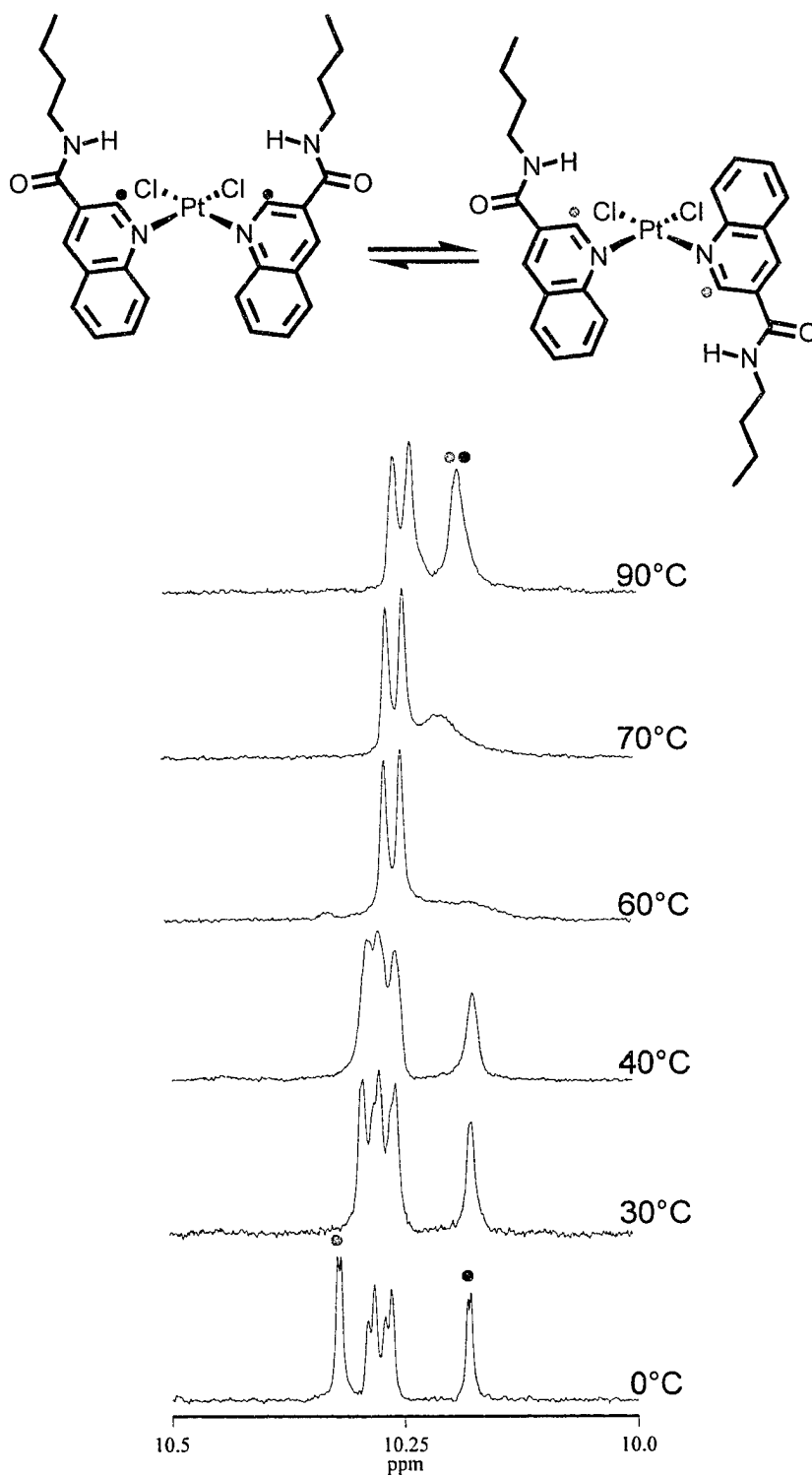


Figure 5.13 ^1H NMR spectra of **7** at several temperatures with the proton H_a highlighted.

Conformational Analysis

Theoretical calculations on **7** were performed by means of molecular mechanics using the MM3 force field. The complex was geometry optimized and a dihedral angle was defined as Cl-Pt-N_(quinoline)-C_(quinoline). The potential energy curve was then calculated by varying the dihedral angle through 360 ° at 1 ° intervals.

The calculations show a difference in stability between the two conformations of 9 kJ/mol, with *anti* being more stable than *syn*. The preference for the *anti* conformation may be due to the unfavourable proximity of the amide groups found in the *syn* conformation. The rotational barrier for this system is 73 kJ/mol and there is no preference in the direction of ligand rotation, as shown in Figure 5.14.

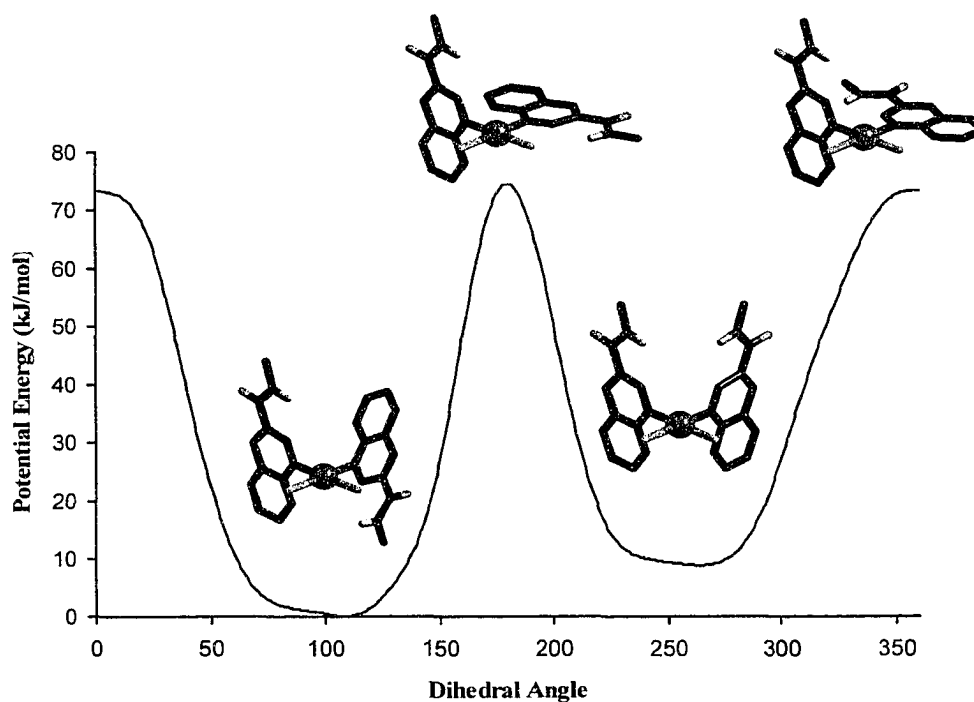


Figure 5.14 Potential energy curve of **7** showing the *anti* conformation as the most stable and the interconversion barrier of 73 kJ/mol.

Conclusions

The model complex **7** was synthesized and studied in terms of the stability of each conformation and their interconversion barrier. The model complex showed two sets of resonances in the ^1H NMR spectrum at room temperature. Therefore, the added bulk of the quinoline based ligand sufficiently raised the interconversion barrier between the two conformations.

Using ^1H NMR, the difference in stability of the conformations was determined to be ~ 1 kJ/mol by the ratio of integrals between the two sets of resonance peaks. The molecular mechanics calculations showed the *anti* conformation as the most stable, therefore the larger set of peaks in the ^1H NMR spectra are tentatively assigned to the *anti* conformation. Finally, a variable temperature ^1H NMR experiment along with full line shape analysis was used to determine the interconversion barrier of the rotamers to be 76 kJ/mol, which is very close to the value determined by molecular mechanics, 73 kJ/mol.

5.2.2 [Pt(3-*n*butylnicotinamide)₂(*t*butylbipy)][PF₆]₂ (**5**)

The [Pt(3-*n*butylnicotinamide)₂(*t*butylbipy)][PF₆]₂, **5**, is the second model compound synthesized and studied is based on receptor **1**. This complex consists of two 3-*n*butylnicotinamide ligands and a bidentate ancillary ligand, *t*butylbipy. The use of only two 3-*n*butylnicotinamide once again reduces the number of possible conformations to two, as shown in Figure 5.15. The placement of the ancillary ligand is the key to the possible increase in interconversion barrier. This ligand is not larger than a pyridine, however, the ligand bulk stems from the placement of the ligand in the plane of the complex. The lack of flexibility of this unit, once coordinated to the metal, may increase the rotational barrier of the Pt-N_(nicotinamide) bond. The stability of the isomers as well as

the dynamics of the complex were derived by molecular mechanics and variable temperature ^1H NMR with the help of a full line shape analysis.

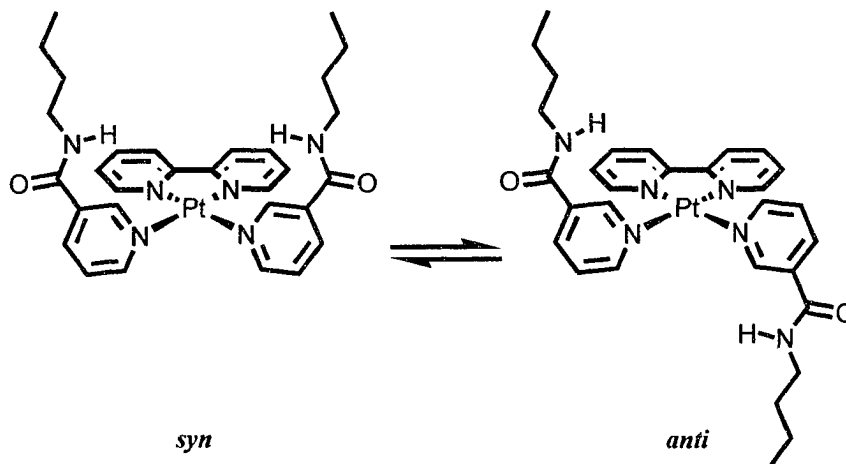


Figure 5.15 Model compound $[\text{Pt}(3\text{-}n\text{butylnicotinamide})_2(\text{tbutylbipy})][\text{PF}_6]_2$, **5**, where only two conformations are possible, *syn* and *anti*.

Synthesis

The synthesis of **5** first involved the preparation of the 3-*n*butylnicotinamide ligand as described in Chapter 2. The inorganic scaffold starting material in this case was $[\text{PtCl}_2(\text{tbutylbipy})]$ which was prepared by literature methods from $[\text{PtCl}_2(\text{C}_2\text{H}_5\text{CN})_2]$ and 4,4'-*t*-butyl-2,2'-bipyridine.⁶⁹ The desired model complex, **5**, was obtained by refluxing $[\text{PtCl}_2(\text{tbutylbipy})]$ with 2 equivalents of both AgPF_6 and 3-*n*butylnicotinamide in MeCN, and isolated in 61 % yield (Figure 5.16).

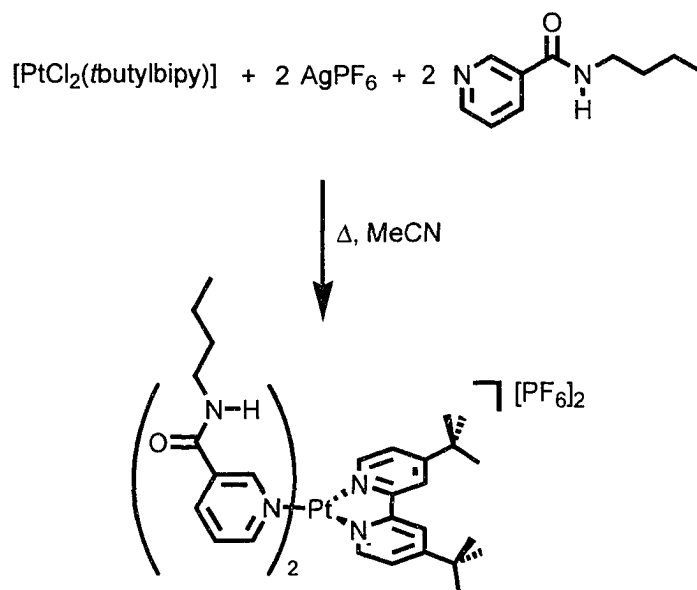


Figure 5.16 Synthesis of **5**.

¹H NMR Spectroscopy

The ¹H NMR spectrum of **5** at 0 °C in MeCN-*d*₃ (Figure 5.17) shows the characteristic chemical shifts for 3-*n*-butylnicotinamide, as they appear in the same sequence as observed for receptor **1** with the added resonances for the *t*-butylbipy ligand. The chemical shifts for H_j, H_k, and H_l are 7.63, 7.60 and 8.54 ppm respectively. The resonance representing the *t*-butyl group, H_m, has a chemical shift of 1.45 ppm.

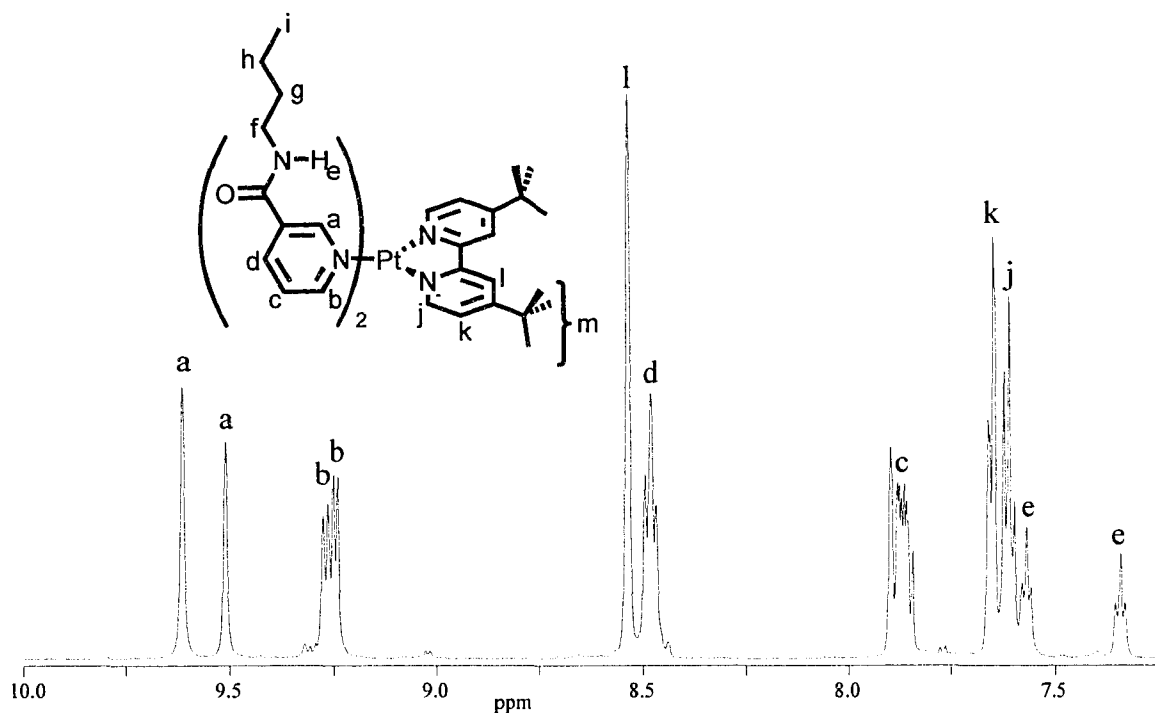


Figure 5.17 Aromatic region of the ^1H NMR spectrum of **5** at $0\text{ }^\circ\text{C}$ in $\text{MeCN-}d_3$. Two sets of peaks representing the *syn* and *anti* conformations are seen.

The ^1H NMR spectrum of this complex also shows two sets of peaks for some of the protons. The splitting of the resonances is due to the two different conformations of the complex. The bidentate *t*butylbipy ligand increases the energy required for the rotation of the 3-*n*butylnicotinamide ligand relative to the tetrasubstituted complex.

Variable temperature ^1H NMR spectra showed slow exchange at $0\text{ }^\circ\text{C}$ where two sets of sharp peaks were obtained, representing the two isomers. Protons H_a and H_e are the most affected, producing the largest resonance splitting of 0.1 ppm . The protons H_d , H_i and H_k are unchanged at all temperatures. The coalescence temperature for this complex is $50\text{ }^\circ\text{C}$ and fast exchange leading to one sharp set of resonances occurs above $60\text{ }^\circ\text{C}$ (Figure 5.18). The population for the two isomers are 0.53 to 0.47 leading to a small experimental difference in stability of 0.3 kJ/mol . Using a full line shape analysis

of this data, the experimental activation energy barrier for this rotation was determined to be 72 kJ/mol.

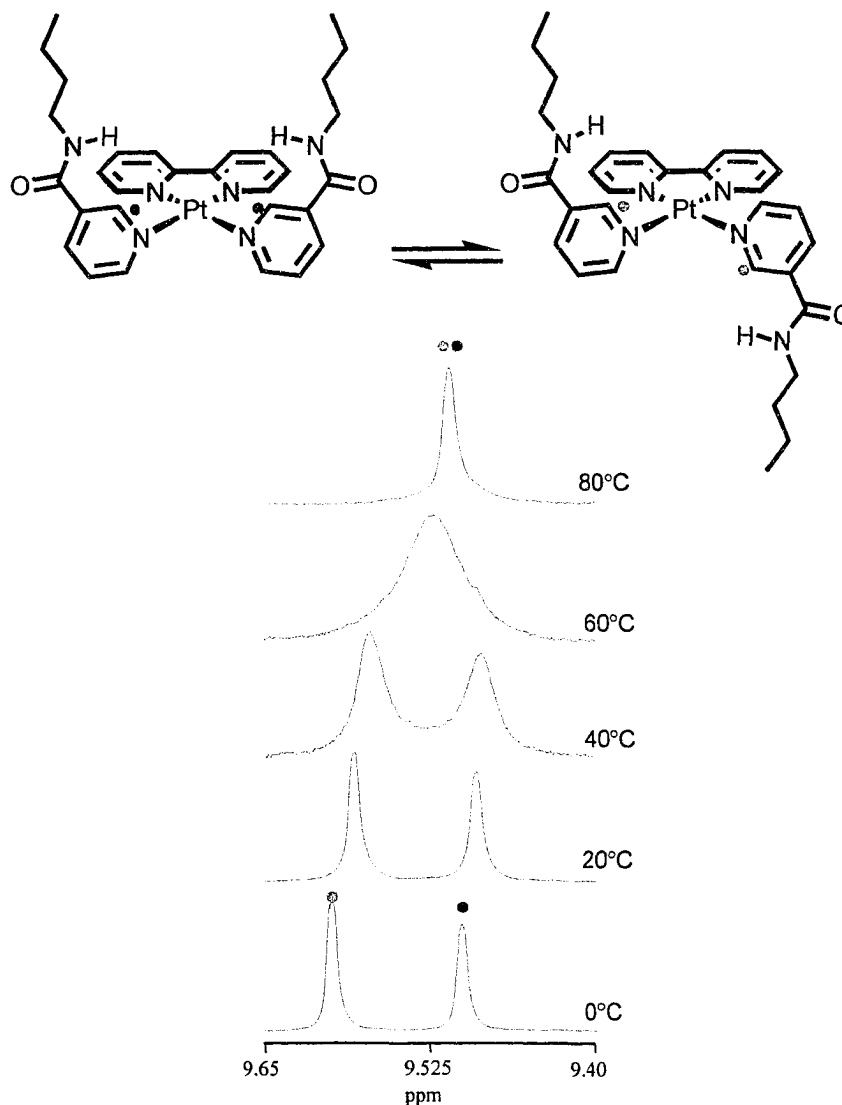


Figure 5.18 1H NMR spectra of **5** at several temperatures with the proton H_a highlighted.

Mass Spectrometry

The mass spectra of **5** shows both the 1+ and 2+ species. The $[5-PF_6]^+$ fragment has an exact mass of 964.3444 which is within 0.3 ppm of the calculated mass, 964.3441. The isotopic profile of the experimental and calculated mass are shown in Figure 5.19.

The $[5]^{2+}$ species was also obtained with an exact mass of 409.6810 that is within 0.1 ppm of the calculated mass. The isotopic profile of the raw data is shown in Figure 5.20.

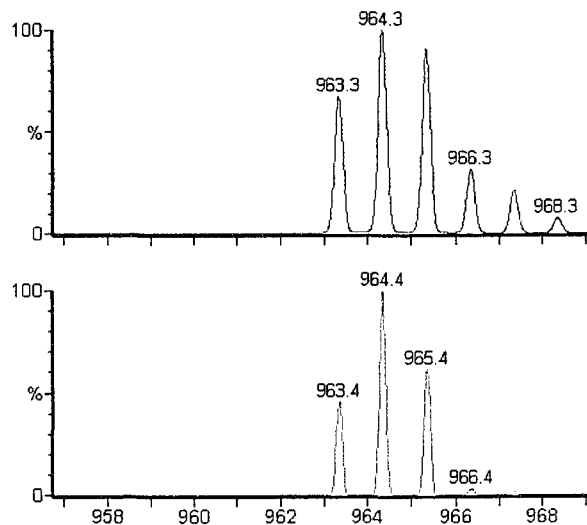


Figure 5.19 The ESI-TOF mass spectra showing the calculated (top) and raw (bottom) isotopic profile of the $[5\text{-PF}_6]^+$ species.

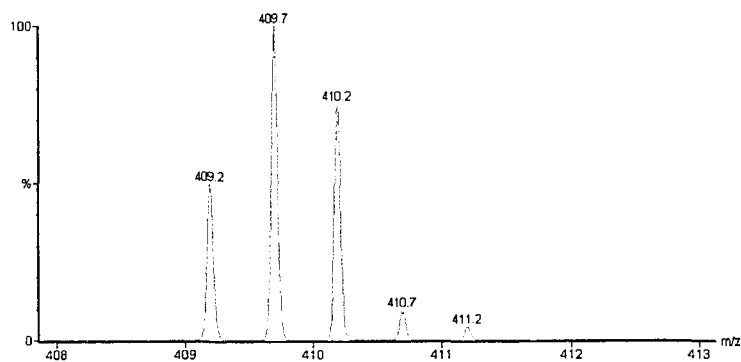


Figure 5.20 The ESI-TOF mass spectrum showing the raw isotopic profile of the $[5]^{2+}$ species.

Conformational Analysis

Molecular mechanics calculation using MM3 were performed on **5** by geometry optimizing the complex. The dihedral angle was defined as $N_{(\text{bipy})}\text{-Pt-N}_{(\text{nicotinamide})}$

$C_{(\text{nicotinamide})}$ and the potential energy curve was calculated through the rotation of the dihedral angle by 360° in 1° intervals.

The plot shows the *anti* conformation is more stable than the *syn* conformation by 0.4 kJ/mol , once again due to the proximity of the amide groups. The rotational energy barrier for this system was determined to be 6 kJ/mol where the most favourable rotation is through the amide rotating towards the neighbouring nicotinamide ligand. The unfavourable maximum of 18 kJ/mol is seen when the amide portion of the ligand is oriented out towards the bipyridine ligand. This demonstrates the unfavourable presence of this bidentate ligand in the plane of the receptor (Figure 5.21).

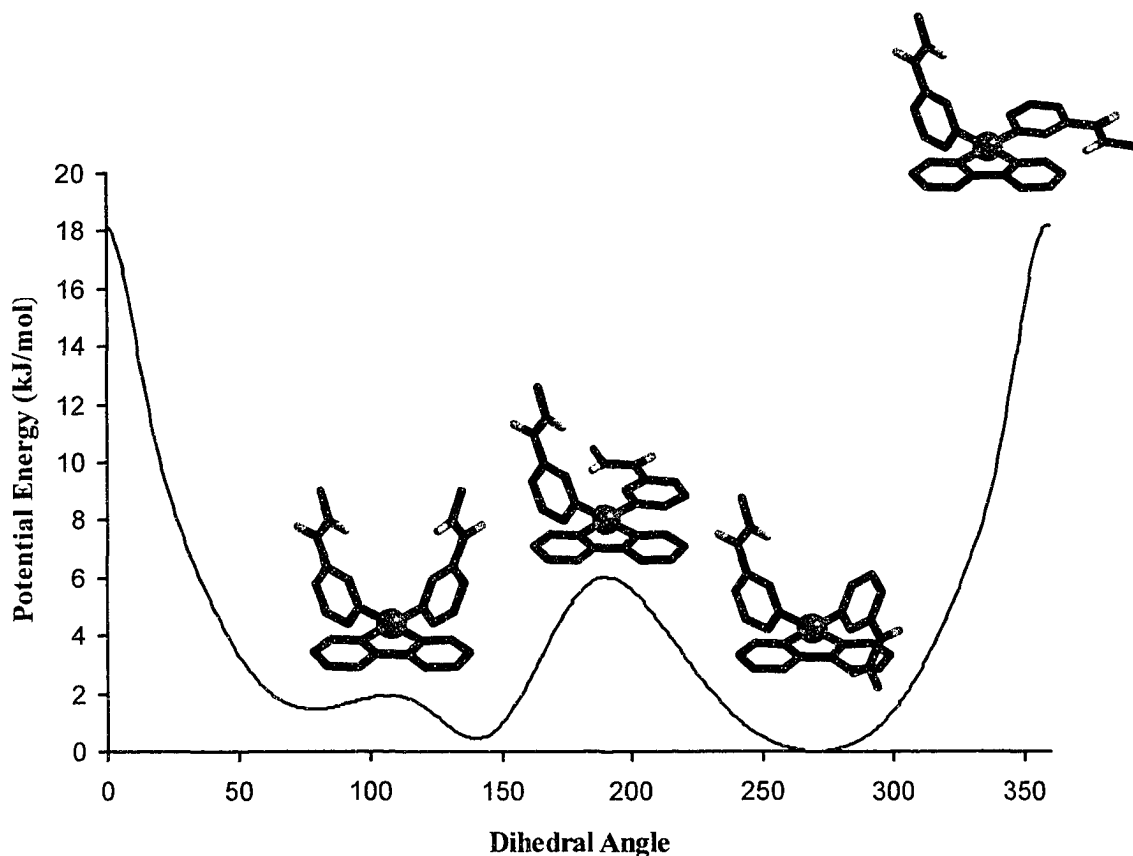


Figure 5.21 Potential energy curve of **5** showing the *anti* conformation as the most stable and the interconversion barrier as 6 kJ/mol .

Conclusions

In the model compound **5** two 3-*n*-butylnicotinamide ligands were utilized to simplify the number of possible conformations and *t*-butylbipy to increase the ligand bulk in the plane of the receptor. The ¹H NMR spectrum at room temperature shows two sets of resonances representing the *syn* and *anti* conformations. Therefore, this model complex was sufficient to study conformational stability and the interconversion barrier of the rotamers.

The difference in stability between the two isomers is 0.3 kJ/mol which was determined using the peak integration from the ¹H NMR spectrum at 0 °C. The molecular mechanics calculations showed the *anti* conformation as slightly more stable than the *syn* conformation (0.4 kJ/mol) therefore, it is inferred that the larger set of proton resonances in the ¹H NMR spectra are due to the *anti* isomer. The interconversion barrier was determined experimentally by recording several variable temperature ¹H NMR spectra followed by full line shape analysis. The barrier is 72 kJ/mol while the calculations showed a barrier of 6 kJ/mol.

5.2.3 [Pt(8-*n*-butylurea*isoquinoline*)₂(*t*-butylbipy)][BF₄]₂ (**6**)

The model complex for the urea based receptor, **3**, is [Pt(8-*n*-butylurea*isoquinoline*)₂(*t*-butylbipy)][BF₄]₂, **6**. This complex consists of two 8-*n*-butylurea*isoquinoline* ligands and a bidentate ancillary *t*-butylbipy ligand, as shown in Figure 5.22. The rationale for this type of modification is the same as for compound **5**.

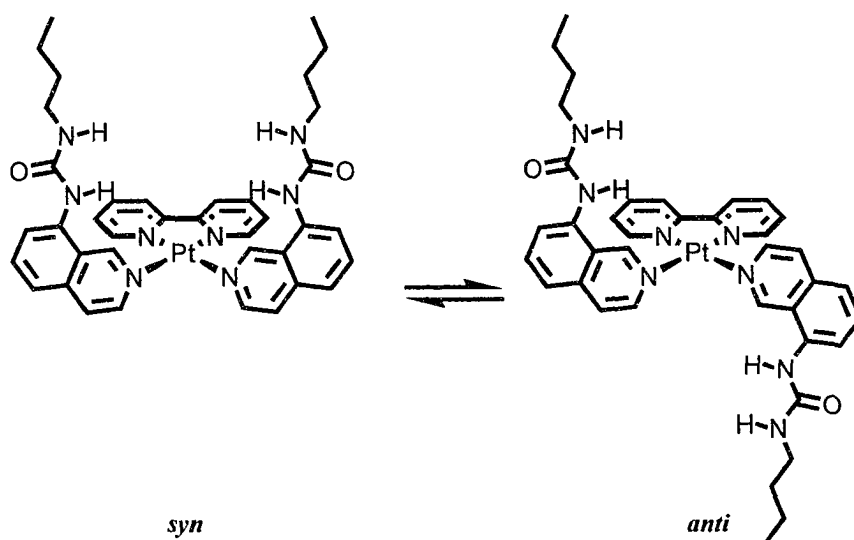


Figure 5.22 Model compound $[\text{Pt}(8\text{-}n\text{butylureaisoquinoline})_2(\text{tbutylbipy})][\text{BF}_4]_2$, **6**, where only two conformations are possible, *syn* and *anti*.

Synthesis

Model compound **6** was synthesized by refluxing $[\text{PtCl}_2(\text{tbutylbipy})]^{69}$ with 2 equivalents of both AgBF_4 and 8-*n*-butylureaisoquinoline in MeCN. After several recrystallizations the product was isolated in 13 % yield (Figure 5.23).

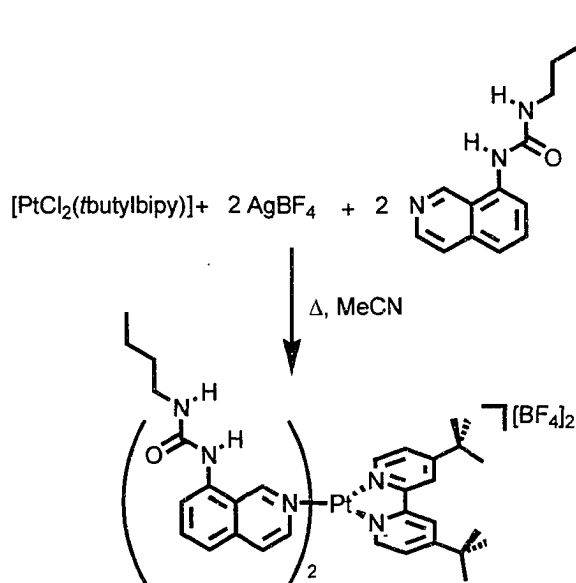


Figure 5.23 Synthesis of the complex **6**.

¹H NMR Spectroscopy

The ¹H NMR spectrum of **6** at -5 °C in MeCN-*d*₃ shows the predicted order of resonances for the 8-*n*butylurea*iso*quinoline and *t*butylbipy ligands when coordinated to the platinum(II). Proton H_a has chemical shifts at the highest frequency of 9.88 and 9.77 ppm while H_b is next with a chemical shift of 8.66 ppm. The chemical shift for H_c is 8.05 ppm, H_d and H_e overlap with a chemical shift of 7.91 ppm. The aromatic H_f proton and the two urea proton H_g and H_h each have two sets of chemical shifts occurring at 7.73 and 7.68 for H_f, 8.29 and 7.13 ppm for H_g and finally 6.11 and 5.80 ppm for H_h. The aromatic *t*butylbipy protons have chemical shifts of 7.91, 7.53 and 8.46 ppm for H_m, H_n and H_o. The *t*butyl protons are found at 1.46 ppm as a singlet. The *n*butyl chain has chemical shift of 3.24, 1.50, 1.37 and 0.89 ppm for H_i to H_l (Figure 5.24).

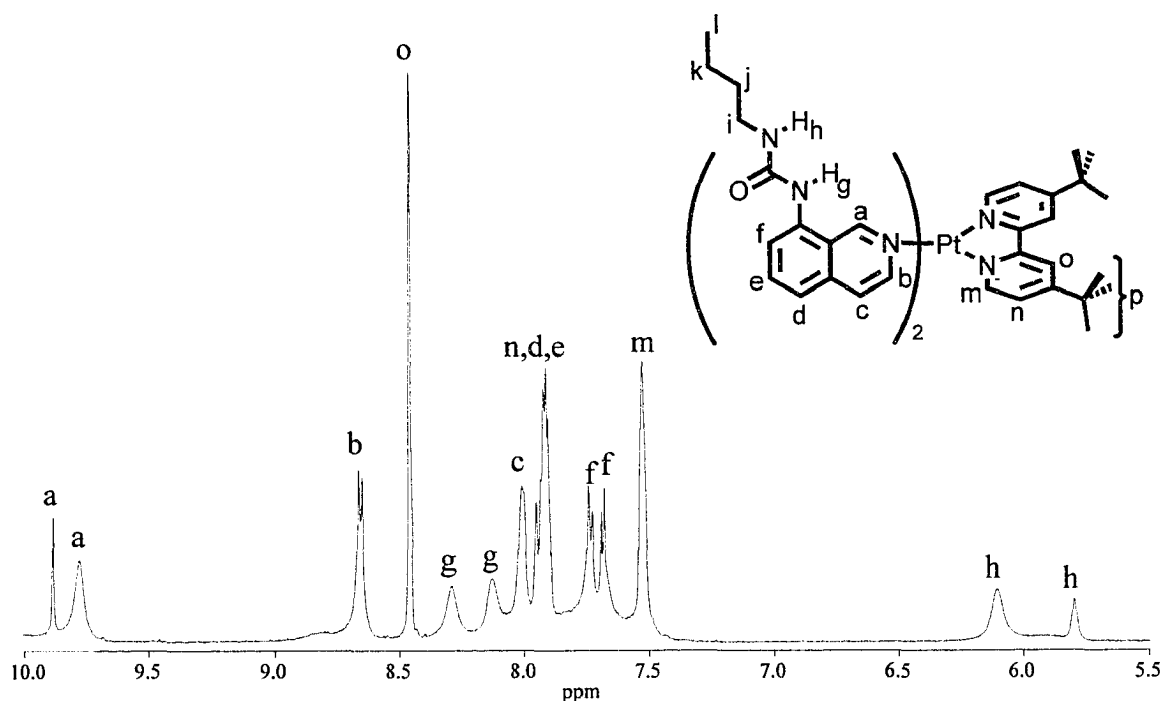


Figure 5.24 Aromatic region of the ¹H NMR spectrum of **6** at -5 °C in MeCN-*d*₃. Two sets of peaks representing the syn and anti conformations are seen for several protons.

The bidentate *t*-butylbipy ligand, when coordinated to the metal, lies perpendicular to the *isoquinoline* ligands. This produces bulk in the plane of the receptor causing an increase in energy required for the rotation of the *isoquinoline* ligands. This phenomenon is seen in the ^1H NMR spectrum where two sets of chemical shifts are observed for some protons. The protons with the largest difference in chemical shift between the two conformers are H_h ($\Delta\delta = 0.3$ ppm), H_g ($\Delta\delta = 0.2$ ppm) and H_a ($\Delta\delta = 0.05$ ppm). The protons closest to the urea, H_i , also experiences some effect from the different environments and produce two resonances approximately 0.04 ppm apart. The two sets of resonances have a peak ratio of 0.75 to 0.25 resulting in an experimental difference in stability between the two conformations of 3 kJ/mol.

The stack plot of the variable temperature ^1H NMR spectra for H_a shows slow exchange below 5 °C. Fast exchange occurs above 65 °C, where one sharp peak is obtained as an average for both conformations and the coalescence temperature is 45 °C (Figure 5.25). The rotational energy barrier for this complex was calculated to be 69 kJ/mol using a full line shape analysis of the spectra.

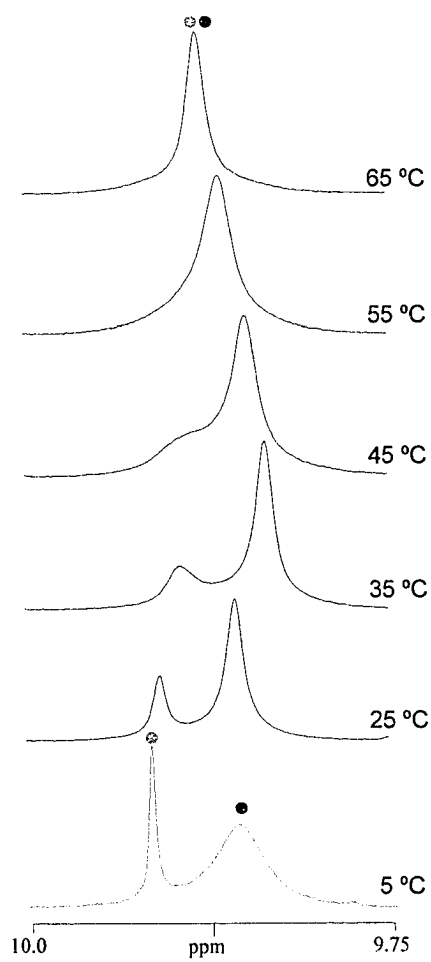
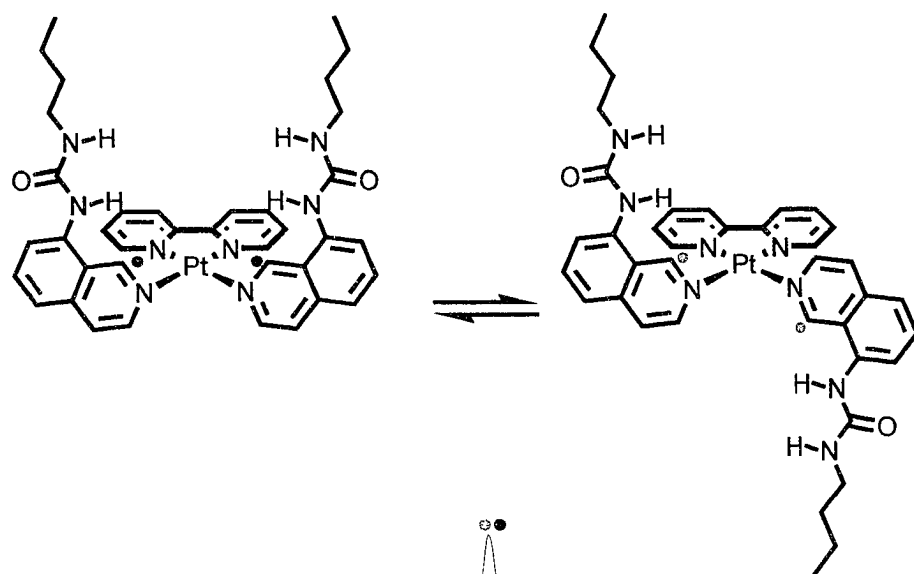


Figure 5.25 ^1H NMR spectra of **6** at several temperatures with the proton H_a highlighted.

X-Ray Crystallography

X-ray quality single crystals of **6** were obtained from the slow diffusion of *i*Pr₂O into an MeCN solution. The clear yellow blocks appeared after several days. The structural information shows the complex in the *anti* conformation where the BF₄⁻ anions are interacting through hydrogen bonds with the urea protons and electrostatically with the platinum(II) metal centre (Figure 5.26).

The hydrogen bonding interactions occur at distances of 3.29 and 3.13 Å and at angles ranging from 151 ° to 162 ° between the orange 8-*n*butylurea*iso*quinoline and the top BF₄⁻. The brown 8-*n*butylurea*iso*quinoline ligand interacts slightly more intimately with the bottom BF₄⁻ anion with distances ranging from 2.92 to 3.17 Å and angle varying from 147 ° to 160 °.

The electropositive platinum(II) metal centre directs the electron rich anions towards itself resulting in the anions being positioned above and below the metal. The interactions occur at Pt...F distances of 4.02 and 3.85 Å for the upper and lower anions respectively.

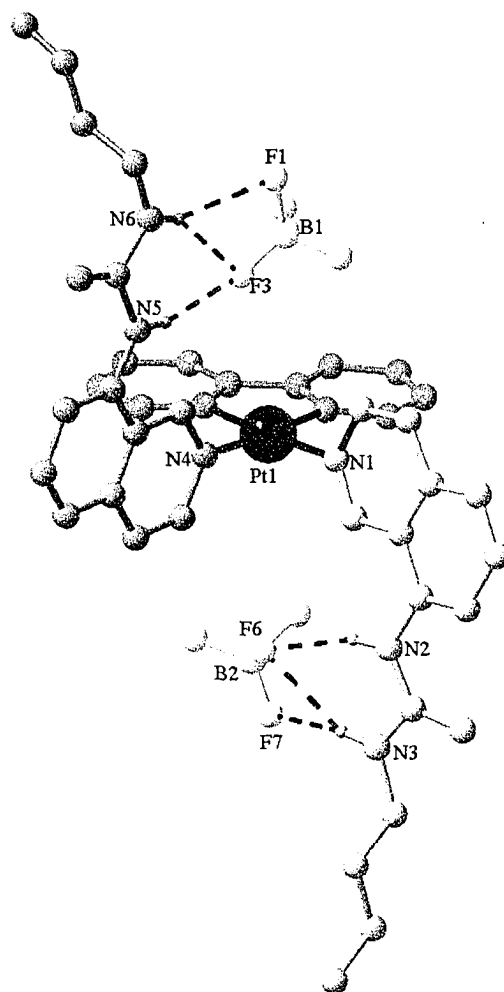


Figure 5.26 X-ray crystal structure of **6** showing the front view with the *t*butyl groups omitted for clarity. N-H...F distances (Å) and angles (°): N(2)...F(6) 2.92, N(2)-H(2B)...F(6) 160; N(3)...F(6) 3.17, N(3)-H(3B)...F(6) 147; N(3)...F(7) 3.01, N(3)-H(3B)...F(7) 157; N(5)...F(3) 3.13, N(5)-H(5B)...F(3) 162; N(6)...F(3) 3.29, N(6)-H(6B)...F(3) 153; N(6)...F(1) 3.29, N(6)-H(6B)...F(1) 152. Pt...F distances (Å) and angles (°): Pt(1)...F(6) 3.85, Pt(1)...F(6)-B(2) 85; Pt(1)...F(3) 4.02, Pt(1)...F(3)-B(1) 109.

Mass Spectrometry

In the ESI-TOF mass spectrum recorded for **6**, the $[\mathbf{6}\text{-BF}_4]^+$ and $[\mathbf{6}]^{2+}$ species were detected. Figure 5.27 shows the isotopic profile of the experimental data of $[\mathbf{6}\text{-BF}_4]^+$ compared to the calculated data. The exact mass obtained was 1036.4353 while the calculated is 1036.4360, resulting in a 0.7 ppm difference. The $[\mathbf{6}]^{2+}$ species has an exact

mass of 474.7167 which is within 0.4 ppm of the calculated mass and the isotopic profile obtained is shown in Figure 5.28.

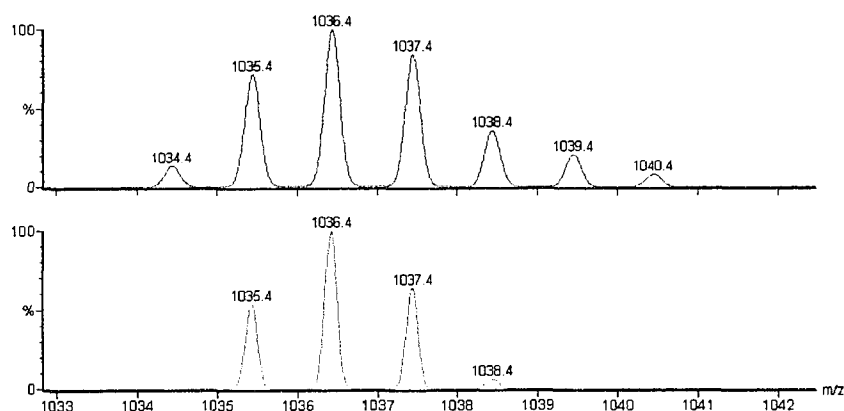


Figure 5.27 The ESI-TOF mass spectra showing the calculated (top) and raw (bottom) isotopic profile of the [6-BF₄]⁺ species.

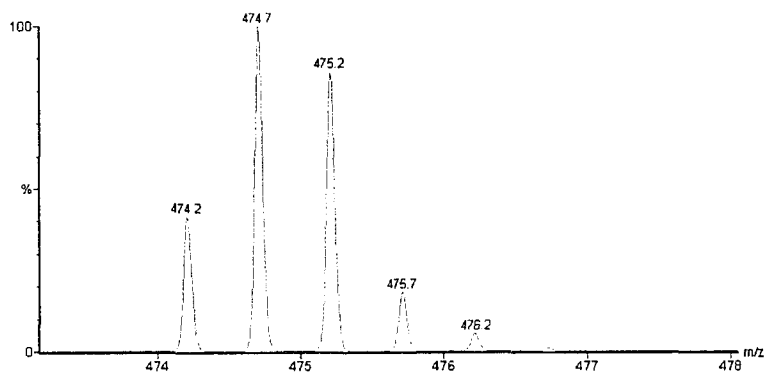


Figure 5.28 The ESI-TOF mass spectrum showing the raw data isotopic profile of the [6]²⁺ species.

Conformational Analysis

The molecular mechanics calculations on **6** were performed using the MM3 force field. The geometry of the complex was first optimized followed by setting the dihedral

angle as $N_{(\text{bipy})}-Pt-N_{(\text{isoquinoline})}-C_{(\text{isoquinoline})}$. The potential energy curve was calculated by rotating the dihedral through 360° at 1° intervals.

The plot of energy potential versus dihedral angle shows the *anti* conformation as the most stable conformation by ~ 1 kJ/mol. The low energy interconversion path occurred when the urea rotated in towards the neighbouring *isoquinoline* ligand with an energy barrier of 2 kJ/mol. The high-energy path occurred when the urea rotated out towards the bipyridine ligand, once again, as observed for **5** and **7** (Figure 5.29).

Interestingly, the overall energy minimum occurred when one *isoquinoline* ligand tilted in, towards the other at a minimum the N-H...O distance. This is due to intramolecular hydrogen bonding between the neighbouring urea groups in the gas phase, but it is not likely a significant contribution to the conformation in polar solutions.

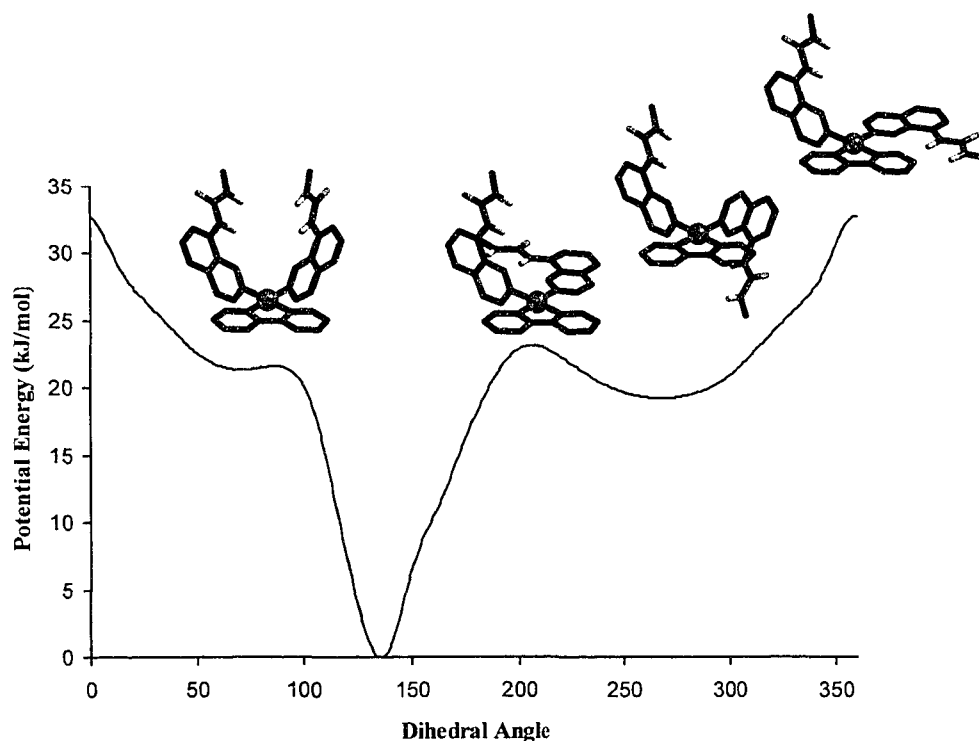


Figure 5.29 Potential energy curve of **6** showing the *anti* conformation as the most stable and the interconversion barrier as 2 kJ/mol.

Conclusions

The model complex **6** was used to study the stability and interconversion barrier between its two conformations. The room temperature ^1H NMR spectrum showed once again two set of peaks representing the *syn* and *anti* conformations.

The stability of one isomer relative to the other was determined to be 3 kJ/mol using the experimental ^1H NMR data. The molecular mechanics calculations showed the *anti* isomer as the most stable conformation (~ 1 kJ/mol) therefore the larger set of peaks in the ^1H NMR spectra are inferred to arise from this conformation. The X-ray crystal structure also displayed the *anti* conformation, with two BF_4^- anions interacting with the metal centre. The experimental interconversion barrier was determined to be 69 kJ/mol using variable temperature ^1H NMR spectra and full line shape analysis.

5.2.4 $[\text{Pt}(3\text{-}n\text{butylamidequinoline})_4][\text{PF}_6]_2$ (**4**)

The simplest variation from the amide base receptor **1** is the model complex $[\text{Pt}(3\text{-}n\text{butylamidequinoline})_4][\text{PF}_6]_2$, **4**. This complex maintains the ability to attain all four *pseudo*-calix[4]arene conformations however, the replacement of the pyridine based ligands with a quinoline based ligand should raise the interconversion barrier for rotation about the Pt-N bond (Figure 5.30).

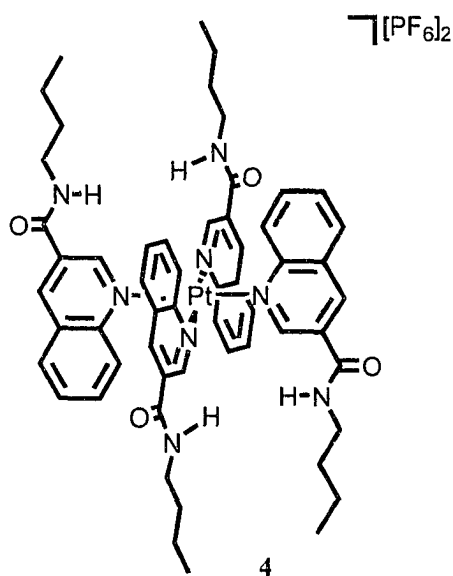


Figure 5.30 Model compound $[Pt(3\text{-}n\text{butylamidequinoline})_4][PF_6]_2$, **4**, in the 1,2-alternate conformation.

Synthesis

The homoleptic platinum(II) quinoline amide complex, **4**, was synthesized by refluxing $[PtCl_2(C_2H_5CN)_2]$ with 4 equivalents of 3-*n*-butylamidequinoline and 2 equivalents of $AgPF_6$ in MeCN. The precipitated complex **4** was isolated in 12 % yield (Figure 5.31).

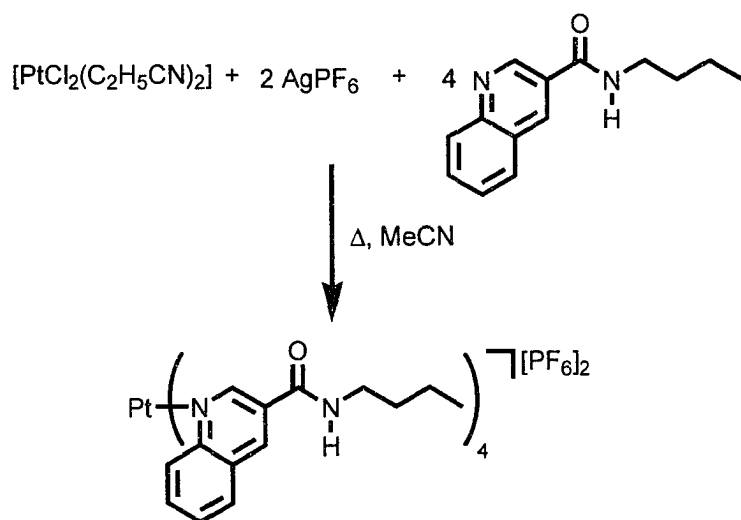


Figure 5.31 Synthesis of **4**.

¹H NMR Spectroscopy

The ¹H NMR spectrum of **4** is quite complex and is shown in Figure 5.32. As previously shown, the ¹H NMR spectrum of *cis*-[PtCl₂(3-*n*butylamidequinoline)₂] displayed two sets of peaks for some of the protons in the complex. Since the homoleptic complex, **4**, maintains the bulk of the quinoline ligands, it is likely that slow rotation occurs and all four different conformations would be observable.

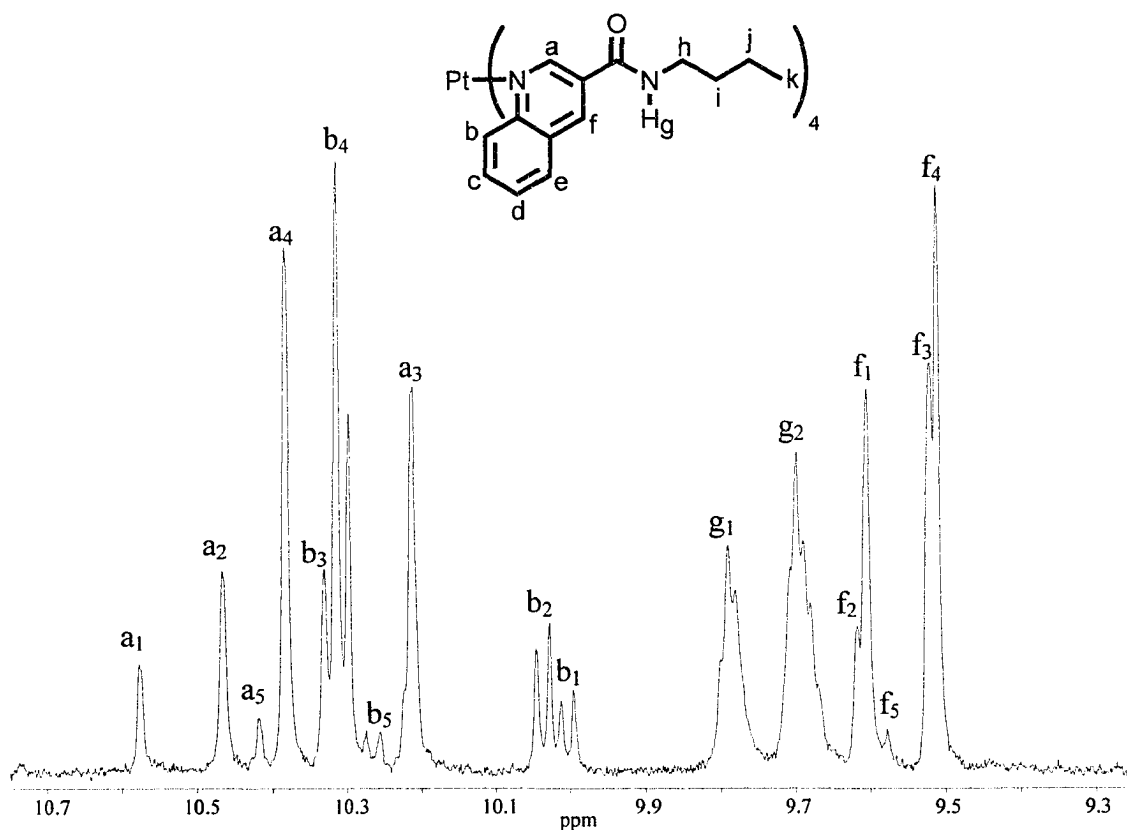


Figure 5.32 Partial ¹H NMR spectrum of **4** at -40 °C in DMF-*d*₇. Several sets of peaks representing the different *pseudo*-calix[4]arene conformations are seen.

Therefore, complex **4** has the possibility of displaying six different sets of proton environments of varying intensities (Figure 5.33). The varying intensities of each set of

peaks depend on two factors, the relative abundance of each isomer in solution and the amount of equivalent protons in each conformation.

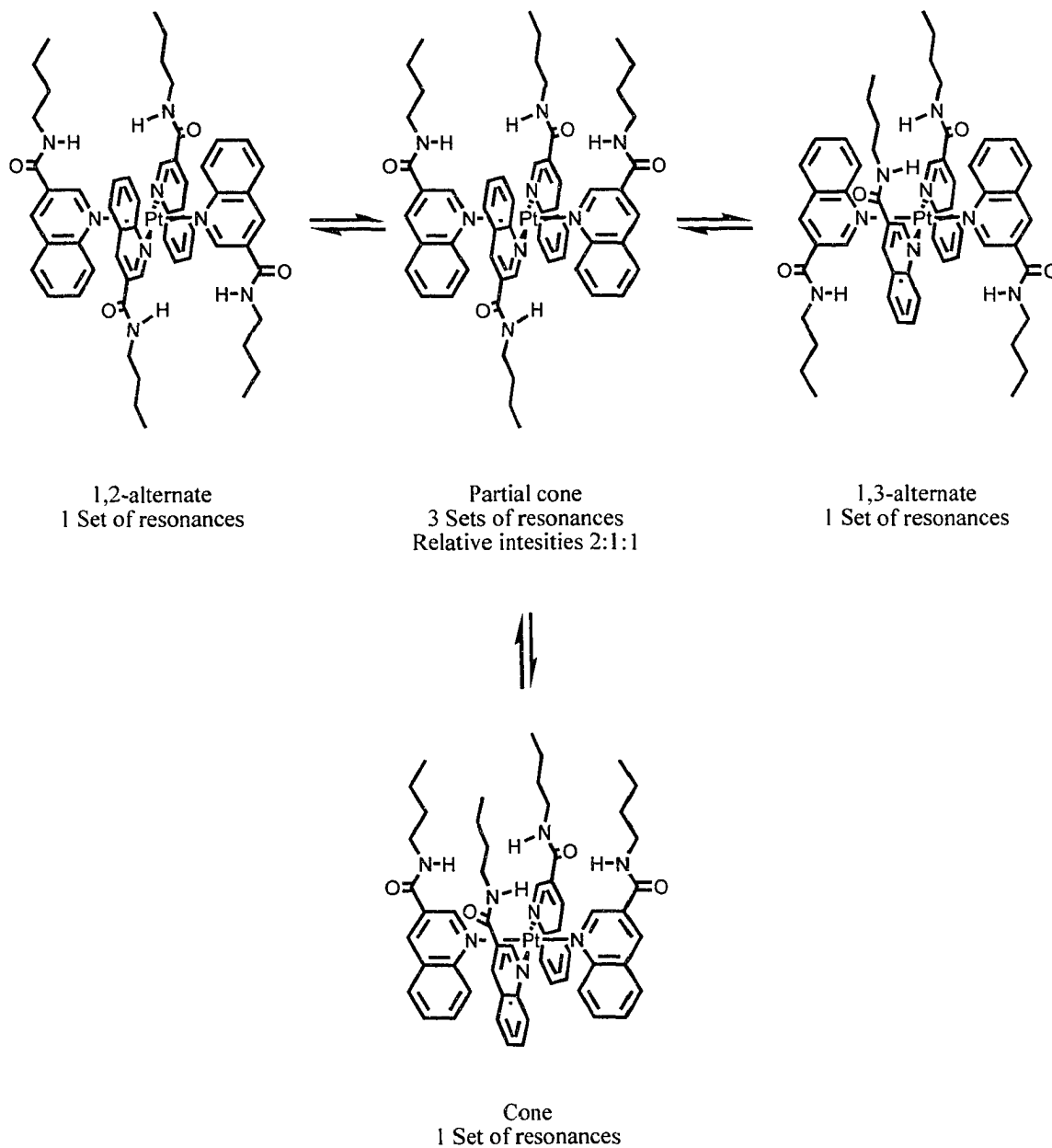


Figure 5.33 Pseudo-calix[4]arene conformations assumed by **4** with the number of sets of peaks possible in the ^1H NMR spectrum.

The cone, 1,2-alternate and 1,3-alternate conformations possess internal symmetry producing four equivalent sets of protons per isomer. The partial cone

conformation possesses three inequivalent proton resonances with 2:1:1 relative intensities. Another difficulty in deciphering the ^1H NMR spectrum for this complex is predicting which environments would give rise to sufficiently different resonances and thus measurable differences in chemical shifts. Therefore, unambiguous assignment of all the resonances to the proper conformations for **4** is an enormous challenge.

In general, the chemical shifts were assigned as H_a having chemical shifts of 10.58, 10.47, 10.43, 10.38 and 10.21 ppm and proton H_b has chemical shifts of 10.34, 10.30, 10.25, 10.03 and 10.00 ppm. Proton H_c , H_d and H_e have chemical shifts of 8.64, 8.18 and 8.59 ppm, respectively. The observed chemical shifts for H_f are 9.62, 9.61, 9.52, 9.51 and 9.50 ppm and the amide proton H_g shows two broad peaks at 9.79 and 9.70 ppm. The protons from the *n*butyl chain have chemical shifts of 3.70, 1.87, 1.65 and 1.15 ppm from H_h , H_i , H_j and H_k , respectively.

The ^1H NMR spectrum at $-40\text{ }^\circ\text{C}$ shows five sets of resonances for H_a and H_b and H_f . As the temperature is increased, the spectrum became less complex however; a single set of peaks was never attained. At $50\text{ }^\circ\text{C}$ the spectrum seemed to be biased to two different conformations and increasing the temperature did not cause any further change.

Conformational Analysis

For complex **4**, the interconversion of four different conformations involves one common transition state. The partial cone conformation is obtained by the rotation of any ligand from any conformation. Therefore, the molecular mechanics calculation involved optimizing the geometry of the conformation. This was followed by defining the dihedral angle as $\text{N}_{(\text{quinoline})}\text{-Pt-N}_{(\text{quinoline})}\text{-C}_{(\text{quinoline})}$. Potential energy curves were obtained from the rotation of a single ligand 360 ° in 1 ° intervals.

The most stable conformation is the 1,3-alternate followed by the 1,2-alternate and the partial cone. The least favourable conformation is the cone conformation. The proximity of the amide groups is the common factor in the relative stabilities of the conformations. The larger the number of proximal amide groups the more unstable the conformation becomes, as shown in Figure 5.34.

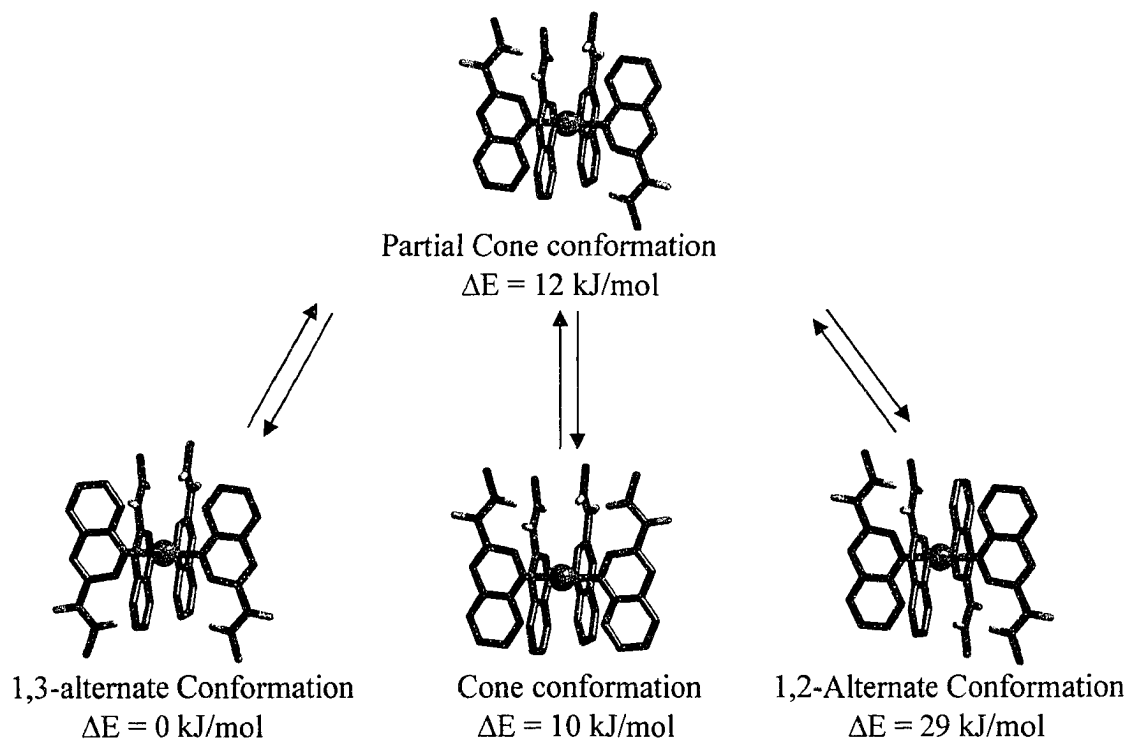


Figure 5.34 Relative stabilities of the isomers compared to the 1,3-alternate conformation.

The rotational energy required to attain the partial cone and the 1,2-alternate conformation from the 1,3-alternate conformation is 48 kJ/mol and 45 kJ/mol, respectively. The cone is the least favoured transition, requiring 51 kJ/mol.

Conclusions

The change of four pyridine ligands to four quinoline ligands in the model compound **4** increased the rotational barrier for the interconversion of the isomers. The

possibility of four interconverting isomers greatly increased the complexity of the ^1H NMR spectra obtained, therefore only a general assignment of the peaks was possible.

The molecular mechanics calculations showed the 1,3-alternate conformation as the most stable followed by the 1,2-alternate and the partial cone. The cone conformation was found to be the least stable.

5.3 Conclusions

Overall, the study of several model complexes lends itself to some understanding of the trends involved in the stability of the conformational isomers and their interconversion barriers.

The molecular mechanics calculations show that all the model complexes prefer the *anti* conformation or the 1,3-alternate conformation which allows for the largest separation of the functional groups. This data was used as a tool to assign the *anti* conformation to the larger set of resonance peaks in the ^1H NMR spectra for **7**, **6** and **5**. The relative stability of the *anti* over the *syn* conformation are 1 kJ/mol for **7**, 0.3 kJ/mol for **5** and 3 kJ/mol for **6**.

The interconversion barrier for **7** is the highest of the simple *syn* and *anti* rotamers with a coalescence temperature of 60 °C and an experimental barrier of 76 kJ/mol. The midrange interconversion barrier is obtained with **5** where the experimental barrier is 72 kJ/mol and the coalescence temperature is 50 °C. The lowest interconversion barrier of 69 kJ/mol was obtained for **6** with a coalescence temperature of 45 °C.

The favourable mechanism of rotation for **5** and **6** is for the functional group to rotate away from the bipyridine ligand due to the bulk it produces in the plane of the

complex. Compound 7 showed both directions of rotation to be similar. The complex 4 results in a very complicated system where unambiguously assigning the resonances in the ^1H NMR spectra was impossible.

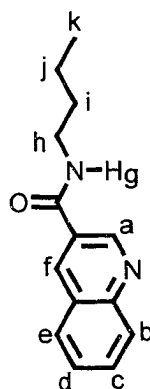
5.4 Experimental

5.4.1 General Methods

See description in section 2.4.1 and 2.4.2 for general procedure and instrumentation used in this chapter.

Interconversion barriers were obtained using full line shape analysis program, gNMR version 5.0.⁷⁷ The molecular mechanics calculations were performed using CAChe Workspace, CAChe Work System Pro Version 6.1.⁷⁸

5.4.2 3-*n*Butylamidequinoline



The 3-quinolinicethyl ester (0.923 g, 4.59 mmol) was refluxed in 15 mL of *n*butylamine for 48 hrs. The solution was cooled to room temperature and the remaining *n*butylamine was removed using dynamic high vacuum. The resulting yellow crystalline powder was obtained with a yield of 1.046 g (100 %). HRMS (ESI): Calcd. for: $\text{C}_{14}\text{H}_{17}\text{N}_2\text{O}$ [L-H]⁺: 229.1341; Found: 229.1343.

¹H NMR data (500 MHz): in MeCN-*d*₃

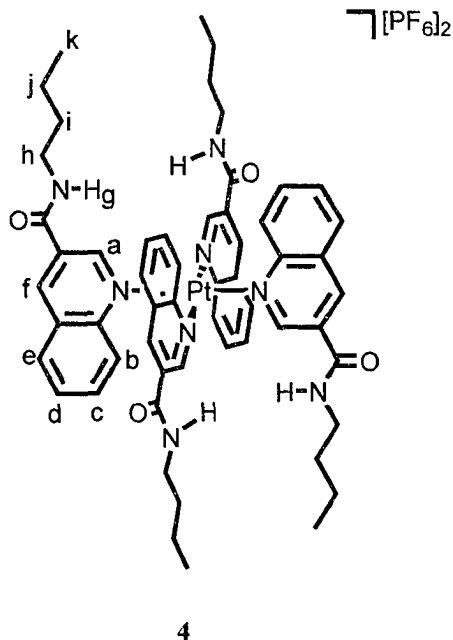
Proton	δ(ppm)	Multiplicity	Coupling Constant (Hz)	# of Protons
a	9.23	d	⁴ J _{af} = 2.1	1
b	8.09	d	³ J _{bc} = 8.3	1
c	7.82	dd	³ J _{cb} = 8.3	1
d	7.64	dd	³ J _{de} = 8.0	1
e	7.99	d	³ J _{ed} = 8.0	1
f	8.64	d	⁴ J _{fa} = 2.1	1
g	7.29	bs	---	1
h	3.42	q	³ J _{hi} = 7.6 ³ J _{hg} = 5.7	2
i	1.61	tt	³ J _{ij} ≈ ³ J _{ih} = 7.6	2
j	1.42	tq	³ J _{ji} ≈ ³ J _{jk} = 7.3	2
k	0.69	t	³ J _{kj} = 7.4	3

¹H NMR data (500 MHz): in DMF-*d*₇

Proton	δ(ppm)	Multiplicity	Coupling Constant (Hz)	# of Protons
a	9.55	d	⁴ J _{af} = 1.8	1
b	8.23	d	³ J _{bc} = 7.5	1
c	8.05	dd	³ J _{cb} = 7.5	1
d	7.86	dd	³ J _{de} = 7.5	1
e	8.23	d	³ J _{ed} = 7.5	1
f	9.04	d	⁴ J _{fa} = 1.8	1

g	8.93	bs	---	1
h	3.70	m	${}^3J_{hi} = 7.4$ ${}^3J_{hg} = 5.7$	2
i	1.89	tt	${}^3J_{ij} \approx {}^3J_{ih} = 7.4$	2
j	1.66	tq	${}^3J_{ji} \approx {}^3J_{jk} = 7.4$	2
k	1.16	t	${}^3J_{kj} = 7.4$	3

5.4.3 [Pt(3-*n*butylamidequinoline)₄][PF₆]₂ (4)

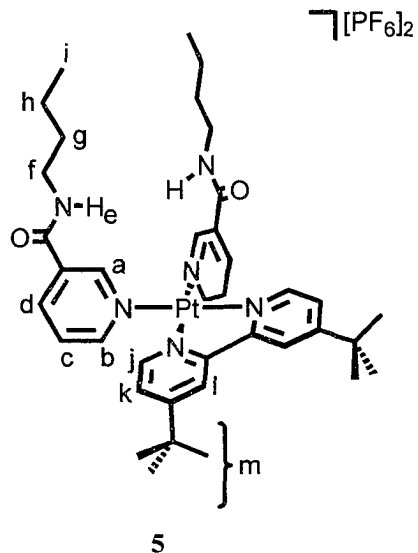


[PtCl₂(C₂H₅CN)₂] (0.100 g, 0.27 mmol), 3-*n*butylamidequinoline (0.242 g, 1.06 mmol) and AgPF₆ (0.134 g, 0.53 mmol) were refluxed together in 20 mL of MeCN for 5 days. The solution was allowed to cool to room temperature and the mixture was centrifuged for 15 minutes. The yellow solution was removed and to the gray powder 4 mL of DMF was added. The solution was heated until boiled and filtered hot through a Büchner funnel with a very fine fritted disc in order to remove the insoluble AgCl. The filtrate was stirred at room temperature for 2 weeks and the white powder was collected. Yield 0.043 g (12 %).

¹H NMR data (500 MHz) in DMF-*d*₇ at -40 °C:

Proton	δ(ppm)	Multiplicity	Coupling Constant (Hz)	# of Protons
a	10.58	s	---	4
	10.47	s		
	10.43	s		
	10.38	s		
	10.21	s		
b	10.34	d	³ J _{bc} = 8.8	4
	10.30	d		
	10.25	d		
	10.03	d		
	10.00	d		
c	8.64	dd	³ J _{cb} = 8.8 ³ J _{cd} = 7.5	4
	8.55	m		
	8.51	m		
d	8.18	m	---	4
e	8.59	d	³ J _{ed} = 8.2	4
f	9.62	s	---	4
	9.61	s		
	9.60	s		
	9.52	s		
	9.51	s		
g	9.79	s	---	4
	9.70	s		
h	3.70	q	³ J _{hg} = 5.8 ³ J _{hi} = 7.4	8
i	1.87	tt	³ J _{ih} ≈ ³ J _{ij} = 7.4	8
j	1.65	tq	³ J _{ji} ≈ ³ J _{jk} = 7.4	8
k	1.15	t	³ J _{kj} = 7.4	12

5.4.4 [Pt(3-*n*butylnicotinamide)₂(*t*butylbipy)] [PF₆]₂ (**5**)

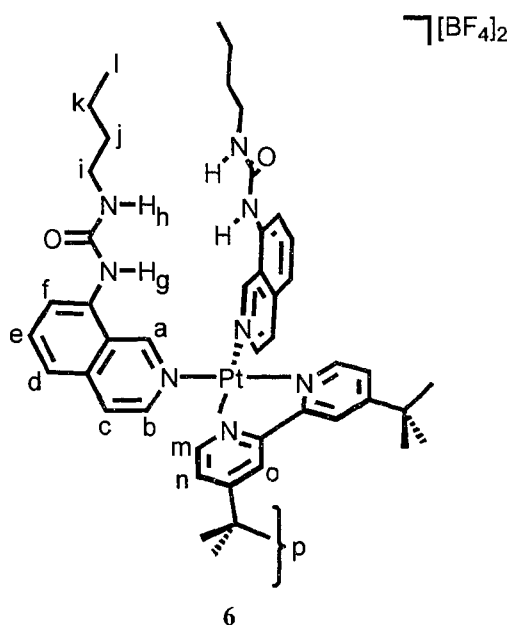


[PtCl₂(*t*butylbipy)]⁶⁹ (0.130 g, 0.24 mmol) was refluxed with 3-*n*butylnicotinamide (0.087 g, 0.49 mmol) and AgPF₆ (0.123 g, 0.49 mmol) in 20 mL of MeCN for 24 hrs. The precipitated AgCl was removed by vacuum filtration using a Buchner funnel with a very fine fritted disc. The yellow filtrate was concentrated to approximately 10 mL and the desired product was obtained by the addition of Et₂O. The yellow precipitate was collected using vacuum filtration and recrystallized from CHCl₃ to give a white crystalline solid. Yield 0.166 g (61 %). HRMS (ESI): Calcd. for C₃₈H₅₂PF₆N₆O₂Pt [**5**-PF₆]⁺: 964.3441; Found: 964.3444 and for C₃₈H₅₂N₆O₂Pt [**5**]²⁺: 409.6810; Found: 409.6894.

¹H NMR data (500 MHz) in MeCN-*d*₃ at 0 °C (see both *syn* and *anti* isomers):

Proton	δ(ppm)	Multiplicity	Coupling Constant (Hz)	# of Protons
a	9.62	s	---	2
	9.51	s		
b	9.27	d	³ J _{bc} = 5.8	2
	9.25	d		
c	7.87	m	---	2
d	8.50	d	³ J _{dc} = 6.8	2
		d		
e	7.51	t	³ J _{ef} = 6.0	2
	7.30	t		
f	3.38	q	³ J _{fe} = 6.0	4
			³ J _{fg} = 7.2	
g	1.58	m	---	4
h	1.39	m	---	4
i	0.95	t	³ J _{hi} = 7.5	6
j	7.60	d	³ J _{jk} = 6.4	2
k	7.63	d	³ J _{kj} = 6.4	2
l	8.54	d	⁴ J _{lk} = 2.0	2
m	1.45	s	---	18

5.4.5 [Pt(8-*n*butylureaisoquinoline)₂(*t*butylbipy)][BF₄]₂ (6)



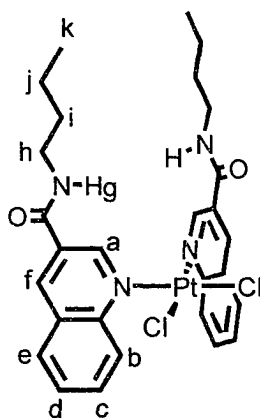
[PtCl₂(*t*butylbipy)]⁶⁹ (0.100 g, 0.19 mmol) was refluxed in 20 mL of MeCN with AgBF₄ (0.073 g, 0.37 mmol) and 8-*n*butylureaisoquinoline (0.091 g, 0.37 mmol) for 24 hrs. The solution was allowed to cool to room temperature and the precipitated AgCl was removed by vacuum filtration using a Büchner funnel with a very fine fritted disc. The filtrate was concentrated to approximately 10 mL and the crude product was precipitated out with Et₂O. The product was recrystallized several times from MeCN by slow diffusion of isopropyl ether. This process was repeated until a yellow crystalline powder was obtained. Yield 0.027 g (13 %). HRMS (ESI): Calcd. for C₄₆H₅₈BF₄N₈O₂Pt [6-BF₄]⁺: 1036.4360; Found: 1036.4353 and for C₃₈H₅₂N₆O₂Pt [6]²⁺: 474.7167; Found: 474.7165. Crystal data: C₄₆H₅₈B₂F₈N₈O₂Pt, M = 1155.71, monoclinic, space group C2/c, a = 31.745(7) Å, b = 18.067(3) Å, c = 20.0929(4) Å, β = 104.34(0)°, V = 11165(4) Å³, T = 173(2) K, Z = 8, μ = 2.585 mm⁻¹, 5827 independent reflections

($R_{\text{int}} = 0.1257$). $R1 = 0.0861$, $wR2 = 0.0724$, ($I > 2\sigma I$), $R1 = 0.2123$, $wR2 = 0.1993$, (all data), Goodness-of-fit = (F^2) = 1.063.

^1H NMR data (500 MHz) in $\text{MeCN-}d_3$ at $-5\text{ }^\circ\text{C}$ (see both *syn* and *anti* isomers):

Proton	δ (ppm)	Multiplicity	Coupling Constant (Hz)	# of Protons
a	9.88	s	---	2
	9.77	s		
b	8.66	d	$^3J_{bc} = 6.2$	2
c	8.05	bs	---	2
d	7.91	m	---	2
e	7.91	m	---	2
f	7.73	d	$^3J_{fe} = 7.7$	2
	7.68	d		
g	8.29	bs	---	2
	7.13	bs		
h	6.11	bs	---	2
	5.80	bs		
i	3.24	q	$^3J_{ih} = 6.4$ $^3J_{ij} = 7.0$	4
j	1.50	m	---	4
k	1.37	m	---	4
l	0.89	t	$^3J_{lk} = 7.5$	6
m	7.53	---	---	2
n	7.91	bs	---	2
o	8.46	s	---	2
p	1.46	s	---	18

5.4.6 *cis*-[PtCl₂(3-*n*butylamidequinoline)₂](7)



7

[PtCl₂(C₂H₅CN)₂] (0.100 g, 0.27 mmol) and 3-*n*butylamidequinoline (0.121 g, 0.53 mmol) were refluxed together in 20 mL of MeCN for 1 week. The solution was allowed to cool to room temperature and the white crystalline powder was collected by vacuum filtration. Yield 0.062 g (32 %).

¹H NMR data (500 MHz, DMF-*d*₇) at 0 °C:

Proton	δ(ppm)	Multiplicity	Coupling Constant(Hz)	# of Protons
a	10.44	d	⁴ J _{ab} = 1.7	2
	10.29	d		
b	10.38	dd	³ J _{bc} = 8.6 ⁴ J _{ba} = 1.7	2
	10.35	dd		
c	8.51	dd	³ J _{cb} = 8.6	2
			³ J _{dc} = 8.6 ³ J _{de} = 7.9	
d	8.19	dd	³ J _{dc} = 8.6	2
			³ J _{de} = 7.9	
e	8.58	d	³ J _{ed} = 7.9	2
f	9.53	s	---	2
	9.52	s		
g	9.70	t	³ J _{gh} = 5.7	2
	9.64	t		
h	3.68	m	³ J _{hg} = 5.7	4
			³ J _{hi} = 7.4	

i	1.88	quintet	${}^3J_{ih} \approx {}^3J_{ij} = 7.4$	4
j	1.66	sextet	${}^3J_{ji} \approx {}^3J_{jk} = 7.4$	4
k	1.52	t	${}^3J_{kj} = 7.4$	6

Chapter 6

Anion Sensing

6.1 Introduction

Chapter 4 described the synthesis and characterization of [Pt(8-*n*butylurea*iso*quinoline)₄][BF₄]₂, **3**, as well as its ability to act as an anion receptor. Association constants for this receptor were obtained using NMR as the spectroscopic method of choice. It was determined that the receptor binds the halides, H₂PO₄⁻ and SO₄²⁻ strongly in polar solvent with a very high affinity for SO₄²⁻.

In this chapter, receptor **3** is used to monitor the receptor:anion interactions using two more analytical techniques. Observing this receptor by mass spectrometry and fluorescence-emission spectroscopy may provide some qualitative information about the selectivity of the receptor in different environments.

Electrospray Ionization (ESI) mass spectrometry uses a relatively soft ionization process allowing non-covalent host-guest interactions to be monitored. This methodology is attractive because it is less tedious, requires much less product and a larger variety of solvent systems are available compared to conventional methods (NMR and UV-VIS).⁷⁹

Fluorescence-emission spectroscopy is also a very sensitive technique that has previously been used to study anion recognition.⁸⁰⁻⁸³ This technique probes the receptors' ability to act as a sensor. Anion sensors have the ability to recognize anions

through a macroscopic change in either their optical or electrochemical properties, as shown in Figure 6.1.

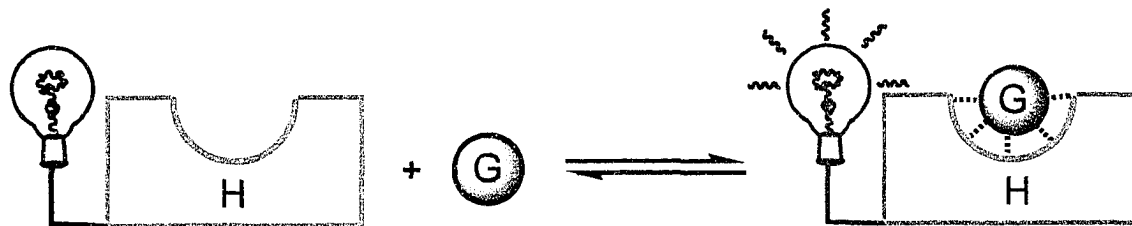


Figure 6.1 Host-guest interaction where the host acts as a sensor and undergoes an optical change when interacting with the guest.

The strategic placement of a luminophore in close proximity to the binding site provides an opportunity for an optical change upon binding the anion. Beer^{43, 45, 84, 85} and co-workers use tris(2,2'-bipyridine)ruthenium(II) as the luminophore in their receptors. The fluorescence-emission properties of this framework are well documented.⁸⁶ By simply appending several functional groups from this unit the electronic effects of binding anions can be monitored.

An example of a ruthenium(II) based anion sensor is shown in Figure 6.2. The fluorescence-emission data shows enhanced emission intensity upon binding Cl^- and Br^- with a shift in the peak maxima of 8 nm. The presence of I^- causes a decrease in emission intensity with no observed shift in peak maxima.⁴³

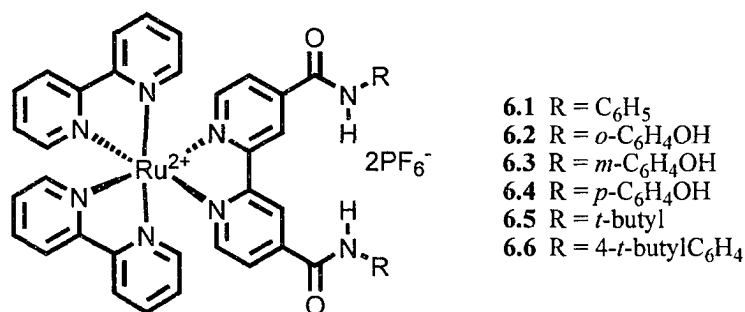


Figure 6.2 Tris(2,2'-bipyridine)ruthenium(II) based anion sensor where a change in fluorescence-emission occurs upon binding anions.

Our [Pt(8-*n*butylureaisoquinoline)₄][BF₄]₂ receptor contains a platinum(II) metal centre and pyridine type donors, a combination which has the potential to exhibit fluorescence due to a metal-to-ligand charge-transfer band (MLCT).⁸⁷ Therefore, a qualitative investigation into the optical sensory properties of this receptor is explored.

6.2 Results and Discussion

6.2.1 ESI-TOF Mass Spectrometric Investigation

There are several methods for determining association constants using mass spectrometry. However, there are a few factors that must be considered before a correlation between peak intensity and association constants can be made. The most influential is the ESI response factor of the ions. The response of an ion depends on its solvation energy, hydrophobicity and surface activity.⁸⁸

Thus far in the literature, when association constants have been determined an assumption of equal ESI response factors has been made, primarily in the case of large biomolecules. For smaller cations such as Na⁺, K⁺, Rb⁺, Cs⁺ and several ammonium cations, *actual* ESI response factors have been determined.⁷⁹

Brodbeck⁸⁹⁻⁹¹ and co-workers have developed a method for determining the relative concentrations of interacting host-guest complexes at equilibrium without determining the actual ESI response factor of each analyte.⁷⁹ This involves applying a correction factor to the peak intensities. The first step involves spraying a single component solution which contains the receptor and a single guest (molecule or ion). This is repeated for all the guests to obtain an ESI response factor. Next, a multi-component solution is made where the receptor and all the guests are present in a single solution. The concentration of the analytes is kept constant in all solutions.

The ratios of intensities observed in the multi-component spectrum are corrected using the relative intensities observed in the single component spectra. In doing so, the ESI response factor is eliminated from the peak intensity in the multi-component solution and the relative binding constants for the series of host-guest complexes can be obtained. In theory, a quantitative association constant can be obtained for each complex; however one value must be established by the use of an alternate conventional method. This in turn is used as a calibration for the relative complexation ratios. This method has been used for neutral host and cationic guest.⁸⁸ Herein, we explore for the first time, the application of this technique to a multi-charged cationic host, receptor **3**, and its interactions with anionic guests.

The experiment

The investigation of the relative strengths of receptor:anion interactions in a multi-component solution first involved the preparation of several sample solutions. The solvent system used was 2:3 MeCN:H₂O solution and the anions tested were CF₃SO₃⁻, NO₃⁻, Cl⁻, Br⁻, I⁻ and H₂PO₄⁻. The concentration of receptor in solution was 1.35 x 10⁻³ M

where the BF_4^- counterion was present at a concentration of 2.70×10^{-3} M. Therefore, in order to ensure equal concentration of all the anions their concentration was also 2.70×10^{-3} M.

The counterion for the anions must be chosen carefully. The presence of certain analytes in the solution can lead to signal suppression of the host-guest complexes. Initially, the tetrabutylammonium salt of the anions was used for consistency with the previous studies. The electrospray response of this cation however is very high and lead to significant signal suppression of the host-guest complexes. On the other hand, the electrospray response for K^+ is quite small compared to Bu_4N^+ and no signal suppression for the complexes was observed. Therefore, the potassium salt was used.

Initially, the mass spectra of the single component species were obtained and the intensities of the peaks were calculated to include the isotopic distribution. The multi-component solution was then run under the same conditions. This spectrum is shown in Figure 6.3. The spectrum shows host-guest interactions with all of the anions added except BF_4^- . The $[\mathbf{3}\text{-BF}_4]^\oplus$ ion has an exact mass of 1254.5 which was not observed, therefore, BF_4^- is not interacting strong enough to be competitive in the presence of the other anions.

The uncorrected peak intensities of the multi-component solution showed the largest peak at 1316.6 from $[\mathbf{3}\text{-CF}_3\text{SO}_3]^\oplus$ followed by the $[\mathbf{3}\text{-I}]^\oplus$ complex at 1294.6. The next complexes were $[\mathbf{3}\text{-Br}]^\oplus$ at 1247.6, $[\mathbf{3}\text{-H}_2\text{PO}_4]^\oplus$ at 1264.6, $[\mathbf{3}\text{-NO}_3]^\oplus$ at 1230.7 and finally with the smallest peaks was $[\mathbf{3}\text{-Cl}]^\oplus$ at 1203.6.

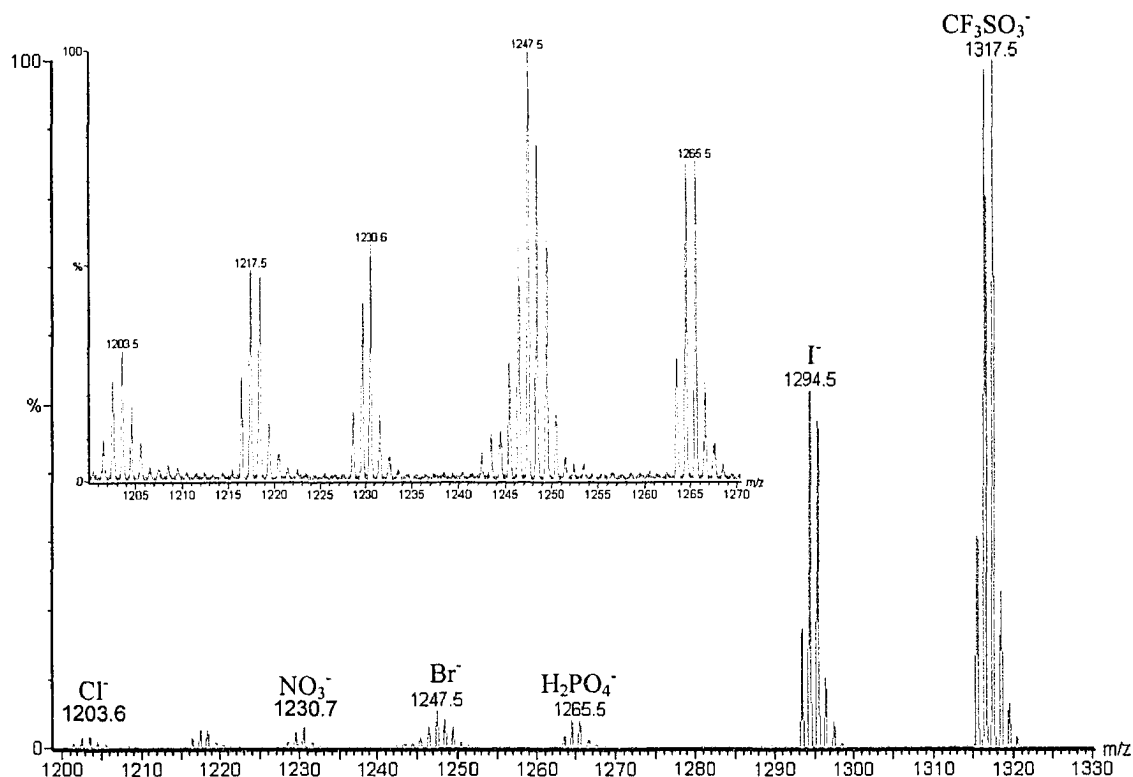


Figure 6.3 Mass spectrum obtained from a mixture of **3** and CF₃SO₃⁻, I⁻, H₂PO₄⁻, Br⁻, NO₃⁻ and Cl⁻.

Using the correction factors from the single component spectra, the relative ranking of receptor:anion interaction strengths showed H₂PO₄⁻ was the strongest binding anion. The halides were next with Br⁻ followed by Cl⁻ and I⁻ and finally the CF₃SO₃⁻ and NO₃⁻ anions. The relative order of association from the corrected intensities was comparable to the ¹H NMR data, where H₂PO₄⁻ binds much more strongly than the other anions. The halides showed moderate binding to **3** while the most weakly bound anions were CF₃SO₃⁻ and NO₃⁻. A bar graph illustrating the relative ratios of binding is shown in Figure 6.4.

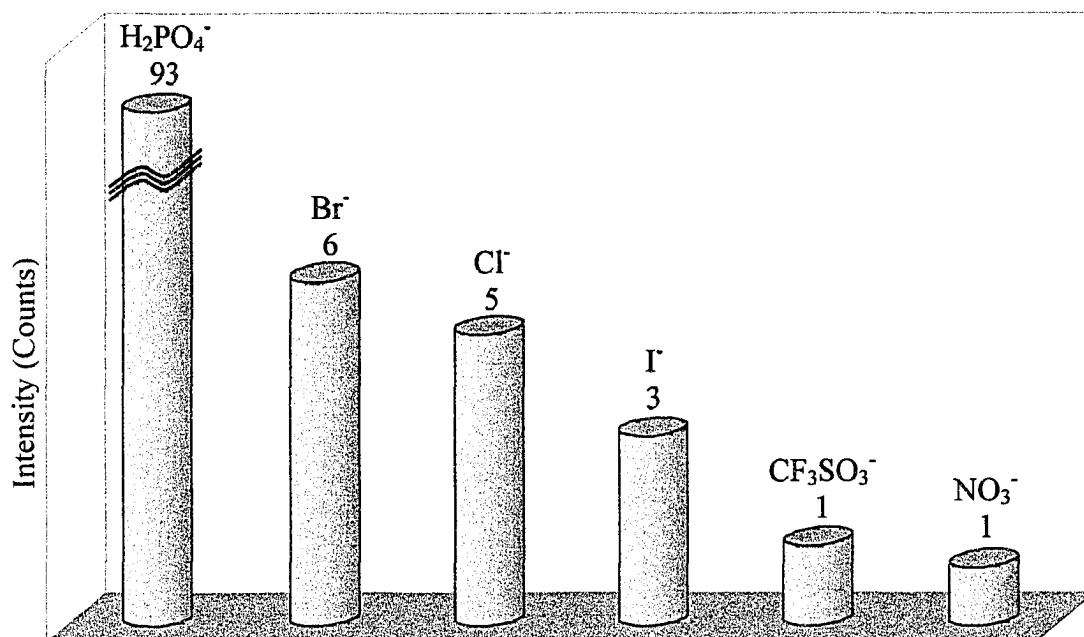


Figure 6.4 The relative binding ratio of the anions with **3** after correction for the ESI response factor.

This is a very effective tool for the screening of relative binding constants. In this case quantitative association constants were not obtained due to the different solvent systems used in the determination of the binding constants by NMR spectroscopy. Therefore, a starting point value was not available to calibrate the relative peak intensities. However, this is a superior tool compared to conventional methods due to the quick and straightforward methodology. An added feature is the very small amount of product required for the experiment.

6.2.2 Fluorescence-Emission Spectroscopic Investigation

An attempt to observe if the receptor acts as a sensor displaying optical properties by fluorescence-emission was undertaken. This study involved titration of the receptor with the desired anion as the tetrabutylammonium salt (CF_3SO_3^- , ReO_4^- , NO_3^- , Cl^- , Br^- , I^- ,

H₂PO₄⁻ and SO₄²⁻). The initial concentration of receptor was 1 x 10⁻⁵ M and anions were added until no further change in fluorescence intensity was observed.

There is very little literature precedence for the examination of the absorbance and fluorescence of tetrasubstituted monodendate pyridine based platinum(II) complexes. However, the UV-VIS spectrum of **3** displayed absorption bands at λ_{max} 270 and 370 nm. When the fluorescence-emission was tested by exciting the sample at 370 nm the intensity of the spectrum was very weak. The excitation at 270 nm however produced a much more intense and well defined spectrum (Figure 6.5). Therefore, the excitation wavelength used was at 270 nm with emission at 350 nm. The emission spectrum for the receptor showed peaks at 410 nm and 452 nm and the addition of anions to the receptor resulted in two notable changes; a change in peak intensity as well as in some cases a shift in the peak maxima.

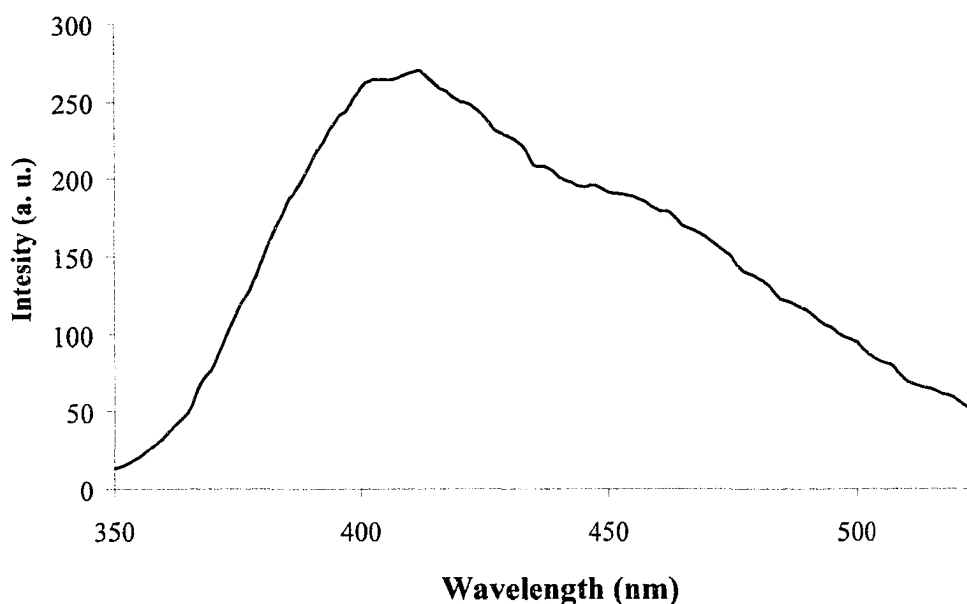


Figure 6.5 Fluorescence-emission spectrum of **3** in MeCN when excited at 270 nm. The peak maxima are 410 nm and 452 nm.

A change in fluorescence-emission intensity is observed with the addition of every anion. When excess anion is added (10 equivalents) the SO_4^{2-} , H_2PO_4^- , Br^- , I^- , and NO_3^- anions show a decrease or quenching of the peak at 410 nm while the Cl^- , CF_3SO_3^- and ReO_4^- show an increase in fluorescence, see Figure 6.6.

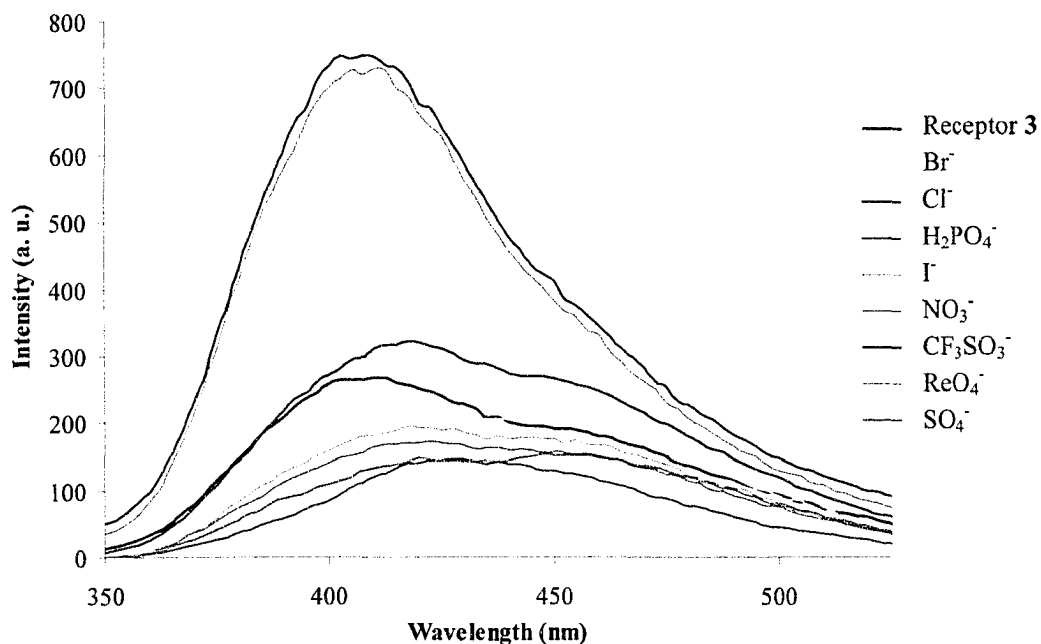


Figure 6.6 Fluorescence-emission spectra of **3** with several anions at 10 equivalents.

The SO_4^{2-} anion shows the largest amount of quenching in this system with a quenching of 57 % or 111 units followed by NO_3^- (63 units), I^- (57 units), H_2PO_4^- (49 units) and Br^- (30 units). The increase in fluorescence-emission intensity is most drastically seen with CF_3SO_3^- with an increase of 479 units or 194 %, ReO_4^- is next with an increase of 460 units and finally Cl^- with an increase of 65 units. Figure 6.7 displays a bar graph showing the amount of change in intensity observed upon addition of 10 equivalent of anion.

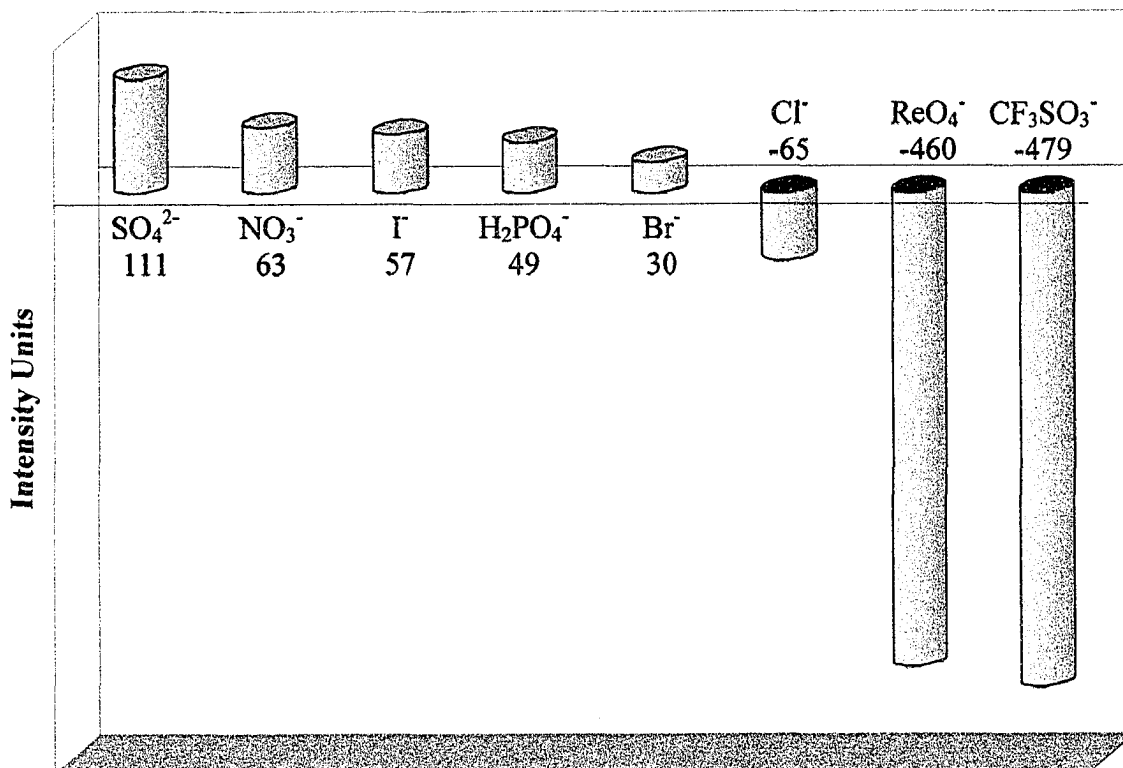


Figure 6.7 Change in intensity observed after the addition of 10 equivalents of anion.

The addition of ReO_4^- and CF_3SO_3^- results in a simple increase in intensity without a shift in the peak maximum. A shift in the peak maximum from 410 nm to 425 nm is observed upon addition of SO_4^{2-} , H_2PO_4^- , Cl^- , Br^- , I^- , and NO_3^- . This red (bathochromic) shift of 15 nm is due to a change in the environment surrounding the receptor (Figure 6.8).

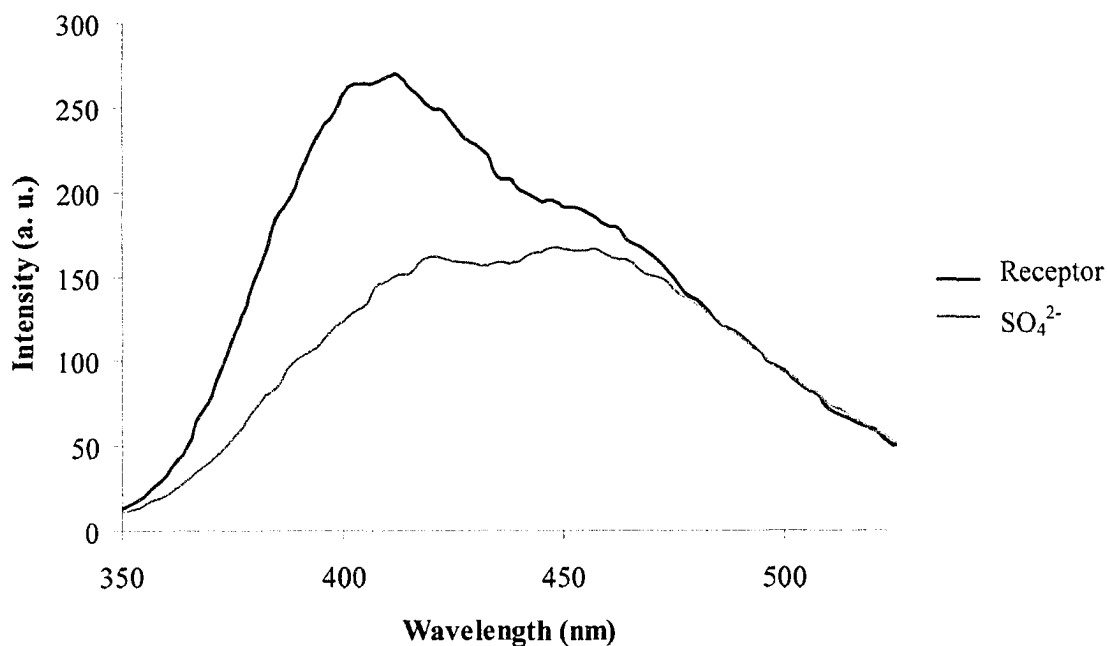


Figure 6.8 Spectra showing the bathochromic shift observed upon addition of 10 equivalents of SO_4^{2-} .

Therefore, the receptor is capable of acting as an optical sensor due its macroscopic optical change in the presence of anions. Several anions cause a quenching of the fluorescence emission while others cause an increase in intensity. The shift in the peak maximum also indicates the receptor undergoes a change in environment. However, with this information a qualitative ranking of the receptor:anion interaction was not possible.

6.3 Conclusions

The behaviour of the receptor $[\text{Pt}(8\text{-}n\text{butylureaisoquinoline})_4][\text{BF}_4]_2$, **3**, in the presence of various anions was detected using two different analytical techniques; ESI-TOF mass spectrometry and fluorescence-emission spectroscopy.

The mass spectrometry experiment showed peaks for all the anions coordinated to the receptor except BF_4^- . This reaffirms our reasoning for choosing BF_4^- as the counterion for the receptor due to its non-competitive nature. The relative peak intensities are due in part to the ESI response factor of the ion, therefore a correction factor was used. A ranking of the corrected binding ratios shows H_2PO_4^- binds very strongly while the halides show moderate binding. The weakest interactions are seen with CF_3SO_3^- and NO_3^- . This relative order is comparable to the values obtained using ^1H NMR titrations. Therefore, this is an effective method for screening receptor:anion interactions.

The fluorescence-emission spectroscopy was used to determine the capability of this receptor to act as a sensor. The changes in peak intensities as well as a shift in the peak maxima in the presence of anions are indicative of an anion sensor. A decrease in intensity was observed in the presence of SO_4^{2-} , H_2PO_4^- , Br^- , I^- , and NO_3^- and an increase in intensity was observed with Cl^- , CF_3SO_3^- and ReO_4^- . The red shift of 15 nm occurred in the presence of SO_4^{2-} , H_2PO_4^- , Cl^- , Br^- , I^- , and NO_3^- while ReO_4^- and CF_3SO_3^- produce no shift in the peak maximum.

The SO_4^{2-} anion caused the greatest amount of quenching as well as a shift in peak maximum, and therefore showed the most effective change in electronic environment in the receptor. This may be interpreted as a strong interaction with receptor **3**, as we have seen by other methods. To the other extreme, ReO_4^- and CF_3SO_3^- showed an increase in fluorescence-emission intensity with no shift in peak maxima. Therefore, lack of ability to change the electronic nature of the receptor may be indicative of weak receptor:anion interactions.

Overall, the fluorescence-emission experiments showed the electronic environment of the receptor is affected by the presence of different anions. A qualitative ranking of the binding efficiencies was not possible at this time however, this method may still have potential with further studies.

6.4 Experimental

6.4.1 General Methods

The mass spectra were obtained using a Micromass LCT electrospray ionization time of flight spectrometer. The samples were run in a 2:3 MeCN / H₂O solvent mixture. Fluorescence-emission data were collected on a Cary Eclipse Fluorescence Spectrophotometer. Both emission spectra and mass spectra were recorded in EM Science OmniSolv[®] High Purity Solvents.

6.4.2 Mass Spectrometry Solution Preparation

For this experiment, separate solutions were made for the receptor and the six anions. The stock solution for the receptor was prepared as 2 mL of MeCN at a concentration of 3.73×10^{-3} M (7.45×10^{-6} mol). From this, 200 μ L (7.45×10^{-7} mol) was used per mass spectrum sample. Six anion solutions as the potassium salts were prepared (KNO₃, KI, KCF₃SO₃, KCl, KH₂PO₄ and KBr). This was accomplished by the addition of 5.96×10^{-5} moles of each potassium salt in 2 mL of a 1:1 mixture of MeCN and H₂O. From this, 50 μ L aliquots of each solution were used for each sample. Each single component sample contained 200 μ L of receptor solution, 50 μ L of anion solution and 250 μ L of MeCN for a total volume of 500 μ L. The multi-component sample

contained 200 μL of receptor solution and 50 μL of each anion solution for a total volume of 500 μL , once again.

The multi-component solution was sprayed first to determine the optimal setting for all the peaks to be observed. Each single component solution was then run under the exact same conditions. The correction factor was obtained by adding up the peak count for each species in the single component spectra, including their isotopic distribution. The response factor was obtained by dividing the total peak intensity of the guest anion by the total peak intensity of the BF_4^- species in the spectrum. The multi-component spectrum was corrected by dividing the total peak intensity by the correction factor obtained from the single component spectra.

6.4.3 Fluorescence-Emission Titration Methods

The receptor stock solution consisted of 10 mL of MeCN at a concentration of 2.51×10^{-4} M (0.0034 g, 2.5×10^{-6} mol). The dilution involved taking 0.4 mL of stock solution and adding it to 9.6 mL of MeCN which resulted in a 1.0×10^{-5} M (1.0×10^{-7} mol) solution. The anion solutions were made with the tetrabutylammonium salts (SO_4^{2-} , H_2PO_4^- , Cl^- , Br^- , I^- , NO_3^- , ReO_4^- and CF_3SO_3^-). Each anion solution consisted of 10 mL of MeCN at a concentration of 1.5×10^{-5} M (1.5×10^{-5} M). The titration involved starting with 1.5 mL of diluted receptor solution. The anion was added in intervals until no further change in intensity was observed. Table 6.1 shows an example of the stepwise additions of anion used during a titration.

Table 6.1 An example of the aliquots of anion added during a titration.

Volume per addition (μL)	Concentration of Receptor (M)	Concentration of Anion (M)	Equivalents of Anion present
0	1.00×10^{-5}	0	0
1	9.99×10^{-6}	9.99×10^{-7}	0.1
1	9.99×10^{-6}	2.00×10^{-6}	0.2
2	9.97×10^{-6}	3.99×10^{-6}	0.4
2	9.96×10^{-6}	5.98×10^{-6}	0.6
4	9.93×10^{-6}	9.93×10^{-5}	1.0
5	9.90×10^{-6}	1.49×10^{-5}	1.5
10	9.87×10^{-6}	1.97×10^{-5}	2.0
10	9.80×10^{-6}	2.94×10^{-5}	3.0
10	9.74×10^{-6}	3.90×10^{-5}	4.0
20	9.62×10^{-6}	5.77×10^{-5}	6.0
20	9.49×10^{-6}	7.59×10^{-5}	8.0

20	9.38×10^{-6}	9.38×10^{-5}	10.0
30	9.20×10^{-6}	1.20×10^{-4}	13.0
40	9.04×10^{-6}	1.45×10^{-4}	16.0
100	8.82×10^{-6}	1.76×10^{-4}	20.0
100	8.33×10^{-6}	2.50×10^{-4}	30.0
200	7.89×10^{-6}	3.16×10^{-4}	40.0
200	7.14×10^{-6}	3.75×10^{-4}	60.0
200	6.52×10^{-6}	4.29×10^{-4}	80.0
200	6.00×10^{-6}	5.22×10^{-4}	100.0
500	5.00×10^{-6}	6.00×10^{-4}	150.0

Chapter 7

Summary and Future Work

7.1 Summary

The thesis focused on the development of anion receptors containing a flexible inorganic framework capable of conformational diversity. The general framework consisted of the cationic complex $[\text{PtL}_4]^{2+}$, where free rotation of the Pt-L bond produced *pseudo-calix[4]arene* type conformations (Figure 7.1). The cationic nature of the platinum(II) metal centre also provided an electrostatic component to our receptors. The ligands contained amide or urea functional groups for the added interaction of hydrogen bonding.

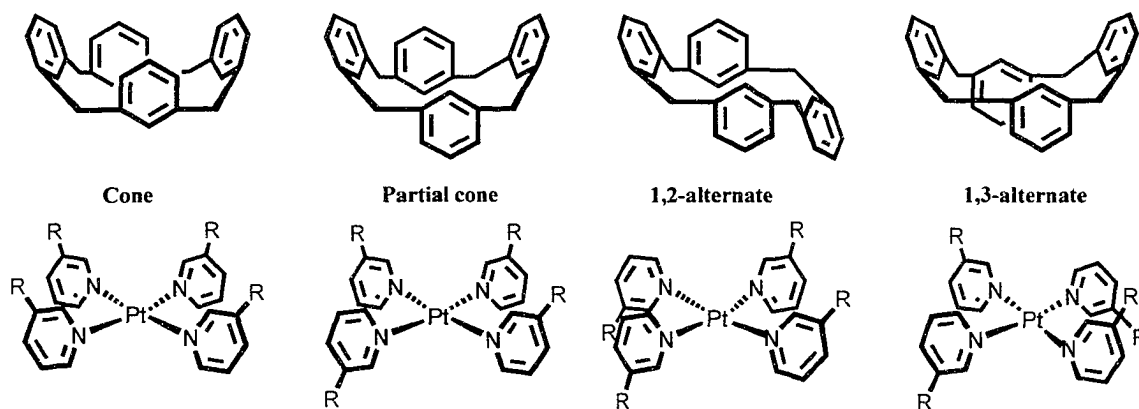


Figure 7.1 Structural similarity between calix[4]arene and our receptor framework.

Chapter 2 investigated the binding efficiency and selectivity of the $[\text{Pt}(3\text{-}n\text{butylnicotinamide})_4][\text{PF}_6]_2$, **1**, receptor (Figure 7.2). The binding studies showed moderate association constants in polar organic solvents with the tetrahedral shaped anions (CF_3SO_3^- , ReO_4^- , HSO_4^- and H_2PO_4^-) binding in a 1:1 ratio. The association constants observed are 129 and 150 M^{-1} for CF_3SO_3^- and ReO_4^- in $\text{MeCN-}d_3$. The HSO_4^-

anion has an association of 149 M^{-1} in 75% MeCN- d_3 25% DMSO- d_6 and H_2PO_4^- is 264 M^{-1} in DMSO- d_6 . The NO_3^- and CH_3CO_2^- anions bound in a 1:2 ratio with association constants of K_1 562 K_2 132 M^{-1} for NO_3^- in MeCN- d_3 and K_1 230 K_2 491 M^{-1} for CH_3CO_2^- in 10 % MeCN- d_3 90% DMSO- d_6 . The strongest interacting anion was CH_3CO_2^- with the second association constant higher than the first due to a positive allosteric interaction. Therefore, this first generation receptor preferred to bind planar bidentate anions such as CH_3CO_2^- .

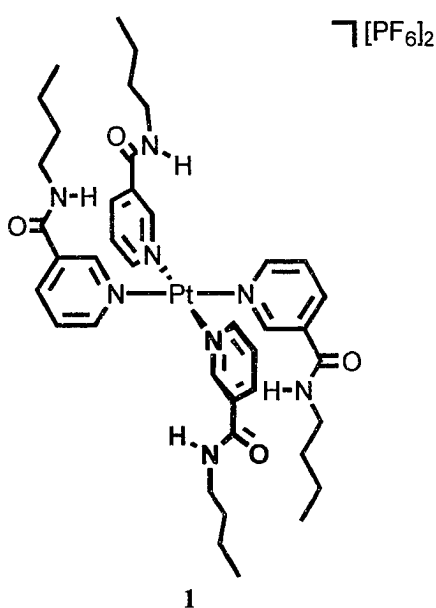


Figure 7.2 First generation receptor $[\text{Pt}(3\text{-}n\text{butylnicotinamide})_4][\text{PF}_6]_2$, **1**, arbitrarily shown in the 1,2-alternate conformation.

The second generation receptor was $[\text{Pt}(3,5\text{-}di\text{-}n\text{butylamidepyridine})_2(\text{zbutylbipy})][\text{PF}_6]_2$, **2**, (Figure 7.3). This receptor was preorganized for a 1:2 interaction with anions by removing the conformational flexibility. The interactions with tetrahedral anions were slightly weaker compared to our first generation receptor. The association constants obtained were 101 and 148 M^{-1} for CF_3SO_3^- and ReO_4^- in MeCN- d_3 . The addition of HSO_4^- , H_2PO_4^- , CH_3CO_2^- and $\text{C}_6\text{H}_5\text{CO}_2^-$ resulted in decomposition of the

receptor due to the increase in reactivity in the Pt-N bond from the presence of two electron withdrawing amide groups in each pyridine ring. Once again, a 1:2 binding of was observed with NO_3^- (K_1 283, K_2 2 M^{-1}); however, much like the tetrahedral anions, the association constants are lower compared to the first generation receptor. The overall decrease in binding strength of the first association constant is attributed to the possibility of only two hydrogen bonds interacting with the anion, since the receptor is locked into the 1,2-alternate conformation. The decrease in the second binding constant is attributed to a negative allosteric effect. The binding of the first anion changes the shape and size of the second binding site hindering a strong interaction with the second anion.

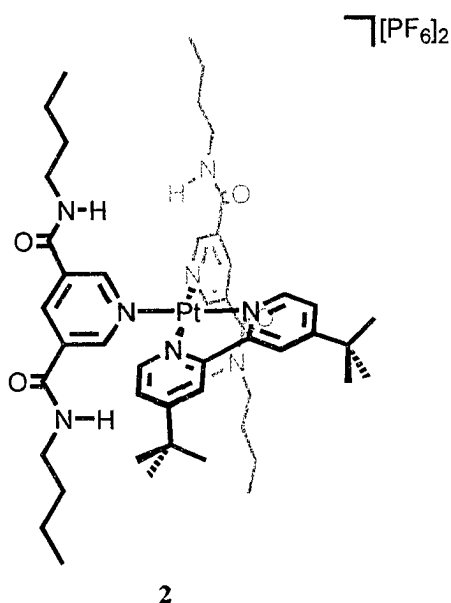


Figure 7.3 Second generation receptor $[\text{Pt}(3,5\text{-di-}n\text{butylamidepyridine})_2(\text{tbutylbipy})][\text{PF}_6]_2$, **2**.

In chapter 4, the amide functional groups of the previous receptors were replaced with urea functional groups which doubles the number of hydrogen bond donors from four to eight (Figure 7.4). The third generation receptor was $[\text{Pt}(8\text{-}n\text{butylureaisoquinoline})_4][\text{BF}_4]_2$, **3**, which shows a substantial increase in binding constant compared to the previously studied receptors. There were two types of

interactions observed with this receptor; 1:2 binding with the halides and 1:1 binding with strongly coordinating tetrahedral shaped anions. The Cl^- anion had the strongest association constants of the halides with K_1 11693 and K_2 2223 M^{-1} while Br^- and I^- gave association constants of K_1 1364 K_2 450 M^{-1} and K_1 1431 K_2 52 M^{-1} . The H_2PO_4^- and SO_4^{2-} anions coordinate to the receptor very strongly with association constants $>10^5 \text{M}^{-1}$. In the solid state, the 1,2-alternate conformation is obtained with Cl^- as the counterion and the cone conformation is observed with SO_4^{2-} present.

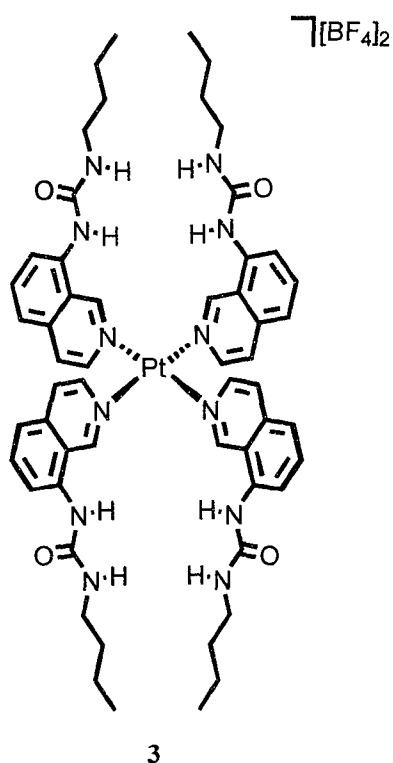


Figure 7.4 Third generation receptor $[\text{Pt}(8\text{-}n\text{butylureaaisoquinoline})_4][\text{BF}_4]_2$, **3**, arbitrarily in the 1,2-alternate conformation.

The stability, conformation flexibility and interconversion barriers between conformations of these receptors was studied in chapter 5. The interconversion between conformations for receptors **1** and **3** was fast on the NMR timescale. In order to slow the

Pt-N rotation, four model complexes based on these receptors were investigated. The model compounds were modified to increase the interconversion barrier of the conformations by adding bulk to the ligands. The addition of a fused ring to receptor 1 resulted in complex $[\text{Pt}(3\text{-}n\text{butylamidoquinoline})_4][\text{PF}_6]_2$, **4**. The rotational barrier of the ligand was increased; however, the presence of four conformations results in a very complex ^1H NMR spectrum, which was impossible to assign to any degree of certainty. As a result, this model complex was simplified by the removal of two bulky ligands to give the model complex $\text{cis-}[\text{PtCl}_2(3\text{-}n\text{butylamidoquinoline})_2]$, **7**. The ^1H NMR spectrum showed two set of peaks of differing integration representing the two possible conformation; *syn* and *anti*. Molecular mechanics was used to assign the larger peak and therefore more stable conformation to the *anti* conformation. The interconversion barrier was measured as 76 kJ/mol using variable-temperature ^1H NMR. (Figure 7.5)

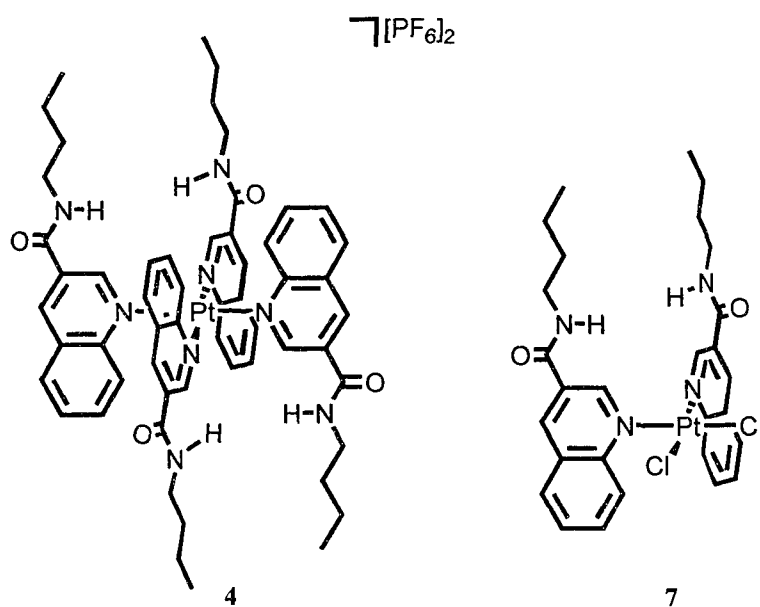


Figure 7.5 Model complexes $[\text{Pt}(3\text{-}n\text{butylamidoquinoline})_4][\text{PF}_6]_2$, **4**, arbitrarily in the 1,2-alternate conformation and $\text{cis-}[\text{PtCl}_2(3\text{-}n\text{butylamidoquinoline})_2]$, **7**, in the *syn* conformation.

Model complexes $[\text{Pt}(3\text{-}n\text{butylnicotinamide})_2(\text{tbutylbipy})][\text{PF}_6]_2$, **5**, and $[\text{Pt}(8\text{-}n\text{butylurea}i\text{isoquinoline})_2(\text{tbutylbipy})][\text{BF}_4]_2$, **6**, were designed as another variation of the two conformation receptor (Figure 7.6). These model complexes have increased interconversion barrier due to the use of a bipy ligand as the added bulk. When coordinated to the metal centre the bipy is in the square plane of the receptor therefore adding indirect bulk as the ligands rotate. The most stable conformation in both cases is the *anti* conformation with interconversion barriers of 72 kJ/mol for **5** and 69 kJ/mol for **6**.

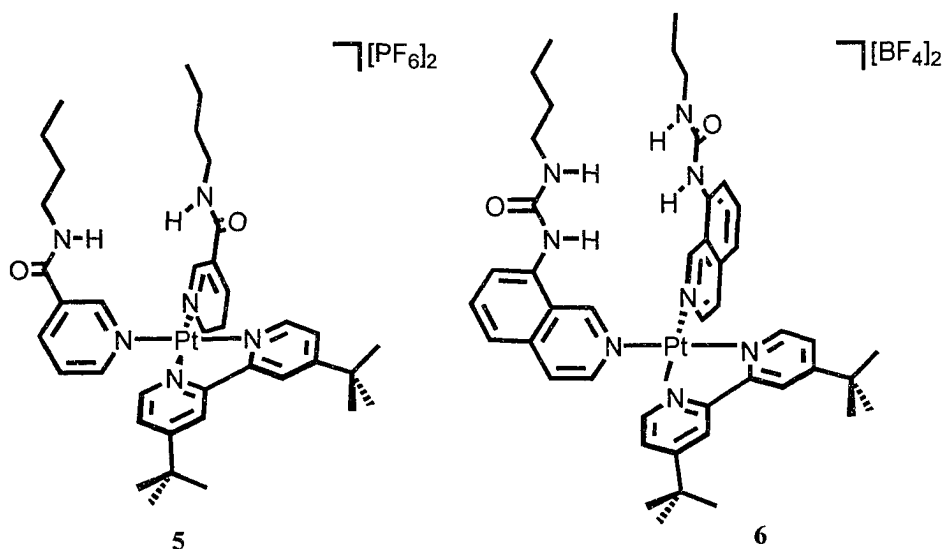


Figure 7.6 Model complexes $[\text{Pt}(3\text{-}n\text{butylnicotinamide})_2(\text{tbutylbipy})][\text{PF}_6]_2$, **5**, and $[\text{Pt}(8\text{-}n\text{butylurea}i\text{isoquinoline})_2(\text{tbutylbipy})][\text{BF}_4]_2$, **6**, arbitrarily in the *syn* conformation.

In a final section described in chapter 6, we investigated the use of different techniques for qualitative evaluation of receptor **3**:anion interactions. Electrospray ionization mass spectrometry was used to show the relative receptor:anion association from a single solution of receptor and six different anions. H_2PO_4^- showed the highest association followed by Br^- , Cl^- , I^- , CF_3SO_3^- and NO_3^- .

Fluorescence-emission spectroscopy showed receptor **3** to be fluorescent. In the presence of SO_4^{2-} , H_2PO_4^- , Br^- , I^- , and NO_3^- the fluorescence is quenched and in the presence of Cl^- , CF_3SO_3^- and ReO_4^- the fluorescence is increased. There was also a bathochromic shift in the peak maxima in the presence of SO_4^{2-} , H_2PO_4^- , Cl^- , Br^- , I^- , and NO_3^- demonstrating a change in environment around the metal centre. Unfortunately, these results did not lead to a qualitative ranking of binding efficiencies, as was possible with the ESI-MS study.

7.2 Future Work

Although this project was ultimately successful and, in particular, produced one of the best anion receptors known to date for the sulphate ion, there is still much of information regarding receptor conformations in solution that is not fully understood. Ideally, if a receptor could be designed so that all four *pseudo-calix*[4]arene conformations were observable in a ^1H NMR spectrum at room temperature, a substantial amount of information about the mechanism of binding anions could be obtained. This mechanistic information would then be very useful in determining the preferred conformation for binding a particular anion and this information used to improve the design. The long term goal would be an improvement in overall binding strengths and most importantly an increase in the selectivity for a particular targeted anion.

We conclude that there are a number of design features that could be addressed in the creation of the *next* generation of metal-organic anion receptors based on the concepts outlined in the scope of this thesis. Some ideas are:

1. *Increase the number of hydrogen-bond donors per ligand.* The increase from one amide to two urea hydrogen bonds had a dramatic effect on

binding so this trend could be continued. It may be possible to determine the optimal number of interactions for each particular target anion.

2. *Increase the acidity of the hydrogen-bond donors.* The strength of a hydrogen-bond is directly related to the polarization of the E-H bond. A simple step would be to look at the thiourea version of receptor **3**. Other functional groups such as pyrrole which contain more acidic N-H's could be included.
3. *Determine the overall contribution of C-H...anion interactions.* It was an added bonus to see that the *ortho*-aromatic hydrogens on the pyridine and *isoquinoline* ligands participate in binding both in solution and the solid state. The significance of these interactions and their inclusion in future receptor design could be beneficial.
4. *Match the spatial distribution of hydrogen-bond donors to the geometrical shape of the target anion.* Strong binding occurred between receptor **3** and the sulphate ion, despite the mismatch between the 4-fold symmetry of the receptor and 3-fold anion symmetry of the anion. Increased selectivity and binding strength may be gained by a better match between guest shape and the host cavity.
5. *Advance application as a sensor.* The fluorescence-emission properties of the receptor may be explored using displacement assays. The selectivity of the receptor for a specific guest in a competitive environment may be fine tuned.

One final point of interest would be the combining of conformational observations with anion binding. That is, if it were possible to design a system that allowed observation of various participating conformations in solution it would be of immense value to be able to directly *watch* the conformational landscape change as anions were introduced. This would provide invaluable information by allowing evaluation of the receptor design as it engaged in anion binding in *real time*.

References

1. J. W. Steed and J. L. Atwood, *Supramolecular Chemistry*, Wiley, **2000**.
2. P. D. Beer and P. A. Gale, *Angewandte Chemie, International Edition*, **2001**, *40*, 486.
3. C. H. Park and H. E. Simmons, *Journal of the American Chemical Society*, **1968**, *90*, 2431.
4. C. J. Pedersen, *Journal of the American Chemical Society*, **1967**, *89*, 7017.
5. A. Bianchi, K. Bowman-James, and E. Garcia-Espana, *Supramolecular Chemistry of Anions*, Wiley-VCH, **1997**.
6. P. A. Gale, *Coordination Chemistry Reviews*, **2001**, *213*, 79.
7. K. Kavallieratos, C. M. Bertao, and R. H. Crabtree, *Journal of Organic Chemistry*, **1999**, *64*, 1675.
8. K. Kavallieratos, S. R. de Gala, D. J. Austin, and R. H. Crabtree, *Journal of the American Chemical Society*, **1997**, *119*, 2325.
9. G. Hennrich and E. V. Anslyn, *Chemistry--A European Journal*, **2002**, *8*, 2218.
10. J. J. Lavigne and E. V. Anslyn, *Angewandte Chemie, International Edition*, **2001**, *40*, 3118.
11. J. J. Lavigne and E. V. Anslyn, *Angewandte Chemie, International Edition*, **1999**, *38*, 3666.
12. L. A. Cabell, M. D. Best, J. J. Lavigne, S. E. Schneider, D. M. Perreault, M.-K. Monahan, and E. V. Anslyn, *Journal of the Chemical Society, Perkin Transactions 2*, **2001**, 315.
13. S. L. Wiskur and E. V. Anslyn, *Journal of the American Chemical Society*, **2001**, *123*, 10109.
14. S. E. Schneider, S. N. O'Neil, and E. V. Anslyn, *Journal of the American Chemical Society*, **2000**, *122*, 542.
15. A. J. Ayling, M. N. Perez-Payan, and A. P. Davis, *Journal of the American Chemical Society*, **2001**, *123*, 12716.

16. A. P. Davis, J. J. Perry, and R. P. Williams, *Journal of the American Chemical Society*, **1997**, *119*, 1793.
17. I. El Drubi Vega, P. A. Gale, M. B. Hursthouse, and M. E. Light, *Organic & Biomolecular Chemistry*, **2004**, *2*, 2935.
18. S. Camiolo, P. A. Gale, M. B. Hursthouse, and M. E. Light, *Organic & Biomolecular Chemistry*, **2003**, *1*, 741.
19. S. Camiolo, P. A. Gale, M. B. Hursthouse, M. E. Light, and A. J. Shi, *Chemical Communications*, **2002**, 758.
20. P. A. Gale, S. Camiolo, G. J. Tizzard, C. P. Chapman, M. E. Light, S. J. Coles, and M. B. Hursthouse, *Journal of Organic Chemistry*, **2001**, *66*, 7849.
21. S. Camiolo, P. A. Gale, M. B. Hursthouse, and M. E. Light, *Tetrahedron Letters*, **2002**, *43*, 6995.
22. T. Clifford, S. Mason, J. M. Llinares, and K. Bowman-James, *Journal of the American Chemical Society*, **2000**, *122*, 1814.
23. M. A. Hossain, J. M. Llinares, C. A. Miller, L. Seib, and K. Bowman-James, *Chemical Communications*, **2000**, 2269.
24. G. Papoyan, K.-J. Gu, J. Wiorcikiewicz-Kuczera, K. Kuczera, and K. Bowman-James, *Journal of the American Chemical Society*, **1996**, *118*, 1354.
25. S. Otto and S. Kubik, *Journal of the American Chemical Society*, **2003**, *125*, 7804.
26. S. Kubik, R. Kirchner, D. Nolting, and J. Seidel, *Journal of the American Chemical Society*, **2002**, *124*, 12752.
27. S. Kubik, R. Goddard, R. Kirchner, D. Nolting, and J. Seidel, *Angewandte Chemie, International Edition*, **2001**, *40*, 2648.
28. S. Kubik and R. Goddard, *European Journal of Organic Chemistry*, **2001**, 311.
29. S. Kubik and R. Goddard, *Chemical Communications*, **2000**, 633.
30. S. Kubik and R. Goddard, *Journal of Organic Chemistry*, **1999**, *64*, 9475.
31. F. Sansone, L. Baldini, A. Casnati, M. Lazzarotto, F. Ugozzoli, and R. Ungaro, *Proceedings of the National Academy of Sciences of the United States of America*, **2002**, *99*, 4842.

32. M. Lazzarotto, F. Sansone, L. Baldini, A. Casnati, P. Cozzini, and R. Ungaro, *European Journal of Organic Chemistry*, **2001**, 595.
33. N. Pelizzi, A. Casnati, A. Friggeri, and R. Ungaro, *Journal of the Chemical Society, Perkin Transactions 2: Physical Organic Chemistry*, **1998**, 1307.
34. J. L. Sessler, W.-S. Cho, D. E. Gross, J. A. Shriver, V. M. Lynch, and M. Marquez, *Journal of Organic Chemistry*, **2005**, 70, 5982.
35. J. L. Sessler, J. Jayawickramarajah, A. Gouloumis, T. Torres, D. M. Guldi, S. Maldonado, and K. J. Stevenson, *Chemical Communications*, **2005**, 1892.
36. C.-H. Lee, J.-S. Lee, H.-K. Na, D.-W. Yoon, H. Miyaji, W.-S. Cho, and J. L. Sessler, *Journal of Organic Chemistry*, **2005**, 70, 2067.
37. K. Kano, H. Kamo, S. Negi, T. Kitae, R. Takaoka, M. Yamaguchi, H. Okubo, and M. Hirama, *Journal of the Chemical Society, Perkin Transactions 2: Physical Organic Chemistry*, **1999**, 15.
38. M. Staffilani, K. S. B. Hancock, J. W. Steed, K. T. Holman, J. L. Atwood, R. K. Juneja, and R. S. Burkhalter, *Journal of the American Chemical Society*, **1997**, 119, 6324.
39. J. W. Steed, C. P. Johnson, R. K. Juneja, J. L. Atwood, and R. S. Burkhalter, *Supramolecular Chemistry*, **1996**, 6, 235.
40. J. L. Atwood, K. T. Holman, and J. W. Steed, *Chemical Communications*, **1996**, 1401.
41. J. W. Steed, R. K. Juneja, and J. L. Atwood, *Angewandte Chemie, International Edition*, **1995**, 33, 2456.
42. P. D. Beer, F. Szemes, V. Balzani, C. M. Sala, M. G. B. Drew, S. W. Dent, and M. Maestri, *Journal of the American Chemical Society*, **1997**, 119, 11864.
43. P. D. Beer, S. W. Dent, and T. J. Wear, *Journal of the Chemical Society, Dalton Transactions: Inorganic Chemistry*, **1996**, 2341.
44. F. Szemes, D. Heseck, Z. Chen, S. W. Dent, M. G. B. Drew, A. J. Goulden, A. R. Graydon, A. Grieve, R. J. Mortimer, T. Wear, J. S. Weightman, and P. D. Beer, *Inorganic Chemistry*, **1996**, 35, 5868.
45. P. D. Beer, C. A. P. Dickson, N. Fletcher, A. J. Goulden, A. Grieve, J. Hodacova, and T. Wear, *Journal of the Chemical Society, Chemical Communications*, **1993**, 828.

46. L. Fabbrizzi and I. Faravelli, *Chemical Communications*, **1998**, 971.
47. P. D. Beer, M. G. B. Drew, D. Hesek, and R. Jagessar, *Journal of the Chemical Society, Chemical Communications*, **1995**, 1187.
48. P. D. Beer, M. G. B. Drew, and R. Jagessar, *Journal of the Chemical Society, Dalton Transactions*, **1997**, 5, 881.
49. P. A. Gale, *Coordination Chemistry Reviews*, **2000**, 199, 181.
50. X. Yang, C. B. Knobler, and M. F. Hawthorne, *Angewandte Chemie, International Edition*, **1991**, 30, 1507.
51. X. Yang, C. B. Knobler, and M. F. Hawthorne, *Journal of the American Chemical Society*, **1992**, 114, 380.
52. J. L. Sessler, A. Gebauer, and P. A. Gale, *Gazzette Chimica Italia*, **1997**, 127, 723.
53. S. Camiolo, S.J. Coles, P.A. Gale, M.B. Hursthouse, T.A. Mayer, and M. A. Paver, *Chemical Communications*, **2000**, 275.
54. J. C. Medina, C. Li, S. G. Bott, J. L. Atwood, and G. W. Gokel, *Journal of the American Chemical Society*, **1991**, 113, 366.
55. C. Li, J. C. Medina, G. E. M. Maguire, E. Abel, J. L. Atwood, and G. W. Gokel, *Journal of the American Chemical Society*, **1997**, 119, 1609.
56. J. C. Mareque Rivas and L. Brammer, *New Journal of Chemistry*, **1998**, 1315.
57. D. R. Turner, E. C. Spencer, J. A. K. Howard, D. A. Tocher, and J. W. Steed, *Chemical Communications*, **2004**, 1352.
58. R. Omi, M. Goto, I. Miyahara, H. Mizuguchi, H. Hayashi, H. Kagamiyama, and K. Hirotsu, *Journal of biological chemistry*, **2003**, 278, 46035.
59. B. R. Cameron and S. J. Loeb, *Chemical Communications*, **1997**, 573.
60. M. Brookhart, B. Grant, and A. F. J. Volpe, *Organometallics*, **1992**, 11, 3920.
61. J. March, *Advanced Organic Chemistry*, McGraw-Hill Book Company, **1977**.
62. V. Y. Kukushkin, A. Oskarsson, and L. I. Elding, *Inorganic Syntheses*, **1997**, 31, 279.
63. A. Job, *Annales de Chimie (10th series)*, **1928**, 9, 113.

64. K. A. Connors, *Binding constants: The measurement of molecular complex stability*, Wiley-Interscience Publication, **1987**.
65. D. Voet and J. G. Voet, *Biochemistry*, John Wiley and Sons, **1995**.
66. M. J. Hynes, *Journal of the Chemical Society, Dalton Transactions: Inorganic Chemistry (1972-1999)*, **1993**, 311.
67. in *SHELXTL version 5.03 Program Library*, Siemens Analytical Instrument Division, **1997**.
68. in *DIAMOND 3.0 - Visual Crystal Information System, Crystal Impact*.
69. K. H. Mitchell and C. M. Jensen, *Inorganic Chemistry*, **1995**, 34, 4441.
70. M. Albrecht, J. Zauner, R. Burgert, H. Rottele, and R. Frohlich, *Materials Science & Engineering, C: Biomimetic and Supramolecular Systems*, **2001**, C18, 185.
71. R. H. F. Manske and M. Kulka, *Can. J. Research*, **1949**, 27B, 161.
72. Y. Ahmad and D. H. Hey, *Journal of the Chemical Society, Abstracts*, **1961**, 3882.
73. U. Bierbach and N. Farrell, *Inorganic Chemistry*, **1997**, 36, 3657.
74. T. W. Hambley, *Inorganic Chemistry*, **1988**, 27, 1073.
75. P. J. Stang, B. Olenyuk, and A. M. Arif, *Organometallics*, **1995**, 14, 5281.
76. M. S. Davies, C. I. Diakos, B. A. Messerle, and T. W. Hambley, *Inorganic Chemistry*, **2001**, 40, 3048.
77. P. H. M. Budzelaar, in *gNMR version 5.0.1.0 - NMR simulation program*, IvorySoft, **2002**.
78. in *CAChe Workspace, CAChe WorkSystem Pro Version 6.1.12.33*, Fujitsu Limited.
79. S. M. Blair, E. C. Kempen, and J. S. Brodbelt, *Journal of the American Society for Mass Spectrometry*, **1998**, 9, 1049.
80. L. Fabbrizzi and I. Faravelli, *Chemical Communications*, **1998**, 971.
81. L. Fabbrizzi, G. Francese, M. Licchelli, A. Perotti, and A. Taglietti, *Chemical Communications*, **1997**, 581.

82. H. Miyaji, J. P. Anzenbacher, J. L. Sessler, E. R. Bleasdale, and P. A. Gale, *Chemical Communications*, **1999**, 1723.
83. A. P. de Silva, H. Q. N. Guarantee, C. McVeigh, M. G. E. Maguire, P. R. S. Maxwell, and E. O'Hanlon, *Chemical Communications*, **1996**, 2191.
84. P. D. Beer and M. Shade, *Gazzette Chimica Italia*, **1997**, 127, 651.
85. P. D. Beer, V. Timoshenko, M. Maestri, P. Passaniti, and V. Balzani, *Chemical Communications*, **1999**, 1755.
86. V. Balzani, F. Bolleta, and M. T. Gandolfi, *Topics Currently in Chemistry*, **1978**, 75, 1.
87. B.-C. Tzeng, S.-C. Chan, M. C. W. Chan, C.-M. Che, K.-K. Cheung, and S.-M. Peng, *Inorganic Chemistry*, **2001**, 40, 6699.
88. J. L. Atwood, J. E. D. Davies, D. D. Macnicol, and F. Vogtle, *Comprehensive Supramolecular Chemistry*, ed. J. E. D. Davies and J. A. Ripmeester, Pergamon, **1996**.
89. E. C. Kempen, J. S. Brodbelt, R. A. Bartsch, M. T. Blanda, and D. B. Farmer, *Analytical Chemistry*, **2001**, 73, 384.
90. C. L. Sherman and J. S. Brodbelt, *Analytical Chemistry*, **2003**, 75, 1828.
91. C. L. Sherman and J. S. Brodbelt, *Analytical Chemistry*, **2005**, 77, 2512.

Vita Auctoris

Name	Chantelle R. Bondy
Date of Birth	Aug. 17, 1977
Place of Birth	Windsor, Ontario, Canada
Citizenship	Canadian
Education	Ph.D., Chemistry, 2005 University of Windsor Windsor, Ontario, Canada
	B.Sc., Honours Biochemistry, 2000 University of Windsor Windsor, Ontario, Canada
Professional Work History	Graduate Teaching Assistant University of Windsor Windsor, Ontario, Canada 2000-2004
	Graduate Research Assistant University of Windsor Windsor, Ontario, Canada 2000-present
	Natural Sciences and Engineering Research Council of Canada Undergraduate Research Assistantship University of Windsor Windsor, Ontario, Canada May-August 1999 and 2000
Scholarships and Awards	NSERC Post-Doctoral Fellowship (2005)
	University of Windsor Tuition Scholarship (2003-2005)
	University of Windsor travel award (2001-2005)
	NSERC Post-Graduate Scholarship (2003-2005)
	Ontario Graduate Scholarship (2001-2003)

Ontario Graduate Scholarship Science and Technology (2003)

CSC Inorganic Post Prize (2002)

University of Windsor Travel Award (2001-2005)

Redmond Memorial Award

NSERC Undergraduate Scholarship (May–August 1999 and 2000)

International
Visits

University of Southampton, School of Chemistry, Southampton,
UK. Supervisor: Dr. Philip A. Gale (May-August 2004)

Publications in
Refereed Journals

C. R. Bondy, P. A. Gale and S. J. Loeb*, “Metal Organic Anion
Receptors: Arranging Urea Hydrogen-Bond Donors to Encapsulate
Sulfate Ions.” *J. Am. Chem. Soc.*, 2004, 5030. Featured in *Science*
– Editors’ choice vol. 304, 361 and *ACCN*.

C. R. Bondy, P. A. Gale and S. J. Loeb*, “Amido Complexes of
Platinum(II) as Receptors for the Nitrate Ion.” *J. Supramol.*
Chem., 2003, 93. (Invited Contribution)

C. R. Bondy, S.J. Loeb*, “Amide-Based receptors for anions.” *In*
35 Years of Synthetic Anion Receptor Chemistry, 1968-2003,
Coord. Chem. Rev., 2003, 77. (Invited Contribution)

C. R. Bondy, P. A. Gale* and S. J. Loeb*, “Platinum (II)
nicotinamide complexes as receptors for oxo-anions.” *Chem.*
Commun., 2001, 729.

Conference
Presentations

C. R. Bondy, P. A. Gale and S. J. Loeb, *Self-Assembled*
Platinum(II) Complexes for Anion Recognition. Departmental
Seminar, University of Windsor, Oct 2005.

P. A. Gale, S. J. Loeb, C.R. Bondy and J. L. Sessler, *Taking*
Inspiration from the chemistry of the Calixarenes. Keynote
Speaker, 8th International Conference on Calixarenes (CALIX
2005), Prague, Czech Republic, July 2005.

C. R. Bondy, P. A. Gale and S. J. Loeb, *Metal Organic Analogs of*
Calix[4]arene Based Anion Receptors. Inorganic Oral
Presentation, 88th Canadian Society for Chemistry Conference,
Saskatoon, Saskatchewan, May 2005.

S. J. Loeb, C. R. Bondy and P. A. Gale, *Metal-Organic Anion Receptors: An alternative Scheme for arranging Hydrogen Bond Donors*. Invited Speaker, 227th American Chemical Society National Meeting, Anaheim, California, March 2004.

C. R. Bondy, P. A. Gale and S. J. Loeb, *Metal Organic Analogs of Calix[4]arene Based Anion Receptors*. Inorganic Poster Presentation, 86th Canadian Society for Chemistry Conference, Ottawa, Ontario, August 2003.

C. R. Bondy, P. A. Gale and S. J. Loeb, *Amide Complexes as Analogs for Calixarene-Based Anion Receptors*. Inorganic Poster Presentation, 85th Canadian Society for Chemistry Conference, Vancouver, British Columbia, June 2002. Inorganic Poster Prize received.

C. R. Bondy, P. A. Gale and S. J. Loeb, *Anions in Supramolecular Chemistry*. Optical Sensors 2001, Prague, Czech Republic, October 2001.

C. R. Bondy, P. A. Gale and S. J. Loeb, *Fundamentals and Applications of Anion Separations*. American Chemical Society National Meeting, Chicago, Illinois, USA, August 2001.

C. R. Bondy, P. A. Gale and S. J. Loeb, *New Inorganic Receptors for Oxo-anions*. Macrocycles 2001 (ISMC-26), Fukuoka, Japan, July 2001.

C. R. Bondy, P. A. Gale and S. J. Loeb, *Platinum (II) Nicotinamide Complexes as Receptors for Oxo- Anions*. Inorganic Poster Presentation, 84th Canadian Society for Chemistry Conference, Montreal, Quebec, Canada, May 2001.

C. R. Bondy, P. A. Gale and S. J. Loeb, *Platinum (II) Nicotinamide Complexes as Anion Receptors*. Poster Presentation, 33rd Annual Inorganic Discussion Weekend, York University, Toronto, Ontario, Canada, October 2000.

C. R. Bondy and S. J. Loeb, *Platinum (II) Nicotinamide Complexes as Anion Receptors*. Undergraduate Poster Presentation, 83rd Canadian Society for Chemistry Conference, Calgary, Alberta, Canada, May 2000.

C. R. Bondy and S. J. Loeb, *Platinum (II) Nicotinamide Complexes as Anion Receptors*. Honour's Thesis Oral Presentation, University of Windsor, Windsor, Ontario, Canada, April 2000.

C. R. Bondy and S. J. Loeb, *Platinum (II) Nicotinamide Complexes as Anion Receptors*. Oral Presentation, 28th Annual Southwestern Ontario Undergraduate Student Chemistry Conference, Brock University, Ste. Catherines, Ontario, Canada, April 2000.